Hypoxia and HIF signalling in the epicardium during development and regeneration

A Thesis submitted for the degree of Doctor of Philosophy (D.Phil)

Department of Physiology, Anatomy and Genetics

University of Oxford

Eleanor Price

Green Templeton College

Supervised by

Professor Paul R Riley and Dr Joaquim M Vieira



2018

Abstract

Heart failure is a major cause of death worldwide due to the inability of the mammalian heart to regenerate after injury. The neonatal mouse heart however mounts a substantial regenerative response; though this capacity is lost one week after birth. The epicardium, which is activated in response to injury, becomes quiescent during this time-frame and may, therefore, be involved in the loss of regenerative potential. Another key change that occurs in the heart after birth is the transition to a post-natal circulation, meaning it becomes less hypoxic. Hypoxia inducible factor (HIF) is a transcription factor, which is activated in response to hypoxia and significantly, activated HIF can directly bind to and upregulate expression of *Wt1*, the master regulator of epicardial activation via epithelial-to-mesenchymal transition (EMT). I, therefore, sought to investigate a functional requirement for hypoxia and HIF-signalling in the activation of the epicardium during murine heart development and neonatal cardiac regeneration.

In the developing heart, co-expression of WT1 with hypoxyprobe at embryonic stages (E)16.5 and E18.5 indicated the epicardium is hypoxic at later stages of embryogenesis. Epicardial-specific loss of *Hif1*α or *Hif2*α during development led to decreased epicardial activation and EMT which impacted on coronary vessel development and myocardial compaction. Furthermore, stabilisation of HIF in epicardial explant cultures, via genetic ablation of prolyl hydroxylase domain 2 gene (*Phd2*), or chemical inhibition of PHD enzymes via FG-4592 (also known as Roxadustat), resulted in enhanced EMT, implicating a role for HIF signalling in epicardial activation. Whilst the epicardium becomes

quiescent within the first postnatal week, stabilisation of HIF signalling after birth through loss of *Phd2* was sufficient to maintain activation of the epicardium. Moreover, genetic knock-down and pharmacological (treatment with FG-4592) inhibition of PHD2 to stabilise HIF augmented the epicardial response to injury and preliminary results suggested an improvement in the regenerative response.

Further analysis into the full impact on neonatal cardiac regeneration, and transition to the injured adult heart, is required. Nevertheless, FG-4592, which is already in clinical trials for patients with anaemia, presents a potential novel therapeutic approach to improve cardiac repair in human patients following myocardial infarction.

Acknowledgments

First and foremost, I would like to thank my two supervisors Paul Riley and Joaquim ‘Joey’ Vieira. Paul, for allowing me to join his lab, for guiding me throughout this process, and for always remaining positive about the research. Joey, for all his support at both the bench and desk, and great mentorship over the years. Thank you to all the members of the Riley, Smart and Mommersteeg lab, new and old. To Tonia and Caroline, my CRM gals, for all the support, laughs and wine over the years, I couldn’t have done it without them. To Mala, for teaching me the MI surgery, and for always keeping faith in my abilities and to Tom for surgical guidance. Thank you to all other members of the group including: Xin, Cristina, Damien, Filipa, Sophia, Christoph, Lorna, Nicola, Tilly, Katie, Dee, Tertia, Sophie, Caitlin, Megan, Irina, Andia, Susann and all the rest, for all their advice, input and entertainment over the years.

Thank you to my Cambridge co-supervisor Dr Sanjay Sinha, for the useful input into the project and advice. Thank you to our collaborators Professor Peter Ratcliffe and Dr Tammie Bishop, for all their advice on hypoxia and HIF, for providing us with animals and compounds and general contributions to the work, the project would not have been possible without them. Thank you to members of the Ratcliffe lab: James, Gloria, Tzu-lan and Rafik.

Thank you to Angela, Richard and all the staff at the BMS for taking care of my animals and for animal welfare guidance.

Thank you to my friends Oxford/home/Bristol, for giving me a life outside the lab and always knowing how to pick me up. Thank you to my Oxford twin, Laurienne, I couldn’t have survived this place without you! Thank you to my

family, to my Dad for inspiring me to do my DPhil, to my Mum and sister Nat for their love and support, and to my wise Owl Chloe, for being my voice of reason this last year.

Thank you to the British Heart Foundation (BHF) for funding this research.

Finally, thank you to Professor Chris Pugh and Professor Mauro Giacca for taking the time to examine this thesis.

‘*I was taught the way of progress was neither swift nor easy.*’

Marie Curie

Table of Contents

1 Introduction 21

1.1 Heart development 22

1.1.1 Ventricular Maturation 23

1.1.2 Coronary vessel development 24

1.2 The epicardium 27

1.2.1 Formation of the epicardium 27

1.2.2 Epicardial epithelial-to-mesenchymal transition 27

1.2.3 The role of Wilm's Tumour 1 in the epicardium 28

1.2.4 The role of the epicardium in ventricular development 29

1.2.5 The epicardium in coronary vessel development 30

1.2.6 The epicardium in fibroblast development 30

1.3 Myocardial infarction 32

1.4 Models of regeneration 33

1.4.1 Zebrafish 33

1.4.2 The neonatal mouse 34

1.4.3 The neonatal human 35

1.5 The epicardium in regeneration 36

1.5.1 The epicardium in zebrafish regeneration 36

1.5.2 Re-activation of the mammalian epicardium. 36

1.5.3 Augmenting the epicardial response to injury 37

1.6 Hypoxia 38

1.6.1 HIF signalling 38

1.6.2 HIF signalling in heart development 41

1.6.3 HIF signalling in cardiac regeneration 43

1.6.4 HIF signalling in the epicardium 44

1.7 Hypothesis 46

1.8 Aims of thesis 46

2 Materials and Methods 47

2.1 Mice 48

2.1.1 Mouse strains 48

2.1.2 Timed matings 48

2.1.3 Hypoxyprobe-1 administration 49
2.1.4 Tamoxifen induced activation of Cre recombinase 49
2.1.5 Embryonic dissection 50
2.1.6 Neonatal and adult dissection 50
2.2 Myocardial infarction 51
2.2.1 Neonatal surgery model 51
2.2.2 FG-4592 administration 53
2.3 Primary Tissue Culture 53
2.3.1 Epicardial explant cultures 53
2.4 Molecular techniques 55
2.4.1 DNA isolation for genotyping 55
2.4.2 Polymerase Chain Reaction (PCR) for genotyping 55
2.4.3 Gel electrophoresis 57
2.4.4 RNA extraction 57
2.4.5 cDNA synthesis 58
2.4.6 Real-time quantitative PCR (RT-qPCR) 59
2.5 Histological and Immunostaining 60
2.5.1 Wax embedding for histology 60
2.5.2 Haematoxylin and Eosin staining 61
2.5.3 Masson's Trichrome Staining 61
2.5.4 Immunostaining of cryosections 62
2.6 Image Analysis 64
2.6.1 Quantification of immunofluorescence of cryosections. 64
2.6.2 Average nuclear fluorescence intensity 64
2.6.3 Fractal analysis 65
2.7 Statistical analysis 67
3 HIF signalling in epicardial development 68
3.1 Background 69
3.2 Aims 70
3.3 Hypoxia in the epicardium during development 71
3.3.1 The epicardium is hypoxic at later stages of development. 71
3.3.2 The HIF-target, GLUT1, is expressed in hypoxic regions in the heart. 76
3.3.3 The HIF family of transcription factors are expressed in the heart during development 79

3.3.4 HIF directly binds to the *WT1* locus 81

3.4 Investigating a functional requirement for HIF1α in the developing epicardium 84

3.4.1 The *Wt1*$^{CreERT2/+}$ driver specifically targets epicardial cells and its derivatives in development..... 84

3.4.2 Generating embryos with epicardial-specific deletion of *Hif1α*..... 86

3.4.3 Loss of Hif1α in the epicardium leads to nodules on the surface of the heart. 88

3.4.4 *Hif1α*$^{fl/fl}$*; Wt1*$^{CreERT2/+}$ embryos display a significant decrease in WT1 expression 89

3.4.5 Loss of HIF1α in the epicardium does not affect cardiomyocyte proliferation 92

3.4.6 Loss of HIF1α in the epicardium impacts on coronary vessel development. 96

3.5 A requirement for HIF2α in epicardial development..... 98

3.5.1 *Hif2α*$^{fl/fl}$*; Wt1*$^{CreERT2/+}$ embryos present with Oedema, haemorrhaging and nodules on the surface of the heart. 100

3.5.2 Loss of *Hif2α* in the epicardium results in a significant reduction in WT1 expression 102

3.5.3 Loss of *Hif2α* in the epicardium leads to a significant reduction in cardiomyocyte proliferation in the compact layer..... 105

3.5.4 Loss of epicardial *Hif2α* results in defective coronary vessel formation. 109

3.6 Discussion..... 111

3.6.1 Hypoxia in early heart development..... 111

3.6.2 Hypoxia in the epicardium 112

3.6.3 Direct interaction of HIF with *Wt1* 115

3.6.4 Differential expression of HIF1α and HIF2α in the heart..... 116

3.6.5 The role of HIF1α in the epicardium 116

3.6.6 The role of HIF2α in the epicardium 118

3.6.7 Complementary roles for HIF1α and HIF2α in the epicardium..... 121

3.7 Conclusions 123

4 HIF signalling in epicardial epithelial-to-mesenchymal transition 124

4.1 Background..... 125

4.2 Aims 126
4.3 Epicardial Explant cultures 127
4.4 Genetic gain-of-function of HIF in epicardial explant cultures. 129
4.4.1 Loss of *Phd2* does not affect epicardial explant size 130
4.4.2 Loss of *Phd2* results in stabilisation of HIF1α 132
4.4.3 Loss of *Phd2* does not affect epicardial cell proliferation 134
4.4.4 Loss of *Phd2* enhances epicardial EMT 135
4.5 Pharmacological gain-of-function of HIF in epicardial explant cultures. 138
4.5.1 Pharmacological inhibition of PHD enzymes results in stabilisation of HIF1α *in vitro*. 139
4.5.2 Pharmacological inhibition of PHDs results in a significant increase in WT1 expression and enhances epicardial EMT. 143
4.6 Genetic ablation of HIF1α in epicardial explant cultures. 147
4.6.1 Loss of *Hif1α* decreases epicardial explant growth 147
4.6.2 Loss of HIF1α results in a reduction in epicardial EMT 151
4.7 Genetic loss of *Hif2α* in epicardial explant cultures 153
4.7.1 Loss of *Hif2α* results in a decrease in epicardial explant growth. 153
4.8 Discussion 155
4.8.1 Genetic gain-of-function of HIF 155
4.8.2 Differences in pharmacological and genetic inhibition of *Phd2* 156
4.8.3 Genetic loss-of-function of HIF 157
4.8.4 Limitations 159
4.8.5 Therapeutic potential 160
4.9 Conclusions 161
5 The epicardial response to injury in the neonatal mouse heart 162
5.1 Background 163
5.2 Aims 165
5.3 The epicardium become quiescent shortly after birth 166
5.4 Learning the injury model 170
5.5 Activation of the epicardium in the regenerating P1 heart 172
5.5.1 Epicardial WT1 expression is increased in response to injury at P1172
5.5.2 The neonatal mouse heart can regenerate following injury at P1 174

5.6 Reactivation of the epicardium in the P7 heart after injury..... 176
5.6.1 The epicardium is partially reactivated following injury at P7 176
5.6.2 Myocardial infarction at P7 results in ventricular remodelling and persistent cardiac fibrosis.....181
5.7 Discussion..... 184
5.7.1 Quiescence of the epicardium after birth 184
5.7.2 HIF signalling in the heart after birth 185
5.7.3 Regeneration in the P1 mouse heart 185
5.7.4 The limited regenerative capacity of the P7 mouse heart.....186
5.8 Conclusions 189
6 HIF signalling in neonatal cardiac regeneration 190
6.1 Background..... 191
6.2 Aims..... 191
6.3 Maintaining HIF signalling after birth..... 192
6.3.1 HIF signalling can be activated postnatally. 192
6.3.2 Loss of *Phd2* results in a significant increase in expression of WT1. 195
6.4 Response to myocardial infarction in the HIF genetic gain-of-function model..... 200
6.4.1 Loss of *Phd2* results in extensive WT1 expression, following myocardial infarction. 201
6.4.2 Stabilisation of HIF does not increase neovascularisation at four days post injury. 206
6.4.3 Loss of *Phd2* does not lead to gross changes in cell proliferation nor monocyte/macrophage recruitment, four days post-infarction. 207
6.4.4 Loss of *Phd2* in cardiac remodelling and fibrosis 208
6.5 Pharmacological activation of HIF signalling..... 211
6.5.1 FG-4592 dose administration. 212
6.5.2 Inhibition of PHDs, post-MI leads to a significant upregulation of epicardial WT1. 213
6.5.3 Activation of HIF does not lead to increased neovascularisation, four days post-MI. 215
6.5.4 Inhibition of PHDs post-MI does not alter global proliferation nor early macrophage proliferation/recruitment. 216

6.5.5 A single dose of FG-4592 results in a decrease in pathological remodelling post-MI. 217
6.6 Discussion.... 221
6.6.1 HIF signalling in the quiescence of the epicardium 221
6.6.2 Activation of WT1 by HIF. 222
6.6.3 Epicardial specific deletion of WT1 224
6.6.4 Loss of *Phd2* in the regenerative response....226
6.6.5 Tamoxifen toxicity in the neonate 226
6.6.6 Maternal cannibalism....228
6.6.7 Differences between the genetic and pharmacological approach. ..229
6.6.8 FG-4592 in the regenerative response 231
6.7 Conclusions 232
7 General discussion 233
7.1 Discussion of aims 234
7.1.1 Levels of hypoxia and HIF in the epicardium during development ..234
7.1.2 A functional requirement for HIF in the developing epicardium 236
7.1.3 A role for HIF signalling in epicardial EMT 239
7.1.4 The epicardial response in neonatal cardiac regeneration 240
7.1.5 The effect of HIF signalling in the epicardial response to injury in the neonate 242
7.2 Conclusions 248
7.3 Future work 249
7.3.1 To Further investigate the role of HIF1α and HIF2α in the epicardium during development 249
7.3.2 Determine if there is an effect of stabilisation of HIF on epicardial development. 251
7.3.3 To investigate if activation of HIF improves myocardial function 252
7.3.4 To determine whether loss of HIF signalling is sufficient to cause early quiescence of the epicardium and inhibit the neonatal regenerative response. 254
7.3.5 To determine a role for HIF signalling in adult mouse regeneration 255
8 Appendices.... 256
8.1 Funding.... 256
8.2 Timing and venue of research 256

8.3 Publications 256
8.3.1 Manuscript in preparation 256
8.3.2 Review in preparation 257
8.4 Presentations at scientific meetings 257
8.4.1 Oral presentations 257
8.4.2 Poster Presentations 257
9 Bibliography 258

List of Figures

Figure 1.1.1 Murine cardiac development.....23
Figure 1.2.1 Epicardial epithelial-to-mesenchymal transition 31
Figure 1.6.1 The HIF pathway 40
Figure 2.2.1 Neonatal LAD ligation surgery.....52
Figure 2.6.1 Average nuclear fluorescence quantification 65
Figure 2.6.2 Fractal Analysis using FracLac.....66
Figure 3.3.1 During development WT1+ cells undergo EMT and migrate into the myocardium as it grows and compacts.....74
Figure 3.3.2 The epicardium is hypoxic at later stages of development 76
Figure 3.3.3 Observed HIF1α antibody immunostaining is only background. ..78
Figure 3.3.4 The HIF-target GLUT1 is expressed in regions of hypoxia during cardiac development. 78
Figure 3.3.5 Hif1α and Hif2α are expressed in the heart during development ..81
Figure 3.3.6 HIF directly binds to the promoter region of *Wt1* in renal cells. 83
Figure 3.4.1 The *Wt1*$^{CreERT2/+}$ line sufficiently targets epicardial cells and EPDCs during development. 85
Figure 3.4.2 Inducible, epicardial-specific deletion of HIF1α during embryonic development 87
Figure 3.4.3 *Hif1α*$^{fl/fl}$; *Wt1*$^{CreERT2/+}$ embryos present with oedema and blood nodules on the surface of the heart. 89
Figure 3.4.4 Epicardial specific loss of *Hif1α* leads to a significant reduction in WT1 expression. 92
Figure 3.4.5 Epicardial loss of *Hif1α* does not lead to reduced cardiomyocyte proliferation 95
Figure 3.4.6 Loss of *Hif1α* in the epicardium results in a significant reduction in coronary vessel formation. 97
Figure 3.5.1 Inducible, epicardial-specific deletion of HIF2α during embryonic development 99
Figure 3.5.2 Embryos lacking epicardial expression of *Hif2α* present with oedema and epicardial surface blood nodules. 101
Figure 3.5.3 Loss of *Hif2α* in the epicardium results in a significant reduction in WT1 expression and hyper-trabeculation of the myocardium. 105
Figure 3.5.4 Epicardial-specific loss of Hif2α expression results in a significant reduction in proliferation in the compact myocardium. 108

Figure 3.5.5 Loss of *Hif2α* in the epicardial results in a significant reduction in the number of coronary vessels.....110
Figure 4.3.1 Murine epicardial explant cultures 127
Figure 4.4.1 4-hydroxytamoxifen treatment of epicardial explant cultures.....129
Figure 4.4.2 Loss of *Phd2* does not affect epicardial explant size.....131
Figure 4.4.3 Loss of *Phd2* results in stabilisation of HIF1α and increased GLUT1 expression. 133
Figure 4.4.4 Loss of *Phd2* does not affect epicardial cell proliferation 134
Figure 4.4.5 Loss of *Phd2* enhances SNAI1/2-mediated epicardial EMT 138
Figure 4.5.1 Pharmacological activation of HIF signalling in epicardial explant cultures. 139
Figure 4.5.2 Pharmacological inhibition of PHD enzymes results in stabilisation of HIF1α.....141
Figure 4.5.3 Selective chemical inhibition of PHD enzymes results in stabilisation of HIF1α and an increase in GLUT1 expression. 142
Figure 4.5.4 Expression of WT1, the master regulator of epicardial EMT, is significantly increased, following PHD inhibition. 146
Figure 4.6.1 Loss of *Hif1α* results in a significant decrease in epicardial surface. 149
Figure 4.6.2 A lower dose, of 1μm of 4-OHT, decreases its toxic effects and results in Cre activation. 150
Figure 4.6.3 Loss of *Hif1α* results in a significant decrease in epicardial EMT. 152
Figure 4.7.1 Loss of *Hif2* results in a significant decrease in epicardial explant size. 154
Figure 5.3.1 The epicardium becomes dormant within 2 weeks after birth.....167
Figure 5.3.2 The epicardium becomes quiescent shortly after birth.....169
Figure 5.5.1 Epicardial expression of WT1 is increased following injury at P1. 173
Figure 5.5.2 The neonatal mouse heart can regenerate in 21 days, following myocardial infarction at P1. 175
Figure 5.6.1 The epicardium is partially reactivated in response to injury at P7. 178
Figure 5.6.2 The epicardium is reactivated proximal to the infarct region. 179
Figure 5.6.3 EMCN expression is increased following injury at P7.....180

Figure 5.6.4 The neonatal mouse heart is unable to regenerate following myocardial infarction at P7. 183
Figure 6.3.1 Tamoxifen administration to neonates at P2 successfully results in reduced *Phd2* and increased *Glut1* and *Wt1* expression by P7. 198
Figure 6.3.2 Loss of *Phd2* results in a significant increase in WT1 199
Figure 6.4.1 Myocardial infarction following activation of HIF signalling..... 200
Figure 6.4.2 WT1 is expressed in endothelial cells following activation of HIF. 205
Figure 6.4.3 Loss of *Phd2* does not lead to changes in vessel formation, four days after myocardial infarction at P7. 206
Figure 6.4.4 Activation of HIF does not lead to notable changes in global cell proliferation or macrophage proliferation/recruitment, four days following MI. 208
Figure 6.4.5 Potential improved myocardial survival and reduced ventricular remodelling following loss of *Phd2*..... 210
Figure 6.5.1 Pharmacological activation of HIF signalling following myocardial infarction. 213
Figure 6.5.2 Pharmacological inhibition of PHDs increases epicardial WT1 expression following myocardial infarction 215
Figure 6.5.3 Pharmacological activation of HIF does not lead to notable differences in neovascularisation, four days post injury. 216
Figure 6.5.4 Global proliferation and early macrophage proliferation/recruitment are not altered following inhibition of PHDs post-MI. 217
Figure 6.5.5 Assessment of cardiac remodelling and collagen deposition 21dpi. 220

List of Tables

Table 2.1.1 Genetic mouse strains **48**
Table 2.3.1 Compounds **54**
Table 2.4.1 PCR primers for genotyping **56**
Table 2.4.2 PCR programmes for genotyping **56**
Table 2.4.3 Solutions **57**
Table 2.4.4 PCR primers for RT-qPCR **60**
Table 2.5.1 Primary antibodies **63**
Table 2.5.2 Secondary antibodies **63**
Table 3.4.1 Survival of *Hif1α$^{fl/fl}$; Wt1$^{CreERT2/+}$* embryos **88**
Table 3.4.2 Phenotype of *Hif1α$^{fl/fl}$; Wt1$^{CreERT2/+}$* embryos **88**
Table 3.5.1 Survival of *Hif2α$^{fl/fl}$; Wt1$^{CreERT2/+}$* embryos. **100**
Table 3.5.2 Phenotype of *Hif2α$^{fl/fl}$; Wt1$^{CreERT2/+}$* embryos. **100**

List of abbreviations

2OG	2-oxoglutarate
4-OHT	4-hydroxytamoxifen
ACTN2	alpha-sarcomeric actinin
ANG2	angiopoietin 2
Atp5f1b	ATP synthase F1 subunit beta
AV	atrioventricular
AVC	atrioventricular canal
cDNA	complementary DNA
ChIP-seq	chromatin immunoprecipitation coupled with RNA sequencing
Cre	Cre recombinase
CreERT2	tamoxifen-dependant cre recombinase
DFO	deferoxamine
DMEM	Dulbecco's modified Eagle medium
DMSO	dimethyl sulphoxide
DNA	deoxyribonucleic acid
dpi	days post-injury
E	embryonic day
ECM	extracellular matrix
ECs	endothelial cells
EGFR	epidermal growt factor receptor
EMCN	endomucin
EMT	epithelial to mesenchymal transition
EndMT	endothelial to mesenchymal transition
EPAS1	Endothelial PAS protein 1
EPDCs	epicardial derived cells
Epi	epicardium
EPO	erythropoietin
ERα	oestrogen receptor alpha
EtOH	ethanol – defined twice
FGF	fibroblast growth factor
FIH	factor inhibiting HIF

GCPs	glycolytic cardiac progenitors
GLUT1	glucose transporter 1
H&E	Haematoxylin and Eosin
HIF	hypoxia inducible factor
HP1	Hypoxyprobe-1
HRE	hypoxia response element
IGF1	insulin-like growth factor 1
IP	intraperitoneal
IQR	interquartile range
IRI	ischaemia reperfusion injury
IVS	interventricular septum
LA	left atria
LAD	left anterior descending
LBD	ligand binding domain
LV	left ventricle
LVNC	left ventricular non-compaction cardiomyopathy – defined twice
MI	myocardial infarction
MRI	magnetic resonance imaging
mRNA	messenger RNA
Myo	myocardium
ODD	oxygen dependant degradation
OFT	outflow tract
P	postnatal day
PBS	phosphate buffered saline
PCR	polymerase chain reaction
PDPN	podoplanin
PECAM (CD31)	Platelet endothelial cell adhesion molecule
PEO	proepicardium
PHD	prolyl hydroxylase domain
PHH3	phosphor-histone H3
RA	retinoic acid
RA	right atria

Raldh2	retinaldehyde dehydrogenase 2
RNA	ribonucleic acid
ROS	reactive oxygen species
RT-qPCR	real-time quantitative PCR
RV	right ventricle
Sdha	succinate dehydrogenase complex flavoprotein subunit A
SEM	Standard error of the Mean
SM-MHC	smooth muscle myosin heavy chain
SM22α	smooth muscle protein 22-alpha
SV	sinus venosus
Tβ4	thymosin beta-4
TAD	transactivation domain
Tbx18	T-box protein 18
Tcf21	transcription factor 21
VECs	vascular endothelial cells
VEGF	vascular endothelial growth factor
VEGFR	VEGF receptor
VSDs	ventricular septal defects
VSMCs	vascular smooth muscle cells
WT1	Wilms tumour 1

1 Introduction

1.1 Heart development

In mice, cardiac development begins around embryonic day (E) 7.5, when mesodermal derived cardiac precursors, referred to as the first heart field, converge on the midline to form the cardiac crescent. At E8.0 the crescent fuses, forming the linear heart tube, which then undergoes rightward looping, giving rise to primitive chambers (DeRuiter et al., 1992). A second cardiogenic mesodermal population, known as the second heart field, lies anterior and dorsal to the linear heart tube. Cells from the second heart field are added to the arterial and venous poles of the developing heart tube, contributing to the outflow tract (OFT), the right ventricle and parts of the atria (Kelly and Buckingham, 2002). Embryonic growth then drives anterior movement of the venous pole, giving rise to the distinct 4-chambered heart. At E10.5 a population of mesoderm-derived cells, known as the proepicardium (PEO), migrate towards the developing heart, enveloping its outer surface and giving rise to the epicardium (Viragh and Challice, 1981). Concomitantly, cardiac neural crest progenitors migrate from the dorsal neural tube, engulfing the pharyngeal arch arteries and contributing to vascular smooth muscle cells (VSMCs) of the OFT, along with OFT septation (Jiang et al., 2000). By E14.5 cardiac maturation is largely complete.

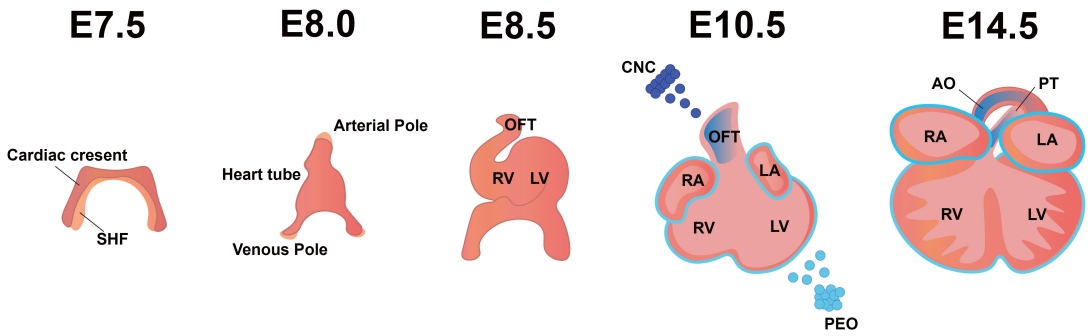


Figure 1.1.1 Murine cardiac development

E7.5. Cardiac progenitors converge to form the cardiac crescent. **E8.0**. The cardiac crescent fuses to form the linear heart tube. Cells from the second heart field (SHF) are added to the arterial and venous poles of the heart tube. **E8.5.** The heart undergoes rightward looping giving rise to the primitive chambers. **E10.5.** Anterior movement of the venous pole gives rise to the 4-chambered heart. Cardiac neural crest (CNC) progenitors contribute to the outflow tract (OFT), whilst cells from the proepicardium (PEO) envelope the surface of the heart giving rise to the epicardium. **E14.5** Cardiac maturation is largely complete. RA= right atria, LA= left atria, RV= right ventricle, LV= left ventricle, AO= aorta, PT= pulmonary trunk.

1.1.1 Ventricular Maturation

Maturation of the ventricular wall during development is essential for creating a functionally competent postnatal heart and requires the co-ordination between myocardial trabeculation and compaction. In early development, the linear heart tube is composed of an inner endocardial cell layer, and an outer single cell myocardial layer, separated by cardiac jelly (Brutsaert and Andries, 1992). As the myocardium begins to thicken, the endocardium invaginates, causing the myocardium to protrude into the lumen of the heart, forming trabeculae, beginning at E9.5. These structures are thought to increase the surface area for oxygen and nutrient exchange, and enhance muscle force generation (Sedmera and Thomas, 1996). Cells of the compact myocardium continue to proliferate, thickening the wall, whilst the trabeculae

cardiomyocytes become more differentiated and have decreased proliferative capacity (Sedmera et al., 2003). Around E12.5, the trabeculae collapse towards the myocardial wall, in a process known as compaction, giving rise to a thicker, mature ventricular wall (Grego-Bessa et al., 2007; Del Monte-Nieto et al., 2018; Sedmera and Thomas, 1996).

Defects in ventricular maturation lead to congenital heart diseases, such as the third most commonly diagnosed cardiomyopathy, left ventricular non-compaction cardiomyopathy (LVNC). LVNC is characterised by hyper-trabeculation, and a thin ventricular wall, which can lead to dilated cardiomyopathy, heart failure, thromboembolism, arrhythmia and sudden cardiac death (Zhang et al., 2013).

Several growth factors and signalling pathways have been shown to be critical in these processes, and work by Kang and Sucov suggests endocardial-derived growth signals, such as neuregulin, predominantly govern trabeculation, whilst epicardial derived growth signals, such as retinoic acid signalling, are particularly important for development of the compact myocardium (Kang and Sucov, 2005).

1.1.2 Coronary vessel development

The establishment of the coronary vasculature is essential as the myocardium grows and thickens. The coronary vasculature begins with the formation of a vascular plexus: a series of discontinuous endothelial patches spread from the sinus venosus (SV), around the ventricles to form a complete plexus which covers the heart (Red-Horse et al., 2010). This plexus then remodels, forming

mature vasculature that connects to the aorta (Dyer et al., 2014). The vascular endothelial cells (VECs), which form the coronary plexus, arise from 3 proposed sources: the proepicardium; the sinuous venosus and the endocardium.

1.1.2.1 The proepicardium

It was long thought VECs were derived from the proepicardium (PEO), due to seminal work conducted in chick embryos (Dettman et al., 1998; Mikawa and Gourdie, 1996; Perez-Pomares et al., 1998). However, later genetic lineage tracing experiments conducted in mice, using epicardial specific Cre drivers such as *Wt1*, *Tbx18* and *Tcf21* revealed varying contributions. Whilst Cano and colleagues reported significant contribution of PEO-derived cells to the endothelial lineage (Cano et al., 2016), others reported only minor contribution (Acharya et al., 2011; Cai et al., 2008; Zhou et al., 2008). In an attempt to resolve this disparity, Katz and colleagues identified a subset of cells from the PEO, which expressed Scleraxis (SCX) and Semaphorin3D (Sema3D) and contributed to cells of the coronary endothelium, sinus venosus and endocardium (Katz et al., 2012). Importantly, these cells were largely distinct from those expressing canonical epicardial markers, such as *Wt1*, *Tbx18* and *Tcf21*, suggesting a non-epicardial contribution of the PEO to the coronary endothelium and therefore accounting for the lack of contribution determined, with the use of epicardial specific Cre drivers. To that end, it is likely that cells of the PEO do contribute to VECs, but the extent to which they do so is likely to be relatively minor compared to the sinus venosus and endocardium.

1.1.2.2 Sinus Venosus

The sinus venosus (SV), is a transient structure, which returns blood to the embryonic heart. Like the PEO, the SV is closely situated to the atrioventricular (AV) groove, from where the first coronary vessels emerge. Work by Red-Horse and colleagues demonstrated that angiogenic sprouting from the SV gives rise to venous endothelial cells, which migrate, invade the myocardium, and differentiate into VECs (Red-Horse et al., 2010). Later work by this group showed these SV-derived ECs contribute to arteries, veins and capillaries on the dorsal and lateral sides of the heart, and this process is dependent on epicardial-expressed vascular endothelial growth factor C (VEGFC) (Chen et al., 2014).

1.1.2.3 Endocardium

The third source of VECs, the endocardium, was initially implicated as the single major source of new coronaries via angiogenesis (Wu et al., 2012). Further work by Red-horse and colleagues demonstrated endocardium-derived VECs contribute to the ventral coronary vessels and those of the inter-ventricular septum (IVS) (Chen et al., 2014; Red-Horse et al., 2010). More recently, a model was put forward by Tian and colleagues for a temporally distinct postnatal endocardial contribution to coronary vessels, in which during trabeculae compaction, endocardial cells become trapped within the compacting myocardium, undergo angiogenesis, migrate and form coronary vessels (Tian et al., 2014).

1.2 The epicardium

1.2.1 Formation of the epicardium

The epicardium, a mesothelial cell sheet that covers the surface of the heart, is derived from a transient extracardiac structure, known as the proepicardium (PEO) (Viragh and Challice, 1981). This structure of coelomic epithelial cells, located dorsal to the developing heart tube, between the SV and the liver, is highly conserved among vertebrates, including human, mouse, chick and zebrafish (Hirakow, 1992; Manner, 1992; Risebro et al., 2015; Serluca, 2008; Viragh and Challice, 1981). In chick, the PEO forms as a single, right-sided cluster, around Hamburger-Hamilton stage (HH) 14, with cells transferring onto the surface of the heart via an extra-cellular matrix bridge (Nahirney et al., 2003). Whilst in mouse and zebrafish the PEO appears as bilateral clusters, around E8.5 and 48 hours post-fertilisation (hpf) respectively, with cells floating in clusters towards the myocardium, driven by pericardial fluid flow (Peralta et al., 2013; Simoes and Riley, 2018). Following attachment the cells collapse and proliferate, giving rise to the epicardium by E10.5 in mouse (Simoes and Riley, 2018).

1.2.2 Epicardial epithelial-to-mesenchymal transition

As the epicardium expands, a subpopulation of cells undergo epithelial to mesenchymal transition (EMT), migrating into the sub-epicardial space and subsequently into the myocardium (Mikawa and Fischman, 1992; Perez-Pomares et al., 1998). During EMT, epicardial cells down-regulate intercellular adhesion junction proteins, such as E-cadherin and β-catenin, and express

EMT-inducing transcription factors, such as SNAI1, allowing them to lose their polarity and become migratory (von Gise and Pu, 2012). Having undergone EMT, these cells have been shown to contribute various cell types, including fibroblasts (Gittenberger-de Groot et al., 1998), vascular smooth muscle cells (VSMCs) (Mikawa and Gourdie, 1996) and to some extent endothelial cells (ECs) (Cano et al., 2016; Perez-Pomares et al., 1998) for the forming coronary vasculature, and cardiomyocytes (CMs), although the latter contribution is still widely debated. Fate mapping studies using *Tbx18* and *Wt1* Cre reporter lines demonstrated an epicardial contribution to the myocardial lineage (Cai et al., 2008; Zhou et al., 2008). However, later studies reported endogenous *Tbx18* expression in cardiomyocytes, (Christoffels et al., 2009), and reported sporadic Cre recombination in all cell types, including cardiomyocytes, in the $Wt1^{creEGFP}$ line used in Zhou's studies (Rudat and Kispert, 2012), thus questioning the suitability of these reporters for investigating an epicardial contribution to cardiomyocytes. In addition to contributing cell types, epicardial derived cells (EPDCs) play an essential role in cardiomyocyte proliferation and coronary vasculature development, through paracrine signalling, and deletion of genes essential for epicardial development, such as, *Gata4, Wt1, Vcam* and *α4β1 integrin*, leads to substantial defects in both processes (Kwee et al., 1995; Moore et al., 1999; Watt et al., 2004; Yang et al., 1995).

1.2.3 The role of Wilm's Tumour 1 in the epicardium

Wilm's tumour 1 (WT1) is a zinc-finger transcription factor which serves as a regulator of epicardial EMT. Epicardial cells in WT1 null mice are unable to detach from the epicardium and migrate into the underlying sub-epicardium

(von Gise et al., 2011; Martínez-Estrada et al., 2010). WT1 has been shown to regulate EMT via multiple mechanisms, including acting via retinoic acid (RA) and both canonical and non-canonical Wnt signalling (von Gise et al., 2011), as well as direct transcriptional regulation of the genes encoding the essential EMT mediators; SNAI1 and E-cadherin (CDH1) (Martínez-Estrada et al., 2010).

Whilst the activation and migration of EPDCs has been set against a requirement for WT1, much is still to be elucidated, regarding the molecular signalling pathways and cellular responses of the epicardium in the context of heart repair and regeneration.

1.2.4 The role of the epicardium in ventricular development

The epicardium is known to play an essential role in ventricular maturation, since mice which have a defective epicardium exhibit reduced cardiomyocyte proliferation and a thinned myocardial wall (von Gise et al., 2011). Further, mice which completely lack an epicardium have both a reduction in trabeculae and a thinner myocardial wall (Watt et al., 2004).

Several mitogenic factors, secreted by the epicardium, have been implicated in this role. Retinoic acid (RA) and erythropoietin (EPO), both secreted from the epicardium, are essential for cardiomyocyte proliferation (Chen et al., 2002; Stuckmann et al., 2003). However, neither RA or EPO directly regulate cardiomyocytes, but instead they induce the production of epicardial-derived mitogens, FGF9 and IGF2, respectively (Brade et al., 2011; Lavine et al., 2005).

1.2.5 The epicardium in coronary vessel development

Whilst the precise contribution of the epicardium to endothelial cells remains contested, it is widely accepted that the vascular smooth muscle cells (VSMCs), which surround the endothelium of the coronaries, originate from the epicardium (Dettman et al., 1998). Additionally, the epicardium secretes growth factors and cytokines, which regulate cells of the coronaries directly, as well as stimulating the myocardium to secrete pro-angiogenic factors. As such, the epicardium is essential for coronary vessel development, with loss of epicardial transcription factor *Wt1* leading to absence of the coronary plexus (Moore et al., 1999). Similarly, disruption of FGF and RA signalling from the epicardium resulted in impaired myocardial secretion of angiopoietin 2 (ANG2), VEGFA and VEGFB, resulting in perturbed coronary vessel development (Lavine et al., 2006).

1.2.6 The epicardium in fibroblast development

Cardiac fibroblasts, typically defined as cells of mesenchymal origin that produce components of the extra cellular matrix (ECM), are essential for the structural and electro-mechanical functions of the heart (Tallquist and Molkentin, 2017). They are considered to be a heterogenous population but remain poorly defined due to the lack of a definitive cardiac fibroblast marker. Markers such as Vimentin, fibroblast specific protein 1 (FSP1) and TCF21, are also expressed in mesenchymal cells, immune cells and the epicardium respectively (Braitsch et al., 2012; Marinas et al., 2012; Osterreicher et al., 2011). Despite this lack of clarity, studies in the chick and mouse have indicated that EPDCs are the principal source of embryonic cardiac fibroblasts (Cai et

al., 2008; Gittenberger-de Groot et al., 1998; Zhou et al., 2008), with the remainder derived from endocardial EMT (Ali et al., 2014; de Lange et al., 2004). Studies in the mouse demonstrated that the majority of *Tcf21*-expressing epicardial cells were committed to a cardiac fibroblast fate, and loss of *Tcf21* resulted in a failure to form cardiac fibroblasts all together (Acharya et al., 2011). Further, platelet derived growth factor (PDGF) and FGF signalling have been implicated as essential inducers of this process (Smith et al., 2011; Vega-Hernandez et al., 2011).

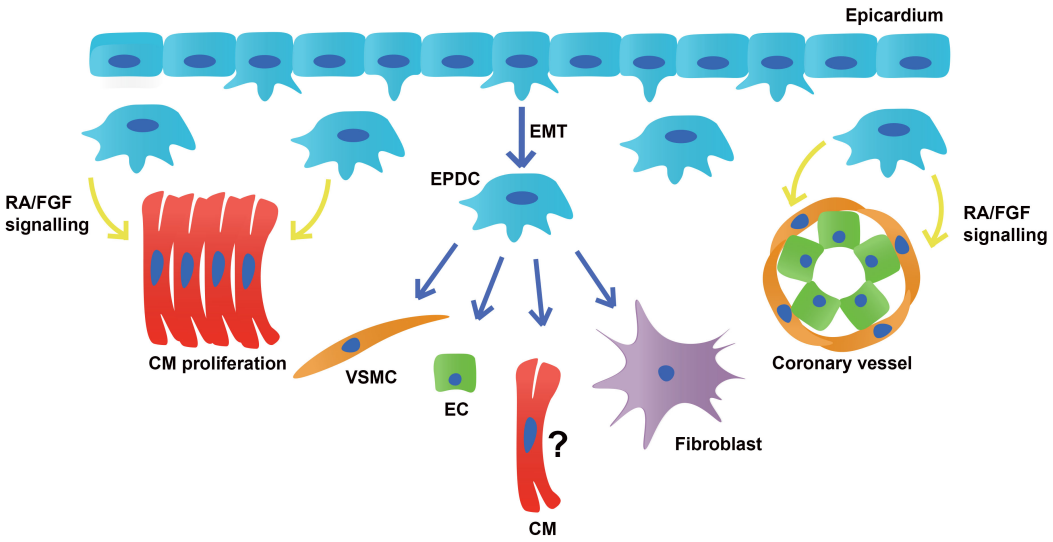


Figure 1.2.1 Epicardial epithelial-to-mesenchymal transition

During development, a subset of epicardial cells, undergo epithelial-to-mesenchymal transition (EMT) and migrate into the underlying myocardium. These epicardial derived cells (EPDCs) can differentiate into vascular smooth muscle cells (VSMCs), endothelial cells (ECs), fibroblasts, and potentially cardiomyocytes (CMs), as well as sending paracrine signals to stimulate cardiomyocyte proliferation and coronary vessel formation.

1.3 Myocardial infarction

Myocardial infarction (MI), commonly caused by coronary artery occlusion, is a leading cause of mortality worldwide. Improved clinical interventions, such as percutaneous coronary intervention (PCI), and the use of drugs to assist the survived myocardium, such as angiotensin-converting enzyme (ACE) inhibitors and beta-blockers, mean the number of people surviving the initial attack has significantly increased (Aros et al., 2006; Puymirat et al., 2012). However, many still eventually die of end-stage heart failure due to the inability of the adult mammalian heart to replace the billions of cardiomyocytes lost during the attack (Velagaleti et al., 2008). Instead, a non-contractile, fibrotic scar is deposited at the site of injury, leading to functional overload and pathological remodelling, characterised by dilation of the myocardium and eventually heart failure (Pfeffer and Braunwald, 1990). Current therapies manage the symptoms and progression of the disease but fail to address the damaged muscle (Gheorghiade et al., 2005). At present, heart transplant is the only *bona fide* cure, but given the issues of immune rejection and lack of donor hearts, there is now, an urgent need to therapeutically stimulate regeneration in the adult mammalian heart.

1.4 Models of regeneration

Whilst the adult human heart has limited regenerative capacity, with only ~1% of cardiomyocytes turned over annually (Bergmann et al., 2009), complete regeneration of damaged tissue and organs is seen in many living organisms across the evolutionary tree. Invertebrates such as Planarians, Echinoderms, Annelids and Hydra, have global regenerative potential (Candia Carnevali et al., 1998; Dawydoff, 1954; Gates, 1950; Ham and Eakin, 1958), with Planarians possessing the capacity to regenerate from as little as ~1/279th of the original organism (Morgan, 1898). Similarly, some vertebrates, such as newts, axolotls and zebrafish are capable of regenerating entire limbs or fins following amputation (Simon and Tanaka, 2013; White et al., 1994), and are able to regenerate several organs, including the heart, following injury (Cano-Martinez et al., 2010; Poss et al., 2002; Witman et al., 2011). The comparative analysis of model organisms of cardiac regeneration provides insight into the evolutionary conserved molecular mechanisms of regeneration. This knowledge could enable the re-activation of such processes in the human adult heart following MI.

1.4.1 Zebrafish

Zebrafish, teleost fish with a two-chambered heart, have been widely studied due to their external and transparent development, genetic amenability and extensive regenerative capabilities. The first definitive description of complete cardiac regeneration was shown in zebrafish, in a seminal study by Poss and colleagues in 2002. They described complete regeneration of the cardiac

muscle, without residual scar, following resection of ~20% of the apex, 60 days after injury (Poss et al., 2002). Since then, alternative methods of injury, including cryoinjury and genetic ablation of cardiomyocytes have been described (Gonzalez-Rosa and Mercader, 2012; Wang et al., 2011). Whilst these different methods vary in the degree of inflammation and transient scarring, and the time-course of regeneration, they all result in the reactivation of developmental pathways, with the majority of new muscle coming from the proliferation of pre-existing cardiomyocytes, which undergo de-differentiation and re-enter the cell cycle (Gonzalez-Rosa et al., 2012; Jopling et al., 2010; Kikuchi et al., 2010, 2011; Poss et al., 2002).

1.4.2 The neonatal mouse

Whilst the adult mammalian heart has limited regenerative capacity, the neonatal mouse is capable of mounting a substantial response after injury. Pioneering work by Porrello and colleagues demonstrated complete cardiac regeneration, in one day old mice (postnatal day 1), following either apical resection or ligation of the LAD (Porrello et al., 2011, 2013). Like the adult zebrafish, genetic fate mapping indicated the majority of new cardiomyocytes came from the proliferation of pre-existing ones (Porrello et al., 2011), however, the molecular mechanisms which govern this process remain largely unknown. This regenerative capacity, however, is restricted to the first week of life, as postnatal day (P)7 mice exhibit a similar fibrotic response to that seen in the adult mouse, following injury (Porrello et al., 2011). Therefore, in recent years, a significant focus of scientific research has been to understand the molecular and physiological changes that occur within this first week of life, the so called

‘regenerative window’, with the aim to extend it and eventually invoke regeneration in the adult mammalian heart.

1.4.3 The neonatal human

It is currently unknown whether humans possess the same regenerative capacity, immediately after birth, as neonatal mice, however, several studies provide intriguing, albeit limited, evidence to suggest this may be the case. In 2015, a new-born child was reported with a severe MI, following thrombotic occlusion of the proximal LAD. Although the echocardiogram and biomarkers suggested there had been significant damage to the myocardium, functional recovery was observed within weeks of the initial injury and normal heart function was observed at 1 year of age (Haubner et al., 2016). Another earlier study reported a similar observation following MI in a new-born infant (Saker et al., 1997). In addition, children with the rare congenital heart disease, anomalous left coronary artery from the pulmonary artery, showed little or no residual scarring following corrective cardiac surgery (Fratz et al., 2011). Taken together, this anecdotal evidence suggests humans, like mice, are capable of cardiac regeneration in early life, therefore, the mechanisms that enable this process in mice, will likely be applicable to humans.

Although much is still to be elucidated on the molecular mechanisms that underpin cardiac regeneration in these model organisms, a common modality seen across all, is the reactivation of developmental gene programmes and signalling pathways. Therefore, understanding the intrinsic mechanisms that govern these processes in development, may provide insight for invoking regeneration in the adult human mammalian heart.

1.5 The epicardium in regeneration

1.5.1 The epicardium in zebrafish regeneration

In zebrafish, along with its role in development, the epicardium has been reported to contribute to cardiac homeostasis throughout life, stimulating cardiomyocyte proliferation and ventricular growth, through FGF signalling (Wills et al., 2008). Moreover, the zebrafish epicardium is activated in response to injury, characterised by re-expression of developmental genes, such as *Raldh2* and *Tbx18,* and rapid expansion (Lepilina et al., 2006). A sub-set of activated cells undergo EMT and invade the underlying myocardium, contributing to coronary vasculature and sending paracrine signals to the myocardium to stimulate proliferation (Kikuchi et al., 2011; Lepilina et al., 2006). Moreover, genetic depletion of the epicardium inhibits cardiomyocyte proliferation and delays muscle regeneration (Wang et al., 2015), demonstrating it's essential role in the regenerative response.

1.5.2 Re-activation of the mammalian epicardium.

In mammals, shortly after birth, canonical epicardial genes are downregulated and the adult epicardium is said to be 'quiescent' (Chen et al., 2002). Following myocardial infarction, the adult epicardium is partially re-activated, characterised by re-expression of developmental gene programmes (Smart et al., 2011; van Wijk et al., 2012; Zhou et al., 2011). However, these activated epicardial cells have been shown to be a highly heterogenous population with a distinct molecular phenotype from their embryonic counterparts (Bollini et al., 2014). The relative contribution of these activated epicardial cells to different

cardiac lineages is widely debated, with Van Wijk and colleagues reporting contribution to cardiomyocytes, fibroblasts and coronary endothelial cells (van Wijk et al., 2012). Whilst Zhou and colleagues reported no contribution to cardiomyocytes or endothelial cells, only fibroblast and smooth muscle cell contributions, along with the secretion of paracrine factors to stimulate angiogenesis (Zhou et al., 2011).

1.5.3 Augmenting the epicardial response to injury

Whilst the ability of activated epicardial cells to differentiate into various cardiac lineages, following injury, is still widely debated, it is clear that the contribution is not sufficient to elicit an adequate regenerative response. However, given the essential role of the epicardium in coronary vessel formation and cardiomyocyte proliferation in development, augmenting epicardial activation post-MI remains a tractable approach for improving the response to injury. To that end, Zhou and colleagues demonstrated that injecting EPDC conditioned media, post-MI, decreased infarct size and improved cardiac function. Further, previous work in our lab demonstrated that 'priming' the adult epicardium with the actin monomer binding protein thymosin beta-4 (Tβ4), resulted in increased mobilisation of epicardial cells, following myocardial infarction, which contributed to neovascularisation and *de novo* cardiomyocytes (Smart et al., 2007, 2011). However, when Tβ4 was administered post-MI, as it would need to be in the clinic, EPDC fate was not effected nor did it improve the regenerative response (Zhou et al., 2012), presenting a caveat for Tβ4 as a treatment following MI.

Gaining a better understanding of the molecular signals that control epicardial gene programmes in development, and what in turn leads to quiescence of the epicardium, alongside insights into how to redeploy developmental signals and re-program adult epicardial cells, could provide the basis for therapeutic strategies to augment the epicardial response post-MI.

1.6 Hypoxia

The ability to maintain oxygen homeostasis is essential for the survival of all vertebrate species. Hypoxia, the term used to describe low or inadequate oxygen supply, is a feature of many human diseases, including myocardial infarction, but also occurs naturally in development, as the *in utero* O_2 concentration is between 1-5%, whilst atmospheric O_2 is around 20%.

There are a number of oxygen-sensing pathways that regulate cellular tolerance to hypoxia. Inhibition of the mammalian target of rapamycin (mTOR) pathway or induction of the unfolded protein response (UPR), inhibit translation, whilst the hypoxia inducible factor (HIF) family of transcription factors activate transcription (Maxwell et al., 1993; Wouters and Koritzinsky, 2008).

1.6.1 HIF signalling

HIF is a heterodimeric transcription factor, made up of two subunits: HIFα and HIF1β (Maxwell et al., 1993; Semenza and Wang, 1992). In mammals, HIF1β is constitutively expressed, whereas expression of HIFα is regulated by the concentration of O_2 (Wang et al., 1995). Under normal conditions (normoxia),

usually defined as between 10-20% O_2, 2-oxoglutarate (2OG)-dependent Prolyl hydroxylase domain proteins (PHD1-3) hydroxylate the oxygen dependant degradation (ODD) domain of HIFα, tagging it for ubiquitin-mediated proteasomal degradation. Additionally, the factor inhibiting HIF (FIH) hydroxylates the transactivation domain (TAD) of HIFα, blocking coactivator binding. In hypoxic conditions, typically defined as less than 5% O_2, PHD1-3 and FIH are no longer able to hydroxylate HIFα, in the absence of oxygen as a substrate. Consequently, HIFα accumulates in the cell, forms a heterodimer with HIF1β and translocates to the nucleus to regulate expression of its target genes (Figure 1.6.1) (Bruick and McKnight, 2001; Epstein et al., 2001; Jaakkola et al., 2001; Mahon et al., 2001; Wang et al., 1995).

HIF activates genes involved in anaerobic glycolysis; therefore, decreasing the cellular requirement for O_2, and activates genes involved in angiogenesis and erythropoiesis, acting to increase the supply of O_2 to the cell (Forsythe et al., 1996; Semenza and Wang, 1992).

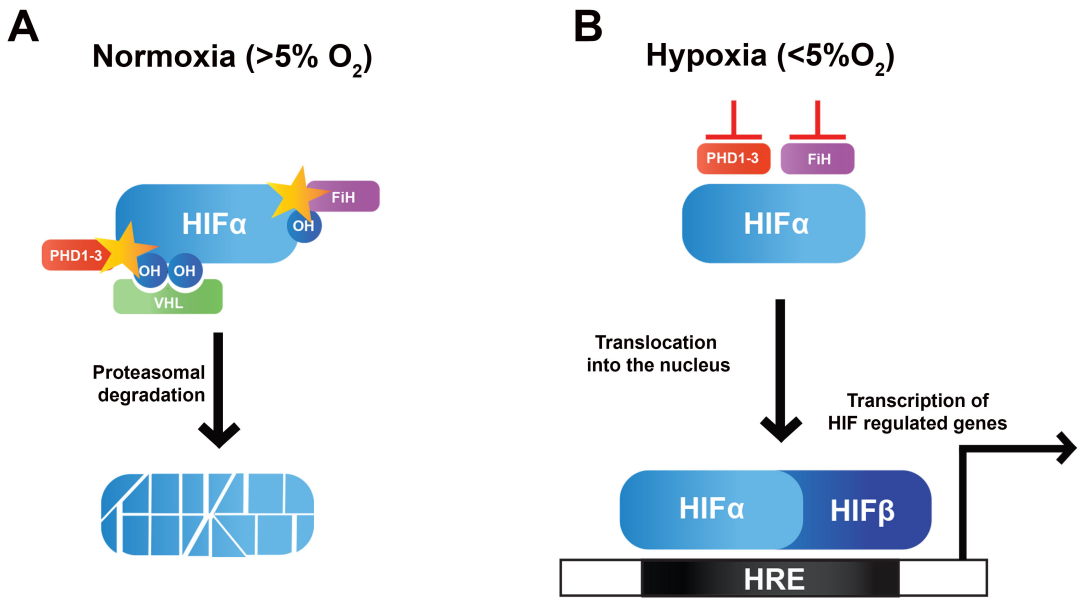


Figure 1.6.1 The HIF pathway

A. Under normoxic conditions 2-oxoglutarate (2OG)-dependant Prolyl hydroxylase domain proteins (PHD1-3) hydroxylate 2 proline residues in the oxygen dependant degradation (ODD) domain of Hif1α, this allows the Von Hippel Lindau (VHL) factor to bind, tagging it for proteasomal degradation. Additionally, the factor inhibiting HIF (FIH) hydroxylates an asparagine residue in the transactivation domain (TAD) of HIFα, blocking transcriptional co-activator binding. **B**. Under hypoxic conditions PHD1-3 and FIH are no longer able to hydroxylate HIFα so it accumulates in the cell, forms a heterodimer with HIF1β and translocates to the nucleus binding to hypoxia response elements (HREs) to regulate expression of its target genes.

There are 3 *Hifα* genes: *Hif-1α; Hif-2α* and *Hif-3α*. HIF1α dimerises with HIF1β to form the HIF1 transcription factor (Wang et al., 1995). Similarly, HIF2α, also known as Endothelial PAS protein 1 (EPAS1), dimerises with HIF1β to produce the HIF2 transcription factor (Wiesener et al., 1998). Both HIF1 and HIF2 activate transcription, but it is thought that HIF3α negatively regulates transcription of HIF target genes due to the lack of a TAD, however, less is known about this third isoform (Hara et al., 2001; Yamashita et al., 2008). Whilst *Hif1α* is ubiquitously expressed, the expression of *Hif2α* and *Hif3α* is

restricted to certain cell types. *Hif2α* is predominantly expressed in vascular endothelial cells and lung epithelia during development (Ema et al., 1997; Flamme et al., 1997; Rosenberger et al., 2002; Tian et al., 1997; Wiesener et al., 1998). HIF1α and HIF2α are similar in structure, with strong homology in the DNA and HIF1β binding domains, they do however differ in their transactivation domains suggesting they have unique target genes and require distinct transcriptional cofactors (Wiesener et al., 1998). In support of this, *Oct4*, which encodes a transcription factor vital for regulating stem cell self-renewal, is a direct target of HIF2α, but not HIF1α (Covello et al., 2006), whilst HIF1α, but not HIF2α, is responsible for regulating the transcription of genes encoding enzymes involved in glycolytic metabolism (Hu et al., 2003b). Furthermore, co-activators, which specifically bind HIF2α have been identified, for example ETS1 which interacts with HIF2α to regulate the transcription of VEGF receptor 2 (VEGFR2) (Elvert et al., 2003).

1.6.2 HIF signalling in heart development

Mammalian development occurs in hypoxic conditions, implicating HIF mediated transcription in many aspects of development, including cardiac morphogenesis. Hypoxia and HIF activation are widespread in the heart at E9.5, but become restricted to the OFT, IVS and AV cushions, following formation of the coronary vasculature at E14.5 (Dunwoodie, 2009). Interestingly, *Hif1α* is predominantly expressed in the myocardium, whilst *Hif2α* is primarily expressed in endothelial cells (Jain et al., 1998), and inactivation of these individual isoforms results in differential effects on cardiac development, suggestive of distinct functions in cardiac morphogenesis. Embryos that lack

Hif1α display myocardial hypoplasia, have reduced or absent myocardial trabeculation and a severely reduced endocardium, resulting in embryonic lethality by E10.5 (Compernolle et al., 2003; Krishnan et al., 2008; Ryan et al., 1998). Conversely, embryos which lack *Hif2α,* display variable outcomes, including extensive vascular defects, but do not exhibit major cardiac structural abnormalities (Peng et al., 2000; Tian et al., 1998).

Whilst HIF activation is required for cardiac development, abnormal upregulation of HIF, via disruption of the major oxygen sensor PHD2, also resulted in cardiac abnormalities, such as septal defects, poorly formed trabeculae and a thin myocardial wall (Takeda et al., 2006), thus highlighting the importance of the tight control of this pathway for normal cardiac development.

Whilst these loss- and gain-of-function genetic studies demonstrate an essential role for HIF signalling in cardiac development, it remains unclear how HIF can drive specific morphogenetic processes. One study found HIF1α directly regulates expression of cardiac genes *Mef2c, Tbx5* and *Ttn* (Krishnan et al., 2008) and HIF1α has also been implicated in the maintenance of cardiomyocyte proliferation during development, by increasing the glycolytic potential of cardiomyocytes and indirectly inhibiting p53 (Guimarães-Camboa et al., 2015).

1.6.3 HIF signalling in cardiac regeneration

1.6.3.1 Neonatal mice

Whilst the mammalian foetal heart is fairly hypoxemic, due to significant mixing of arterial and venous blood (Dawes, 1955), after birth transition to a postnatal circulation dramatically changes the oxygenation state of cardiomyocytes. They switch from anaerobic glycolytic metabolism to oxygen-dependant mitochondrial oxidative phosphorylation (Fisher et al., 1980; Lopaschuk et al., 1991; Wisneski et al., 1985). It was reported, this metabolic switch results in permanent cardiomyocyte cell cycle arrest via activation of the DNA damage response pathway, mediated by a build-up of reactive oxygen species (ROS) (Puente et al., 2014). Significantly, postnatal hypoxemia, ROS scavenging or inhibition of the DNA damage response pathway all prolonged the proliferative capacity of cardiomyocytes, resulting in an improved regenerative response beyond the first week of life (Puente et al., 2014). This suggests changes in the oxygen environment after birth results in permanent cardiomyocyte cell cycle arrest, thus contributing to the loss of regenerative capacity.

1.6.3.2 Zebrafish

Unlike in mammals, the zebrafish heart remains relatively hypoxemic throughout life, due to its more primitive 2-chambers, and the hypoxic aquatic environment in which zebrafish reside. Correspondingly, hypoxia and HIF signalling promote cardiac regeneration in the zebrafish, by inducing cardiomyocyte dedifferentiation and proliferation (Jopling et al., 2012).

1.6.3.3 Adult mice

Due to the role of hypoxia and HIF signalling on cardiomyocyte proliferation in the regenerative neonatal mouse and zebrafish, Nakada and colleagues subjected adult mice to severe hypoxia following myocardial infarction. This induced a regenerative response, including a significant increase in cardiomyocyte proliferation, resulting in a decrease in fibrotic scarring and an improvement in cardiac function (Nakada et al., 2017).

1.6.4 HIF signalling in the epicardium

It has not yet been established whether HIF is required for the formation of the epicardium or the subsequent coronary vasculature in the mouse as loss of *Hif1α* causes embryonic lethality at E10 (Iyer et al., 1998). However, since HIF activity is required for systemic vasculature development, it is likely to be involved in the formation of the coronary vasculature (Ryan, Lo, and Johnson 1998). Furthermore, expression of the transcription factor WT1, the master regulator of the embryonic epicardium, can be upregulated via HIF1α binding to a HRE in the promoter region of *Wt1* (Duim et al., 2015; Wagner et al., 2002). Therefore, hypoxia may regulate epicardial activation during development by activating transcription of key epicardial genes such as *Wt1*. Moreover, it was shown that overexpression of stable HIF1α in the avian epicardium impaired EPDC migration and invasion into the myocardium *in ovo* through inhibition of the VEGF pathway (Tao et al., 2013). More recently the same group demonstrated hypoxia induces immortalised epicardial cells to differentiate into VSMCs *in vitro* (Tao et al., 2018). Kocabas and colleagues also established a role for HIF1α in the adult epicardium, identifying the adult mouse ventricular

epicardium/sub-epicardium as a hypoxic niche, in which self-renewing, glycolytic, cardiac progenitors reside (Kocabas et al., 2012). A role for hypoxia and HIF signalling in murine epicardial development and EMT, and whether this can be exploited in the injured heart to promote optimal tissue repair and regeneration, remains to be elucidated.

1.7 Hypothesis

Hypoxia and HIF-mediated signalling play a role in epicardial activation during mouse heart development, and transition to a postnatal circulation, not only leads to cardiomyocyte cell cycle arrest, but also to quiescence of the epicardium. Therefore, mimicking the hypoxic environment after birth, via activation of HIF signalling, may act to extend the window of cardiac regeneration.

1.8 Aims of thesis

The primary aims of this thesis were to investigate a role for HIF signalling in the epicardium in development and in neonatal cardiac regeneration.

To test the above hypothesis, the following experimental aims were established:

1. Characterise levels of hypoxia and HIF in the epicardium during murine heart development.

2. Investigate a functional requirement for HIF in epicardial development.

3. Explore a role for HIF signalling in epicardial EMT.

4. Characterise the potential of the epicardium in neonatal mouse cardiac regeneration.

5. Determine the effect of activation of HIF signalling on the epicardial response to injury in the neonate.

2 Materials and Methods

2.1 Mice

2.1.1 Mouse strains

All mice were housed in the biomedical services building (BSB), within the University of Oxford. All mice were on a pure C57BL/6 background and were either wild type or one of the genetically modified lines outlined in Table 2.1.1. All animal experiments were carried out in accordance with the UK Animals (Scientific Procedures) Act 1986 under project licences PPL 30/2987, PPL 30/3155 and PPL PDDE89C84.

Table 2.1.1 Genetic mouse strains

Name	Promoter	Genetic background	Construct	References
Hif1α$^{fl/fl}$; Wt1$^{CreERT2/+}$	*Wt1*	C57BL/6	LoxP-Hif1α(exon2)-LoxP & Cre-ERT2 recombinase	(Higgins et al., 2004; Zhou et al., 2008)
Hif2α$^{fl/fl}$; Wt1$^{CreERT2/+}$	*Wt1*	C57BL/6	LoxP-Hif2α(exon2)-LoxP & Cre-ERT2 recombinase	(Gruber et al., 2007; Zhou et al., 2008)
Hif1α$^{fl/fl}$;Rosa26$^{+/CreERT2}$	*Rosa26*	C57BL/6	LoxP-Hif1α(exon2)-LoxP & Cre-ERT2 recombinase	(Higgins et al., 2004; Vooijs et al., 2001)
Hif2α$^{fl/fl}$;Rosa26$^{+/CreERT2}$	*Rosa26*	C57BL/6	LoxP-Hif2α(exon2)-LoxP & Cre-ERT2 recombinase	(Gruber et al., 2007; Vooijs et al., 2001)
Phd2$^{fl/fl}$;Rosa26$^{+/CreERT2}$	*Rosa26*	C57BL/6	LoxP-Phd2(exon2)-LoxP & Cre-ERT2 recombinase	(Mazzone et al., 2009; Vooijs et al., 2001)

2.1.2 Timed matings

For developmental experiments, 8-12 week old mice were set-up overnight and females checked for the presence of a vaginal plug the following morning. The date of a vaginal plug was designated as embryonic day (E)0.5.

2.1.3 Hypoxyprobe-1 administration

Solid pimonidazole-HCl (Hypoxyprobe-1 Inc) was dissolved in sterile saline to give a final concentration of 15mg/ml. Pregnant dams were injected with 100µl of solution via intraperitoneal (IP) injection. Mice were then sacrificed 2 hours later, and tissue was collected as outlined in section 2.1.5 below.

2.1.4 Tamoxifen induced activation of Cre recombinase

Tamoxifen was initially dissolved in 100% ethanol (EtOH) to give a concentration of 200mg/ml, and then diluted in peanut oil (Sigma) to give a final concentration of 20mg/ml.

2.1.4.1 Activation of Cre recombinase in embryos

For embryonic studies, pregnant dams were injected with 2 doses of 1mg per kg of body weight, at embryonic stages (E)9.5 and E11.5 to maximise *Cre-ERT2* activity in the developing epicardium, via IP injection.

2.1.4.2 Activation of Cre recombinase in neonates

For neonate studies, pups were injected with a single 10µl dose of 20mg/ml tamoxifen, at postnatal day (P)2, via IP injection, using a 25-gauge needle (Pitulescu et al., 2010). Following injection, pups were cleaned, covered in faeces from the breeding cage, and then briefly warmed by an infra-red heat lamp to reduce maternal cannibalism.

2.1.5 Embryonic dissection

Embryos were harvested from pregnant dams at the required embryonic stages. The dam was euthanised by cervical dislocation and the uterus was removed and placed in ice-cold PBS to anesthetise the embryos. Embryos were isolated from the uterus using fine forceps, under a microscope, and subsequently the hearts were removed. The hearts were briefly washed in PBS and then fixed in 2% formaldehyde overnight (O/N) at 4°C. Tail tips were collected for DNA isolation (see section 2.4.1 below).

2.1.6 Neonatal and adult dissection

Mice were euthanised by Schedule 1 using a method appropriate for their age: cervical dislocation for adult mice and hindbrain destruction for neonates. Ear biopsies were collected for DNA isolation. Hearts were then removed and washed in ice-cold PBS. For staining protocols hearts were fixed in 2% formaldehyde O/N at 4°C. For RNA extraction hearts were snap-frozen in liquid nitrogen and stored at -80°C.

2.2 Myocardial infarction

2.2.1 Neonatal surgery model

Left anterior descending (LAD) coronary artery ligation in the neonatal mouse has previously been described (Mahmoud et al., 2014; Porrello et al., 2013), and has been adapted by the Riley group to comply with UK regulation (Masters, 2015). Before the litter was born, the stud male was removed from the cage, to reduce the risk of cannibalism. At either postnatal day (P)1 or P7, the entire litter was removed from the dam and placed in a 31ºC incubator. Before surgery, general anaesthesia was induced with 4% isoflurane inhalation for 1-2 minutes. The pup was then immersed in ice for 2-4 minutes to induce apnoea and asystole to prevent excessive blood loss during surgery.

The pup was taped onto an ice block in the supine position and a sterile field was made using sterile drapes. Surgical scissors were used to a make a small transverse incision in the skin, which was subsequently widened by blunt dissection of the skin from the underlying muscles (Figure 2.2.1A). A lateral thoracotomy was achieved by puncturing the fourth intercostal space using sharp forceps and widened using blunt forceps (Figure 2.2.1B). A light pressure was then applied to the abdomen and the right thorax to expose the heart (Figure 2.2.1C). A taper-point 7-0 prolene suture was passed through the anterior wall of the left ventricle and tied off to occlude blood flow through the LAD and induce an infarction (Figure 2.2.1D). The blunt forceps were then removed to allow the heart to return to its position inside the thoracic cavity. The ribs were first sutured closed, followed by the skin, both with a 7-0 prolene suture (Figure 2.2.1E). The pup was then gently warmed under an infrared heat

lamp to return circulation and breathing (Figure 2.2.1F). Littermates were used to aid the recovery as physical stimulation is critical to the process. Once normal breathing had returned, the pup was placed back in the incubator. Once surgery had been completed on the whole litter, pups were covered in faeces from the breeding cage, in order to reduce the risk of maternal cannibalism, and returned to the dam.

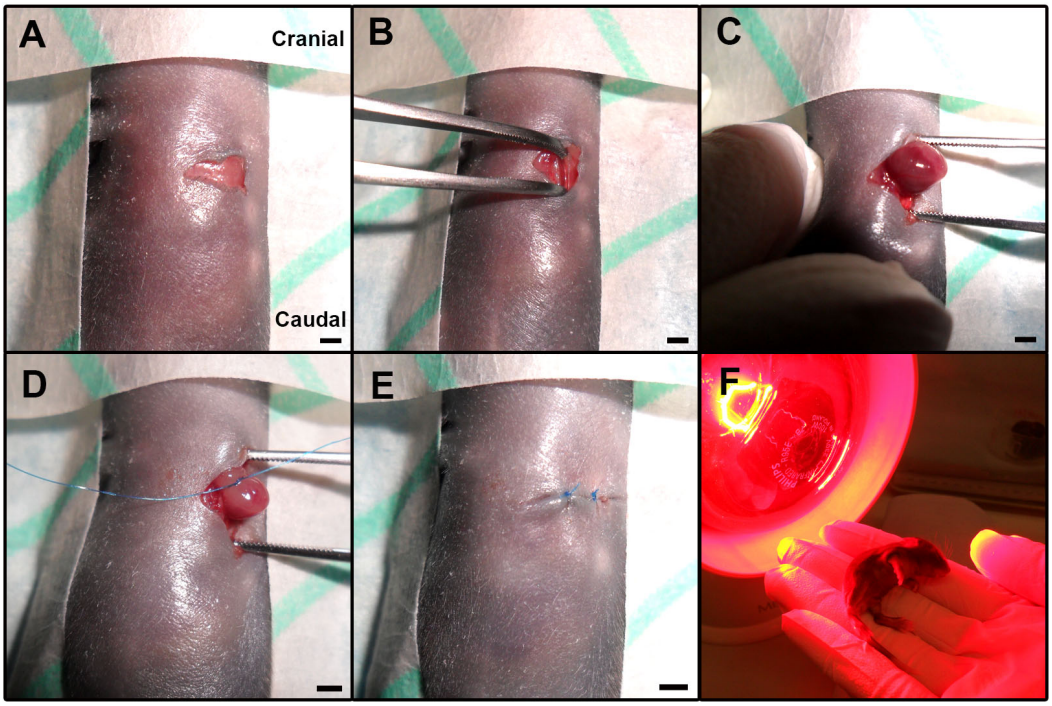


Figure 2.2.1 Neonatal LAD ligation surgery

A. Following induction of cardiorespiratory arrest, the mouse is placed in the supine position, an incision in the skin is made, and the muscles are removed. **B**. A lateral thoracotomy is performed. **C**. The heart is manipulated out of the thoracic cavity. **D**. A suture is then tied through the anterior left ventricular wall, to ligate the LAD. **E**. The ribs are then sutured closed, followed by the skin. **F**. The mouse is rapidly warmed by an infrared lamp to return circulation and breathing. Scale bars = 2mm.

2.2.2 FG-4592 administration

FG-4592 (Selleck), also known as Roxadustat, was initially dissolved in sterile dimethyl sulphoxide (DMSO) (Sigma) to a concentration of 50mg/ml and then further diluted to 1mg/ml in sterile PBS, and stored at -80°C (Hoppe et al., 2016). Following LAD ligation surgery, before recovery, pups were injected with a single 10μl dose, of 10mg/ml of FG-4592 in PBS, via IP injection, with a 31-gauge needle. Pups were then recovered as described above.

2.3 Primary Tissue Culture

2.3.1 Epicardial explant cultures

Sterile 12-well plates (Fisher Scientific), containing sterile 13-mm diameter coverslips were coated with 0.1% gelatin and allowed to stand for 20mins. The gelatin was then replaced by Dulbecco's Modified Eagle Medium (DMEM) (Sigma) containing 10% FBS (Sigma), 1% Penicillin/Streptomycin (Sigma). Hearts were isolated from E11.5 embryos and the outflow tract and atria were removed. Each ventricle was then cut in half and placed epicardial side down on the coverslip (Chen et al. 2002). Explants were placed in a 37°C/5% CO_2 incubator for 48hours. After 48 hours, the explant tissue was carefully peeled off using a sterile 10μl pipette tip, leaving only the epicardial sheet remaining on the coverslip. Plates were then returned to the incubator for a further 24 hours. After a total of 72 hours in culture, the media was removed, coverslips were washed briefly in ice-cold PBS and then fixed in 4% formaldehyde at room temperature for 15 minutes. Coverslips were subsequently washed in PBS for 2x 5 minutes, and then stored in fresh PBS at 4ºC prior to staining.

2.3.1.1 Tamoxifen treatment of explant cultures

For explants produced from embryos from the genetically modified lines outlined in Table 2.1.1, 4-hydroxytamoxifen (4-OHT) was added to the cultures to induce activation of Cre recombinase. 4-OHT (ToCris) was initially dissolved in 100% ethanol (EtOH) to give a concentration of 100mg/ml, and then diluted in peanut oil (Sigma) to give a final concentration of 10mg/ml. Either 1μM or 5μM of 4-OHT was added directly to the media in each well 24 hours after plating, to allow time for explant attachment before treatment.

2.3.1.2 Pharmacological treatment of explant cultures

Explants were prepared from wild type C57BL/6 embryos, as described in section 2.3.1 above. After 48 hours in culture the explant tissue was carefully peeled of and removed along with the media. Fresh media was then added to the explant along with one of the compounds outlined in Table 2.3.1.

Table 2.3.1 Compounds

Name	Concentration (μM)	Source	Reference
Deferoxamine (DFO)	250	Sigma	(Theriault et al., 2010)
ML-228	20	ToCris	(Theriault et al., 2010)
FG-4592 (Roxadustat)	50	Professor PJ Ratcliffe laboratory	(Besarab et al., 2015)
Bay 85-3934 (Molidustat)	50	Professor PJ Ratcliffe laboratory	(Beck et al., 2018)
IOX4	50	Professor PJ Ratcliffe laboratory	(Chan et al., 2015)

2.4 Molecular techniques

2.4.1 DNA isolation for genotyping

Tissue collected for genotyping was incubated with 500µl of tail lysis buffer (Table 2.4.3) and 0.5µl of 10mg/ml Proteinase K (Sigma) at 55°C O/N. The following day 500µl isopropanol (Sigma) was added to the digesting tissue to precipitate the DNA, spun on a rotating wheel for 30min at room temperature (RT) and then centrifuged at 17,000g for 10min. The supernatant was discarded and the pellet was washed in 1ml 70% Ethanol (Sigma). After centrifuging at 17,000g for 5min, the supernatant was discarded, and the pellet re-suspended in 150µl of 1xTE (Table 2.4.3).

2.4.2 Polymerase Chain Reaction (PCR) for genotyping

Genotyping PCR was conducted using PCR beads (GD Healthcare) in a 96 well Veriti™ thermal cycler (Applied Biosystems). For each reaction 0.05pmol/µl of forward and reverse primers was added to 2.5µl of DNA; RNase-free water was added to give a total volume of 25µl. Details of the PCR programme and primers are given in Table 2.4.1 and Table 2.4.2.

Table 2.4.1 PCR primers for genotyping

Allele	Primer (5'-3' orientation)	PCR programme
Wt1^{CreER}	F: AGGAGCGGAGAACCGTC R: TCTTGCGAACCTCATCACTC	Taqgenom2
Cre	Fwd: GTTCGCAAGAACCTGATGGACA Rev: CTAGAGCCTGTTTTGCACGTTC	Taqgenom2
Phd2	F: TTGCAGTGTGCAACAGTCAG R (wild type allele): CACGGGGAACTCTGATTCAT R (floxed allele): CCAAAATCACCAATCTAGAATAACTTC	PHD2
Phd2 recombination	F: TGGGAGGGGATTTGTAGTTG R: TGTACCTCAACCTCCGCTCT	HIF
Hif1α	F (recombined allele): TTGGGGATGAAAACATCTGC F (non-recombined allele): GCAGTTAAGAGCACTAGTTG R: GGAGCTATCTCTCTAGACC	HIF
Hif2α	F: CAGGCAGTATGCCTGGCTAATTCCAGTT R: CTTCTTCCATCATCTGGGATCTGGGACT	HIF

Table 2.4.2 PCR programmes for genotyping

Taqgenom2

Stage	Temperature (ºC)	Time (min)	Cycles
1	94	2.00	1
2	94	0.50	35
	60	0.50	
	72	0.75	
3	72	5.00	1
4	4	∞	1

HIF

Stage	Temperature (ºC)	Time (min)	Cycles
1	95	2.00	1
2	95	0.50	40
	56	0.75	
	72	0.75	
3	72	10.00	1
4	4	∞	1

Phd2

Stage	Temperature (ºC)	Time (min)	Cycles
1	95	3.00	1
2	95	0.50	35
	60	0.75	
	72	0.75	
3	72	10.00	1
4	4	∞	1

2.4.3 Gel electrophoresis

DNA samples were separated by gel electrophoresis. A 1.5% agarose gel was prepared by adding 1.5g agarose (Sigma) to 100ml of 1x TBE buffer (Table 2.4.3), before heating in a microwave to fully dissolve. 5µl of GelRed (Cambridge Biosciences) was added to the gel, to allow UV visualisation of DNA, before pouring the gel into a mould to set. Samples were mixed with Orange DNA loading dye (Life Technologies) prior to loading, gels were then run at 120V for 45 minutes. PCR products were visualised on the gel using a UV lightbox.

Table 2.4.3 Solutions

Solution	Components
Tail lysis buffer	100mM Tris pH 8.5, 5mM EDTA, 0.2% SDS, 200mM NaCl
Tris-EDTA (TE) buffer	10mM Tris pH 8.0, 1mM EDTA
Tris-borate-EDTA (TBE) buffer	40mM Tris pH 8.0, 20mM Boric acid, 1mM EDTA

2.4.4 RNA extraction

Frozen hearts were homogenised in Trizol (750µl per 50-100mg of tissue; Invitrogen) using a teflon homogeniser followed by aspiration with a sterile 25G needle and syringe (BD sciences). Homogenised samples were incubated at RT for 5 minutes and then chloroform was added (200µl per 750µl trizol). After 15 seconds of vigorous shaking, samples were incubated at RT for 15 minutes, followed by centrifugation at 11,600 g for 15 minutes and 4°C. The aqueous phase was then moved to a new 1.7ml Eppendorf and the RNA was precipitated from the aqueous solution by incubation with isopropanol O/N at -

20°C. The following day, samples were centrifuged at 11,600 g for 10 minutes at 4°C and the supernatant was discarded. To wash the pellet 70% ethanol was added, vortexed and then centrifuged at 7,800 g for 5 minutes at 4°C. After discarding the supernatant, the pellet was allowed to air-dry for 5 minutes before being resuspended in 30µl DEPC-H_2O. RNA quantity and quality was measured using a Nanodrop2000 (ThermoScientific, UK)

2.4.5 cDNA synthesis

Complementary (c)DNA was synthesised via reverse transcription using the messenger (m)RNA as a template. Reactions were prepared in 200µl reaction tubes. To each tube 1µg of RNA, 0.5µl of 20µg/ml random primers (Promega) and 1µl of 10mM deoxynucleotide triphosphates (dNTPs) (GE Healthcare) was added, diethyl pyrocarbonate (DEPC)- H_2O was then added to bring the total volume up to 10µl. Reaction tubes were then placed in a 96 well Veriti^{TM} thermal cycler (Applied Biosystems) and incubated for 5 minutes at 65°C, followed by 5 minutes at 4°C. The following was then added to each reaction tube: 4µl 5x First Strand buffer; 2µl 25mM $MgCl_2$ (Thermo Scientific); 2µl 0.1 Dithiothreitol (DTT) (Life Technologies) and 1µl RNAsin (Promega). After incubation for 2 minutes at 25°C, 1µl of Superscript Reverse Transcriptase III (Life Technologies) was added to each sample. Samples were then incubated for 10 minutes at 25°C; followed by 50 minutes at 42°C and then 15 minutes at 70°C. The resulting cDNA was diluted in DEPC-H_2O to give a final concentration of 2ng/µl.

2.4.6 Real-time quantitative PCR (RT-qPCR)

Primers used (see Table 2.4.4) were predesigned from NIH mouse primer depot (http://mouseprimerdepot.nci.nih.gov/). Reactions were prepared in 0.1ml Fast 96-well plates (Invitrogen). To each reaction tube the following was added: 0.5µl of each 10µM primer; 12.5µl SYBR Green (Invitrogen), 6.5 µl H_2O and 2µl of 2ng/µl cDNA. All samples were run in triplicate. Reactions were performed on a ViiA™ 7 Real-Time PCR System using the following thermal cycles: 95°C for 15 minutes and then 40 cycles of 95°C for 15 seconds and 60°C for 1 minute. A melt-curve was used to detect non-specific primers. Cycle Threshold (Ct) values were determined using the ViiA 7 software. For each set of samples, a panel of 11 housekeeping genes were first tested. The most stable reference genes were then determined using formulas extracted from qBase software (Hellemans et al., 2007). Briefly, the stability of each housekeeping gene was determined by calculating the pairwise variation with all other housekeeping genes, those with the lowest average pairwise variation were defined as the most stable. The $2^{-\Delta\Delta Ct}$ value of the gene of interest was then calculated, and normalised to the average of the $2^{-\Delta\Delta Ct}$ values for the two most stable reference genes (Livak and Schmittgen, 2001). The resulting value is referred to as 'fold change' throughout the remainder of this thesis.

Table 2.4.4 PCR primers for RT-qPCR

	Gene	Forward Primer	Reverse Primer
Housekeeping panel	Atp5f1b	GGTTCATCCTGCCAGAGACTA	AATCCCTCATCGAACTGGACG
	Sdha	GGAACACTCCAAAAACAGACCT	CCACCACTGGGTATTGAGTAGAA
	18s	CATTCGAACGTCTGCCCTAT	GTTTCTCAGGCTCCCTCTCC
	B2m	TTCTGGTGCTTGTCTCACTGA	CAGTATGTTCGGCTTCCCATTC
	Cyc1	CAGCTTCCATTGCGGACAC	GGCACTCACGGCAGAATGAA
	Ubc	GCCCAGTGTTACCACCAAGA	CCCCATCACACCCAAGAACA
	Ywhaz	GAAAAGTTCTTGATCCCCAATGC	TGTGACTGGTCCACAATTCCTT
	Canx	ATGGAAGGGAAGTGGTTACTGT	GCTTTGTAGGTGACCTTTGGAG
	Eif4a2	ACACCATCGGGGTCCATTCC	ACCTTTCCTCCCAAATCGAC
	Rpl13a	GTTCGGCTGAAGCCTACCAG	TTCCGTAACCTCAAGATCTGCT
Genes of interest	Wt1	TTCAAGGACTGCGAGAGAAG	GGGAAAACTTTCGCTGACAA
	Tbx18	ACGAAATAGGCACCGAGATG	TTGTCCACCGGCACAATATC
	Tcf21	CGACAAGTACGAGAACGGTTAC	TGTAGTTCCACACAAGCGGTT
	Raldh2	TGCCACCCGCGACAA	TTGTTGTGAGGCAAGAGTGG
	Phd2	TTGTTACCCAGGCAACGGAAC	CCTTGGCGTCCCAGTCTTT
	Glut1	CTCTGTCGGCCTCTTTGTTAAT	CCAGTTTGGAGAAGCCCATAAG

2.5 Histological and Immunostaining

2.5.1 Wax embedding for histology

Following O/N fixation in 2% formaldehyde at 4°C, hearts were washed 3x in PBS. Hearts were then dehydrated by passage through rising concentrations of ethanol: 50%, 70%, 80%, 90%, 100% and 100%, at RT, for 2 hours each. Samples were then washed in Butanol O/N, at RT, before being placed in molten 50:50 butanol: Histoplast paraffin wax (Fisher) at 56°C. After 1 hour the solution was replaced with 100% Histoplast paraffin wax. After several changes of 100% wax, to remove residual butanol, hearts were oriented and embedded into a mould pre-loaded with paraffin. The wax was then rapidly cooled on a bed of ice and stored at 4°C. A microtome was used to cut 10μm-thick sections through the heart, which were transferred onto Superfrost plus slides (VWR).

For all staining procedures, sections were first deparaffinised in Histoclear solution (Fisher) for 2x 5min, followed by rehydration through a decreasing concentration of ethanol: 100%, 90%, 80%, 70% and 50%, for 5min each.

2.5.2 Haematoxylin and Eosin staining

Haematoxylin and Eosin (H&E) staining was used to assess left ventricular dilation and cardiac remodelling post-MI. Post rehydration, slides were washed in PBS, before immersion in Haematoxylin (Sigma) for 5 minutes. Slides were then washed under a running tap, until the distilled water ran clear. Slides were subsequently immersed in Eosin (Sigma) for 1 minute and then rinsed again in distilled water. Sections were then dehydrated, through a rising ethanol concentration (reverse of above), prior to coverslip mounting using DPX mounting media (Sigma). Sections were imaged using a Zeiss Stereomicroscope.

2.5.3 Masson's Trichrome Staining

Staining was performed using a Masson's Trichrome kit (Sigma) as per the manufacturer's instructions. This stained muscle fibres in red, and collagen in blue, allowing the assessment of collagen deposition and cardiac fibrosis. Following rehydration, slides were immersed in Bouin's solution, for 15 minutes at 56°C. Sections were then stained by serial immersion in the following solutions: Weigert's Iron Haemotoxylin solution (5 minutes); Biebrich Scralet-acid Fuchsin (5 minutes); Aniline Blue (5 minutes); Phosphotungstic/ Phosphomolybdic acid solution (5 minutes) and finally 1% Acetic acid solution (2 minutes). Samples were then rinsed in distilled water and dehydrated

through a rising concentration of ethanol (reverse of above). Finally, sections were cleared in Xylene and mounted using DPX mounting media. Sections were imaged using a Zeiss Stereomicroscope.

2.5.4 Immunostaining of cryosections

For immunostaining, embryonic, neonatal and adult hearts, were initially fixed O/N in 2% formaldehyde at 4°C. After briefly washing in PBS, hearts were equilibrated in 30% sucrose in PBS (pH 7.4) O/N at 4°C. The following day, hearts were placed in 50:50 30% sucrose/PBS: Tissue-Tek OCT (VWR) for 30min at RT, before being washed in 100% OCT. The hearts were then embedded in 100% OCT and placed at -80°C. A Cryostat was then used to cut 10µm-thick cryosections through the heart, slides were stored at -80°C.

Before use slides were removed from -80°C and left to dry at RT for 10 minutes. Slides were washed in PBS for 5 minutes to remove the OCT. Sections were then permeabilised with 0.5% Triton X-100 in PBS (PBTr 0.5%) for 10min at RT and subsequently rinsed twice in PBS. Sections were blocked in 10% Serum (from the species in which the secondary antibody (Ab) was raised, to reduce background levels), 1% bovine serum albumin (BSA), 0.1% Triton X-100 in PBS (PBTr 0.1%) for 1hr at RT prior to incubation in the Primary Ab (Table 2.5.1), diluted in block, overnight at 4°C. The following day slides were washed 3x 5 min in PBTr 0.1%. Samples were then incubated with Alexa Fluor 2° Ab's (Table 2.5.2), and 4',6-Diamidino-2-Phenylindole, Dihydrochloride (DAPI; concentration 0.1 µg/ml), diluted in block for 1hr at RT. Slides were subsequently washed 1x 5min in PBTr 0.1% and then 2 x 5min in PBS. A small volume of mounting medium (50:50 gylcerol:PBS) was added to each section

and then a coverslip was placed on top. Slides were stored at 4°C. Fluorescent images were captured with either a Zeiss Leica microscope or an Olympus FluoView 3000 confocal microscope.

Table 2.5.1 Primary antibodies

Antibody	Supplier	Catalogue	Clone	Reactivity	Species	Dilution
WT1	Abcam	Ab89901	CAN-R9(IHC)-56-2	Epicardial cells	Rabbit	1:100
PDPN	Fitzgerald	10R-P155a	103-M40	epicardium	Hamster	1:100
EMCN	Santa Cruz	Sc-55341	V.5C7	Coronary vasculature endocardium	Rat	1:100
PECAM (CD31)	Abcam	ab119341	2H8	Coronary vasculature	Armenian Hamster	1:100
PHH3	Santa Cruz	SC-8656-R	Polyclonal	Proliferating cells	Rabbit	1:100
CD68	Bio-Rad	MCA1957	Polyclonal	Macrophages	Mouse	1:100
ACTN2	Sigma	A7811	EA-53	Cardiomyocytes	Mouse	1:500
SM-MHC	Abcam	ab125884	Polyclonal	Smooth muscle	Rabbit	1:100
SM-22α	Abcam	ab14106	Polyclonal	Smooth muscle	Rabbit	1:100
α-SMA	Sigma	C6198	1A4	Smooth muscle, mesenchymal cells	Mouse-cy3	1:100
HIF1α	Novus	NB100-105	H1alpha67	Hypoxic cells	Mouse	1:100
GLUT1	Alpha diagnostic	GT11-A	Polyclonal	Cells utilising glycolysis	Rabbit	1:100
ERα	Abcam	ab1660	SP1	cells expressing activated CreERT2	Rabbit	1:100
ZEB1	Santa Cruz	Sc-25388	Polyclonal	Cells undergoing EMT	Rabbit	1:100
SNAI1/2	Abcam	ab180714	Polyclonal	Cells undergoing EMT	Rabbit	1:100

Table 2.5.2 Secondary antibodies

Antibody	Supplier	Catalogue	Dilution
Alexafluor 647 phalloidin	Life Technologies	A222287	1:40
Alexafluor® goat anti-Hamster 488	Invitrogen	A21110	1:200
Alexafluor® goat anti-Rabbit 488	Invitrogen	A11008	1:200
Alexafluor® goat anti-Rabbit 546	Invitrogen	A11035	1:200
Alexafluor® donkey anti-Rabbit 647	Invitrogen	A31573	1:200
Alexafluor® donkey anti-mouse546	Invitrogen	A10036	1:200
Alexafluor® goat anti-Rat 546	Invitrogen	A11081	1:200
Alexafluor® goat anti-Armenian Hamster 488	Abcam	Ab173003	1:100

2.6 Image Analysis

2.6.1 Quantification of immunofluorescence of cryosections.

For quantification of immunofluorescence of cryosections, images were captured on an Olympus FluoView 3000 confocal microscope and analysed using ImageJ software. For each heart, images were captured from at least 2 sections, over 100μm apart, and from a comparable plane to other samples. For each section, at least 6 images were captured, of comparable regions. The channel(s) of interest was then over-layed onto DAPI in ImageJ, and the number of positive cells, across a defined area, were counted using the cell counter Plugin. An average, per section, was then determined.

2.6.2 Average nuclear fluorescence intensity

Images of explants were captured using a Leica epi-fluorescence microscope. Average nuclear fluorescence intensity was then measured using ImageJ software. Initially, channels were separated and the DAPI nuclear stain was used to create a mask. Briefly, a threshold was set, to highlight all DAPI stained nuclei (Figure 2.6.1A), a binary image was then created and converted to a mask (Figure 2.6.1B). The nuclear mask was then overlayed onto the channel of interest (Figure 2.6.1C). The fluorescence intensity (grey value) was then measured inside each outlined nuclei. The average intensity, across all the nuclei, for each image was then calculated. For each experiment, at least 4 images were captured and quantified per explant.

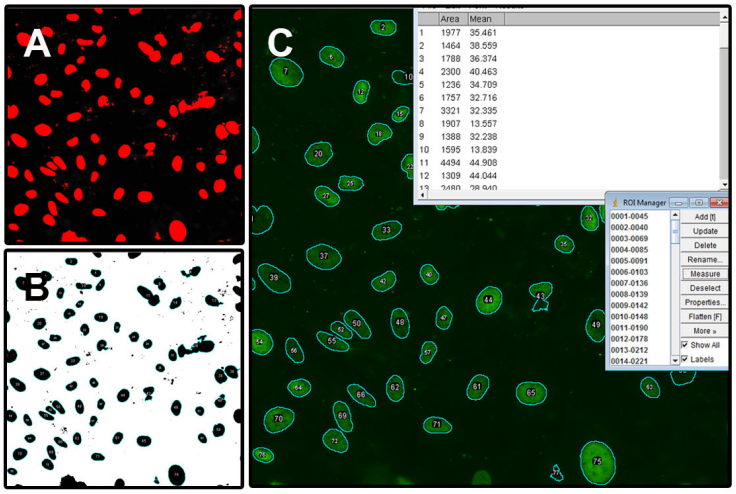


Figure 2.6.1 Average nuclear fluorescence quantification

A. A threshold was set, using the DAPI channel, to highlight all cell nuclei. **B**. This was converted to a binary image and the nuclei were outlined. **C**. The outlined nuclei were overlaid onto the channel of interest, and the fluorescence intensity within each nucleus was measured.

2.6.3 Fractal analysis

Fractal analysis, is the assessment of fractal characteristics in a set of data, and has previously been used, and validated, to determine endocardial and trabeculae complexity (Captur et al., 2014, 2015, 2016). Images were captured on an Olympus FluoView 3000 confocal microscope, and analysed in ImageJ, using the FracLac plugin. For each heart, images were captured from at least 2 sections, over 100μm apart, and from a comparable plane. For each section, at least 6 images were captured, 3 from the left ventricle, 3 from the right. The endomucin (EMCN, which labels endocardium and allows visualisation of trabeculae) channel was opened in ImageJ, a threshold was then set to highlight the positive staining, and a binary image was created (Figure 2.6.2A-C). Any EMCN staining that did not mark the trabeculae was then removed and the resulting pattern was outlined (Figure 2.6.2D). The fractal analysis box

counting method was then used to analyse the data. Briefly, the image is repeatedly segmented, into boxes of varying size, demonstrated in Figure 2.6.2E-F, and the complexity is measured. This generates the mean fractal dimension value (D_B), which can be between 1 and 2, the closer to 2, the more complex the pattern. An average D_B value for each section was then determined.

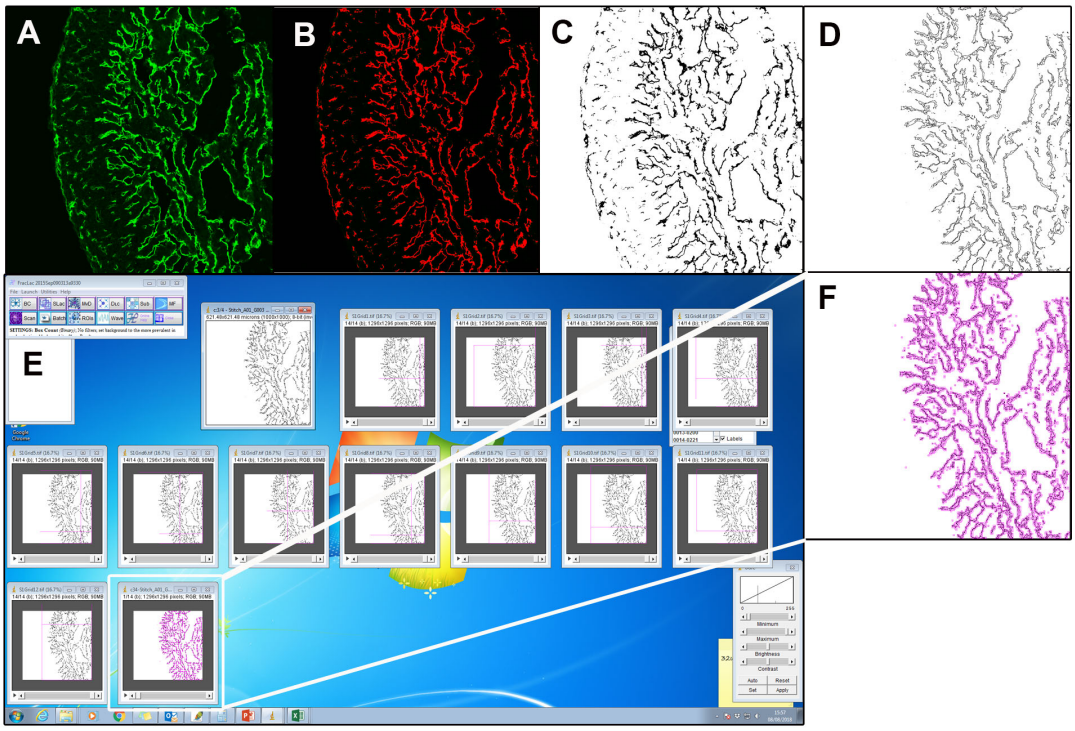


Figure 2.6.2 Fractal Analysis using FracLac

A. Representative image of EMCN (green) staining of the trabeculated myocardium used in fractal analysis. **B**. Threshold of EMCN staining. **C**. Binary image of EMCN staining. **D**. Outline of trabeculae, following removal of non-endocardial EMCN staining. **E**. Example of box sampling used by FracLac to determine the mean D_B value. **F**. High magnification of boxed region in **E**, highlighting how the image is segmented during box counting analysis.

2.7 Statistical analysis

All statistical analyses were performed in GraphPad Prism 7 software. A two-tailed, unpaired Student t-test was used for comparing two experimental groups. Comparisons between three of more experimental groups were made using a one-way ANOVA, with Tukey's multiple comparisons post-hoc test. A p-value of less than or equal to 0.05 was considered statistically significant.

3 HIF signalling in epicardial development

3.1 Background

During development a population of mesoderm-derived cells, known as the proepicardium, migrate towards the developing heart and envelope its outer surface, giving rise to the epicardium by embryonic day (E) 10.5 (Viragh and Challice, 1981). As the epicardium expands, a subpopulation of epicardial derived cells (EPDCs), undergo EMT and invade the developing myocardium, contributing to various cells types of the heart including: interstitial and perivascular fibroblasts (Gittenberger-de Groot et al., 1998), VSMCs (Mikawa and Gourdie, 1996) and to some extent coronary ECs (Cano et al., 2016). Further, EPDCs secrete essential mitogens, such as EPO, RA and FGFs, which stimulate cardiomyocyte proliferation and coronary vessel formation (Brade et al., 2011; Lavine et al., 2005, 2006; Stuckmann et al., 2003).

WT1 is a transcription factor which functions as a “master regulator” of epicardial EMT and is essential for epicardial development (Moore et al., 1999). Epicardial cells in mice lacking WT1 are unable to delaminate and migrate into the underlying sub-epicardium. This leads to a thin ventricular wall, coupled with the absence of a coronary vasculature network. These mice die from cardiovascular failure between E16.5-E18.5, highlighting the essential role of the epicardium in myocardial maturation and coronary vessel development (von Gise et al., 2011; Martínez-Estrada et al., 2010).

Whilst the activation and migration of EPDCs has been set against a requirement for WT1, much is still to be elucidated, regarding the upstream signalling pathways which govern its expression during development. One such pathway that has been implicated in regulating WT1 *in vitro* is HIF-

signalling, whereby HIF1α directly binds to the *Wt1* promoter in an oxygen-dependant manner, to upregulate expression of *Wt1* (Wagner et al., 2003), suggesting HIF may play an important role during epicardial development.

3.2 Aims

This chapter addressed two main experimental aims, pertaining to a possible role for HIF signalling in epicardial development. Firstly, to investigate the physiological levels of hypoxia in the developing heart, focusing on mid- to late gestation stages, when the epicardium forms. Secondly, to determine a functional requirement for epicardial HIF signalling during development, in particular to assess a requirement for HIF1α or HIF2α transcription factors.

3.3 Hypoxia in the epicardium during development

3.3.1 The epicardium is hypoxic at later stages of development.

The marker Pimonidazole-HCl (Hypoxyprobe-1) (Raleigh et al., 1999) was used to assess hypoxia in the heart during development. At low pO_2 ($\leq$10mm Hg), pimonidazole forms adducts with thiol-containing proteins, which can be detected using an anti-pimonidazole fluorescence-conjugated monoclonal Antibody (HP1). Embryonic hearts were harvested at stages E12.5-E18.5, following *in utero* pimonidazole treatment, fixed and sectioned for immunostaining. HP1 was co-stained with antibodies against the endothelial marker, endomucin (EMCN), and the epicardial marker, WT1. At embryonic day (E)12.5, when the myocardium is highly trabeculated, to increase the surface area exposed to blood and ensure an efficient exchange of nutrients and oxygen (Figure 3.3.1A-B) (Sedmera and Thomas, 1996), and the epicardium is fully formed (Figure 3.3.1C), HP1 staining revealed extensive regions of hypoxia, mostly in areas of compact myocardium, and most strikingly in the compact wall of the atrioventricular (AV) groove (Figure 3.3.2A-E).

At E14.5, when a sub-set of $WT1^+$ epicardial cells have undergone EMT and started extending into the sub-epicardial space (Figure 3.3.1D-F), HP1 staining was observed in areas of thicker compact myocardium, specifically in the inter-ventricular septum (IVS) region (Figure 3.3.2F-J). However, this signal became weaker by E16.5 and E18.5, a time-point when $WT1^+$ derivatives were observed throughout the ventricular wall and the compact myocardium was already being nourished by the newly formed coronary vessels (Figure 3.3.1D-L; Figure 3.3.2K-T). Instead, HP1 staining was almost exclusively restricted to

the WT1-expressing epicardium (Figure 3.3.2N,O,S,T), suggesting that the most outer layer of the heart becomes hypoxic at later stages of development.

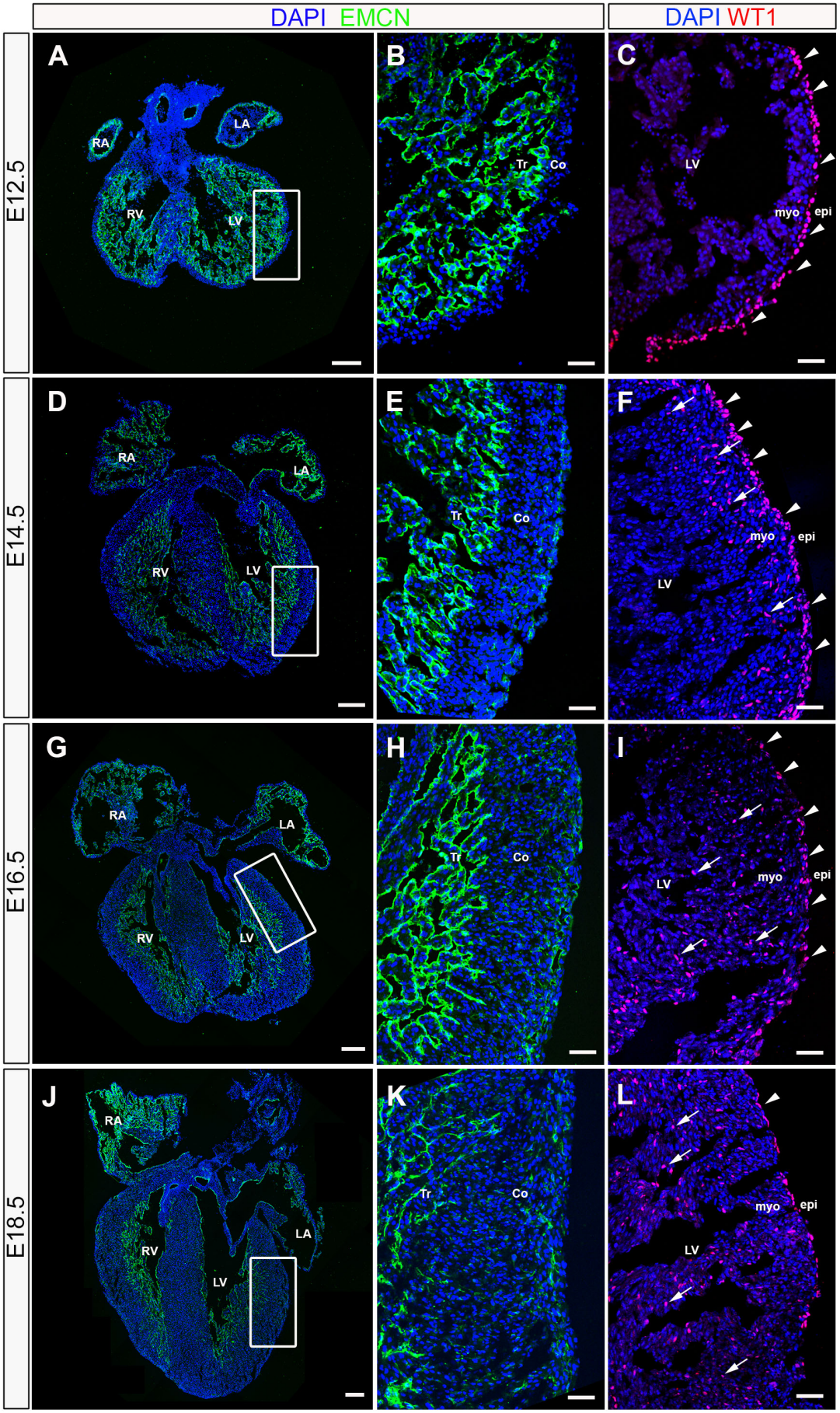

DAPI EMCN
DAPI WT1
E12.5
E14.5
E16.5
E18.5
A
B
C
D
E
F
G
H
I
J
K
L
RA
LA
RV
LV
Tr
Co
myo
epi

Figure 3.3.1 During development WT1+ cells undergo EMT and migrate into the myocardium as it grows and compacts

Representative images of immunostaining for endomucin (EMCN) (green), WT1 (red) and DAPI nuclear stain (blue) on **A-C**. E12.5, **D-F**. E14.5, **G-I**. E16.5 and **J-L**. E18.5. Images **B**, **E**, **H** and **K** are magnifications of boxed regions in **A**, **D**, **G** and **J** respectively. Images **C**, **F**, **I** and **L** are equivalent regions to **B**, **E**, **H** and **K** respectively. Arrowheads highlight WT1+ epicardial cells, arrows highlight WT1+ EPDCs. RA= right atria, LA= left atria, RV in right ventricle, LV= left ventricle, Tr= trabeculae myocardium, Co= compact myocardium, Epi= epicardium, myo= myocardium. Whole heart scale bars= 200μm, high magnification scale bars= 50μm. n= 2-4 hearts per stage.

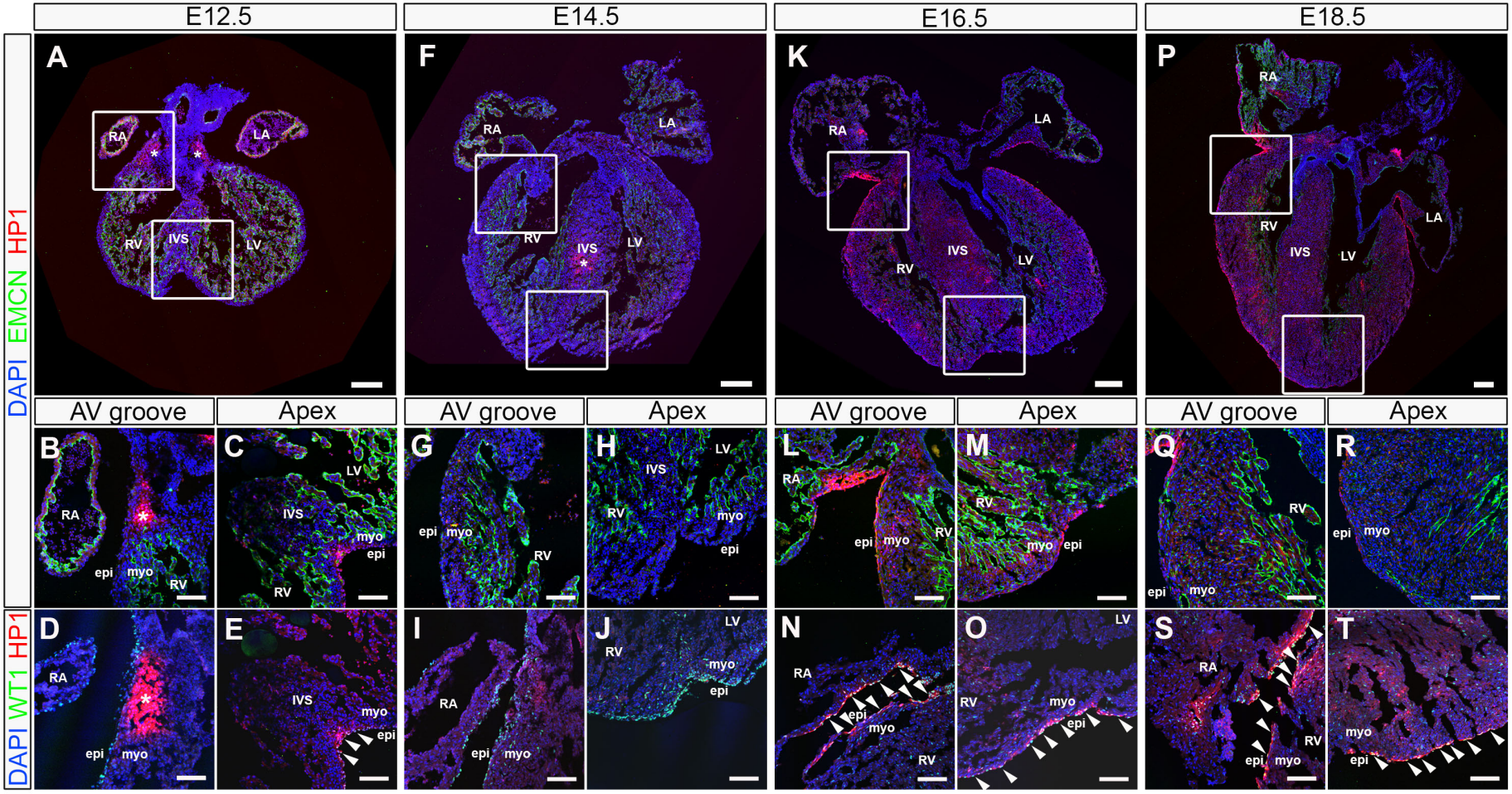

E12.5
E14.5
E16.5
E18.5
DAPI EMCN HP1
DAPI WT1 HP1
A
F
K
P
RA
LA
RV
IVS
LV
AV groove
Apex
B
C
G
H
L
M
Q
R
D
E
I
J
N
O
S
T
epi
myo

Figure 3.3.2 The epicardium is hypoxic at later stages of development

A-T. Representative images of immunostaining for DAPI (blue), HP1 (red) and EMCN or WT1 (green) on cryosections of hearts from stages **A-E**. E12.5, **F-J**. E14.5, **K-O**. E16.5 and **P-T**. E18.5. Images **B-C**, **G-H**, **L-M** and **Q-R** are magnifications of boxed regions in images **A**, **F**, **K** and **P** respectively. Images **D-E**, **I-J**, **N-O** and **S-T** represent equivalent regions of the heart to the images above them. * indicate hypoxic regions in compact myocardium, arrowheads indicate overlap between HP1 and WT1. AV groove= atrioventricular groove, IVS= interventricular septum RA= right atria, LA= left atria, RV= right ventricle, LV= left ventricle, epi= epicardium, myo= myocardium. Apex= tip of left ventricle. Whole heart scale bars= 200μm, high magnification scale bars= 50μm. n=2-4 hearts per stage.

3.3.2 The HIF-target, GLUT1, is expressed in hypoxic regions in the heart.

During hypoxia, transcription factor HIFα is stabilised, dimerises HIFβ and activates transcription of a variety of genes which enable the cell to survive under hypoxic conditions. To determine whether HIF-mediated transcription was active in the hypoxic epicardium during development, and to validate the hypoxyprobe staining, serial sections were immunostained with an antibody against HIF1α. However, immunostaining of HIF1α is particularly problematic, due to its rapid proteasomal degradation in the presence of oxygen. When the embryos were initially harvested from the uterus, they were exposed to atmospheric O_2, leading to the rapid degradation of HIF1α before the hearts were fixed. Further, current HIF1α antibodies are not sensitive enough to detect the small amount of protein that remains. Therefore, whilst several attempts were made to optimise the staining protocol using primary antibodies from different sources and testing multiple fixative conditions, successful immunostaining of HIF1α was not achieved, with only high levels of

background immunofluorescence from the AlexaFluor® secondary antibody observed (Figure 3.3.3).

Stabilised HIF activates transcription of genes involved in anaerobic glycolysis, such as glucose transporter 1 (*Glut1*), which enables the cell to generate energy in the absence of O_2 (Ouiddir et al., 1999). As such, immunostaining against GLUT1, on serial sections, was used as a surrogate read-out for HIF activity. At E12.5 and E14.5 GLUT1 expression was strongest in the AV groove and IVS respectively (Figure 3.3.4A-B), in comparable areas to the hypoxyprobe staining (Figure 3.3.2A-J). Moreover, at E16.5 and E18.5 GLUT1 expression was observed in the epicardium, both validating the hypoxyprobe staining and suggesting HIF-mediated transcription is activated in the hypoxic epicardium (Figure 3.3.4C-D).

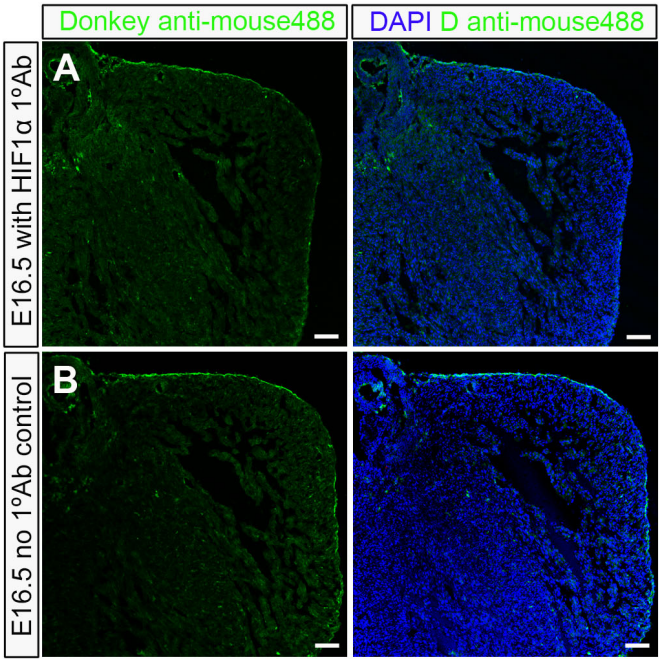


Figure 3.3.3 Observed HIF1α antibody immunostaining is only background.

A. Representative image of immunostaining for HIF1α (green) and DAPI (blue) on a cryosection from an E16.5 heart. **B**. Serial section incubated with DAPI (blue) and the donkey anti-mouse 488 AlexaFluor® secondary antibody only (no primary antibody (1° Ab) control). Scale bars= 100μm.

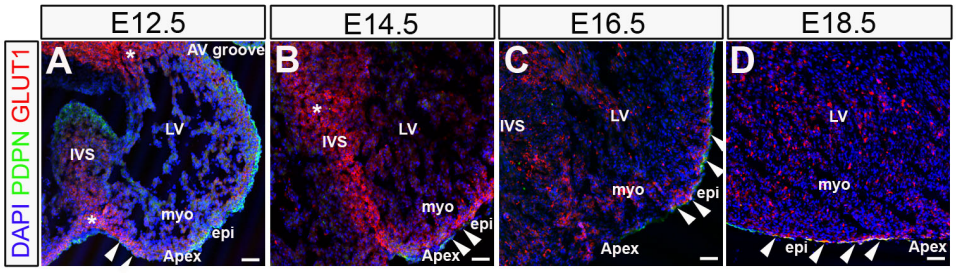


Figure 3.3.4 The HIF-target GLUT1 is expressed in regions of hypoxia during cardiac development.

A-D. Representative images of immunostaining for PDPN (green), GLUT1 (red) and DAPI (blue) on cryosections of hearts from stages **A**. E12.5, **B**. E14.5, **C**. E16.5 and **D**. E18.5. * indicates overlapping region with hypoxyprobe staining. Arrowheads indicate GLUT1 expression in the epicardium. AV groove= atrioventricular groove, IVS= interventricular septum LV= left ventricle, epi= epicardium, myo= myocardium, Apex= tip of left ventricle. Scale bars= 50μm. n=2-4 hearts per stage.

3.3.3 The HIF family of transcription factors are expressed in the heart during development

As HIF1α and HIF2α are regulated at the protein level, by PHDs1-3 and FIH-mediated hydroxylation, RNA transcript levels do not necessarily reflect protein activity. However, given the difficulties associated with HIFα immunostaining, to confirm whether the HIF family of transcription factors were at least transcribed in the heart during development, messenger (m)RNA transcript levels were assessed, in whole ventricular lysates, using RT-qPCR. Levels of hallmark epicardial genes: *Wt1*, *Tcf21, Tbx18* and *Raldh2* were also assessed. Expression of epicardial genes was highest at E11.5, when epicardial signalling/activity is highest, with levels decreasing thereafter (Figure 3.3.5A-D). Concomitantly, expression of *Hif1α* significantly decreased from E11.5-E14.5, when the heart becomes perfused by the coronaries (Mean fold change ± SEM; E11.5: 12.06 ± 0 (n=1); E14.5: 1.815 ± 0.1423 (n=2); E16.5: 0.3001 ± 0.0859 (n=2); E18.5: 0.5573 ± 0.0667 (n=2); p<0.0001 [E11.5 vs E14.5]; Figure 3.3.5E). Expression of *Hif2α* also decreased from E11.5-E14.5 but remained high (Mean fold change ± SEM; E11.5: 1.472 ± 0; E14.5: 0.986 ± 0.04678; E16.5: 0.8206 ± 0.1181; E18.5: 1.037 ± 0.1147; p=0.1813 [E11.5 vs E14.5]; Figure 3.3.5F), suggesting HIF2α may be important in the hypoxic epicardium at later stages of development. Expression of the ubiquitously expressed *Hif1β* was observed at all stages (Figure 3.3.5G).

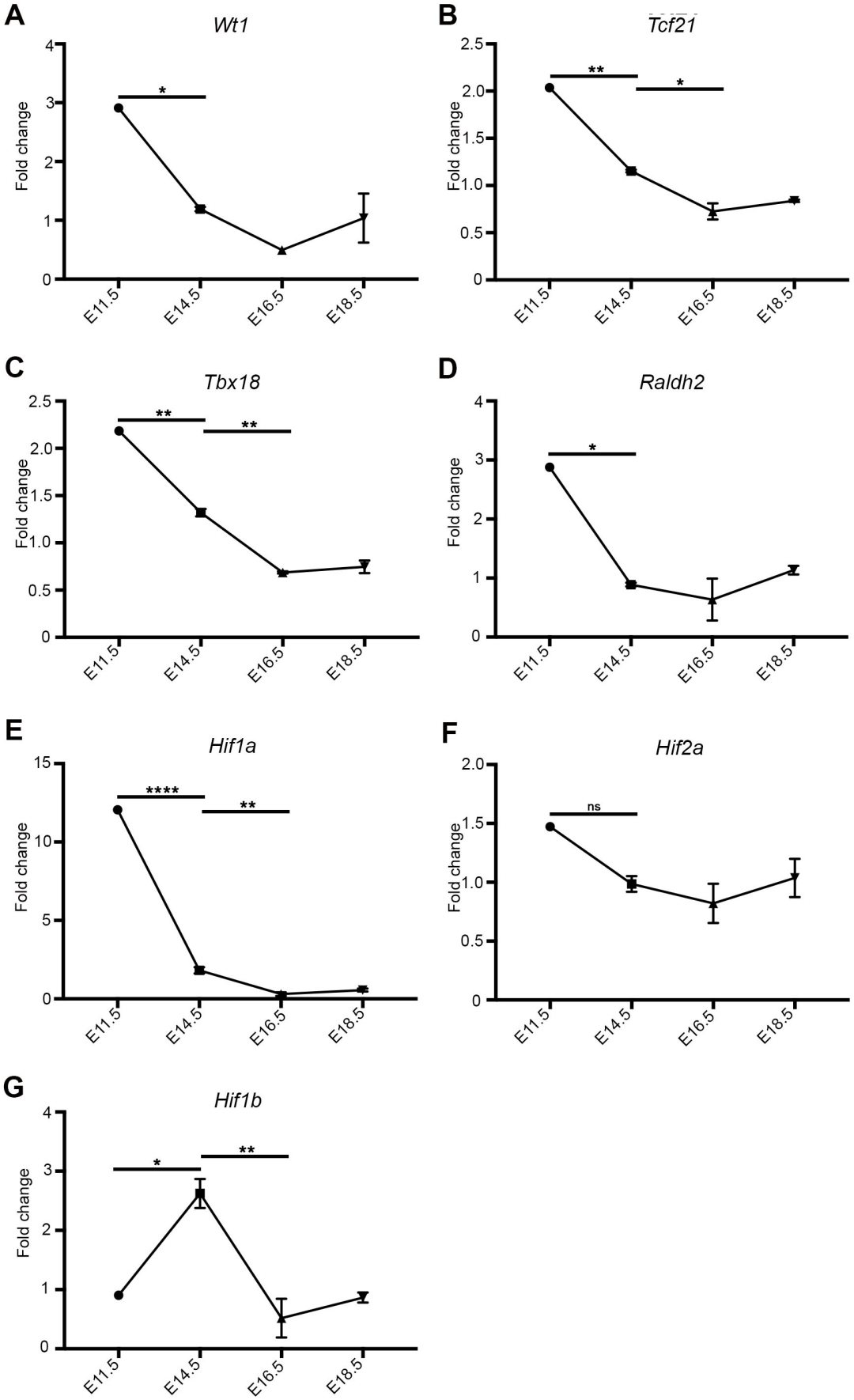

A
Wt1
Fold change
E11.5
E14.5
E16.5
E18.5
*
B
Tcf21
**
*
C
Tbx18
**
**
D
Raldh2
*
E
Hif1a
****
**
F
Hif2a
ns
G
Hif1b
*
**

Figure 3.3.5 Hif1α and Hif2α are expressed in the heart during development

A-F. mRNA levels of epicardial genes **A**. *Wt1*, **B**. *Tcf21*, **C**. *Tbx18* and **D**. *Raldh2* and HIF transcription factor genes: **E**. *Hif1α,* **F**. *Hif2α* and **G**. *Hif1β* taken from whole ventricles of E11.5, E14.5, E16.5 and E18.5, normalised to *18s* expression and analysed by the ΔΔCT method. E11.5: n=1 embryo, E14.5/E16.5/E18.5: n=2 embryos. Data presented as Mean ± SEM. Data analysed by one-way ANOVA with Tukey's post-hoc test *p<0.05; **p<0.01; ***p<0.001; ****p<0.0001; ns = not significant.

3.3.4 HIF directly binds to the *WT1* locus

Wagner and colleagues previously demonstrated that hypoxia increases expression of the master epicardial regulator *WT1,* in human U-2OS osteosarcoma cells*,* and deletion of a HIFα consensus binding element, known as a hypoxia response element (HRE), in the *WT1* promoter abrogated this effect, suggesting HIF1α directly binds to and regulates expression of *WT1*. Our collaborator Prof Peter Ratcliffe's lab conducted chromatin immunoprecipitation coupled with next generation sequencing (ChIP-seq) on three human clear cell renal cell carcinoma (ccRCC) lines: 786-O, RCC4 and UMRC3, in which VHL is mutated and HIF is therefore constitutively active. In this technique, transcription factor bound DNA is fixed *in situ*, by cross-linking with formaldehyde, sheared, and then precipitated out using an antibody against the transcription factor of interest. The extracted DNA is then sequenced to determine where the transcription factor binds (Johnson et al., 2007; Ren et al., 2000). An antibody against HIF1β (rabbit polyclonal, Novus Biologicals, NB100-110) was used to precipitate out the bound DNA, as HIF1β dimerises with both HIF1α and HIF2α to activate transcription, therefore enabling the determination of all HIF targets. To confirm a direct interaction of HIF with *WT1*, we asked Rafik Salama, a bioinformatician in the Ratcliffe lab to

interrogate the data for signal in the *WT1* locus, along with other hallmark epicardial genes: *TCF21, TBX18* and *RALDH2*. A clear peak was observed in the promoter region of *WT1*, in the 786-O cell line, indicating HIF directly binds (Figure 3.3.6B). Taken together with the study by Wagner and colleagues (Wagner et al., 2003), this suggest HIF is able to directly bind and regulate expression of *WT1*. No peaks were observed in the loci of *TCF21, TBX18* or *RALDH2* for any of the cell lines (Figure 3.3.6C-E), although a peak around 200kb away from the promoter of *TBX18* was observed (Figure 3.3.6D).

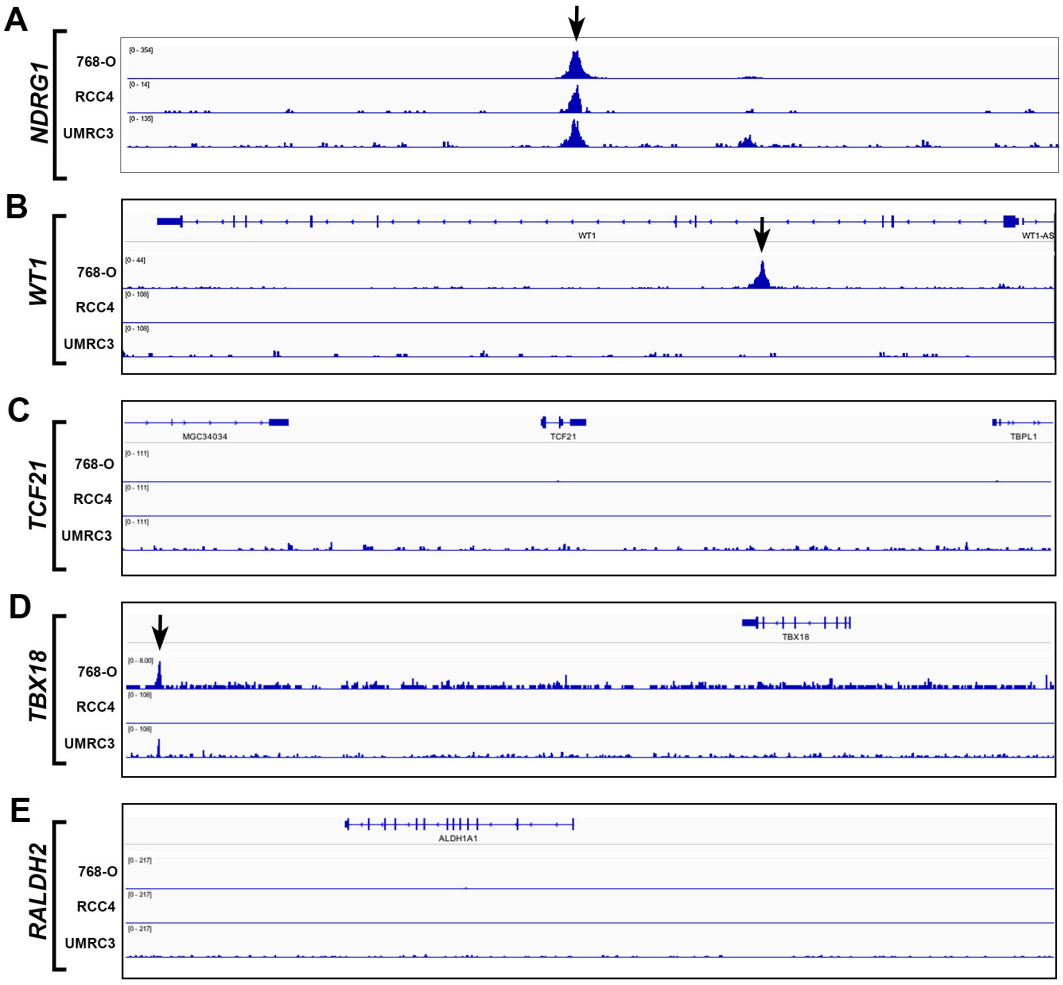


Figure 3.3.6 HIF directly binds to the promoter region of *Wt1* in renal cells.

A-E. HIF1β ChIP-seq analysis of **A**. *NDRG1* (positive control), **B**. *WT1*, **C**. *TCF21*, **D**. *TBX18* and **E**. *RALDH2* loci, conducted on human clear cell renal cell carcinoma (ccRCC) lines: 786-O, RCC4 and UMRC3. Arrows highlight positive peaks.

3.4 Investigating a functional requirement for HIF1α in the developing epicardium

Following the observation that the epicardium is hypoxic at later stages of development, and expresses the HIF-target GLUT1, and having confirmed HIF directly binds the promoter region of *Wt1*, in renal cells, we hypothesised that hypoxia and downstream HIF signalling has a functional role, impacting on epicardium development.

To determine a functional requirement for HIF signalling in the epicardium, an *in vivo* genetic loss-of-function approach of HIF was employed. Whilst there are 3 isoforms of HIFα, Wagner and colleagues reported regulation of *Wt1* by the ubiquitously expressed HIF1α (Wagner et al., 2003), therefore, initial experiments aimed to target HIF1α specifically and probe for a potential effect on epicardial development and closely-associated myocardial maturation and coronary vessel formation.

3.4.1 The *Wt1*$^{CreERT2/+}$ driver specifically targets epicardial cells and its derivatives in development

To target expression of *Hif1α* in the epicardium, the tamoxifen-inducible epicardial-specific CreERT2 driver, *Wt1*$^{CreERT2/+}$ was utilised (Zhou et al., 2008). Initially, to confirm sufficient Cre-mediated recombination in epicardial cells upon tamoxifen administration, the *Wt1*$^{CreERT2/+}$ line was crossed with a *Rosa26 tdTomato* reporter (*R26R*^{tdTomato}) which has a *LoxP*-flanked STOP cassette preventing transcription of a red fluorescent protein variant (tdTomato). In resulting *Wt1*$^{CreERT2/+}$*;R26R*^{tdTomato} embryos, following tamoxifen administration,

cells expressing *Wt1* which have successfully undergone Cre-mediated recombination, and therefore excised the STOP cassette, will express tdTomato. Dams were injected with 100mg/kg of tamoxifen at E9.5 and E11.5 and embryos were harvested at E12.5, E14.5 and E16.5 to assess for recombination. Imaging of sections at E12.5 revealed successful targeting in the majority of epicardial cells and a high specificity to the epicardial layer (Figure 3.4.1A). Imaging of sections at E14.5 and E16.5 revealed successful targeting in most epicardial cells, along with a substantial proportion of EPDCs (Figure 3.4.1B-C). These experiments demonstrated the specificity of the *Wt1*$^{CreERT2/+}$ Cre driver for the epicardium and its derivatives and revealed that sufficient Cre-mediated recombination could be achieved following prenatal administration of 100mg/kg of tamoxifen at E9.5 and E11.5.

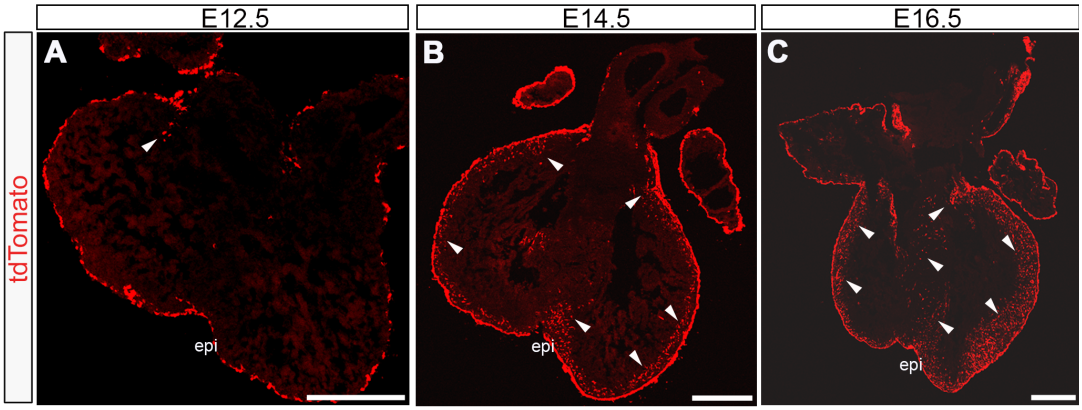


Figure 3.4.1 The *Wt1*$^{CreERT2/+}$ line sufficiently targets epicardial cells and EPDCs during development.

A-C. Representative images of tdTomato fluorescence (red) at stages **A**. E12.5, **B**. E14.5 and **C**. E16.5, following administration of 100mg/kg of tamoxifen at E9.5 and E11.5. Arrowheads indicate WT1+ EPDCs. Epi= epicardium.

3.4.2 Generating embryos with epicardial-specific deletion of *Hif1α*

Following confirmation of the *Wt1*$^{CreERT2/+}$ (Zhou et al., 2008) line as an epicardial-specific CreERT2 driver, it was crossed with a mouse model in which exon 2, containing the DNA binding region, of *Hif1α* was flanked by *LoxP* sites (hereafter, *Hif1α*$^{fl/fl}$) (Higgins et al., 2004), for two generations, to generate *Hif1α*$^{fl/fl}$; *Wt1*$^{CreERT2/+}$ mutant embryos; *Hifα*$^{fl/fl}$ embryos negative for *CreERT2* were used as controls. Pregnant *Hif1α*$^{fl/fl}$ dams were injected with 100mg/kg of tamoxifen at E9.5 and E11.5 to target epicardial development; embryos were subsequently collected at E15.5-E16.5 for analysis of epicardial cell migration, coronary vessel formation and ventricular maturation. (Figure 3.4.2).

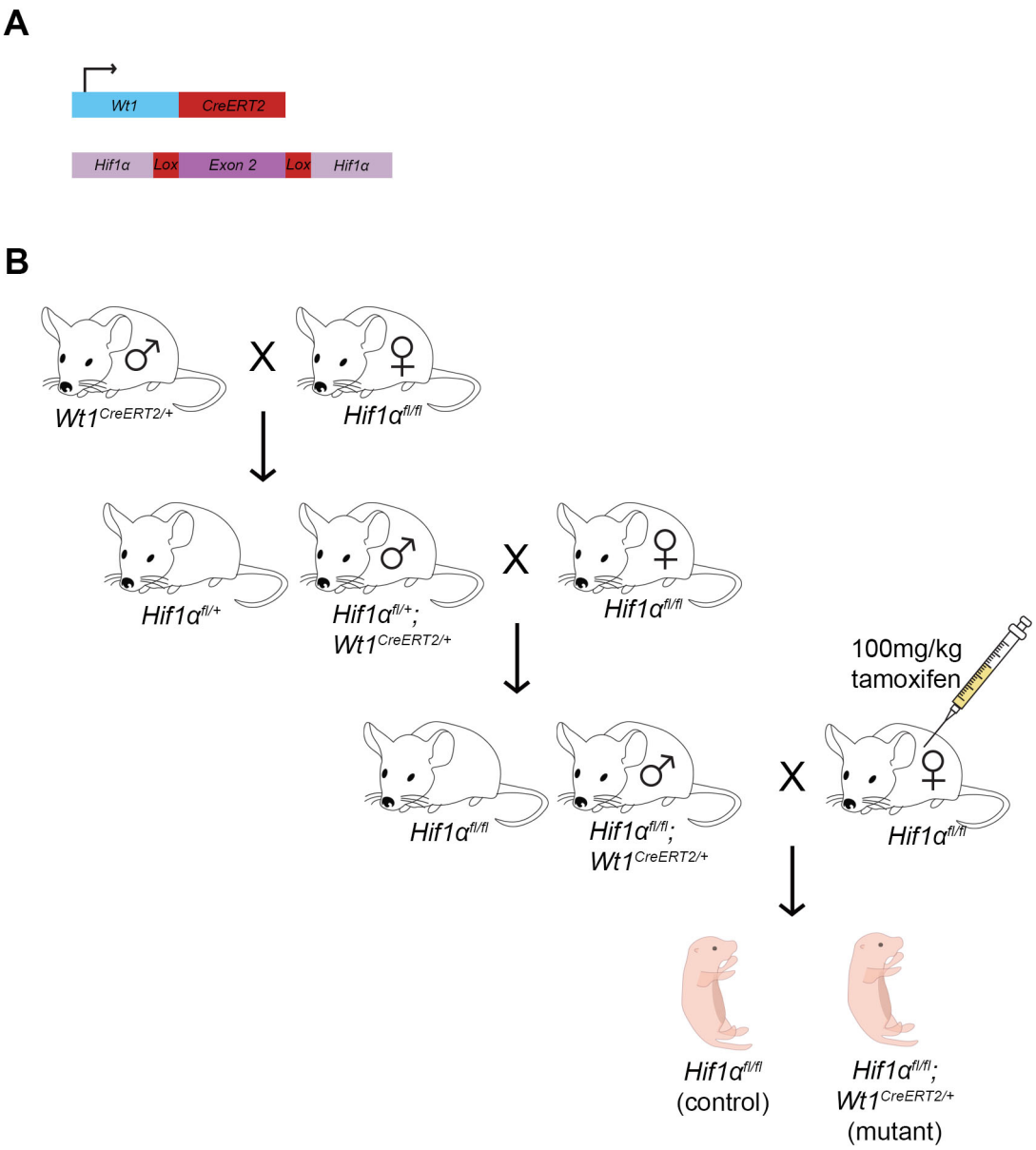


Figure 3.4.2 Inducible, epicardial-specific deletion of HIF1α during embryonic development

A. Hif1$\alpha^{fl/+}$;*Wt1*$^{CreERT2/+}$ construct: *CreERT2* is under the control of the *Wt1* promoter, exon 2 of *Hif1α* is flanked by LoxP sites. **B**. Schematic of the generation of epicardial-specific *Hif1α* KO embryos. A *Wt1*$^{CreERT2/+}$ stud male was crossed with a *Hif1α*$^{fl/fl}$ female to produce Hif1$\alpha^{fl/+}$;*Wt1*$^{CreERT2/+}$ males, which were then used for timed-matings with *Hif1α*$^{fl/fl}$ females to generate mutant (Hif1$\alpha^{fl/fl}$;*Wt1*$^{CreERT2/+}$) and control (Hif1$\alpha^{fl/fl}$) embryos. Hif1$\alpha^{fl/fl}$ dams were injected with 100mg/kg of tamoxifen at E9.5 and E11.5 to induce Cre-mediated recombination in the Hif1$\alpha^{fl/fl}$;*Wt1*$^{CreERT2/+}$ embryos.

3.4.3 Loss of Hif1α in the epicardium leads to nodules on the surface of the heart.

Tail tips were collected from each embryo to determine genotype. Expected mendelian ratios of inheritance were observed, suggesting loss of *Hif1α* in the epicardium does not cause embryonic lethality by E16.5 (Table 3.4.1), however, *Hif1α$^{fl/fl}$; Wt1$^{CreERT2/+}$* mutant embryos exhibited gross anatomical and morphological defects, which varied in severity across mutant embryos, even within the same litter. Specifically, 3 out of 4 mutant embryos presented with widespread oedema, in the back of the head and trunk, and haemorrhaging on the skin surface (Figure 3.4.3C). Further, 3 out of the 4 mutants displayed abnormal spots/nodules on the surface of the heart, resembling a previously described phenotype resulting from impaired epicardial development (Smart et al., 2007) (Figure 3.4.3D). These phenotypes are summarised in Table 3.4.2.

Genotype	Harvested	Alive when harvested	Expected
Hif1α$^{fl/fl}$	64%	50%	50%
Hif1α$^{fl/fl}$; Wt1$^{CreERT2/+}$	36%	50%	50%

Table 3.4.1 Survival of *Hif1α$^{fl/fl}$; Wt1$^{CreERT2/+}$* embryos

Percentage of embryos from each genotype, collected at E15.5 and E16.5 along with expected mendelian ratios of inheritance.

Genotype	Pale	oedema	haemorrhaging on skin	Nodule on heart
Hif1αfl^{fl}	0%	25%	0%	0%
Hif1αfl^{fl}; Wt1$^{CreERT2/+}$	75%	75%	25%	75%

Table 3.4.2 Phenotype of *Hif1α$^{fl/fl}$; Wt1$^{CreERT2/+}$* embryos

Summary of gross anatomical and morphological phenotypes observed in *Hif1α$^{fl/fl}$; Wt1$^{CreERT2/+}$* mutant embryos.

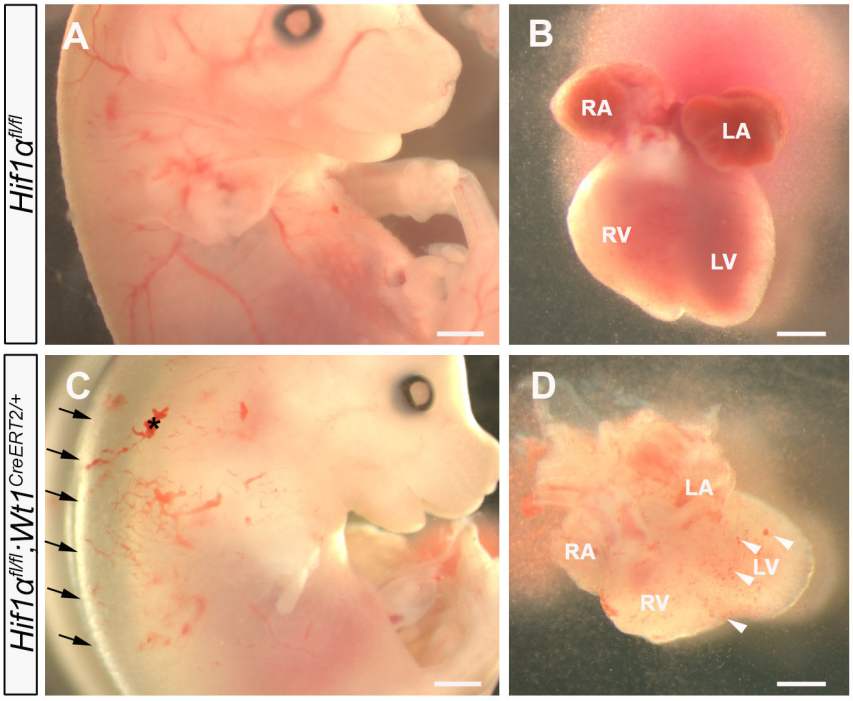


Figure 3.4.3 *Hif1α*$^{fl/fl}$*; Wt1*$^{CreERT2/+}$ embryos present with oedema and nodules on the surface of the heart.

A-D. Representative brightfield images captured of **A-B**. *Hif1α*$^{fl/fl}$ (control) or **C-D**. *Hif1α*$^{fl/fl}$*; Wt1*$^{CreERT2/+}$ E15.5 embryos. **A, C**. Whole-embryos, **B, D**. Whole-hearts. * indicates blood haemorrhaging. Arrows highlight widespread oedema. Arrowheads denote blood spots. RA= right atria, LA= left atria, RV= right ventricle, LV= left ventricle. A,C scale bars= 1mm, B, D scale bars= 0.5mm. n=4 per group.

3.4.4 *Hif1α*$^{fl/fl}$*; Wt1*$^{CreERT2/+}$ embryos display a significant decrease in WT1 expression

Hearts were sectioned and prepared for immunostaining to assess the effect of epicardial loss of *Hif1α* on heart development. Antibodies against epicardial markers WT1 and podoplanin (PDPN), a mucin-like transmembrane glycoprotein, were used to asses formation of the epicardium (Mahtab et al., 2008). The endothelial marker (veins and capillaries) endomucin (EMCN), which also marks the endocardium was used to outline myocardial trabeculae.

In all *Hif1α*$^{fl/fl}$ control hearts, PDPN marked the continuous, single cell-thick epicardial layer, with the majority of cells positive for WT1. At this stage, cells expressing WT1 were also present in the underlying sub-epicardium and myocardium. EMCN staining marked the distinction between the trabeculated (non-compacted) myocardium and thick, compacted myocardium, alongside the newly formed sub-epicardial coronary vessels (Figure 3.4.4A).

Hearts from *Hif1α*$^{fl/fl}$*; Wt1*$^{CreERT2/+}$ mutants showed variation in the severity of phenotype. Two of the three mutants had a continuous epicardial layer, marked by PDPN, similar to controls (Figure 3.4.4B). However, one mutant showed a partially detached, loose, epicardium (Figure 3.4.4C) and was grossly dysmorphic. All mutants exhibited fewer WT1+ cells in the epicardium and WT1^{+}EPDCs in the underlying myocardium, compared to controls, and quantification revealed this difference was statistically significant (Mean number of WT1+ cells per area ± SEM; control, 24.29 ± 1.934, n=4; mutant, 13.4 ± 1.572, n=3; $p<0.0001$; Figure 3.4.4D) (control, 20.13 ± 2.623; mutant, 4.35 ± 0.9242; $p<0.0001$; Figure 3.4.4E). EMCN staining suggested an increase in myocardial trabeculation in mutant hearts, with the most extreme example displaying EMCN-labelled protrusions that extended into the epicardial layer (Figure 3.4.4C). To quantitatively analyse the extent of myocardial trabeculation, fractal analysis, which measures the complexity of the EMCN+ trabeculae, was used (Captur et al., 2014, 2015, 2016), but no significant differences were found between mutants and controls (Figure 3.4.4F). In addition, *Hif1α*$^{fl/fl}$*; Wt1*$^{CreERT2/+}$ mutant hearts exhibited a thinner, under-developed compact myocardium than control littermate hearts, however, measurement of the average width of compact myocardium revealed there was

not a significant difference between mutants and controls (Mean width of compact myocardium (μm) ± SEM; control, 89.73 ± 11.73, n=4; mutant, 74.25 ± 10.98, n=3; p=0.3952; Figure 3.4.4G).

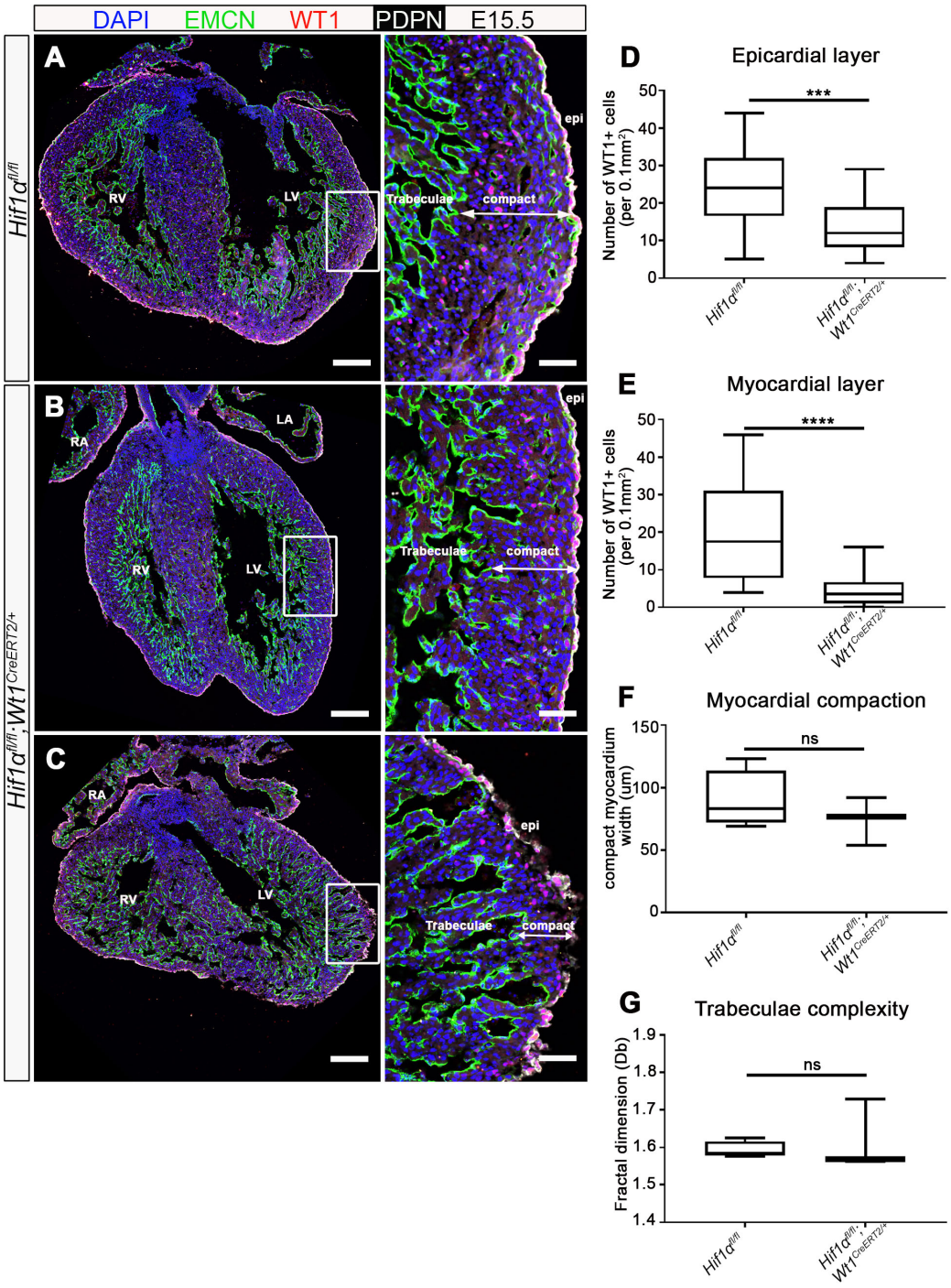


Figure 3.4.4 Epicardial specific loss of *Hif1α* leads to a significant reduction in WT1 expression.

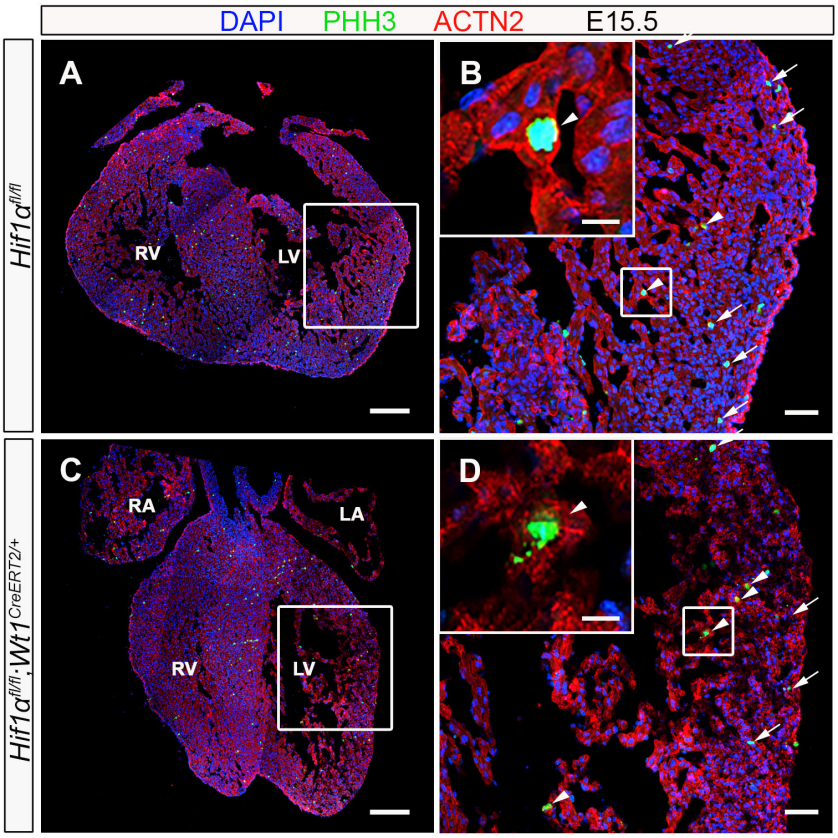
A-C. Representative images of immunostaining for EMCN (green), WT1 (red), PDPN (white) and DAPI (blue), on coronal sections of hearts from **A**. *Hif1α$^{fl/fl}$* (control) or **B-C.** *Hif1α$^{fl/fl}$;Wt1$^{CreERT2/+}$* embryos at stage E15.5. Images to right represent high magnifications of boxed regions. RA= right atria, LA= left atria, RV= right ventricle, LV= left ventricle, epi= epicardium. Double-edge arrow highlights width of compact myocardium. Scale bars= 200μm, high magnification scale bars= 50μm. **D-E**. Quantification of the number of WT1+ cells per 0.1mm^2 **D**. the epicardium or **E**. the myocardium. **F**. Fractal analysis used to determine the complexity of myocardial trabeculae. **G**. Average width of compact myocardium. n=4 hearts for control and n=3 hearts for mutant. Data presented as median, inter-quartile range (IQR) and upper and lower limits, data analysed by a student t-test, ***p<0.001; ****p<0.0001; ns= not significant.

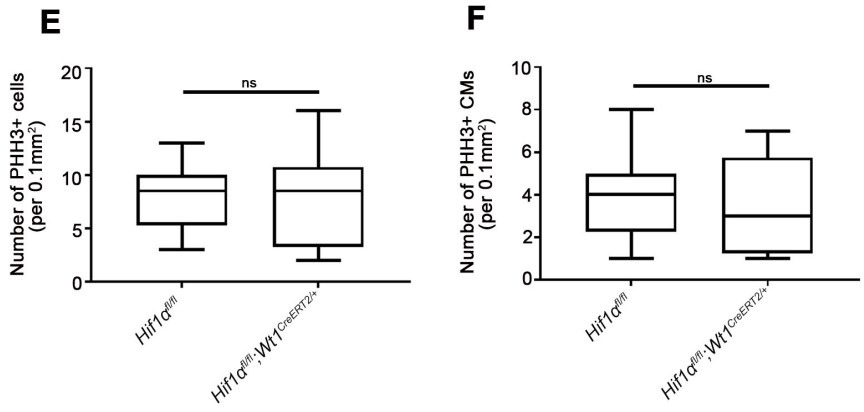
3.4.5 Loss of HIF1α in the epicardium does not affect cardiomyocyte proliferation

Migration of EPDCs, during development, has been linked to myocardial compaction (Vicente-Steijn et al., 2015). Further, mice lacking epicardial *Wt1* exhibit diminished proliferation of the compact myocardium (von Gise et al., 2011). Since *Hif1α$^{fl/fl}$; Wt1$^{CreERT2/+}$* hearts presented with a reduction in WT1+ epicardial cells and EPDCs, combined with a thinned compact myocardium, we hypothesised there would be decreased cardiomyocyte proliferation in the compact layer.

Proliferation was assessed using phospho-histone H3 (PHH3), which marks mitotically active cells (Tetzlaff et al., 2013) (Figure 3.4.5). Initial quantification off all PHH3+ cells revealed no differences in global proliferation between groups (Figure 3.4.5E). The number of proliferating cardiomyocytes, specifically, was then determined, via co-staining with the cardiomyocyte marker, alpha-actinin 2 (ACTN2), but again no differences were observed (Figure 3.4.5F). Finally, to exclude the possibility that an effect on proliferation

within the highly proliferative compact myocardium was being masked by the abundant, less proliferative trabeculae myocardium, the two distinct layers were quantified separately, however, no significant difference was found (Figure 3.4.5G). To determine proliferation levels in the epicardium, PHH3 staining was combined with PDPN, however only 1-2 PHH3+ cells were observed per section in both controls and mutants, suggesting low proliferative rates in the epicardium at this stage (data not shown).


DAPI PHH3 ACTN2 E15.5
A
B
C
D
RV
LV
RA
LA
Hif1α^fl/fl
Hif1α^fl/fl;Wt1^CreERT2/+


E
Number of PHH3+ cells (per 0.1mm²)
ns
Hif1α^fl/fl
Hif1α^fl/fl;Wt1^CreERT2/+
F
Number of PHH3+ CMs (per 0.1mm²)
ns
Hif1α^fl/fl
Hif1α^fl/fl;Wt1^CreERT2/+

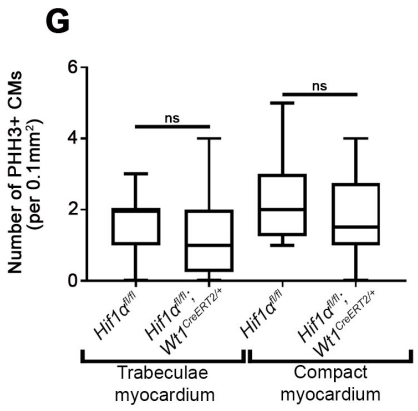

G
Number of PHH3+ CMs (per 0.1mm²)
ns
ns
Hif1α^fl/fl
Hif1α^fl/fl; Wt1^CreERT2/+
Hif1α^fl/fl
Hif1α^fl/fl; Wt1^CreERT2/+
Trabeculae myocardium
Compact myocardium

Figure 3.4.5 Epicardial loss of *Hif1α* does not lead to reduced cardiomyocyte proliferation

A-D. Representative images of immunostaining for PHH3 (green), ACTN2 (red), and DAPI (blue), on coronal sections of hearts from **A-B**. *Hif1α*$^{fl/fl}$ (control) or **C-D.** *Hif1α*$^{fl/fl}$*; Wt1*$^{CreERT2/+}$ embryos at stage E15.5. Images **B** and **D** are magnifications of boxed regions in **A** and **C** respectively. Images in top left corner of **B** and **D** are high magnifications of boxed PHH3+ cardiomyocytes (CMs). Arrowheads highlight PHH3+ CMs in the trabeculae myocardium, Arrows indicate PHH3+ CMs in compact myocardium. RV= right ventricle, LV=left ventricle. Scale bars: A, C= 200μm, B, D=50μm, high magnification= 10μm. **E-G**. Quantification of the number of **E**. PHH3+ cells, **F**. PHH3+ cardiomyocytes and **G.** PHH3+ cardiomyocytes in compacted vs. non-compacted (trabeculated) myocardium. n=4 hearts for control and n=3 hearts for mutant. Data presented as median, IQR and upper and lower limits. Data analysed by **E-F**. student t-test or **G.** one-way ANOVA with Tukey's post-hoc multiple comparisons test. ns= not significant.

3.4.6 Loss of HIF1α in the epicardium impacts on coronary vessel development.

Formation of the coronaries was assessed by immunostaining using antibodies specific for the endothelial cell marker CD31 (aka platelet-endothelial cell adhesion molecule-1, PECAM-1) and smooth muscle cell marker, smooth muscle protein 22-alpha (SM22α). Quantification of CD31+ and SM22α+ vessels, in the compact myocardium, revealed a significant decrease in the number of vessels in *Hif1α*$^{fl/fl}$*;Wt1*$^{CreERT2/+}$ hearts compared to littermate controls (Mean number of vessels per area ± SEM; control, 22.6 ± 3.244, n=4; mutant, 12.51 ± 1.674, n=3; p=0.0148; Figure 3.4.6).

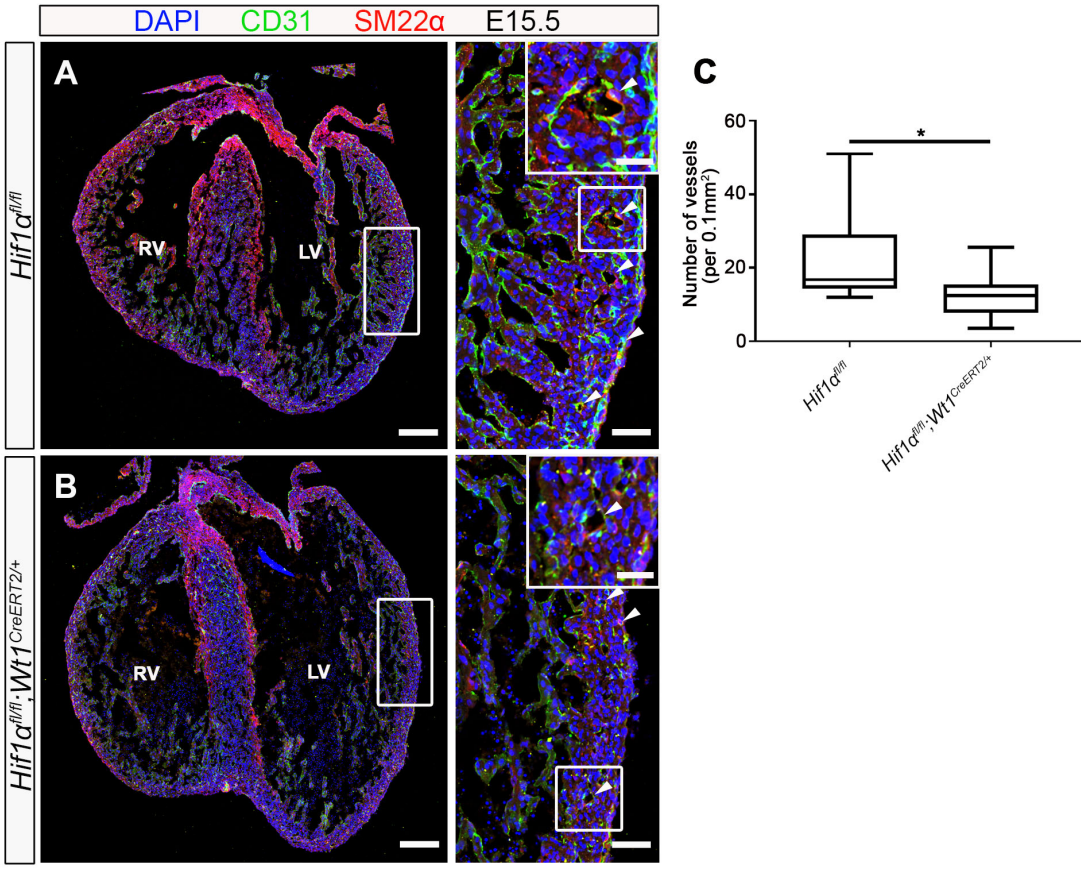


Figure 3.4.6 Loss of *Hif1α* in the epicardium results in a significant reduction in coronary vessel formation.

A-B. Representative images of immunostaining for CD31 (green), SM22α (red) and DAPI (blue) on coronal sections from **A**. *Hif1α*$^{fl/fl}$ (control) or **B**. *Hif1α*$^{fl/fl}$;*Wt1*$^{CreERT2/+}$ E15.5 hearts. Images to right represent high magnifications of boxed regions. Images in top right corner highlight coronary vessels. Scale bars= 200μm, high magnification scale bars= 50μm and 25μm. Arrowheads mark CD31+ SM22α+ vessels. **C**. Quantification of the number of CD31+ SM22α+ vessels per 0.1mm^2. n=4 hearts for control and n=3 hearts for mutant. Data presented as median, IQR and upper and lower limits, and analysed by student t-test, *p<0.05.

3.5 A requirement for HIF2α in epicardial development

During development, HIF1α and HIF2α have been shown to display distinct tissue-specific expression patterns (Jain et al., 1998), indicative of differential roles. Despite this, they share many common target genes, such as the pro-angiogenic VEGF (Ema et al., 1997; Zhang et al., 2012). Therefore, to explore a possible role for HIF2α in the developing epicardium, epicardial specific loss of *Hif2α* studies were conducted.

A mouse model expressing exon 2, containing the DNA binding region, of *Hif2α* flanked by *LoxP* sites (hereafter, *Hif2α*$^{fl/fl}$) (Gruber et al., 2007) was crossed with the tamoxifen-inducible, epicardial-specific *CreERT2* driver, *Wt1*$^{CreERT2/+}$ (Zhou et al., 2008), for two generations, to produce *Hif2α*$^{fl/fl}$*; Wt1*$^{CreERT2/+}$ embryos; *Hif2α*$^{fl/fl}$ embryos negative for *CreERT2* were used as controls. Pregnant *Hif2α*$^{fl/fl}$ dams were injected with 100mg/kg of tamoxifen at embryonic stages (E)9.5 and E11.5 to target epicardial development; embryos were collected at E16.5 for analysis (Figure 3.5.1).

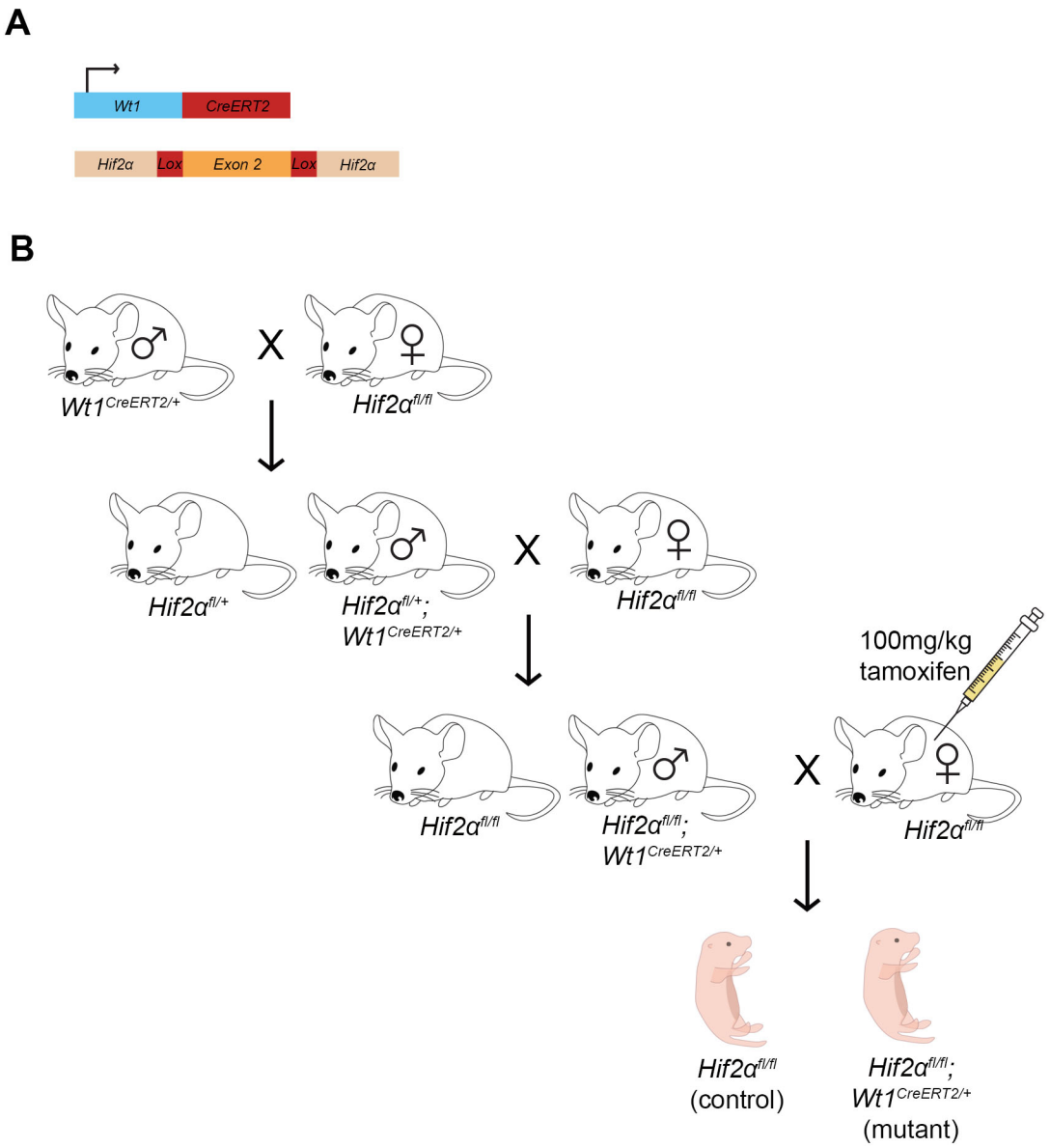


Figure 3.5.1 Inducible, epicardial-specific deletion of HIF2α during embryonic development

A. *Hif2α*$^{fl/fl}$;*Wt1*$^{CreERT2/+}$ construct: *CreERT2* is under the control of the *Wt1* promoter, exon 2 of *Hif2α* is flanked by LoxP sites. **B**. Schematic of the generation of epicardial-specific *Hif2α* KO embryos. A *Wt1*$^{CreERT2/+}$ stud male was crossed with a *Hif2α*$^{fl/fl}$ female to produce *Hif2α*$^{fl/+}$;*Wt1*$^{CreERT2/+}$ males, which were then used for timed-matings with *Hif2α*$^{fl/fl}$ females to generate mutant (*Hif2α*$^{fl/fl}$;*Wt1*$^{CreERT2/+}$) and control (*Hif2α*$^{fl/fl}$) embryos. Hif2α$^{fl/fl}$ dams were injected with 100mg/kg of tamoxifen at E9.5 and E11.5 to induce Cre-mediated recombination in the *Hif2α*$^{fl/fl}$;*Wt1*$^{CreERT2/+}$ embryos.

3.5.1 *Hif2α$^{fl/fl}$; Wt1$^{CreERT2/+}$* embryos present with Oedema, haemorrhaging and nodules on the surface of the heart.

A total of 3 litters were harvested at E16.5 (12 embryos). Genotyping using DNA for tail tips revealed that 50% of embryos collected were *Hif2α$^{fl/fl}$; Wt1$^{CreERT2/+}$,* suggesting epicardial loss of *Hif2α* does not lead to embryonic lethality by E16.5 (Table 3.4.1). Yet, *Hif2α$^{fl/fl}$; Wt1$^{CreERT2/+}$* embryos presented with a remarkably similar phenotype to *Hif1α$^{fl/fl}$; Wt1$^{CreERT2/+}$* mutant embryos, i.e. widespread oedema, skin surface haemorrhaging and nodules on the surface of the heart (Figure 3.5.2). As with the *Hif1α* mutant embryos, the frequency and severity of defects were variable across samples, even in the same litter; this is summarised in Table 3.5.2.

Genotype	Harvested	Alive when harvested	Expected
Hif2α$^{fl/fl}$	57%	58%	50%
Hif2α$^{fl/fl}$; Wt1$^{CreERT2/+}$	43%	42%	50%

Table 3.5.1 Survival of *Hif2α$^{fl/fl}$; Wt1$^{CreERT2/+}$* embryos.

Genotype	Pale	oedema	haemorrhaging on skin	Nodules on heart
Hif2α$^{fl/fl}$	14%	14%	0%	0%
Hif2α$^{fl/fl}$; Wt1$^{CreERT2/+}$	40%	40%	40%	60%

Table 3.5.2 Phenotype of *Hif2α$^{fl/fl}$; Wt1$^{CreERT2/+}$* embryos.

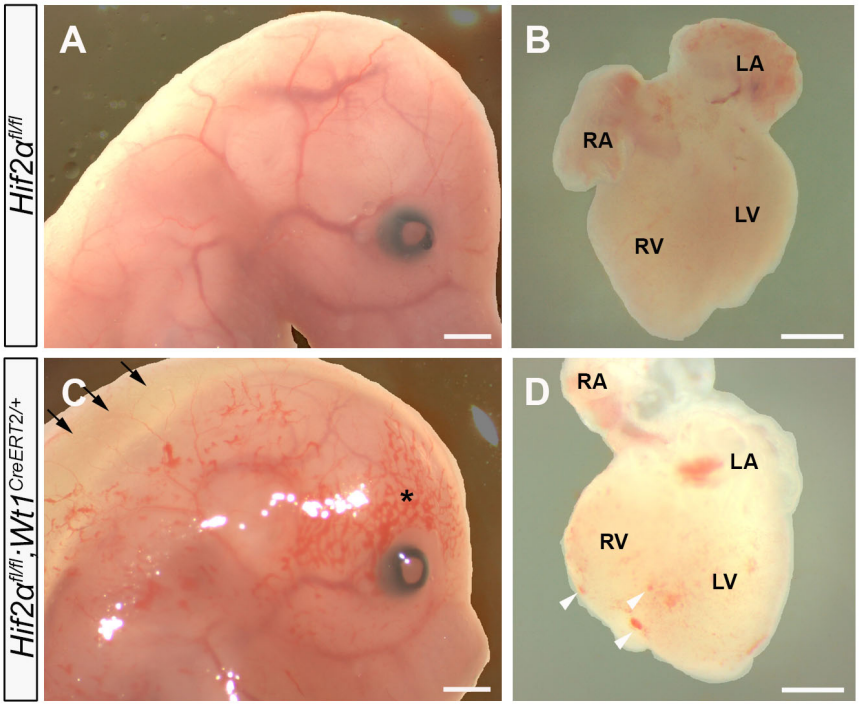


Figure 3.5.2 Embryos lacking epicardial expression of *Hif2α* present with oedema and epicardial surface blood nodules.

A-D. Representative brightfield images captured of **A-B**. *Hif2α*$^{fl/fl}$ (control) or **C-D**. *Hif2α*$^{fl/fl}$*; Wt1*$^{CreERT2/+}$ E16.5 embryos. **A, C**. Whole-embryos, **B, D**. Whole-hearts. * indicates blood haemorrhaging. Arrows highlight oedema. Arrowheads denote blood spots. RA= right atria, LA=left atria, RV= right ventricle, LV= left ventricle. A, C scale bars= 1mm, B, D scale bars= 0.5mm. n=7 *Hif2α*$^{fl/fl}$, n=5 *Hif2α*$^{fl/fl}$*; Wt1*$^{CreERT2/+}$.

3.5.2 Loss of *Hif2α* in the epicardium results in a significant reduction in WT1 expression

Collected hearts were sectioned and prepared for immunostaining. The epicardial markers WT1 and PDPN were used to assess integrity of the epicardium and epicardial EMT. The endothelial marker EMCN was used to visualise the trabeculated myocardium.

In all *Hif2α*$^{fl/fl}$ controls, PDPN and WT1 marked a continuous, single cell-thick epicardial layer. Additionally, WT1 marked a subset of EPDCs that had undergone EMT and migrated into the underlying sub-epicardium and myocardium. EMCN staining marked the trabeculated myocardium, which was phenotypically distinct from the adjacent thick compact layer (Figure 3.5.3A).

Whilst *Hif2α*$^{fl/fl}$*; Wt1*$^{CreERT2/+}$ hearts exhibited a continuous epicardium, labelled by PDPN, a significant reduction in epicardial expression of WT1 was determined (Mean number of WT1+ cells, in the epicardial layer, per area ± SEM; control, 31.74 ± 1.545; mutant, 21.28 ± 1.125; n=4 hearts per group; $p<0.0001$; Figure 3.5.3B-D). Moreover, a significant decrease in WT1 positive EPDCs, in the underlying sub-epicardium and myocardium, was observed (Mean number of WT1+ cells, in the myocardial layer, per area ± SEM; control, 45.11 ± 3.415; mutant, 12.49 ± 1.676; n=4 hearts per group; $p<0.0001$; Figure 3.5.3E). EMCN staining revealed hyper-trabeculation of the myocardium, with protrusions extending into the epicardial layer and fractal analysis determined a significant increase in trabeculae complexity in *Hif2α*$^{fl/fl}$*; Wt1*$^{CreERT2/+}$ hearts compared to controls (Mean fractal dimension (Db) ± SEM; control, 1.595 ± 0.01773; mutant, 1.661 ± 0.01378; n=4 hearts per group; $p=0.0256$; Figure

3.5.3F). Lastly, a reduction in thickness of the compact myocardium was observed, although this was not significant (Mean width of compact myocardium (μm) $\pm$ SEM; control, 166.1 $\pm$ 31.22; mutant, 125.7 $\pm$ 9.616; n=4 hearts per group; p=0.3030; Figure 3.5.3G.)

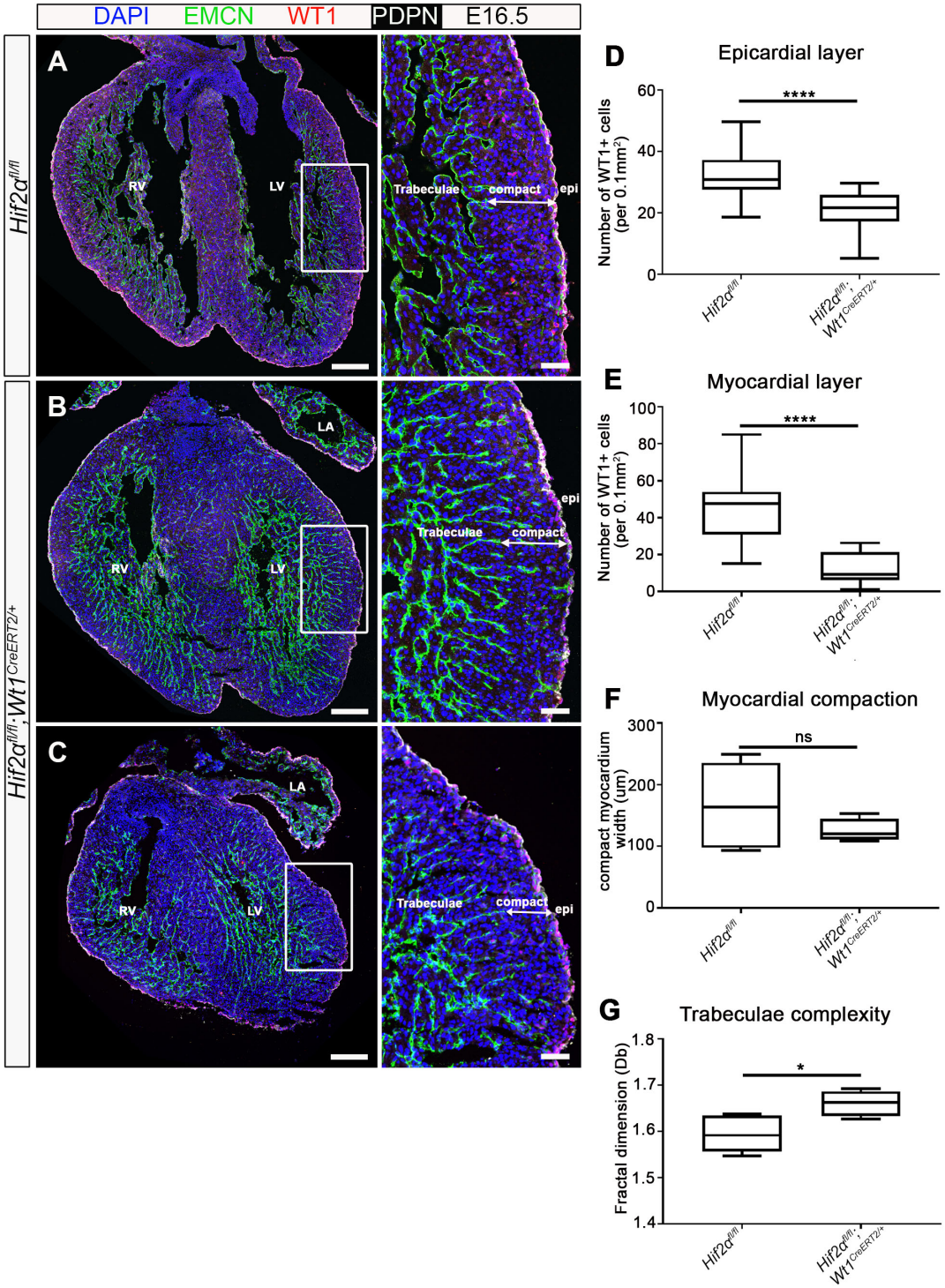

DAPI EMCN WT1 PDPN E16.5
Hif2α fl/fl
Hif2α fl/fl;Wt1 CreERT2/+
A
B
C
RV
LV
LA
Trabeculae
compact
epi
D
Epicardial layer
Number of WT1+ cells (per 0.1mm²)
****
E
Myocardial layer
F
Myocardial compaction
compact myocardium width (um)
ns
G
Trabeculae complexity
Fractal dimension (Db)
*
Hif2α fl/fl
Hif2α fl/fl; Wt1 CreERT2/+

Figure 3.5.3 Loss of *Hif2α* in the epicardium results in a significant reduction in WT1 expression and hyper-trabeculation of the myocardium.

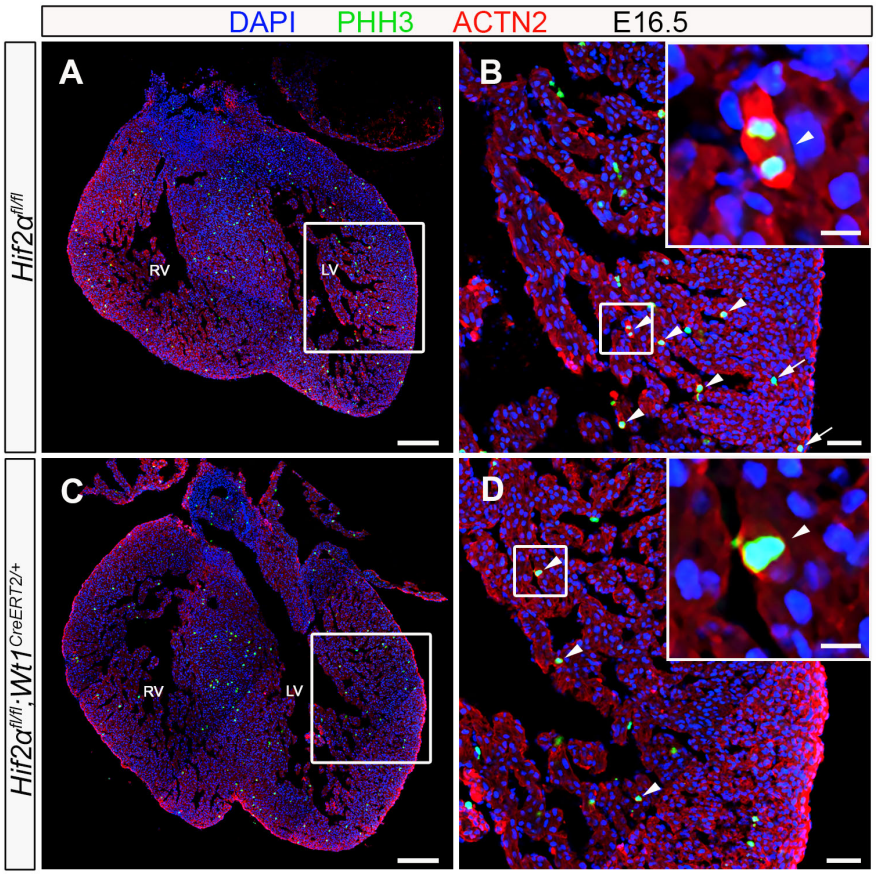
A-C. Representative images of immunostaining for EMCN (green), WT1 (red), PDPN (white) and DAPI (blue), on coronal sections of hearts from **A**. *Hif2α$^{fl/fl}$* (control) or **B-C.** *Hif2α$^{fl/fl}$; Wt1$^{CreERT2/+}$* embryos at stage E16.5. Images to right represent high magnifications of boxed regions. RA= right atria, LA= left atria, RV= right ventricle, LV= left ventricle, epi= epicardium. Double-edge arrow highlights width of compact myocardium. Scale bars= 200μm, high magnification scale bars= 50μm. **D-E**. Quantification of the number of WT1+ cells per area (0.1mm^2) in **E**. the epicardium or **F**. the myocardium. **F**. Fractal analysis used to determine the complexity of myocardial trabeculae **G**. Average width of compact myocardium. n=4 hearts per group. Data presented as median, IQR and upper and lower limits, data analysed by a student t-test, *p<0.05; ****p<0.0001; ns= not significant.

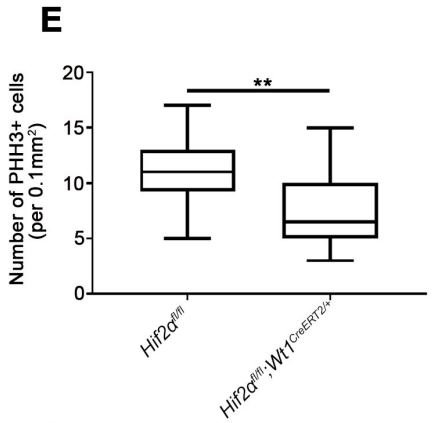
Due to the strikingly similar phenotype observed in the *Hif2α$^{fl/fl}$; Wt1$^{CreERT2/+}$* and *Hif1α$^{fl/fl}$; Wt1$^{CreERT2/+}$* hearts, cardiomyocyte proliferation and coronary vessel development were again assessed by immunofluorescence, to determine the downstream consequences of reduced, WT1-mediated, epicardial EMT.

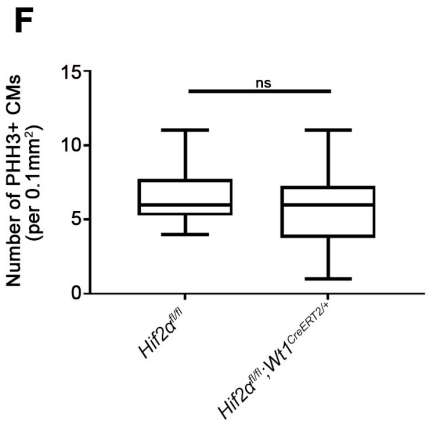
3.5.3 Loss of *Hif2α* in the epicardium leads to a significant reduction in cardiomyocyte proliferation in the compact layer.

To assess cell proliferation, an antibody against phosphorylated histone H3 (PHH3) was used (Figure 3.5.4). Initial quantification of PHH3+ cells, revealed a significant reduction in global levels of proliferation in *Hif2α$^{fl/fl}$; Wt1$^{CreERT2/+}$* hearts compared to controls (Mean number of PHH3$^+$ cells per area ± SEM; control, 11.15 ± 0.7007; mutant, 7.5 ± 0.801; n=4 hearts per group; p=0.0016; Figure 3.5.4E). The number of PHH3+ cardiomyocytes in particular was then quantified, via co-labelling with an anti-ACTN2 antibody, but no substantial differences were found (Mean number of PHH3$^+$,ACTN2$^+$ cells per area ± SEM; control: 6.6 ± 0.4255; mutant: 5.722 ± 0.6458; n=4 hearts per group; p=0.255;

Figure 3.5.4F). However, since the *Hif2α*$^{fl/fl}$*; Wt1*$^{CreERT2/+}$ hearts exhibited a thinned compact myocardial layer, we hypothesised there would be a reduction in cardiomyocyte proliferation in the compact layer specifically. Indeed, whilst no significant difference in cardiomyocyte proliferation was observed in the trabeculated layer, there were statistically less myocytes proliferating in the compact layer of *Hif2α*$^{fl/fl}$*; Wt1*$^{CreERT2/+}$ hearts compared to controls (Mean number of PHH3^{+},ACTN2^{+} cells per area ± SEM; control trabeculae: 2.3 ± 0.1638; mutant trabeculae: 2.5 ± 0.2887; control compact: 4.55 ± 0.3871; mutant compact: 2.0 ± 0.3764; n=4; $p<0.0001$ [control compact vs mutant compact]; Figure 3.5.4G).


DAPI PHH3 ACTN2 E16.5
A
B
C
D
RV
LV
RV
LV
Hif2α fl/fl
Hif2α fl/fl;Wt1 CreERT2/+


E
Number of PHH3+ cells (per 0.1mm²)
20
15
10
5
0
**
Hif2α fl/fl
Hif2α fl/fl;Wt1 CreERT2/+


F
Number of PHH3+ CMs (per 0.1mm²)
15
10
5
0
ns
Hif2α fl/fl
Hif2α fl/fl;Wt1 CreERT2/+

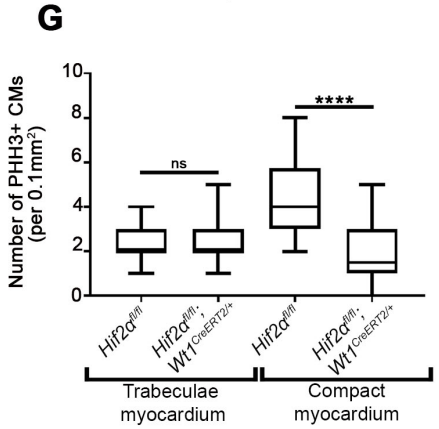

G
Number of PHH3+ CMs (per 0.1mm²)
10
8
6
4
2
0
ns
****
Hif2α fl/fl
Hif2α fl/fl; Wt1 CreERT2/+
Hif2α fl/fl
Hif2α fl/fl; Wt1 CreERT2/+
Trabeculae myocardium
Compact myocardium

Figure 3.5.4 Epicardial-specific loss of Hif2α expression results in a significant reduction in proliferation in the compact myocardium.

A-D. Representative images of immunostaining for PHH3 (green), ACTN2 (red), and DAPI (blue), on coronal sections of hearts from **A-B**. *Hif2α$^{fl/fl}$* (control) or **C-D.** *Hif2α$^{fl/fl}$; Wt1$^{CreERT2/+}$* embryos at stage E16.5. Images **B** and **D** are magnifications of boxed regions in **A** and **C** respectively. Images in top right corner of **B** and **D** are high magnifications of boxed PHH3+ cardiomyocytes (CMs). Arrowheads highlight PHH3+ CMs in the trabeculae myocardium, Arrows indicate PHH3+ CMs in compact myocardium. RV= right ventricle, LV=left ventricle. Scale bars: A, C= 200μm, B, D=50μm, high magnification= 10μm. **E-G**. Quantification of the number of **E**. PHH3+ cells, **F**. PHH3+ cardiomyocytes and **G.** PHH3+ cardiomyocytes in compacted vs. non-compacted (trabeculated) myocardium. n= 4 hearts per group. Data presented as median, IQR and upper and lower limits. Data analysed by **E-F**. student t-test or **G.** one-way ANOVA with Tukey's post-hoc multiple comparisons test. **p<0.01; ****p<0.0001; ns= not significant.

3.5.4 Loss of epicardial *Hif2α* results in defective coronary vessel formation.

The formation of the coronary vasculature was visualised by co-staining of the endothelial marker CD31 with the smooth muscle marker SM22α (Figure 3.5.5A-B). Quantification, of the number of CD31+ and SM22α+ vessels in the compact myocardium, revealed a significant reduction in the number of coronary vessels in *Hif2α$^{fl/fl}$; Wt1$^{CreERT2/+}$* hearts compared to controls (Mean number of vessels per area ± SEM; control: 25.24 ± 1.926; mutant: 14.5 ± 0.8085; n=4 hearts per group; $p<0.0001$; Figure 3.5.5C).

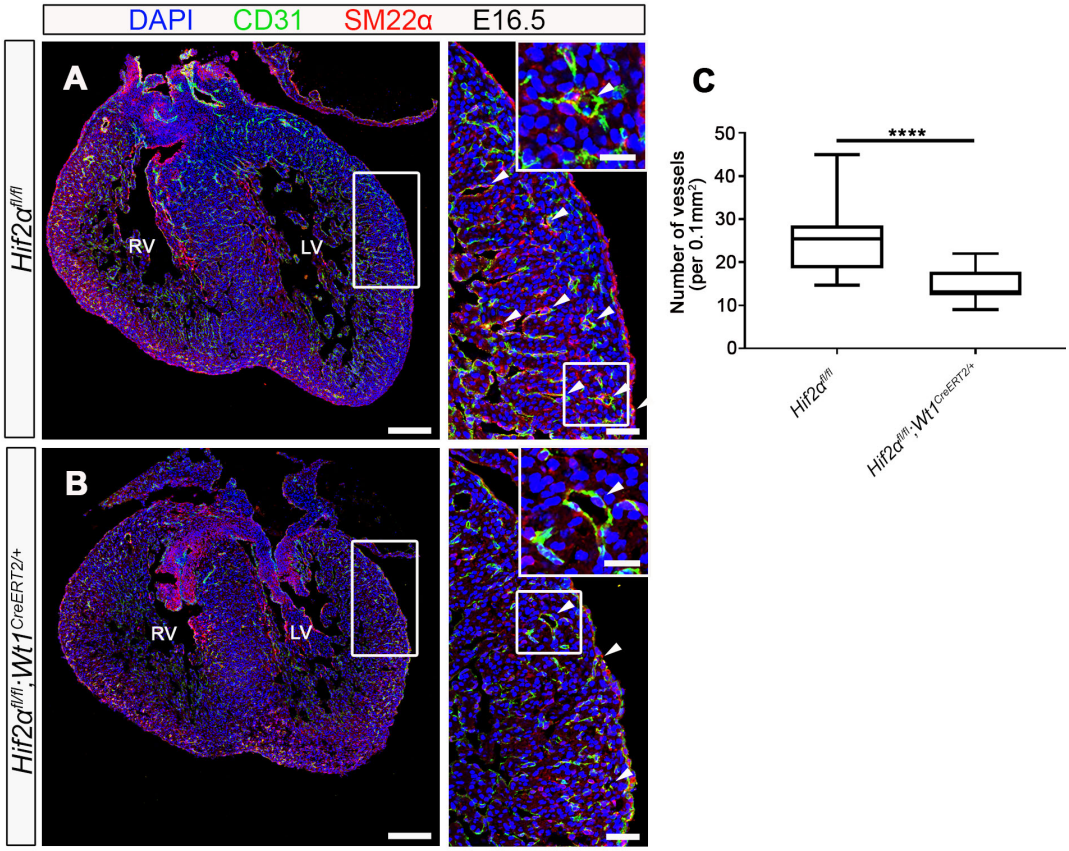


Figure 3.5.5 Loss of *Hif2α* in the epicardial results in a significant reduction in the number of coronary vessels.

A-B. Representative images of immunostaining for CD31 (green), SM22α (red) and DAPI (blue) on coronal sections from **A**. *Hif2α*$^{fl/fl}$ (control) or **B**. *Hif2α*$^{fl/fl}$*; Wt1*$^{CreERT2/+}$ E16.5 hearts. Images to right represent high magnifications of boxed regions. Images in top right corner highlight coronary vessels. Scale bars= 200μm, high magnification scale bars= 50μm and 25μm. Scale bars= 200μm, high magnification scale bars= 50μm. Arrowheads mark CD31+ SM22α+ vessels. **C**. Quantification of the number of CD31+ SM22α+ vessels per 0.1mm^2. n=4 hearts per group. Data presented as median, IQR and upper and lower limits, and analysed by student t-test. ****p<0.0001.

3.6 Discussion

3.6.1 Hypoxia in early heart development

The hypoxia marker, pimonidazole (Hypoxyprobe), has previously been used to assess levels of hypoxia in early heart development. Krishnan and colleagues observed overlap of pimonidazole with cardiomyocytes between E9.0 and E10.0, indicating the early heart develops in hypoxia (Krishnan et al., 2008), but reported negligible pimonidazole expression at E11.5. Conversely, Dunwoodie and colleagues reported expression of pimonidazole in the IVS, the AV canal, and the AV endocardial cushions at E11.5 and E14.5 (Dunwoodie, 2009). Whilst levels of hypoxia in early heart development have been studied extensively, little is known about the later stages of development.

Data presented in this chapter demonstrated that by E12.5 hypoxia was restricted to areas of compact myocardium. Of significance, the strongest signal was observed in the compact wall of the AV groove. Red-horse and colleagues demonstrated coronary vessels originate from near the SV, and spread around the atrioventricular canal (AVC) and outflow tract (OFT) between E11.5-E12.5 (Red-Horse et al., 2010). Therefore, these hypoxic regions near the AV groove may be stimulating coronary vessel formation. In support of this, Lee and colleagues demonstrated that endothelial cells proliferate and form vessels in hypoxic regions of developing organs (Lee et al., 2001).

Hypoxyprobe signal was also present in the IVS at E12.5, which became stronger by E14.5, similar to findings reported by Dunwoodie (Dunwoodie, 2009). Coronary blood flow begins around E13.5, when the coronary vascular

plexus connects to the aortic root (Dyer et al., 2014). Therefore, it is unsurprising that the majority of the heart is no longer hypoxic by E14.5, as it is sufficiently perfused. Interestingly, Tian and colleagues observed that, whilst coronary vessels of the ventricle-free wall arose from sub-epicardial endothelial cells, the majority of coronary vessels of the IVS arose from a different, unknown source. They then demonstrated that the central portion of the septum was not perfused as early as the remainder of the ventricles (Tian et al., 2013). Therefore, the IVS may still be hypoxic by E14.5 as it is not sufficiently perfused, which in turn may act as a signal for coronary vessel formation in the IVS. Further, ventricular septal defects (VSDs) have been reported, following both loss of *Hif1*α or loss of the HIF inhibitor, *Phd2,* or gestational hypoxia, therefore, highlighting the importance of the regulation of HIF signalling in the IVS during development (O'Reilly et al., 2014; Takeda et al., 2006; Yuan et al., 2017).

3.6.2 Hypoxia in the epicardium

Of significance, by E16.5 and E18.5, hypoxyprobe staining was seen almost exclusively in the epicardium, overlapping with the epicardial marker WT1. By E16.5, the heart is sufficiently perfused, by the coronary vessels, therefore, this raised the question as to why the epicardium remains hypoxic, and suggested it is less perfused than the rest of the heart. Whilst perfusion of the epicardium in development has not been explored, Kocabas and colleagues reported the adult mouse epicardium had a lower capillary density than the ventricular myocardium and endocardium (Kocabas et al., 2012). Further, studies in dogs demonstrated, at rest, coronary blood flow to the sub-epicardium was lower

than the myocardium and sub-endocardium (Ball et al., 1975). Taken together, these experiments suggest the epicardium is less perfused than the remainder of the heart and may therefore account for why it is hypoxic during development.

The hypoxic nature of the epicardium during development also raises the question as to whether it has a functional role. The observed hypoxia in the epicardium coincided with the presence of WT1+ EPDCs in the underlying sub-epicardium and myocardium, which had undergone EMT and migrated inward. Hypoxia-induced HIF signalling is a known promoter of EMT (Joseph et al., 2015; Scully et al., 2016). Further HIF1α has previously been shown to regulate expression of *Wt1* (Wagner et al., 2003), and ChIP-seq of the 786-0 ccRCC line, conducted by our collaborators, suggested HIF directly binds to the *Wt1* locus. Therefore, the hypoxic epicardium may be stimulating WT1 positive cells to undergo EMT and migrate. This hypothesis forms the focus of the next chapter of this thesis.

Whilst a hypoxic epicardium during murine development has not been described previously, Kocabas and colleagues reported the adult mouse epicardium as a hypoxic niche in which glycolytic, self-renewing, cardiac progenitors reside (Kocabas et al., 2012). However, most of the characterisation of these cells, termed glycolytic cardiac progenitors (GCPs), was done *in vitro* and, therefore, it remains to be determined whether GCPs exist *in vivo*, under normal homeostatic conditions. As such, we sought to determine if the observed developmental hypoxic epicardium was maintained after birth, in the postnatal period, and continued into adulthood. However,

injecting large volumes of pimonidazole into comparatively small postnatal mice proved technically challenging, and the optimal time-point in which to harvest the hearts, following administration of pimonidazole was unknown. Moreover, the lack of an appropriate positive control made it difficult to determine whether the observed lack of expression was because the heart was no longer hypoxic after birth, or because the adapted protocol was ineffective. As such, postnatal hypoxyprobe staining was not achieved. Future experiments could optimise the protocol on pups born under hypoxic conditions, to act as a positive control, although this would require a home office licence amendment.

In order to validate the hypoxyprobe staining, and to determine if HIF1α was co-expressed with WT1, immunofluorescence with an antibody against HIF1α was tested. However, immunostaining for HIF1α is problematic, due to its rapid degradation upon exposure to oxygen, which occurs during isolation of the tissue, therefore, successful immunostaining was not achieved. Nevertheless, pimonidazole, as a marker of hypoxic tissues, has been validated on numerous occasions (Arteel et al., 1995; Raleigh et al., 1999), hence we can be reasonably confident with the result obtained. Further, immunostaining for the HIF-target GLUT1, used as a surrogate for HIF expression, at stages E12.5 and E14.5 revealed extensive overlap with hypoxyprobe in the AV groove and IVS respectively. Moreover, at E16.5 and E18.5 GLUT1 expression was observed in the epicardium, both validating the hypoxyprobe and suggesting HIF-mediated transcription is active in the epicardium.

3.6.3 Direct interaction of HIF with *Wt1*

During development *Wt1* is expressed in the developing kidneys, as well as the epicardium, and mice lacking *Wt1* exhibit defects in the urogenital system along with heart failure (Moore et al., 1999). ChIP-seq analysis revealed direct binding of HIF to *WT1* in human 786-0 renal cancer cells indicating HIF directly binds and regulates expression of *WT1* in renal cells which may therefore be true in development. To confirm a direct interaction of HIF with *Wt1* in the murine epicardium during development, ChIP-seq on epicardial cells would needed to be performed, initially using an antibody against HIF1β to confirm direct HIF binding, followed by HIF1α and HIF2α, to determine which of the two binds.

Direct binding of HIF to epicardial genes *TCF21, TBX18* and *RALDH2* was not observed in any of the renal cancel cell lines, suggesting they are not directly regulated by HIF, however, they may be indirectly regulated, through *WT1* (Guadix et al., 2011). All three genes are expressed in the kidney during development (Maezawa et al., 2014; Niederreither et al., 2002; Xu et al., 2014a), suggesting the lack of binding was not because these genes are not expressed in renal cells, however, hypermethylation of *TCF21* leading to its silencing, was reported in 786-O cells (Gooskens et al., 2018) and may therefore account for the lack of interaction. Therefore ChIP-seq on developmental epicardial cells would be need to be performed, as described above.

3.6.4 Differential expression of HIF1α and HIF2α in the heart

Expression of both *Hif1α* and *Hif2α,* in the developing mouse heart, has previously been described. *In situ* hybridisation (ISH) analysis, at various developmental stages demonstrated *Hif1α* expression is mainly myocardial, whilst expression of *Hif2α* is restricted to vascular endothelial cells, suggestive of differential roles in cardiac development (Jain et al., 1998). Epicardial-specific expression of *Hif1α* or *Hif2α,* during mouse heart development, has not been previously described. However, it remains unclear whether this is due to a lack of expression, or because studies into their expression patterns in the heart did not look into epicardial expression specifically (Jain et al., 1998). Given our observations, that the epicardium is hypoxic at later stages of development, we hypothesised that either HIF1α or HIF2α would be expressed in the epicardium and would be essential to its function.

3.6.5 The role of HIF1α in the epicardium

Data presented in this chapter revealed that epicardial-specific deletion of *Hif1α* led to a significant reduction in expression of WT1, both in the epicardium and underlying myocardium. Direct regulation of *Wt1* by HIF1α has previously been described (Wagner et al., 2003), and ChIP-seq analysis of ccRCC cells revealed direct binding of HIF to the *Wt1* locus, therefore, during heart development HIF1α may directly bind the promoter of *Wt1* and induce its transcription. Still, a direct, *in vivo* interaction would need to be confirmed, which could be achieved in an unbiased manner by ChIP-seq analysis on mouse epicardial cells.

During development, a subpopulation of epicardial cells undergo EMT, migrate into the developing myocardium and secrete paracrine signals, stimulating cardiomyocyte proliferation and coronary vessel development (Brade et al., 2011; Lavine et al., 2005, 2006). Further, EPDCs have been shown to differentiate into various cell types of the heart, including VSMCs and to some extent endothelial cells, for the coronary vasculature (Cano et al., 2016; Mikawa and Gourdie, 1996; Perez-Pomares et al., 1998). WT1 is an essential mediator of epicardial EMT , therefore, it is likely that a significant reduction in WT1 expression would impair epicardial EMT (von Gise et al., 2011; Martínez-Estrada et al., 2010), having a downstream effect on myocardial maturation and coronary vessel development. In evidence of this, loss of *Hif1*α resulted in a significant reduction in coronary vessels at E15.5, though, it did not affect cardiomyocyte proliferation.

Whilst the decrease in coronary vessels indicates loss of *Hif1*α resulted in an impairment in epicardial EMT, to confirm this, a genetic lineage-tracing approach would need to be utilised, to map epicardial cells and their progeny *in vivo*, in particular to assess changes in VSMC and coronary endothelium fate contribution. However, the most common *Cre*-based lineage tracing system for epicardial fate mapping utilises *Cre* knocked in to the *Wt1* locus, leading to haploinsufficiency (Zhou et al., 2008). Given WT1 expression is significantly reduced following loss of *Hif1*α*,* this lineage tracing system would not be appropriate. A *Tbx18-Cre* reporter could instead be used (Cai et al., 2008), however, reported *Tbx18* expression in cardiomyocytes would confound the interpretation of any results generated with such approach (Christoffels et al., 2009).

Whilst the decrease in coronary vessels could be due to impairment of WT1-mediated EMT, it may have also resulted from a direct effect of aberrant epicardial HIF-signalling on vasculogenesis. HIF1α is known to bind to, and directly regulate expression of pro-angiogenic factors such as *Vegf*, Angiopoietins *Ang1* and A*ng*2 (Forsythe et al., 1996; Kelly, 2003). Thus, loss of H*if1α* in the epicardium may result in a significant reduction in pro-angiogenic signalling, resulting in a decrease in coronary vessel formation. To address this, immunostaining against candidate proangiogenic factors could be performed, however, EPDCs themselves secrete angiogenic factors, thus, a direct regulation by HIF1α would not be determined. Instead, RNA sequencing of *Hif1α*$^{fl/fl}$*; Wt1*$^{CreERT2/+}$ and control hearts could be used to identify differentially expressed genes in an unbiased manner. This could then be coupled with ChIP-seq on epicardial cells, to identify which differentially regulated genes are a direct target of HIF1α in the epicardium.

3.6.6 The role of HIF2α in the epicardium

As for loss of *Hif1α* expression, epicardial-specific deletion of *Hif2α* resulted in a significant decrease in WT1 expression, both in the epicardium and underlying myocardium (reduced EPDC mobilisation). Direct regulation of *Wt1* by HIF2α has not been previously described, however, since a hypoxia responsive element (HRE) has been reported within the *Wt1* locus (Wagner et al., 2003), and HIF1α and HIF2α both bind the same HRE, direct regulation is plausible.

Loss of *Hif2α* in the epicardium resulted in a significant decrease in cardiomyocyte proliferation in the compact layer of the myocardium, along with a significant decrease in coronary vessel number. Transitioning WT1+ EPDCs secrete mitogens, such as FGFs and RA, which stimulate cardiomyocyte proliferation and coronary vessel formation (Chen et al., 2002; Lavine et al., 2006). Therefore, the observed disruption in both of these processes is likely to be directly associated to decreased WT1 expression and subsequent reduction in EPDC mobilisation and signalling.

It is important to note, coronary vessel development and myocardial growth are themselves intrinsically linked, therefore disruption of one could lead to perturbation of the other. Epicardium-derived FGF signalling stimulates cardiomyocytes to proliferate and secrete ANG2, VEGFA and VEGFB to stimulate coronary vasculature development (Lavine et al., 2006). Further, as the myocardium grows and thickens it creates a hypoxic environment, resulting in HIF-mediated induction of VEGF, therefore stimulating coronary vessel development (Nanka et al., 2006). Therefore, at this stage it cannot be ruled out the possibility that impairment in coronary vessel development lies downstream of the effect on cardiomyocyte proliferation. Having said that, it should be mentioned that HIF2α is known to directly bind and activate transcription of pro-angiogenic factors, such as *Vegfa*, *Vegfc* and *Ang4* (Downes et al., 2018), therefore, the significant reduction in coronary vessel number may also be a direct consequence of losing HIF2α-driven angiogenesis.

Loss of *Hif2α* in the epicardium resulted in a thinned compact myocardium coupled with hyper-trabeculation. Myocardial thinning is seen in a number of loss-of-function mutant embryos with epicardial defects (von Gise et al., 2011; Martínez-Estrada et al., 2010; Watt et al., 2004), and in this case, is likely due to the significant reduction in cardiomyocyte proliferation in the compact layer. Whilst signals from the epicardium are particularly important for the development of the compact myocardium, the endocardium acts as an important mitogenic source for the trabeculae myocardium (Grego-Bessa et al., 2007; Del Monte-Nieto et al., 2018). Therefore, it is unlikely the observed hyper-trabeculation is a direct result of perturbed epicardial signalling, but instead is due to the imbalance of the tightly linked processes of myocardial trabeculation and compaction (Grego-Bessa et al., 2007). In support of this, several other studies have reported hyper-trabeculation of the myocardium, following defects in proliferation and growth of the compact layer (Zhang et al., 2013; Zou et al., 2018). Further, the common congenital heart disorder, left ventricular non-compaction cardiomyopathy (LVNC), characterised by hyper-trabeculation and a thinned ventricular wall, is thought to be caused by non-compaction of the ventricular wall (Towbin et al., 2015), however, this remains unproven. Alternatively, hyper-trabeculation may be a compensatory mechanism, to increase perfusion of the cardiac muscle, due to the significant decrease in coronary vessels.

3.6.7 Complementary roles for HIF1α and HIF2α in the epicardium

HIF1α and HIF2α share strong homology in their DNA and HIF1β binding domains, however, they differ in their transactivation domains, and have been shown to have distinct expression patterns and target genes (Covello et al., 2006; Hu et al., 2003a). Therefore, it is interesting that both loss of *Hif1α* and *Hif2α* in the epicardium resulted in a remarkably similar phenotype. Both loss-of-function models resulted in reduced expression of WT1 in the epicardial layer and lower numbers of EPDCs in the sub-epicardial space, coupled with a significant decrease in the number of coronary vessels, suggesting both are expressed in the epicardium and are essential for its activity. It could be argued that the similar phenotype observed in both models was the result of the *Wt1*$^{CreERT2/+}$ driver alone, as the CreERT2 is knocked-in to the endogenous *Wt1* locus, resulting in the functional loss of one *Wt1* allele. However, in initial experiments in which the *Wt1*$^{CreERT2/+}$ line was crossed with a *Rosa26 tdTomato* reporter to assess Cre activity, following tamoxifen administration at E9.5 and E11.5, no phenotype was observed at E12.5, E14.5 or E16.5, suggesting the Cre alone is not sufficient to induce a phenotype. Despite having unique targets, HIF1α and HIF2α do still share some common targets, such as the proangiogenic factor, VEGF, and the epidermal growth factor receptor (EGFR) (Ema et al., 1997; Schodel et al., 2011; Zhang et al., 2012). Thus, functional redundancy by these transcription factors to directly regulate the *Wt1* locus is feasible. However, they may also have distinct targets in the epicardium, and the similar phenotype is as a result of aberrant epicardial signalling as oppose to the dysregulation of one specific gene. Finally, it cannot be ruled out that the similar phenotypes are as a result of perturbing HIF signalling and therefore

altering the hypoxic environment of the developing heart. To address both hypotheses, unbiased assessment of differential expression of transcripts, by RNA-seq, will need to be used to determine dysregulated pathways, coupled with ChIP-seq, to determine unique or common targets of both transcription factors.

Despite similarities in phenotype, following epicardial loss of *Hif1α* or *Hif2α,* loss of *Hif2α* resulted in a more severe phenotype than loss of *Hif1α*. This increase in severity may reflect the fact that whilst both HIF1α and HIF2α are important in the developing epicardium, HIF2α may play a more significant role. However, it is important to note, hearts analysed following loss of *Hif1α,* were collected earlier, at E15.5, when the compact myocardium and coronary vasculature are less developed (Vicente-Steijn et al., 2015). Therefore, in order to properly compare the phenotypes of both loss-of-function models it will be important to harvest and analyse *Hif1α* mutant hearts at E16.5. Likewise, to further examine the role of HIF signalling during epicardial development, specifically complementary roles or functional redundancy across the two transcription factors, it will be important to generate compound double knockouts samples (discussed in 7.3.1).

3.7 Conclusions

The data presented in this chapter demonstrated the epicardium is hypoxic during the later stages of development. Furthermore, loss of function of *Hif1α* or *Hif2α*, resulted in a phenotype indicative of defective epicardial EMT, indicating an as yet unappreciated functional requirement for these transcription factors in the epicardium. Further studies are needed to identify the molecular mechanisms by which HIF signalling converges on epicardium development and identify the essential downstream targets.

4 HIF signalling in epicardial epithelial-to-mesenchymal transition

4.1 Background

During development a sub-set of epicardial cells lose their polarity and migrate into the developing myocardium, in a process known as epithelial-to-mesenchymal transition (EMT). WT1 is a key regulator of this process, with epicardial-specific deletion of *Wt1* resulting in a failure of these cells to undergo EMT (Moore et al., 1999). I*n vivo*, WT1 has been shown to directly bind and upregulate expression of EMT-inducing transcription factor, *Snai1*, whilst directly repressing expression of cell adhesion molecule, e-cadherin (*Cdh1*) (Martínez-Estrada et al., 2010). Further, retinoic acid (RA) and both canonical and non-canonical wnt signalling have been implicated as downstream targets in WT1-mediated EMT (von Gise et al., 2011). However, little is known about the upstream regulators of WT1 in this context.

Hypoxia is a known inducer of EMT, in normal development and cancer progression, with HIF1α acting as an upstream regulator of key mediators of EMT. In glioblastoma, hypoxia was shown to promote a mesenchymal shift, via interaction of HIF1α with the EMT-inducing transcription factor ZEB1 (Joseph et al., 2015). In chick embryos, HIF1α promoted migration of neural crest cells, via upregulation of transcription factors *Sox10* and *Snai2* (Scully et al., 2016). Further, HIF1α was shown to induce endothelial-to-mesenchymal transition (EndMT) in human coronary endothelial cells *in vitro*, through direct upregulation of *Snai1* (Xu et al., 2015).

Importantly, HIF1α has been implicated in epicardial EMT, as persistent HIF1α in the avian epicardium impaired EPDC migration and invasion into the

myocardium *in ovo,* through inhibition of the VEGF pathway (Tao et al., 2013). Further, hypoxia was shown to induce immortalised epicardial cells to differentiate into vascular smooth muscle cells (VSMCs) *in vitro*, although the role of HIF1α was not investigated (Tao et al., 2018). As such, a role for HIF signalling in mammalian and specifically murine epicardial EMT has yet to be elucidated.

4.2 Aims

Work in the previous chapter indicated both HIF1α and HIF2α are important for activation of *Wt1* in the epicardium. Further, loss of *Hif1*α and *Hif2*α resulted in downstream defects on coronary vessel formation and myocardial maturation, indicative of an impairment in epicardial EMT. Given the known role of HIF signalling in EMT in other systems, it was hypothesised that HIF signalling is an inducer of epicardial EMT and may act via *Wt1*. The aim of this chapter was to test this hypothesis by investigating the role of HIF signalling on mouse epicardial EMT *in vitro*, using primary murine explant cultures.

4.3 Epicardial Explant cultures

To assess the importance of HIF signalling on epicardial cell survival and EMT, an *in vitro* epicardial explant approach was used (Chen et al., 2002). Briefly, hearts were isolated from E11.5 embryos, the ventricles halved, and then cultured, epicardial-side down. Epicardial cells migrated out of the cardiac tissue, forming an epithelial sheet, with cells on the outer edge beginning to undergo EMT after 72 hours in culture, much like what is seen *in vivo* during development (Figure 4.3.1).

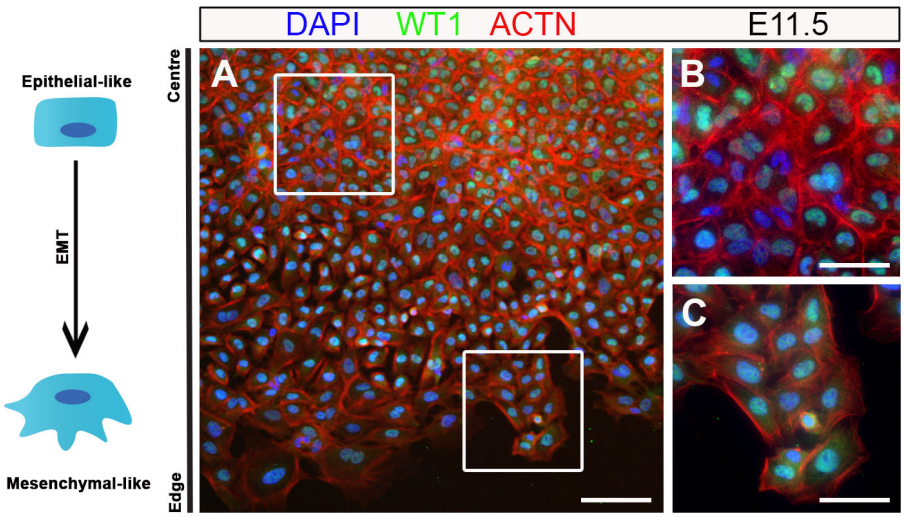


Figure 4.3.1 Murine epicardial explant cultures

A-C. Immunofluorescent images of an epicardial explant, from an E11.5 mouse heart, following 72 hours in culture. WT1 (green) marks epicardial cells, ACTN marks the actin cytoskeleton, and DAPI (blue) marks the nucleus. B and C represent high magnifications of boxed regions in A. **B**. cells at the centre of the explant exhibit an epithelial-like, cobblestone morphology. **C**. cells at the edge exhibit a mesenchymal-like morphology. Scale bar= 100μm, high magnification scale bars= 25μm. EMT= epithelial-to-mesenchymal transition.

To assess the effect of loss-of-function of HIF signalling on epicardial EMT, explants were generated from *Hif1α*$^{fl/fl}$;*Rosa26*$^{+/CreERT2}$ embryos and *Hif2α*$^{fl/fl}$;*Rosa26*$^{+/CreERT2}$ embryos (Gruber et al., 2007; Higgins et al., 2004), in which a tamoxifen-inducible Cre is under the control of the ubiquitous *Rosa26* promoter, thus targeting *Hif1α* or *Hif2α* in all cell types respectively. These mouse strains were obtained from a collaboration with Professor Peter Ratcliffe and Dr Tammie Bishop. Additionally, the effect of a gain-of-function of HIF signalling on epicardial EMT was assessed using explants generated from the previously described, *Phd2*$^{fl/fl}$;*Rosa26*$^{+/CreERT2}$ strain (Mazzone et al., 2009; Takeda et al., 2006), again obtained from the Ratcliffe laboratory. In this model, exon 2 of *Phd2* can be excised by tamoxifen-induced, CRE-mediated recombination, in cells expressing the ubiquitous *Rosa26* locus, resulting in a null allele. In normoxia, PHD2 hydroxylates HIFα, promoting its degradation by the proteasome, therefore, loss of PHD2 leads to stabilisation of HIFα, and consequently a gain-of-function of HIF signalling, independent of oxygen levels (Bruick and McKnight, 2001; Jaakkola et al., 2001). The genetic gain-of-function studies were complemented by the use of PHD inhibitors: Deferoxamine (DFO), ML-228, FG-4592 (Roxadustat), BAY 85-3934 (Molidustat) and IOX4 (Beck et al., 2018; Besarab et al., 2015; Chan et al., 2015; Theriault et al., 2010), on explants generated from wildtype C57BL/6 embryos.

4.4 Genetic gain-of-function of HIF in epicardial explant cultures.

Hearts were harvested from *Phd2*$^{fl/fl}$;*Rosa26*$^{+/CreERT2}$ embryos, and explants generated. After 24 hours in culture, allowing for explant attachment, the active metabolite of tamoxifen, 4-hydroxytamoxifen (4-OHT), was added directly to the culture to induce loss of *Phd2* expression. After a further 24 hours, the cardiac tissue was removed and the remaining epicardial cells were left for an additional 24 hours before fixing (Figure 4.4.1).

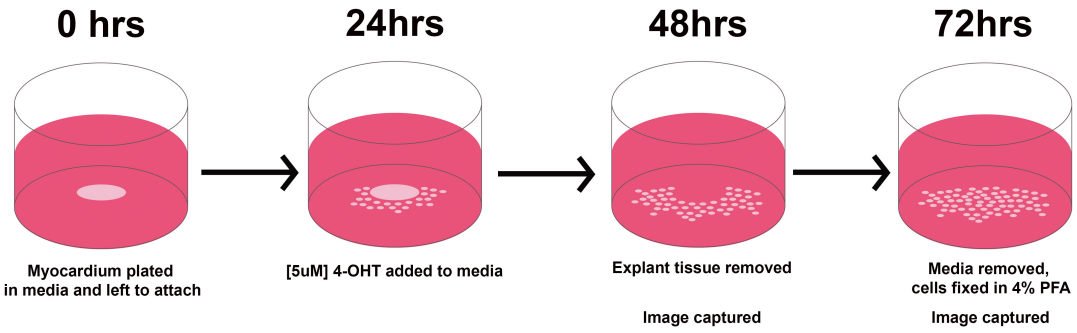


Figure 4.4.1 4-hydroxytamoxifen treatment of epicardial explant cultures
Schematic of 4-OHT treatment of epicardial explant cultures.

4.4.1 Loss of *Phd2* does not affect epicardial explant size

Images of the explants were captured, 24 and 48 hours following 4-OHT administration (i.e. 48 hours and 72 hours in culture, respectively), to enable assessment of growth and survival. ImageJ software was then used to measure the total epicardial surface at these time points, along with the percentage change in size. There was no significant difference in total epicardial surface, following loss of *Phd2* for 24 or 48 hours, when compared to controls (Mean size of epicardial surface [mm^2] ± SEM; [control 24hrs: 1.168 ± 0.189, n=22 explants; mutant 24hrs: 1.486 ± 0.352, n=8 explants; p=0.4074]; [control 48hrs: 2.701 ± 0.380, n=22 explants; mutant 48hrs: 3.421 ± 0.687, n=8 explants; p=0.3387]; Figure 4.4.2A-B). Similarly, the percentage increase in size, over 24 hours, did not reveal any significant differences in rate of growth between mutant and control cultures (Mean % change ± SEM; control: 78.48 ± 10.79, n=22 explants; mutant: 96.48 ± 10.85, n=8 explants; p=0.3364; Figure 4.4.2C). However, large variations in size were observed from explants within the same experimental group, highlighting the variability of this approach.

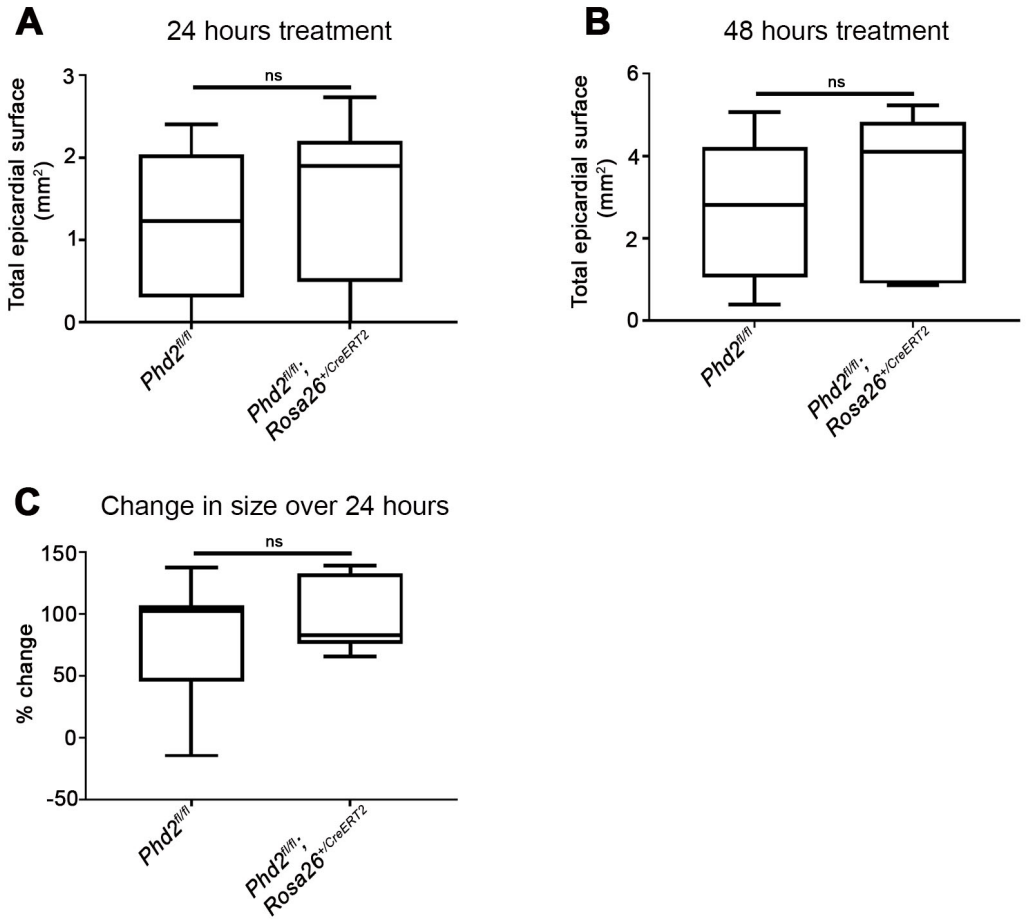


Figure 4.4.2 Loss of *Phd2* does not affect epicardial explant size

A-B. Box and Whiskers plots of the total epicardial surface covered by explants from control (*Phd2*$^{fl/fl}$) or *Phd2*$^{fl/fl}$*;Rosa26*$^{+/CreERT2}$ E11.5 hearts, following **A**. 24 hours or **B**. 48 hours treatment with 4-OHT. **C**. Box and Whiskers plot of the % change in total epicardial surface, from 24 to 48 hours treatment with 4-OHT. n= 22 control explants, n=8 mutant explants. Data presented as median, interquartile range (IQR) and upper and lower limits. Student t-test was used to test for significance, ns = not significant.

4.4.2 Loss of *Phd2* results in stabilisation of HIF1α

The number of epicardial cells obtained per explant was relatively small, therefore, even after pooling 10-12 explants of the same genotype, sufficient levels of RNA or protein could not be extracted to confirm loss of *Phd2* by RT-qPCR or western blot, respectively. As such, the efficiency of gene-targeting was assessed via nuclear expression of the oestrogen receptor alpha (ERα). *Phd2$^{fl/fl}$;Rosa26$^{+/CreERT2}$* mice express a CreER recombinase, consisting of Cre, fused to a mutated ligand binding domain (LBD) of the Oestrogen receptor (ER). Upon binding of 4-OHT to ERα via its LBD, activated CreER recombinase translocates to the nucleus, where it recombines Lox-P flanked DNA (Feil et al., 1997). Therefore, nuclear expression of ERα can be used as a surrogate read-out for Cre activation. Clear nuclear expression of ERα was observed in all *Phd2$^{fl/fl}$;Rosa26$^{+/CreERT2}$* explants, following administration of 5μM of 4-OHT, whilst no nuclear localisation was observed in *Phd2$^{fl/fl}$* controls (Figure 4.4.3A-B).

HIF1α antibody staining is usually problematic, due to the rapid degradation of HIF1α *in vivo*, but given that HIF1α should be stabilised in loss of function models of *Phd2*, immunostaining against ERα was combined with an anti-HIF1α antibody. Control explants showed no nuclear expression of either ERα or HIF1α. In contrast, *Phd2$^{fl/fl}$;Rosa26$^{+/CreERT2}$* explants showed clear nuclear expression of both (Figure 4.4.3A-B), indicating successful stabilisation of HIF1α and therefore a gain-of-function of HIF. To further validate this, expression of the HIF target GLUT1 was assessed, revealing an increase in

GLUT1 expression in *Phd2*$^{fl/fl}$;*Rosa26*$^{+/CreERT2}$ explants compared to littermate controls (Figure 4.4.3C-D).

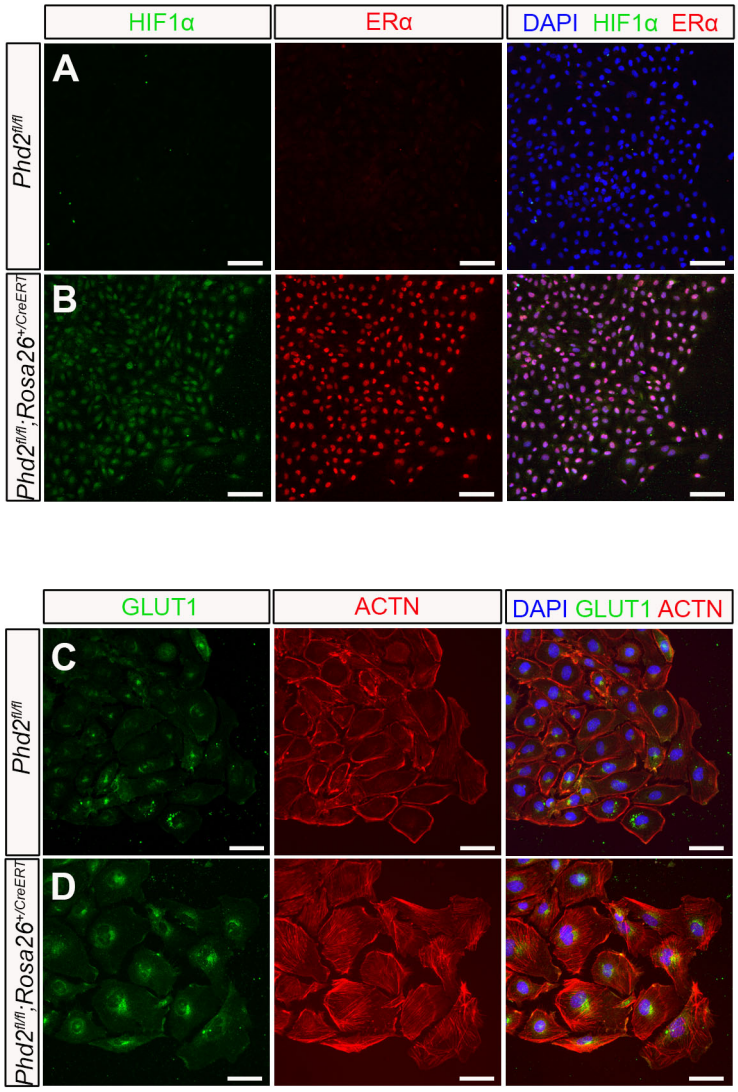


Figure 4.4.3 Loss of *Phd2* results in stabilisation of HIF1α and increased GLUT1 expression.

A-D. Representative images of immunostaining, on explants from E11.5 hearts following treatment with 4-OHT for 48 hours. **A-B**. HIF1α (green), ERα (red) and DAPI nuclear stain (blue) on explants from **A**. Control (*Phd2*$^{fl/fl}$) and **B**. *Phd2*$^{fl/fl}$;*Rosa26*$^{+/CreERT2}$ hearts. Scale bars= 100μm. **C-D**. GLUT1 (green), ACTN (red) and DAPI (blue) on explants from **C**. Control (*Phd2*$^{fl/fl}$) and **D**. *Phd2*$^{fl/fl}$;*Rosa26*$^{+/CreERT2}$ hearts. Scale bars= 50μm. n=4 explants per group.

4.4.3 Loss of *Phd2* does not affect epicardial cell proliferation

To determine if there were any differences in proliferation, the number of epicardial cells expressing Ki67, which is expressed in all active phases of the cell cycle (G_1, S, G_2 and mitosis) but is absent in quiescent cells (G_0), was determined (Gerdes et al., 1983). Both groups had a considerable proportion of cells positive for Ki67 (~30%), but no differences between them were observed (Figure 4.4.4A-C), concordant with the earlier observed lack of difference in size of explant (Figure 4.4.2).

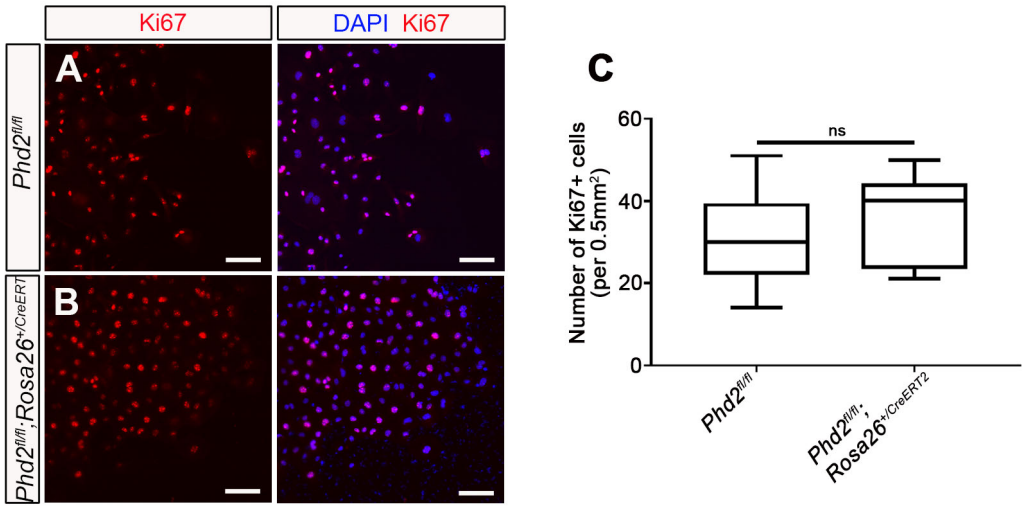


Figure 4.4.4 Loss of *Phd2* does not affect epicardial cell proliferation

A-B. Representative images of immunostaining for Ki67 (red) and DAPI (blue) on explants from **A**. Control (*Phd2*$^{fl/fl}$) and **B**. *Phd2*$^{fl/fl}$;*Rosa26*$^{+/CreERT2}$ E11.5 hearts following treatment with 4-OHT for 48 hours. Scale bars= 100μm. **C**. Quantification of the number of Ki67 positive nuclei, per 0.05mm^2 of explant. Data presented as median, IQR and upper and lower limits. Statistics test= Student t-test, ns= not significant. n=5 control explants, n=3 mutant explants.

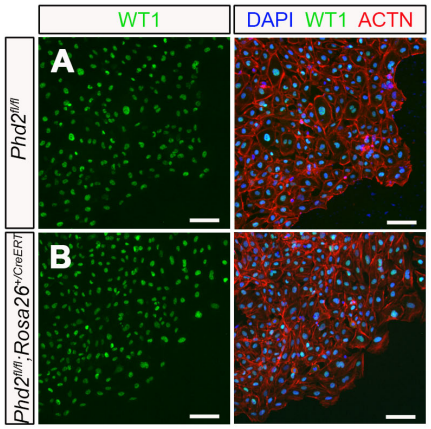
4.4.4 Loss of *Phd2* enhances epicardial EMT

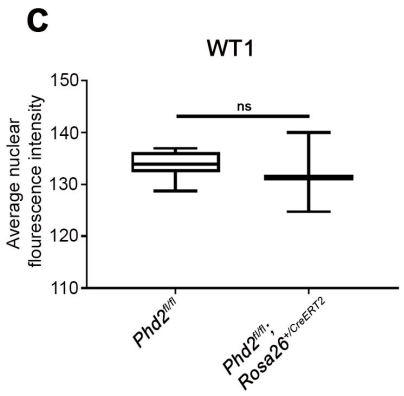
To mechanistically assess the effect of gain-of-function of HIF, explants were initially stained with an antibody against WT1, the master regulator of epicardial EMT. WT1 was widely expressed in both control and KO explants (Figure 4.4.5A-B). ImageJ software was used to measure the nuclear fluorescence intensity of WT1 in each cell, but no significant difference was observed between mutant and control explant cultures (Mean nuclear fluorescence intensity ± SEM; control: 133.90 ± 1.17, n=6 explants; mutant: 132.00 ± 4.42, n=3 explants; p=0.6024; Figure 4.4.5C).

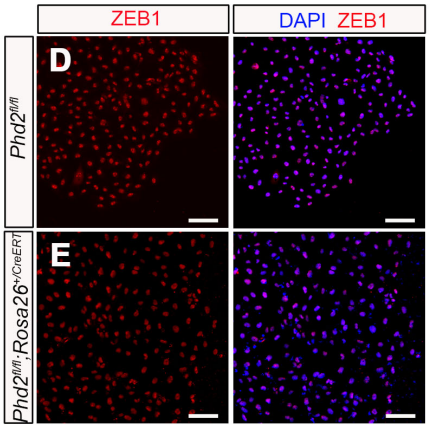
The direct regulation of EMT-inducing transcription factors, ZEB1, SNAI1 and SNAI2 (also known as SLUG), by HIF1α has previously been described and all have been implicated in HIF-mediated EMT, therefore, their expression in the explant cultures was evaluated by immunostaining (Cho et al., 2015; Huang et al., 2009a; Joseph et al., 2015; Xu et al., 2015; Zhang et al., 2015). Surprisingly, expression of ZEB1 was not increased in *Phd2*$^{fl/fl}$*;Rosa26*$^{+/CreERT2}$ versus control epicardial-derived cells (Mean nuclear fluorescence intensity ± SEM; control: 172.20 ± 2.93, n=8 explants; mutant: 162.30 ± 3.64, n=2 explants; p=0.1565; Figure 4.4.5D-F). However, expression of SNAI1/2 significantly increased in *Phd2*$^{fl/fl}$*;Rosa26*$^{+/CreERT2}$ explants compared to controls, indicating that stabilisation of HIF signalling induced SNAI1/2-mediated EMT (Mean nuclear fluorescence intensity ± SEM; control: 636.20 ± 108.20; mutant: 1454.00 ± 334.20; n=6 explants per group p=0.0092; Figure 4.4.5G-I).

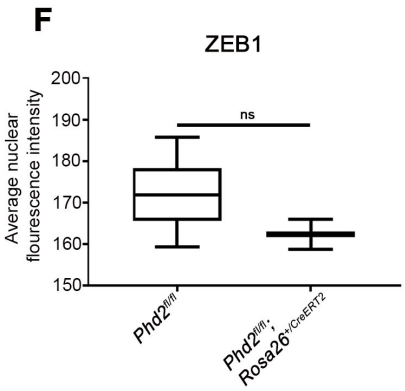
The extent and distribution of filamentous (f)-actin (ACTN) was then visualised using Phalloidin, a toxin which binds to and stabilises f-actin (Chazotte, 2010).

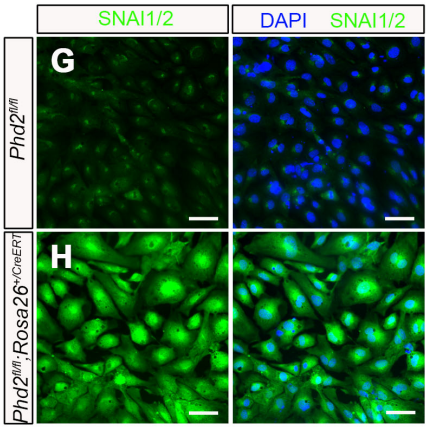
F-actin distribution was used to determine if a cell was more epithelial-like, with actin associated to the cell junctions, in cortical filaments, or more mesenchymal-like, with actin redistributed across the cell in stress fibres, aligned with the direction of cell migration (Bax et al., 2011). The number of epithelial-like and mesenchymal-like cells were counted across several areas per explant, both close to the centre of the explant, where it could be expected for cells to be more epithelial-like, and at the edge where cells should be undergoing mesenchymal transition (Figure 4.4.5J-K). When analysing the explants as a whole there were no significant differences in the proportion of mesenchymal cells, however, when the analysis was focussed on the centre versus the edge of the explant, a considerable increase in mesenchymal-like cells was determined in the centre of *Phd2*$^{fl/fl}$*;Rosa26*$^{+/CreERT2}$ explants compared to controls (Mean % of mesenchymal cells ± SEM; control centre: 29.69 ± 5.42; control edge: 53.15 ± 10.82; mutant centre: 52.35 ± 10.81; mutant edge: 51.09 ± 11.10 n=4 control, n=6 mutant; p=0.5575 [control centre vs mutant centre]; Figure 4.4.5L). This result is important because normally epicardial differentiation is expected to take place at the leading edge of the cell outgrowth by 72 hours, and as such it suggests that loss of *Phd2* led to augmentation of EMT across the explant.

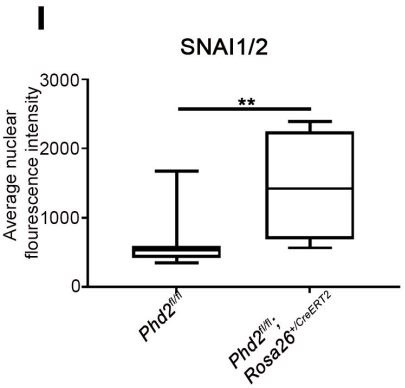

WT1
DAPI WT1 ACTN
A
B
Phd2fl/fl
Phd2fl/fl;Rosa26+/CreERT

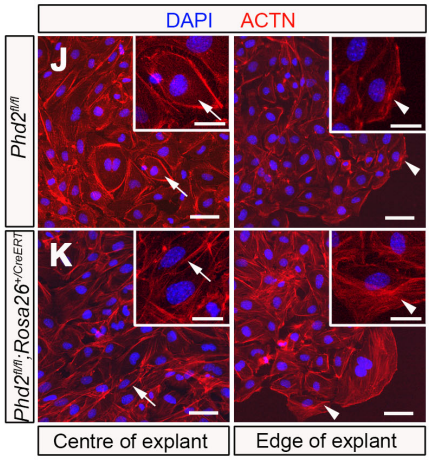

C
WT1
Average nuclear flourescence intensity
150
140
130
120
110
ns
Phd2fl/fl
Phd2fl/fl; Rosa26+/CreERT2


ZEB1
DAPI ZEB1
D
E
Phd2fl/fl
Phd2fl/fl;Rosa26+/CreERT


F
ZEB1
Average nuclear flourescence intensity
200
190
180
170
160
150
ns
Phd2fl/fl
Phd2fl/fl; Rosa26+/CreERT2


SNAI1/2
DAPI SNAI1/2
G
H
Phd2fl/fl
Phd2fl/fl;Rosa26+/CreERT


I
SNAI1/2
Average nuclear flourescence intensity
3000
2000
1000
0
**
Phd2fl/fl
Phd2fl/fl; Rosa26+/CreERT2


DAPI ACTN
J
K
Phd2fl/fl
Phd2fl/fl;Rosa26+/CreERT
Centre of explant
Edge of explant

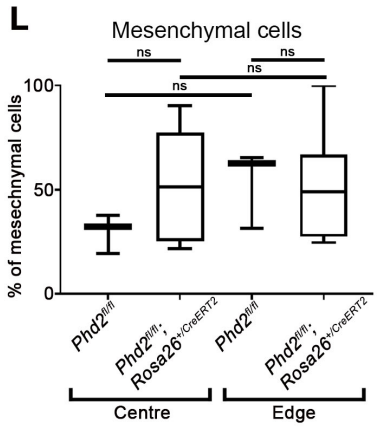

L
Mesenchymal cells
% of mesechnymal cells
100
50
0
ns
ns
ns
ns
Phd2fl/fl
Phd2fl/fl; Rosa26+/CreERT2
Phd2fl/fl
Phd2fl/fl; Rosa26+/CreERT2
Centre
Edge

Figure 4.4.5 Loss of *Phd2* enhances SNAI1/2-mediated epicardial EMT

A-L. Representative images and quantification of immunostaining, to asses EMT, on explants from E11.5 hearts following treatment with 4-OHT for 48 hours. **A-B**. Immunostaining for WT1 (green) and DAPI nuclear stain (blue) on explants from **A**. Control (*Phd2$^{fl/fl}$*) and **B**. *Phd2$^{fl/fl}$;Rosa26$^{+/CreERT2}$* hearts. Scale bars= 100μm. **C**. Quantification of the average nuclear fluorescence intensity for WT1 staining. n=6 control and n=3 mutant explants. **D-E**. Immunostaining for ZEB1 (red) and DAPI (blue) on explants from **D**. Control (*Phd2$^{fl/fl}$*) and **E**. *Phd2$^{fl/fl}$;Rosa26$^{+/CreERT2}$* hearts. Scale bars= 100μm. **F**. Quantification of the average nuclear fluorescence intensity for ZEB1 staining. n=8 control and n=2 mutant explants. **G-H**. Immunostaining of SNAI1/2 (green) and DAPI (blue) on explants from **G**. Control (*Phd2$^{fl/fl}$*) and **H**. *Phd2$^{fl/fl}$;Rosa26$^{+/CreERT2}$* hearts. Scale bars= 50μm. **I.** Quantification of the average nuclear fluorescence intensity for SNAI1/2 staining. n=6 explants per group. **J-K**. Immunostaining for f-actin (red) and DAPI (blue) on explants from **J**. Control (*Phd2$^{fl/fl}$*) and **K**. *Phd2$^{fl/fl}$;Rosa26$^{+/CreERT2}$* hearts. Images in top right corner are high magnifications of example epithelial-like cells (marked by arrow) or mesenchymal-like cells (marked by arrowheads). Scale bars= 50μm, high magnification scale bars= 25μm. **L**. Quantification of the proportion of mesenchymal cells at the centre and edge of explants. n= 4 control and n=6 mutant explants. All graphical data presented as median, IQR and upper and lower limits. **C,F,I.** Student t-test, **L**. one-way ANOVA with Tukey's post-hoc test. **p<0.01; ns= not significant.

4.5 Pharmacological gain-of-function of HIF in epicardial explant cultures.

To complement the genetic approach (above), we aimed to pharmacologically stabilise HIF signalling on epicardial explant cultures, using PHD inhibitors, to further determine its effect on EMT.

Explants were generated from wildtype C57BL/6 E11.5 embryos. After 48 hours in culture, following removal of the cardiac tissue, epicardial cells were treated with either a PHD inhibitor, or DMSO as a vehicle control. After 24 hours treatment, explants were fixed and prepared for immunostaining (Figure 4.5.1).

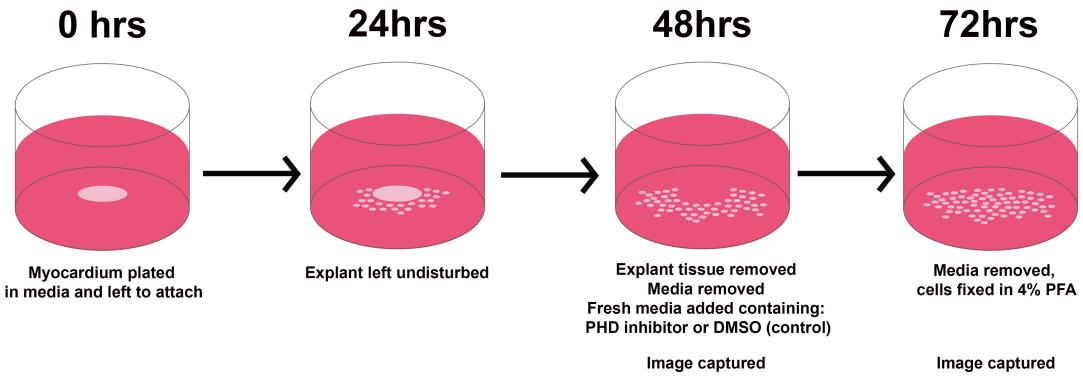


Figure 4.5.1 Pharmacological activation of HIF signalling in epicardial explant cultures.

Schematic of the protocol used for pharmacological activation of HIF signalling in explant cultures from E11.5 C57BL/6 embryos.

4.5.1 Pharmacological inhibition of PHD enzymes results in stabilisation of HIF1α *in vitro*.

Pilot studies were performed using iron chelating compounds, Deferoxamine (DFO) and ML-228, which inhibit the activity of iron-dependant PHDs (Theriault et al., 2010). As reported above, sufficient RNA or protein amounts could not be collected from explant cultures to validate compound efficacy in stabilisation of HIF by qPCR and western-blotting, respectively. Instead, immunostaining for HIF1α was performed, with control explants showing no expression of HIF1α, whilst those treated with DFO and ML-228 exhibited a clear nuclear HIF1α staining signal, suggesting effective stabilisation of HIF. Moreover, actin staining revealed that treated cells were larger in size and more loosely attached, in comparison to the cobblestone morphology (epithelial-like) seen in vehicle-treated controls (Figure 4.5.2A-C). Whilst these pilot studies were

promising, DFO and ML-228 are considered as non-specific inhibitors, affecting not only other 2-oxoglutarate-dependent oxygenases, but also other iron-dependant enzymes beyond PHDs, consequently, the effect observed may not be a direct result of HIF stabilisation and subsequent signalling activation.

Accordingly, the selective and potent PHD inhibitors, FG-4592 (Roxadustat), BAY 85-3934 (Molidustat) and IOX4, kindly provided by our collaborators Professor Peter Ratcliffe and Dr Tammie Bishop, were tested, at a concentration of 50μM (Beck et al., 2018; Besarab et al., 2015; Chan et al., 2015). Co-staining of HIF1α and GLUT1 was performed, to confirm stabilisation of HIF1α. Control explants showed weak or no nuclear HIF1α expression and weak GLUT1 expression (Figure 4.5.3A). In contrast, following treatment with either FG-4592 or BAY 85-3934, epicardial cells showed clear nuclear expression of HIF1α, along with an increase in GLUT1 expression (Figure 4.5.3B-C). However, IOX4 was shown to be toxic at a concentration of 50μM and did not induce nuclear HIF1α expression (Figure 4.5.3D). Additional experiments trialled a lower dose of 10μM of IOX4, but whilst this was not toxic, it led to reduced stabilisation of HIF1α, compared to other PHD inhibitors, and was therefore not carried forward (Figure 4.5.3E). Both treatment with FG-4592 or BAY 85-3934 led to the stabilisation of HIF1α, however, since FG-4592 is already in a phase 3 clinical trial for patients with anaemia, whilst BAY 85-3934 is only in phase 2, the use of FG-4592 was favoured for future experiments, as this pharmacological agent holds greater therapeutic value (Besarab et al., 2015; Provenzano et al., 2016a).

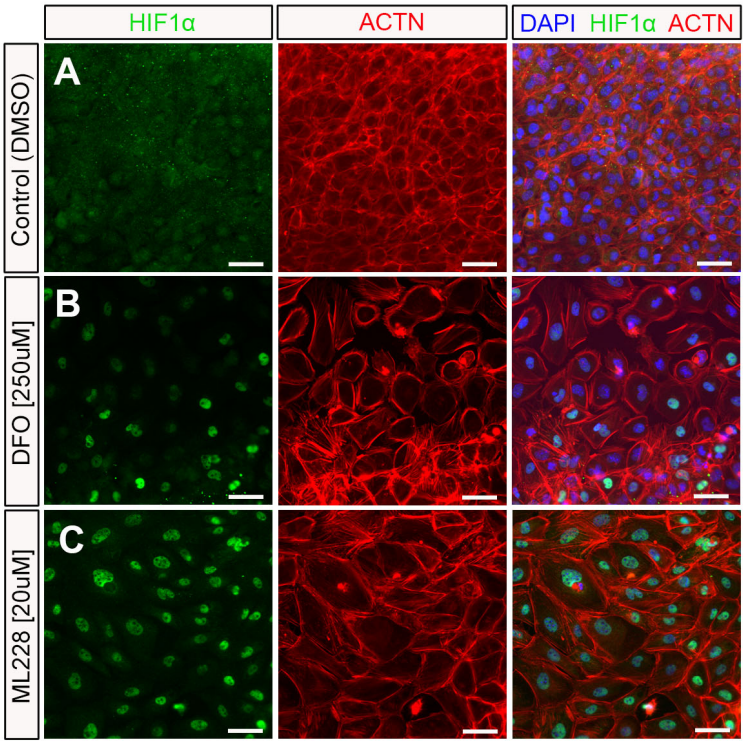


Figure 4.5.2 Pharmacological inhibition of PHD enzymes results in stabilisation of HIF1α

A-C. Representative images of immunostaining for HIF1α (green), ACTN (red) and DAPI (blue), on 72-hour cultured explants from wildtype C57BL/6 E11.5 hearts, following 24 hours treatment with **A.** DMSO (vehicle control), **B.** DFO [250μM] or **C**. ML228 [20μM]. Scale bars= 50μm. n=3 explants per group.

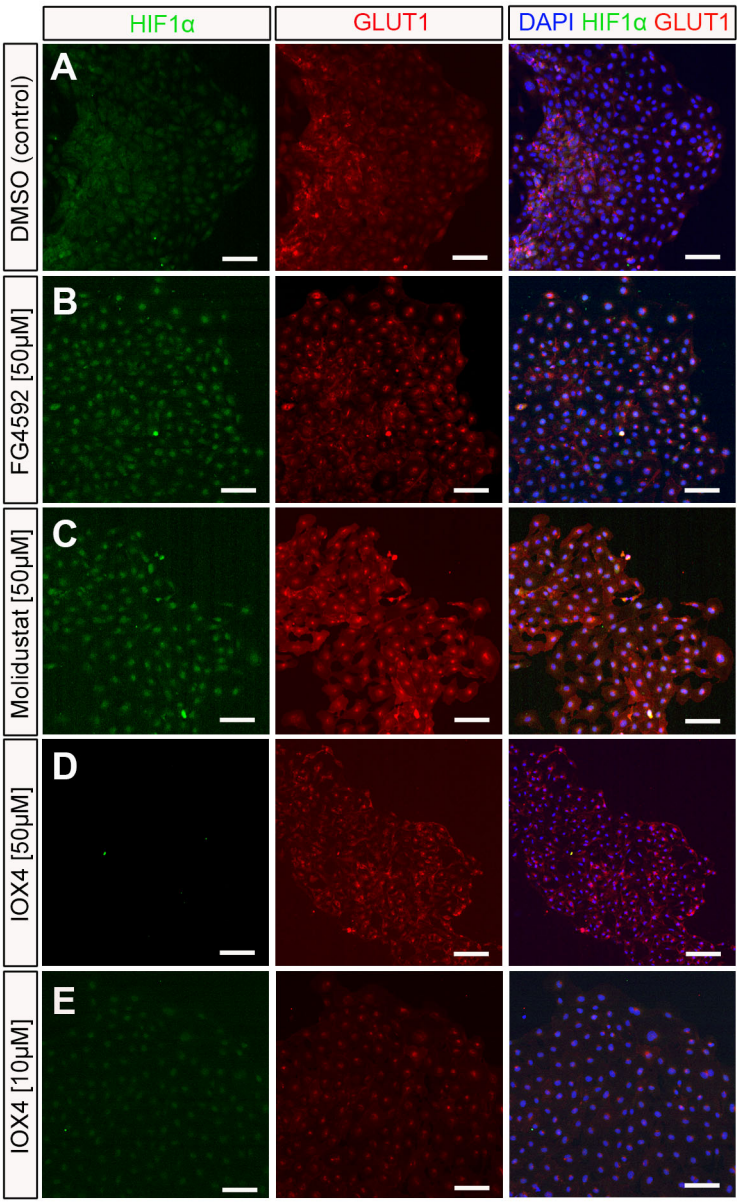


Figure 4.5.3 Selective chemical inhibition of PHD enzymes results in stabilisation of HIF1α and an increase in GLUT1 expression.

A-E. Representative images of immunostaining for HIF1α (green), GLUT1 (red) and DAPI (blue), on 72-hour cultured explants from wildtype C57BL/6 E11.5 hearts, following 24 hours treatment with **A.** DMSO (vehicle control), **B.** FG4592 [50μM] or **C**. BAY 853934 [50μM] or **D**. IOX4 [50μM]. **E**. IOX4 [10μM]. Scale bars= 100μm. n=2 explants per group.

4.5.2 Pharmacological inhibition of PHDs results in a significant increase in WT1 expression and enhances epicardial EMT.

To assess the effect of chemical PHD inhibition on epicardial EMT, expression of EMT regulators, WT1, ZEB1 and SNAI1/2 was again assessed by immunofluorescence. Interestingly, in contrast to genetic loss of *Phd2*, explant analyses revealed inhibition of PHDs1-3, following treatment with FG-4592, led to a significant increase in nuclear WT1 expression, compared to DMSO-treated controls, indicating that stabilisation of HIF signalling leads to *Wt1* activation (Mean nuclear fluorescence intensity ± SEM; control: 311.30 ± 11.89; treated: 392.10 ± 15.99; n=2; p= 0.0037; Figure 4.5.4A-C). Expression of ZEB1 significantly decreased in treated cells (Mean nuclear fluorescence intensity ± SEM; control: 166.80 ± 6.11; treated: 140.20 ± 1.43; n=2; p= 0.0054; Figure 4.5.4D-F), whilst expression of SNAI1/2 increased, although not significantly (Mean nuclear fluorescence intensity ± SEM; control: 192.90 ± 18.81; treated: 232.60 ± 8.56; n=2; p= 0.1268; Figure 4.5.4G-I), indicating a trend towards induction of SNAI1/2-mediated EMT.

The proportion of mesenchymal cells was assessed via distribution of f-actin. In the centre of treated-explants, the proportion of mesenchymal cells was higher than controls, although this was not statistically significant. Moreover, no significant differences in mesenchymal-like cell numbers were found between treated and control explants at the edge of the explants. Nevertheless, whilst in control explants there was a significant increase in the number of mesenchymal cells at the edge of the explant, compared to the centre, in treated-explants there was no difference between the centre and edge of the

explants, suggesting that PHD inhibition by FG-4592 enhanced widespread EMT activation in the explant cultures (Mean % of mesenchymal cells ± SEM; control centre: 14.04 ± 7.86; treated centre: 33.77 ± 6.71; control edge: 73.23 ± 14.79; treated edge: 65.97 ± 12.32; n=2; p= 0.0153 [control centre vs control edge]; p= 0.1151 [treated centre vs treated edge]; p= 0.6321 [control centre vs treated centre]; p=0.6321 [control edge vs treated edge]; Figure 4.5.4J-L).

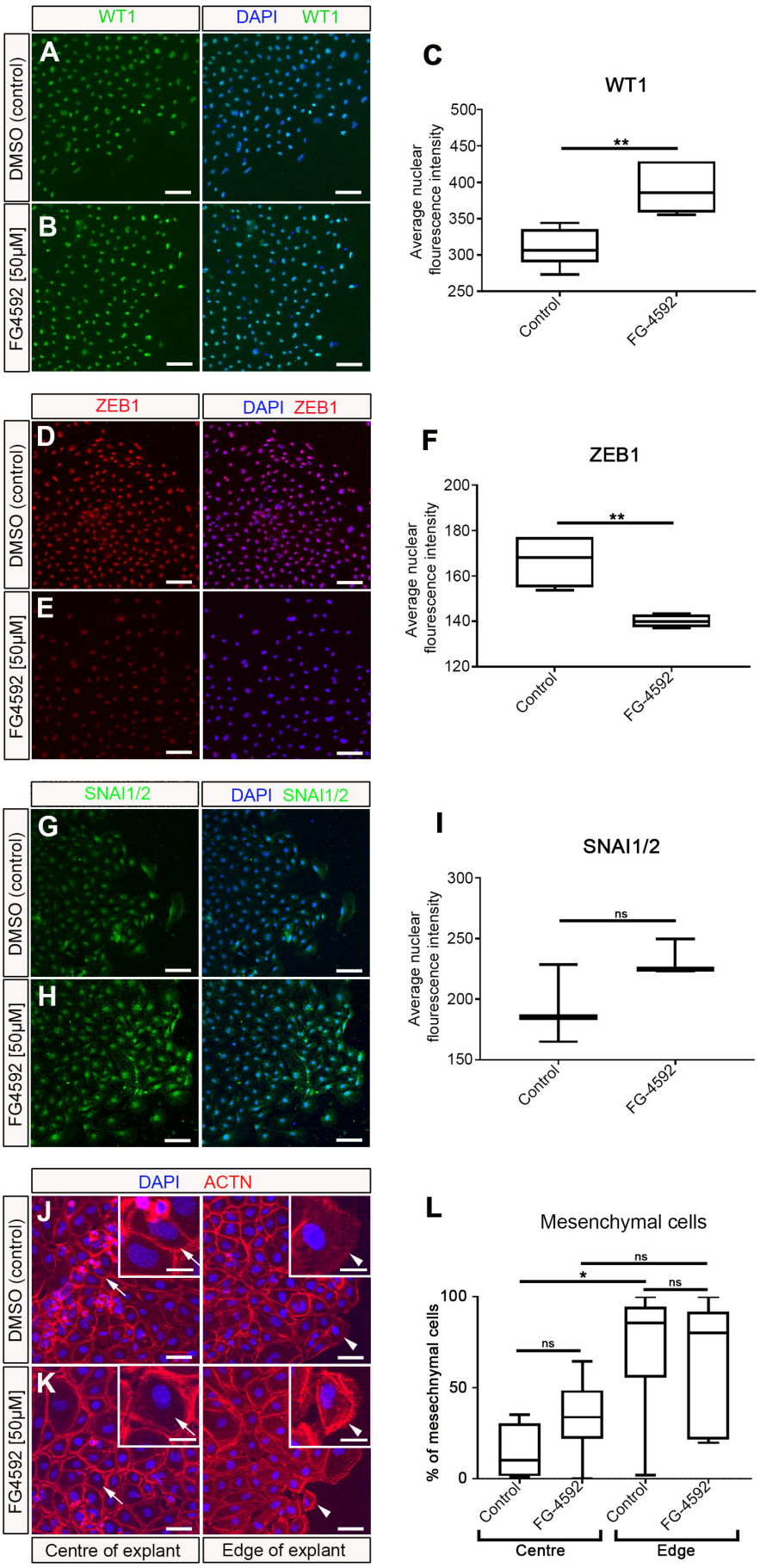

WT1
DAPI WT1
A
DMSO (control)
B
FG4592 [50μM]
C
WT1
Average nuclear flourescence intensity
500
450
400
350
300
250
**
Control
FG-4592
ZEB1
DAPI ZEB1
D
E
F
ZEB1
200
180
160
140
120
SNAI1/2
DAPI SNAI1/2
G
H
I
SNAI1/2
300
250
200
150
ns
DAPI ACTN
J
K
L
Mesenchymal cells
% of mesechnymal cells
100
50
0
*
Centre
Edge
Centre of explant
Edge of explant

Figure 4.5.4 Expression of WT1, the master regulator of epicardial EMT, is significantly increased, following PHD inhibition.

A-K. Representative images and quantification of immunostaining, to asses EMT, on 72-hour cultured explants from wildtype C57BL/6 E11.5 hearts, following 24 hours treatment with a pharmacological agent. **A-B**. Immunostaining for WT1 (green) and DAPI nuclear stain (blue) on explants treated with **A**. DMSO (vehicle-control) or **B**. FG-4592 [50μM]. Scale bars= 100μm. **C**. Quantification of the average nuclear fluorescence intensity for WT1 staining. **D-E**. Immunostaining for ZEB1 (red) and DAPI (blue) on explants treated with **D**. DMSO (vehicle-control) or **E**. FG-4592 [50μM]. Scale bars= 100μm. **F**. Quantification of the average nuclear fluorescence intensity for ZEB1 staining. **G-H**. Immunostaining of SNAI1/2 (green) and DAPI (blue) on explants treated with **G**. DMSO (vehicle-control) or **H**. FG-4592 [50μM]. Scale bars= 100μm. **I.** Quantification of the average nuclear fluorescence intensity for SNAI1/2 staining. **J-K**. Immunostaining for ACTN (red) and DAPI (blue) on explants treated with **J**. DMSO (vehicle-control) or **K**. FG-4592 [50μM]. Images in top right corner are high magnifications of example epithelial-like cells (marked by arrow) or mesenchymal-like cells (marked by arrowheads). Scale bars= 50μm, high magnification scale bars= 25μm. **L**. Quantification of the proportion of mesenchymal cells at the centre and edge of explants. All graphical data presented as median, IQR and upper and lower limits. **C,F,I.** Student t-test, **L**. one-way ANOVA with Tukey's post-hoc test. *$p<0.05$; **$p<0.01$; ns= not significant. n=2 explants per group.

4.6 Genetic ablation of HIF1α in epicardial explant cultures.

4.6.1 Loss of *Hif1α* decreases epicardial explant growth

Explants were generated from *Hif1α$^{fl/fl}$;Rosa26$^{+/CreERT2}$* explants and treated with 4-OHT as previously outlined (Figure 4.3.1). The total epicardial surface of *Hif1α$^{fl/fl}$;Rosa26$^{+/CreERT2}$* explants was significantly smaller than control explants, following 24- and 48-hours treatment with 4-OHT, suggesting that loss of *Hif1α* decreased cell proliferation and/or migration (Mean epicardial surface [mm^2] ± SEM; [control 24hrs: 1.34 ± 0.17, n=22; mutant 24hrs: 7.74 ± 0.08, n=15; p=0.0123]; [control 48hrs: 1.32 ± 0.34, n=22; mutant 48hrs: 0.30 ± 0.06, n=15; p=0.0207]; Figure 4.6.1A-B). Interestingly, calculation of the percentage change in size, from 24 to 48 hours treatment, revealed all *Hif1α$^{fl/fl}$;Rosa26$^{+/CreERT2}$* explants decreased in size over this period, indicating *Hif1α* is important for epicardial cell survival (Mean % change ± SEM; control: -12.34 ± 14.11, n=22; mutant: -60.15 ± 6.76, n= 15; p=0.0136; Figure 4.6.1C), although this would need to be confirmed by a cell death assay, such as terminal deoxynucleotidyl transferase dUTP nick end labelling (TUNEL) staining, which marks double-strand DNA breaks generated during apoptosis. However, whilst an increase in size, over this period, was seen in around half of control explants, a decrease in size was observed in the other half, something that was not observed in control explants in the previous gain-of-function studies. Thus, the concentration of 4-OHT used (5μM) may be toxic to explants from embryos on a Hif1α$^{fl/fl}$ background, and a concentration of 1μM of 4-OHT was trialled instead.

Administration of 1μM of 4-OHT led to no significant differences in total epicardial surface area between *Hif1α$^{fl/fl}$;Rosa26$^{+/CreERT2}$* explants and controls, after either 24- or 48-hours incubation with 4-OHT (Figure 4.6.2A-B). Indeed, all explants increased substantially in size, over this 24-hour period, with no significant difference between the two groups (Figure 4.6.2C).

In order to confirm Cre activity, following a lower dose of 4-OHT, nuclear localisation of ERα was assessed by immunofluorescence. Clear nuclear staining signal was observed in cells from *Hif1α$^{fl/fl}$;Rosa26$^{+/CreERT2}$* explants, indicating activation and nuclear translocation of Cre following binding of 4-OHT (Figure 4.6.2D-E).

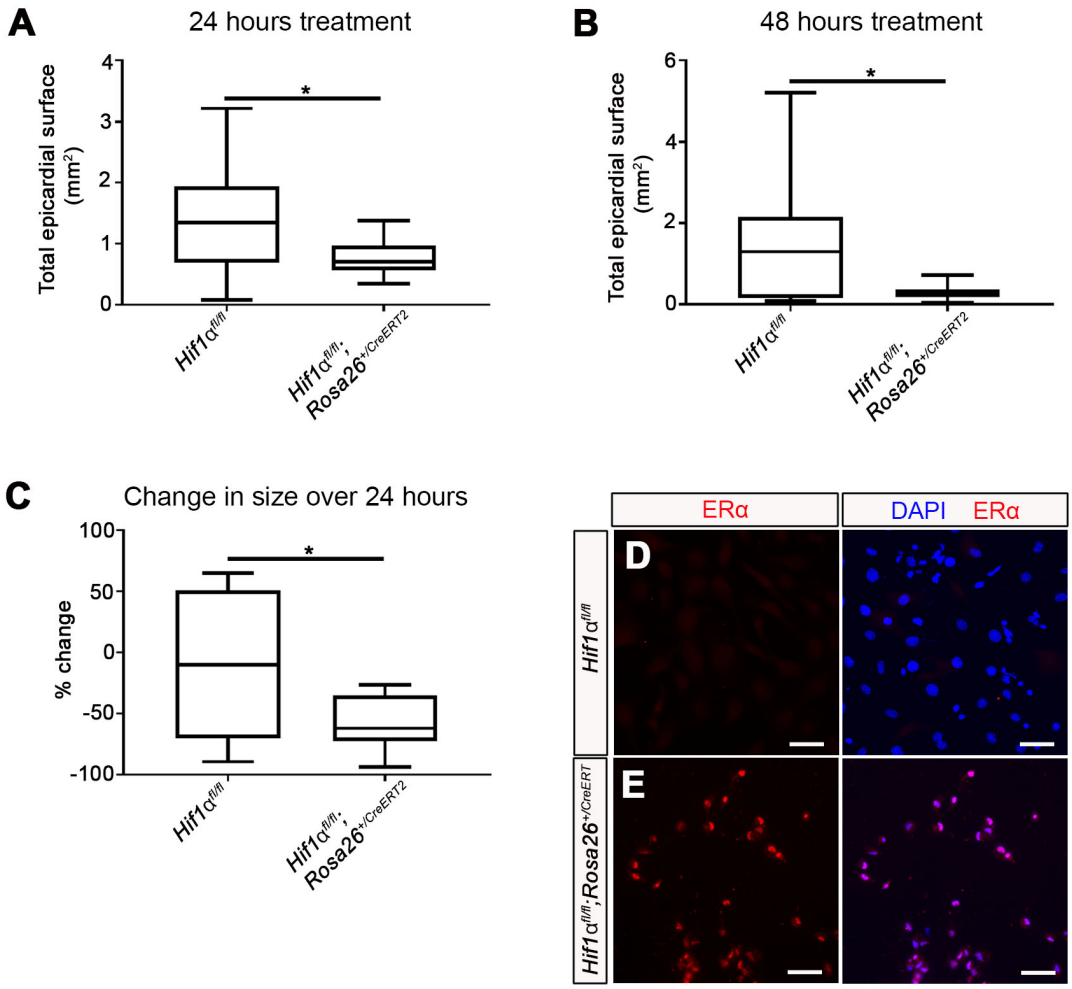


Figure 4.6.1 Loss of *Hif1α* results in a significant decrease in epicardial surface.

A-B. Box and Whiskers plots of the total epicardial surface covered by 72-hour cultured explants from control (*Hif1α*$^{fl/fl}$) or *Hif1α*$^{fl/fl}$*;Rosa26*$^{+/CreERT2}$ E11.5 hearts, following **A**. 24 hours and **B**. 48 hours treatment with 5 μM 4-OHT. **C**. Box and Whiskers plot of the % change in total epicardial surface, from 24 to 48 hours treatment with 5μM of 4-OHT. n= 22 control, n=15 mutant explants. Data presented as median, IQR and upper and lower limits. Statistical tests= Student t-test; *p<0.05. **D-E**. Representative images of immunostaining for ERα (red) and DAPI (blue) on **D**. control (*Hif1α*$^{fl/fl}$) or **E**. *Hif1α*$^{fl/fl}$*;Rosa26*$^{+/CreERT2}$ E11.5 hearts. n= 6 explants control n=4 explants mutant. Scale bars= 50μm.

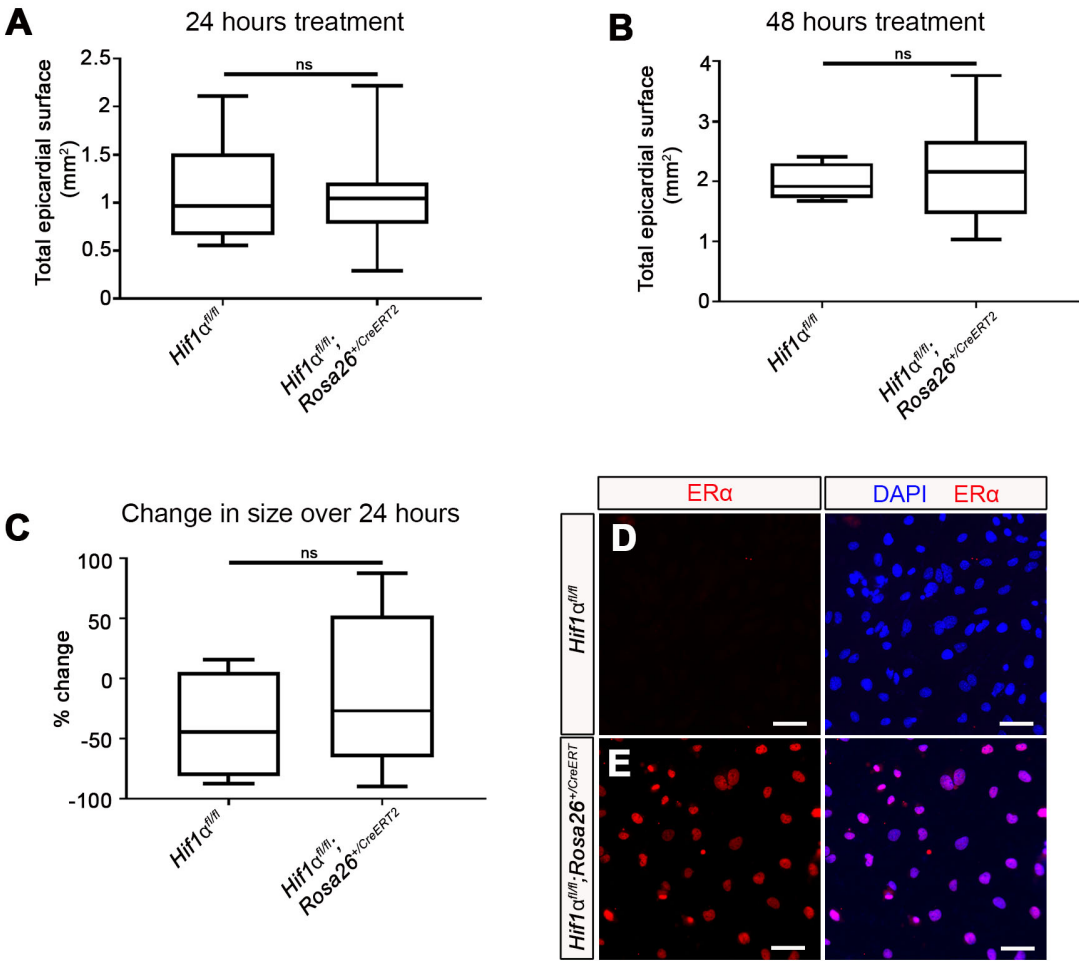


Figure 4.6.2 A lower dose, of 1μm of 4-OHT, decreases its toxic effects and results in Cre activation.

A-B. Box and Whiskers plots of the total epicardial surface covered by 72-hour cultured explants from control (*Hif1α*$^{fl/fl}$) or *Hif1α*$^{fl/fl}$*;Rosa26*$^{+/CreERT2}$ E11.5 hearts, following **A**. 24 hours and **B**. 48 hours treatment with 1 μM 4-OHT. **C**. Box and Whiskers plot of the % change in total epicardial surface, from 24 to 48 hours treatment with 1μM of 4-OHT. n= 15 control, n=26 mutant explants per group. Data presented as median, IQR and upper and lower limits. Statistical tests= Student t-test; ns= not significant. **D-E**. Representative images of immunostaining for ERα (red) and DAPI (blue) on **D**. control (*Hif1α*$^{fl/fl}$) or **E**. *Hif1α*$^{fl/fl}$*;Rosa26*$^{+/CreERT2}$ E11.5 hearts. n= 4 control, n=7 mutant explants. Scale bars= 50μm.

4.6.2 Loss of HIF1α results in a reduction in epicardial EMT

Immunofluorescence was used to assess the effect of loss of *Hif1α* on epicardial EMT. Explants were stained with an antibody anti-WT1, which revealed widespread expression in *Hif1α$^{fl/fl}$;Rosa26$^{+/CreERT2}$* explants. Accordingly, quantification of nuclear fluorescence intensity revealed no difference in expression compared to controls (Figure 4.6.3A-C).

Actin distribution was used to determine the number of epithelial-like and mesenchymal-like cells, both at the centre and edge of the explant. There was no significant difference, in the proportion of mesenchymal cells in the centre of explants, between mutant and control, with the majority of cells exhibiting an epithelial-like morphology. In contrast, a significant reduction in the proportion of mesenchymal cells at the edge in *Hif1α$^{fl/fl}$;Rosa26$^{+/CreERT2}$* explants was observed, indicating an inhibition of EMT (Mean % of mesenchymal cells ± SEM; control centre: 23.95 ± 5.75; control edge: 69.14 ± 14.62; mutant centre: 20.18 ± 3.75; mutant edge: 33.90 ± 8.59 n=4 control, n=6 mutant; ; p= 0.9681 [control centre vs mutant centre]; p=0.0237 [control edge vs mutant edge]; Figure 4.6.3D-F).

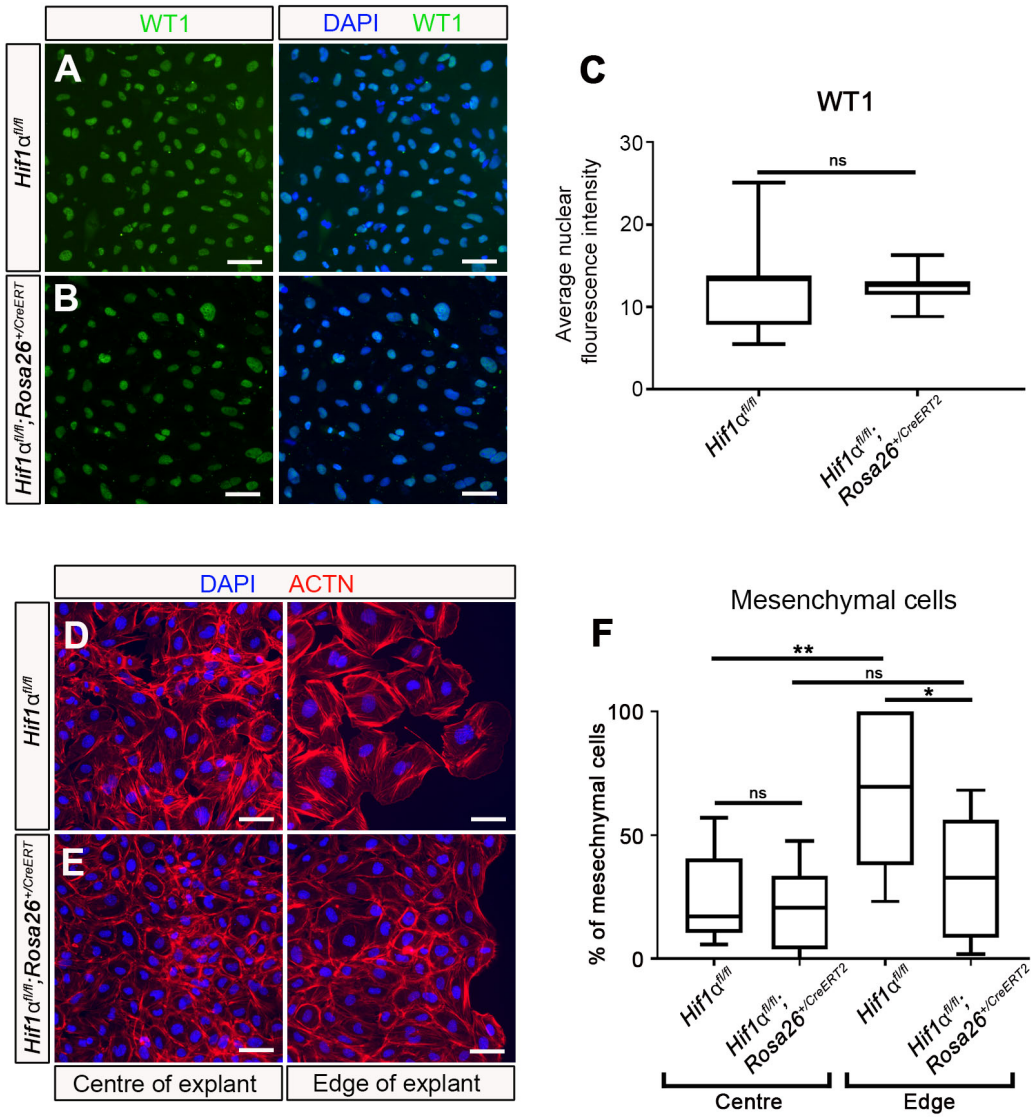


Figure 4.6.3 Loss of *Hif1α* results in a significant decrease in epicardial EMT.

A-F. Representative images and quantification of immunostaining, to asses EMT, on 72-hour cultured explants from E11.5 hearts following treatment with 4-OHT for 48 hours. **A-B**. Immunostaining for WT1 (green) and DAPI nuclear stain (blue) on explants from **A**. Control (*Hif1α*$^{fl/fl}$) and **B**. *Hif1α*$^{fl/fl}$*;Rosa26*$^{+/CreERT2}$ hearts. Scale bars= 100μm. **C**. Quantification of the average nuclear fluorescence intensity for WT1 staining. **D-E**. Immunostaining for f-actin (red) and DAPI (blue) on explants from **D**. Control (*Hif1α*$^{fl/fl}$) and **E**. *Hif1α*$^{fl/fl}$*;Rosa26*$^{+/CreERT2}$ hearts. Scale bars= 50μm. Arrows highlight example epithelial-like cells, arrowheads highlight example mesenchymal cells. **F**. Quantification of the proportion of mesenchymal cells at the centre and edge of explants. All graphical data presented as median, IQR and upper and lower limits. **C.** Student t-test, **F**. one-way ANOVA with Tukey's post-hoc test. *p<0.05; **p<0.01; ns= not significant. n=4 controls, n=7 mutants.

4.7 Genetic loss of *Hif2α* in epicardial explant cultures

Experiments in the previous chapter indicated a role for HIF2α in epicardial development, therefore, the role of HIF2α on epicardial EMT *in vitro* was assessed through a similar approach as above, using embryos generated from a *Hif2α$^{fl/fl}$; Rosa26$^{+/CreERT2}$* line (Gruber et al., 2007).

4.7.1 Loss of *Hif2α* results in a decrease in epicardial explant growth.

Following culture with 5μM of 4-OHT, explants derived from *Hif2α$^{fl/fl}$; Rosa26$^{+/CreERT2}$* hearts were significantly smaller in size than controls, after 24 hours incubation with 4-OHT, suggesting that HIF2α may be important for epicardial cell proliferation and/or migration (Mean ± SEM; control 24hrs: 1.359 ± 0.138, n=17; mutant 24hrs: 0.503 ± 0.077, n= 30; $p<0.0001$; Figure 4.7.1A). However, as for the HIF1α loss-of-function experiments, many of the explants, including the controls had decreased in size by 48 hours, indicating toxicity of tamoxifen at this concentration (Figure 4.7.1B-C). Additional explants were not treated with a lower dose of 4-OHT, as with the *Hif1α$^{fl/fl}$; Rosa26$^{+/CreERT2}$* explants, due to a lack of available mice. Therefore, future experiments, discussed in section 7.3.1, will be conducted to investigate a role for *Hif2α* in epicardial EMT *in vitro*.

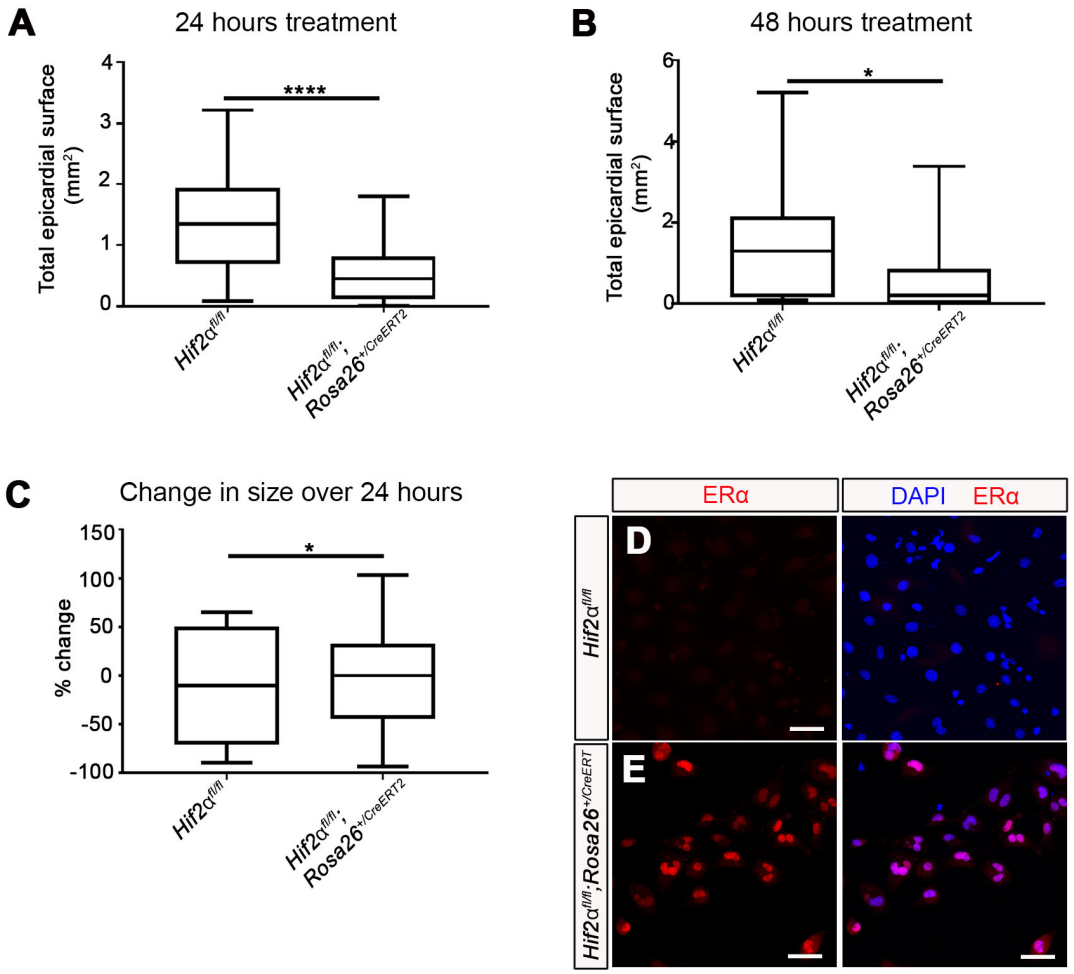


Figure 4.7.1 Loss of *Hif2* results in a significant decrease in epicardial explant size.

A-B. Box and Whiskers plots of the total epicardial surface covered by explants from control (*Hif2α*$^{fl/fl}$) or *Hif2α*$^{fl/fl}$*;Rosa26*$^{+/CreERT2}$ E11.5 hearts, following **A**. 24 hours and **B**. 48 hours treatment with 5 μM 4-OHT. **C**. Box and Whiskers plot of the % change in total epicardial surface, from 24 to 48 hours treatment with 5μM of 4-OHT. n= 17 control, n= 30 mutant explants. Data presented as median, IQR and upper and lower limits. Statistical tests= Student t-test *p<0.05; ****p<0.0001. **D-E**. Representative images of immunostaining for ERα (red) and DAPI (blue) on **D**. control (*Hif2α*$^{fl/fl}$) or **E**. *Hif2α*$^{fl/fl}$*;Rosa26*$^{+/CreERT2}$ E11.5 hearts. n= 5 control, n=8 mutant explants. Scale bars= 50μm.

4.8 Discussion

4.8.1 Genetic gain-of-function of HIF

Following stabilisation of HIF, via genetic loss of *Phd2* expression, a significant increase in the EMT-inducing transcription factors SNAI1/2, along with an increase in proportion of mesenchymal cells was observed *in vitro*, indicating HIF induces epicardial EMT.

Surprisingly, increased SNAI1/2 expression was not coupled with an increase in WT1, suggesting induction of EMT independent of WT1. Whilst this is possible, since HIF1α is known to directly bind *Snai1* and *Snai2* (Huang et al., 2009a; Xu et al., 2015), it is unexpected since WT1 had been shown to be essential for epicardial EMT (von Gise et al., 2011; Martínez-Estrada et al., 2010). Importantly, *in vivo*, following induction of EMT and migration into the myocardium, EPDCs downregulate WT1 expression as they differentiate into VSMCs and ECs (Perez-Pomares et al., 2002). Therefore, a difference in WT1 expression may not be observed since some cells have already undergone EMT and begun to downregulate expression of WT1. SNAI1/2 are extremely liable proteins, readily degraded by the proteasome, therefore, downregulation, following induction of EMT would also be expected. However, F-box E3 ubiquitin ligase (FBX114), which usually promotes the ubiquitylation and degradation of SNAI1, is potently downregulated in hypoxia, leading to the stabilisation of SNAI1 (Vinas-Castells et al., 2010). Therefore, HIF may be inducing transcription of SNAI1/2 (directly or via WT1) and concomitantly promoting its stabilisation.

4.8.2 Differences in pharmacological and genetic inhibition of *Phd2*

Pharmacological activation of HIF signalling, following treatment with the selective and potent PHD inhibitor FG-4592, resulted in a significant increase in WT1 expression and a significant decrease in ZEB1 expression, whilst the increase in SNAI1/2 was not significant.

These differences in outcome may be due to technical differences in experimental approaches. In the genetic studies, explants were treated with 4-OHT for 48 hours, to allow for sufficient time for CRE-mediated recombination, before fixation (Fuhrmann-Benzakein et al., 2000). However, in the pharmacological inhibition studies, explants were treated with FG-4592 for only 24 hours, since it is fast acting (Hansson et al., 2017). Whilst Cre-mediated recombination in culture can take up to 24 hours it may occur more quickly, therefore, explants with genetic loss of *Phd2* may have been exposed to active HIF signalling for longer than those treated with FG-4592. As previously mentioned, WT1 expression is downregulated following epicardial EMT, therefore, genetic loss of *Phd2* may have resulted in a significant increase in WT1, similar to FG-4592 treatment, but expression may have already been downregulated at the point of fixation. Moreover, the peak in SNAI1/2 expression, following treatment with FG-4592, may not have been reached, after only 24 hours treatment, particularly if it is downstream of *Wt1* activity. To assess this further *Phd2*$^{fl/fl}$*;Rosa26*$^{+/CreERT2}$ explants and FG-4592 treated explants would need to be collected at various time points to determine the effect on WT1 and SNAIL expression over-time.

Another possible reason for the difference between the genetic and pharmacological approach, is because FG-4592 is a selective and potent inhibitor of all PHD enzymes (PHD1-3), whilst the genetic approach only resulted in loss of *Phd2* expression. Therefore, in the genetic model, *Phd2* loss may be compensated for by an increase in PHDs1 and 3, resulting in decreased stabilisation of HIF compared to FG-4592 treatment. Additionally, whilst all 3 PHD enzymes act on HIF1α and HIF2α, the more abundantly expressed, PHD2, appears to be more important for controlling levels of HIF1α, whilst the more tissue restricted isoforms, PHD1 and PHD3, appear to preferentially regulate HIF2α (Appelhoff et al., 2004; Berra et al., 2003). Therefore, the increased WT1 expression, following treatment with FG-4592, could be due to stabilised HIF2α. Genetic loss-of-function studies of other PHDs separately and in combination could be used to assess this further. Likewise, loss-of-function of HIF1α and HIF2α could be informative to further dissect out the role of HIF signalling in epicardial EMT.

4.8.3 Genetic loss-of-function of HIF

To that end, loss-of-function of *Hif1α* and *Hif2α* epicardial explant studies were carried out. Following loss of *Hif1α* or *Hif2α,* epicardial explants exhibited a significant reduction in size and growth compared to controls, arguing for a functional requirement for explant outgrowth and survival. However, a similar effect in explant size was also observed in control explants, indicating that the levels of 4-OHT used may be toxic and contribute directly to the observed changes in size/survival. This was unforeseen, since it was not observed in *Phd2$^{fl/fl}$* experiments conducted in parallel, under the same conditions, and may

therefore reflect differences in the genetic background of the different models used.

As such, a concentration of 1μM of 4-OHT was trialled in *Hif1α;Rosa26*$^{+/CreERT2}$ explants. Treatment with the lower concentration of 4-OHT led to nuclear accumulation of ERα as well, and therefore likely CRE activity, but did not result in a significant change in explant size. This suggests that the observed difference in explant size was likely due to tamoxifen toxicity, therefore, experiments with *Hif2α;Rosa26*$^{+/CreERT2}$ explants will also need to be repeated at a lower dose of 4-OHT. Immunofluorescence staining revealed no significant difference in WT1 expression following loss of *Hif1α*, which was unexpected given that epicardial specific loss of *Hif1α in vivo* led to a significant reduction in WT1. This may reflect differences between *in vitro* and *in vivo* systems (discussed in section 4.8.4) or may be due to insufficient knockdown (KD) of *Hif1α in vitro*. Therefore, different doses of 4-OHT should be trialled and a protocol for RNA extraction optimised to enable absolute quantification of KD. However, the experiments did reveal a significant decrease in proportion of mesenchymal cells, suggesting loss of *Hif1α* results in a decrease in epicardial EMT, therefore, it would be interesting to look at expression of SNAI1/2 in these explants to determine if they were decreased.

Corresponding experiments were not conducted for *Hif2α;Rosa26*$^{+/CreERT2}$ explants due to a lack of available mice, therefore, future experiments are needed to determine the role of HIF2α in epicardial EMT *in vitro* (discussed in 7.3.1). Furthermore, double knock-out *Hif1α;Hif2α;Rosa26*$^{+/CreERT2}$ explants

should be generated to determine the effect that complete loss of HIF signalling has on epicardial EMT.

4.8.4 Limitations

Whilst the *in vitro* experiments presented in this chapter indicate that HIF signalling impacts on WT1 and SNAI1/2 expression and enhances epicardial EMT, there are several limitations to the approach. Firstly, analysis of control explants revealed substantial changes in total size, and variations in morphology of cells, thus highlighting the inherent variability associated with this approach arising from difficulties in controlling explant size and attachment timing, which affect cell outgrowth capacity, across different experiments. To overcome these technical limitations, more *n* numbers would be needed to account for variability.

Secondly, due to low cells numbers, genetic recombination could not be confirmed by RT-qPCR or western blot. Instead, a surrogate approach based on the nuclear translocation of the ERα upon binding of 4-OHT was used to infer Cre activity. This is suboptimal, as nuclear localisation of ERα does not directly reflect efficient Cre recombination of “floxed” alleles. To overcome this caveat, the alleles of interest could be crossed into a reporter background, which expresses a fluorescent protein upon successful Cre recombination, e.g. *Rosa26-EYFP* or *Rosa26-tdTomato* (Hasegawa et al., 2013). Additionally, RNA extraction could be optimised, to enable measurement of transcript levels of the target gene by RT-qPCR.

Experiments conducted in this chapter used the ubiquitous *Rosa26*$^{+/CreERT2}$ driver, due to the readily availability of these mice. Whilst the observed widespread expression of WT1 indicated the vast majority of outgrown cells were epicardial, or epicardial derivatives, the presence of non-epicardial cells cannot be excluded, further, the myocardial tissue was also present in the culture. Therefore, to exclude the possibility of non-epicardial cells masking the epicardial phenotype, future studies should utilise the epicardial specific *Wt1*$^{CreERT2/+}$ driver (Zhou et al., 2008).

Finally, the major caveat of this approach, is that whilst epicardial explant cultures more closely recapitulate epicardial development, than an epicardial cell line, the cells have still been removed from their natural microenvironment which is likely to have a significant impact on their behaviour. Of significance, whilst *in vivo* O_2 conditions range from around 1-11%, *in vitro* oxygen tension can vary substantially between wells, due to factors such as the surface area and volume of liquid, and the number and activity of the cells. Moreover, the mechanical properties, bought about by the extracellular matrix (ECM), such as stiffness and confinement, along with direct interaction with ECM proteins, such as laminin and fibronectin, are lost, which could affect EMT (Chen et al., 2013; Kumar et al., 2014; Mercer et al., 2013).

4.8.5 Therapeutic potential

Despite the limitations with this approach, genetic GOF of HIF, through loss of *Phd2*, led to an enhancement of epicardial EMT. Taken together with the *in vivo* HIF studies (Chapter 3), they implicate a role for HIF signalling in epicardial EMT. This highlights the need to conduct *in vivo* studies involving loss of *Phd2*

in the epicardium to determine if an increase in epicardial EMT would be observed (discussed in 7.3.2). Importantly, it raises the question of whether activating HIF signalling following myocardial infarction, could enhance epicardial EMT following injury, and improve the regenerative response.

Of significance, the observed enhancement of EMT, following loss of *Phd2*, was replicated, following treatment with the potent and selective inhibitor of PHDs 1-3, FG-4592. FG-4592 is currently in a phase III clinical trial for patients with anaemia and *in vitro* work has demonstrated its therapeutic potential for both Parkinson's disease and wound healing (Li et al., 2018; Tang et al., 2018). Therefore, FG-4592 presents an exciting potential therapeutic for augmenting epicardial EMT.

4.9 Conclusions

The experiments presented in this chapter suggest HIF signalling induces epicardial EMT *in vitro*, through increased expression of transcription factors WT1 and SNAI1/2. Taken together, with the results from the previous chapter, these findings support a previously unappreciated role for HIF signalling in epicardial activation and EMT during development.

5 The epicardial response to injury in the neonatal mouse heart

5.1 Background

The neonatal mouse is capable of mounting a substantial response to heart injury, though this capacity is lost a week after birth (Porrello et al., 2011, 2013). Determining the molecular mechanisms that underpin this regeneration, and what in turn leads to its loss, could enable extension of the regenerative window and reactivation of such mechanisms in the injured/diseased adult heart.

Complete regeneration following myocardial infarction requires replacement of lost cardiomyocytes. Additionally, re-establishment of adequate blood flow to the regenerating tissue is essential, which can either be via the formation of new vessels (vasculogenesis) or from the growth of pre-existing ones (angiogenesis). In the regenerating P1 heart, Porrello and colleagues observed organ-wide cardiomyocyte proliferation, along with newly formed vessels in the heart, 7 days following injury, which subsequently connected to the ligated LAD, to restore blood flow, by 21 days post injury (dpi) (Porrello et al., 2013).

During development, the activated epicardium acts as a mitogenic source, secreting retinoic acid (RA) and erythropoietin, to stimulate cardiomyocyte proliferation, whilst secreting VEGF to promote coronary vessel development (Chen et al., 2002; Lavine et al., 2006; Stuckmann et al., 2003). Further, EPDCs differentiate into VSMCs and to some extent endothelial cells to form mature vessels (Cano et al., 2016; Mikawa and Gourdie, 1996; Perez-Pomares et al., 1998).

Concurrent with the loss of regenerative capacity in the neonatal mouse, the epicardium becomes quiescent during the first week of life. A comparative analysis, previously conducted in the lab, of P1 and P7 hearts, revealed a

significant decrease in expression of hallmark epicardial genes: *Wt1, Tbx18, Tcf21* and *Raldh2*, along with a reduction in WT1 and RALDH2 protein levels, at P7 compared to P1 (Masters, 2015).

Given the essential role of the epicardium in cardiomyocyte proliferation and coronary vessel formation in development, and the importance of these two processes in the regenerative response, the observed quiescence of the epicardium within the first week of life may contribute to the loss of regeneration by P7. Given this, re-activation of the epicardium, following MI at P7, may act to extend the window of regeneration.

Of significance, previous studies in the lab demonstrated upregulation of embryonic epicardial genes post-MI, in the regenerative P1 heart, most markedly at 7 dpi. In the non-regenerative P7 heart, partial re-activation of the epicardium was also observed, most markedly at 4dpi, but the extent of this re-activation was not fully characterised (Masters, 2015). Moreover, the signalling pathways that result in this upregulation and the downstream consequences on regeneration, have yet to be elucidated.

The postnatal heart resides in an oxygen rich environment in comparison to the embryonic heart. Work in Chapters 3 and 4 revealed a key role for hypoxia and HIF signalling in the epicardium during development, therefore, changes in oxygen levels and HIF signalling after birth may result in quiescence of the epicardium.

5.2 Aims

This chapter aims to fully characterise the potential of the epicardium and assess levels of HIF signalling in the neonatal regenerative setting. Specifically, to analyse in greater depth, former observations that the epicardium becomes dormant within the first postnatal week and is activated in response to injury at P1 and P7. Previous work was conducted on an outbred CD1 background, but the genetically modified strains used to investigate a role for HIF signalling were kept in an inbred C57BL/6 genetic background, therefore, experiments in this chapter aimed to characterise the baseline response to injury in the P1 and P7 wildtype C57BL/6 mouse.

5.3 The epicardium become quiescent shortly after birth

To assess epicardial potential during the postnatal period, mRNA levels of characteristic epicardial genes: *Wt1, Tbx18, Tcf21* and *Raldh2,* were measured, in ventricular lysates, at days P0 – P7, P14, P21, P28 and adult (8 weeks old) (n=4 hearts per timepoint). Data was normalised to housekeeping genes, ATP synthase F1 subunit beta (*Atp5f1b)* and succinate dehydrogenase complex flavoprotein subunit A (*Sdha).* HIF1α and HIF2α are regulated at the protein level, by proteasomal degradation, therefore, transcript levels do not reflect their activity. As such, HIF activity was assessed via expression of the HIF regulator, *Phd2*, and the HIF target gene, *Glut1* (Figure 5.3.1A-F). Expression levels of *Phd2* were low during the first week of life, indicating HIF signalling is active. Levels then increased by P7, and further still in the adult heart, suggesting an inhibition of HIF signalling beyond the first week of life (Figure 5.3.1A). Concomitantly, levels of the HIF target gene, *Glut1*, decreased over this time period, with the most dramatic decrease in expression occurring from P0 to P1, indicating changes in cardiac metabolism occur rapidly after birth (Figure 5.3.1 B). Interestingly expression of the epicardial transcription factor *Wt1* increased from P1 to P7, contrary to previous findings, but then decreased thereafter (Figure 5.3.1 C) (Masters, 2015). The transcription factor *Tcf21* followed a similar pattern of expression (Figure 5.3.1 D). Expression of *Tbx18* remained relatively constant within the first postnatal week. Finally, a peak in *Raldh2* expression was seen from P4-P7, indicating an increase in retinoic acid (RA) signalling during this period; expression of *Raldh2* decreased thereafter (Figure 5.3.1 E).

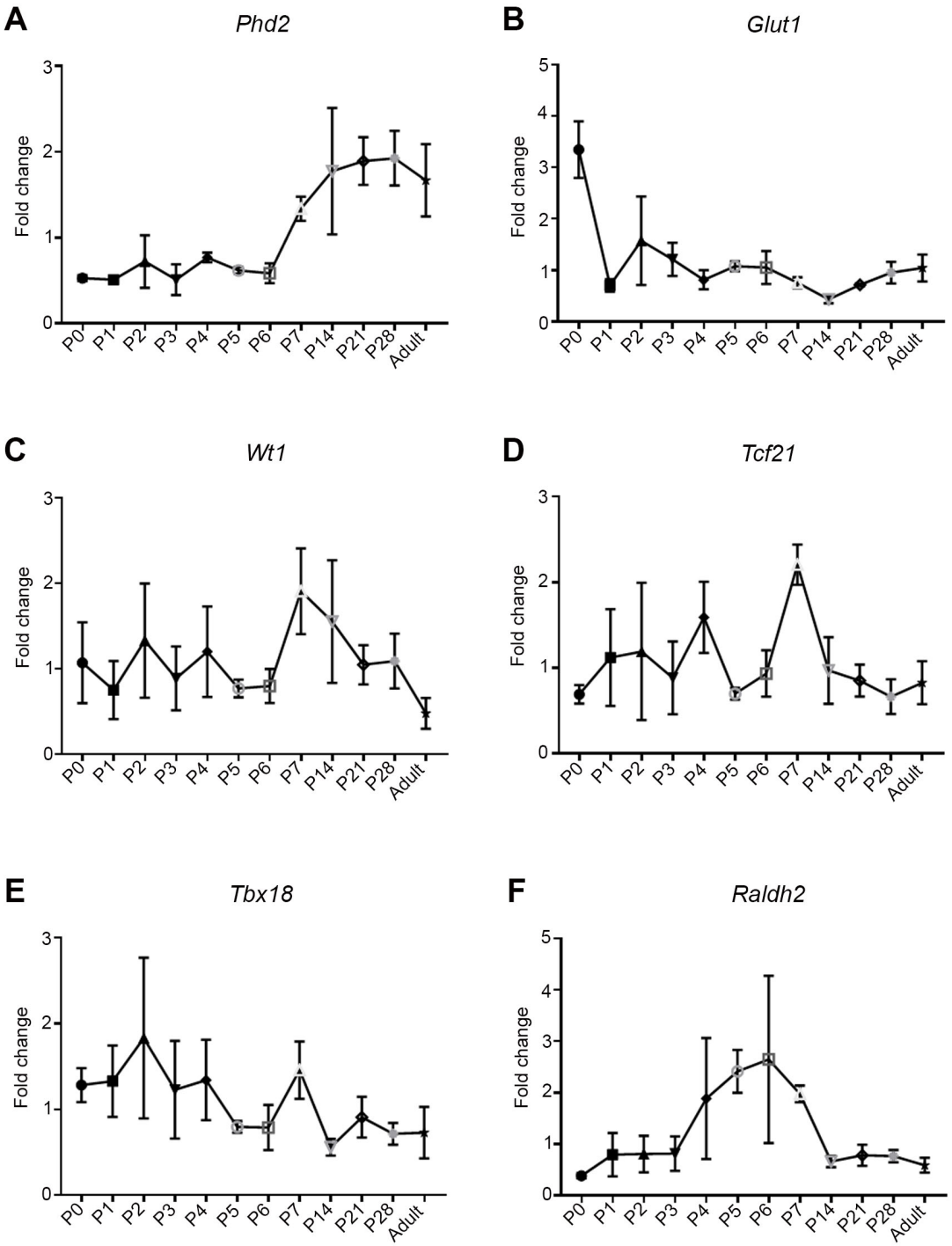


Figure 5.3.1 The epicardium becomes dormant within 2 weeks after birth.

A-F. mRNA levels of **A**. *Phd2*, **B**. *Glut1* and epicardial genes **C**. *Wt1*, **D**. *Tcf21*, **E**. *Tbx18* and **F**. *Raldh2* taken from whole ventricles of P0-P7, P14, P21, P28, and adult (6-week-old) mice, normalised to *Atp5b* and *Sdha* expression and analysed by the $2^{-\Delta\Delta CT}$ method. n=4 mice per group. Data presented Mean ±SEM.

In C57BL/6 mice, whilst expression of epicardial genes decreased by P14, indicating a dormancy of the epicardium after birth, it did not significantly decrease by P7, coinciding with the loss of regenerative capacity, as previously described in a CD1 background (Masters, 2015). This may be a result of intrinsic differences between mice of different genetic backgrounds, since this is known to influence cardiac development, function and response to injury (Barnabei et al., 2010; van den Borne et al., 2009; Jelinek et al., 2018; Villar et al., 2004). Furthermore, expression levels were measured in whole ventricular lysates and whilst these genes are primarily expressed in the epicardium, expression of *Wt1, Tcf21* and *Tbx18* has been reported in endothelial cells, mesenchymal cells and cardiomyocytes, respectively (Christoffels et al., 2009; Duim et al., 2015; Hidai et al., 1998; Robb et al., 1998) which may, therefore, mask potential changes in epicardial expression. In addition, it may also reflect differences between gene expression and protein translation, the protein may no longer be present, yet transcript remains. Therefore, immunohistochemistry of WT1 was used to assess the extent and distribution of WT1 protein during the regenerative window, at stages P1, P4 and P7 (Figure 5.3.2). WT1 was expressed throughout the majority of the epicardium at P1, with expression decreasing by P4 and further still by P7. This supports a quiescence of the epicardium within the first week of life, coincident with the loss of regenerative potential by P7.

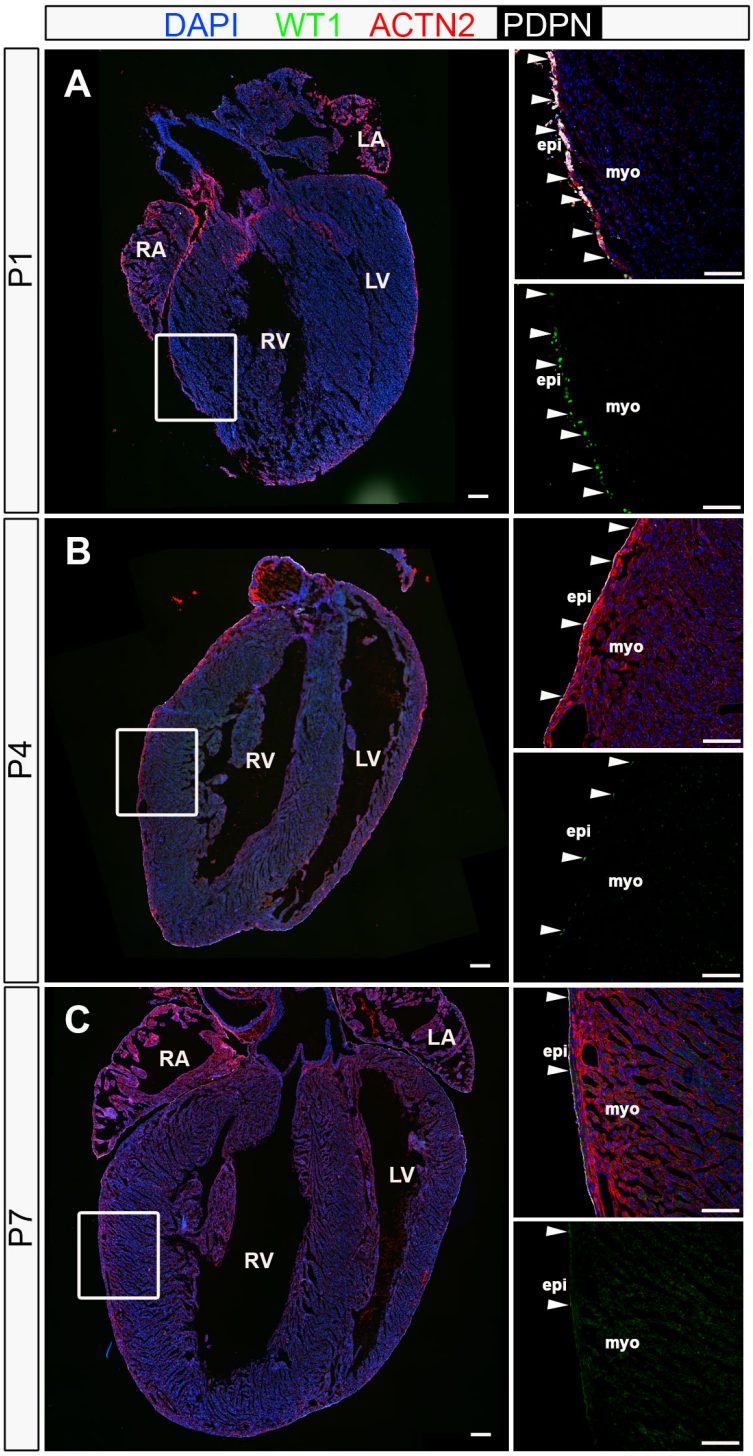


Figure 5.3.2 The epicardium becomes quiescent shortly after birth.

A-C. Representative images of immunostaining for WT1 (green), ACTN2 (red), PDPN (white) and DAPI nuclear stain (blue) at stages **A**. P1, **B**. P4 and **C**. P7. Images to the right are magnifications of boxed regions. Arrowheads highlight expression of WT1 in the epicardium. RA= right atria, LA= left atria, RV= right ventricle, LV= left ventricle, epi= epicardium, myo= myocardium. Scale bars are 200μm, high magnification scale bars = 100μm. n=3 hearts per group.

5.4 Learning the injury model

To assess the epicardial response to injury in the neonate, I undertook surgical training to perform the LAD ligation procedure, outlined in section 2.2.1, on both P1 and P7 pups. Briefly, for each pup, following hypothermia to induced cardiorespiratory arrest, I performed a thoracotomy and manipulated the heart out of the thoracic cavity. I then placed a suture through the left ventricle to ligate the LAD. The heart was then manoeuvred back into position and the ribs and skin were subsequently sutured closed. I then rapidly warmed the pup to stimulate recovery.

I was trained in the procedure, first established by Porrello and Colleagues in 2013 (Porrello et al., 2013) and adapted by our lab to meet UK home office regulations (Masters, 2015), by our surgical technician Mala Rohling, who routinely performs the procedure. Initial training was conducted on the outbred CD1 mouse strain as this was the strain our lab, and others, had previously used (Gunadasa-Rohling et al., 2018; Masters, 2015; Porrello et al., 2013). Having not worked with animals prior to my DPhil, and with no previous surgical training, learning the technique proved technically challenging. In particular, as the LAD was generally not visible, and the hearts exhibited varied orientations upon manipulation out of the thoracic cavity, suture placement differed, resulting in variations in infarct size. Once I was proficient in the procedure, able to induce a substantial and reproducible infarct, I then had to adapt the technique for C57BL/6 mice, as this was the background of the genetic strains used in this thesis. Adult C57BL/6 mice are reported to have lower survival rates following MI than mice on other genetic backgrounds (van den Borne et

al., 2009). Moreover, C57BL/6 pups are substantially smaller than CD1 pups of the same age, making the microscopic procedure more technically challenging and resulting in lower survival rates following MI. Furthermore, C57BL/6 dams are known to be less nurturing (Weber and Olsson, 2008; Weber et al., 2013), which resulted in increased rates of maternal cannibalism. Finally, C57BL/6 dams produce much smaller litters, ~8 pups as oppose to ~15 from CD1 dams. Taken together, this meant there were less pups to operate on per litter, and of the few that survived the surgery, the majority were cannibalised. Therefore, substantial time was spent refining my surgical technique to improve survival rates, eventually leading to comparable survival rates achieved by members of the lab on CD1 mice. Additionally, dams who had previously had a litter were used, and paired with another female where possible (Jo Manning et al., 1995), as we found this reduced the risk of maternal cannibalism.

5.5 Activation of the epicardium in the regenerating P1 heart

5.5.1 Epicardial WT1 expression is increased in response to injury at P1

To assess epicardial activity in the regenerative neonatal mouse, LAD ligation surgery was performed at P1, and hearts were collected for analysis at 7 dpi (n=3). Uninjured, age-matched, controls were collected at P8 for comparison (n=3). Immunohistochemistry of WT1, on transverse apical sections, revealed a significant upregulation of WT1 in the epicardium following injury, compared with uninjured controls (Mean number of $WT1^+$ in the epicardium per area ± SEM; control: 2.33 ± 1.20; infarct zone: 99.17 ± 4.31; remote zone: 6.25 ± 4.31; n=3, p=0.0043 [control vs infarct zone]; Figure 5.5.1).

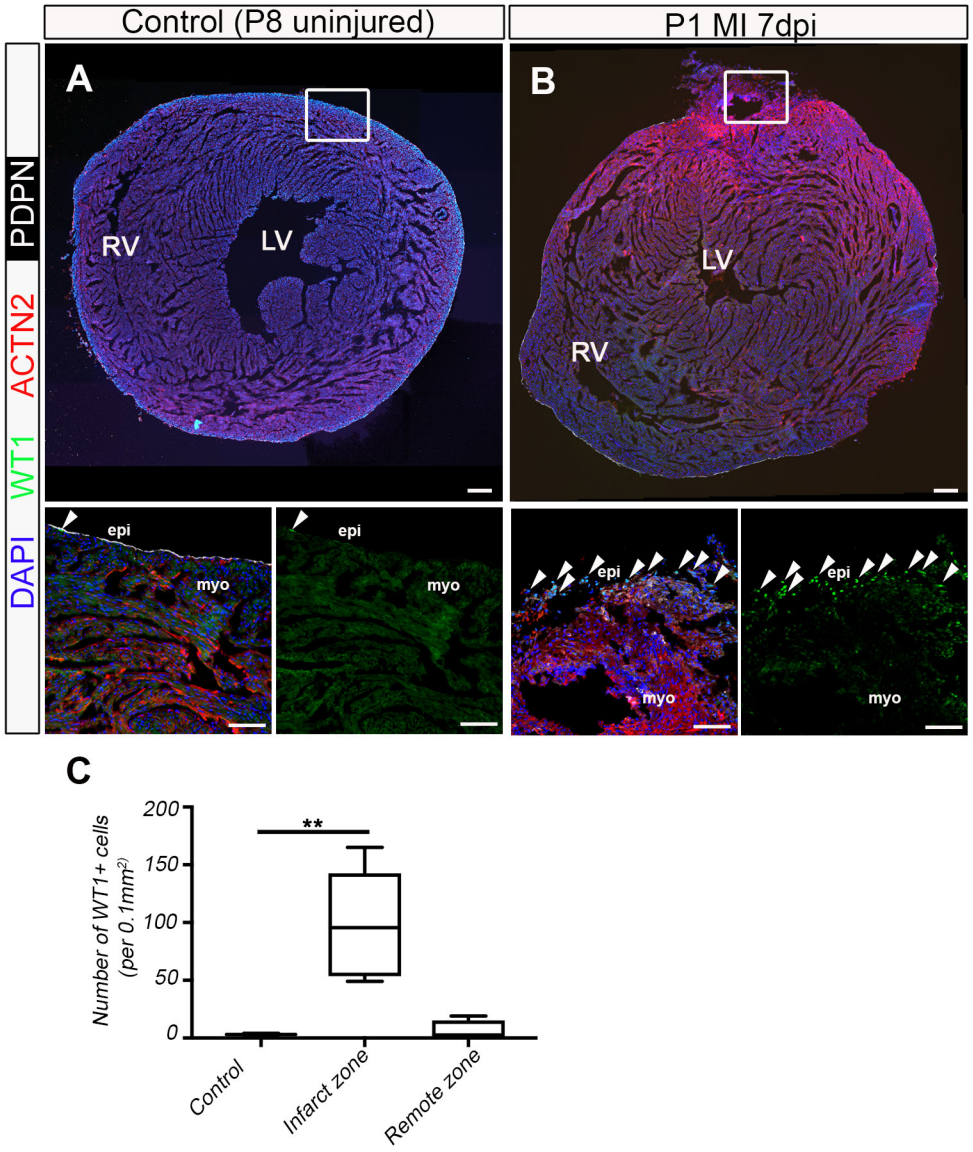


Figure 5.5.1 Epicardial expression of WT1 is increased following injury at P1.

A-B. Immunostaining for WT1 (green), ACTN2 (red), PDPN (white) and DAPI nuclear stain (blue), on transverse apical sections of hearts from C57BL/6 mice, **A**. at P8 uninjured or **B**. at P8 following myocardial infarction at P1 (7dpi). Images below represent high magnifications of boxed regions. Arrowheads highlight expression of WT1 in the epicardium. Epi= epicardium, myo= myocardium. Scale bars are 200μm, high magnification scale bars = 100μm. **C**. Quantification number of WT1 positive cells in the epicardium, near the injury (infarct zone) and away from the injury (remote zone), compared to P8 uninjured hearts (control). n=3 hearts per group. Data presented as median, IQR and upper and lower limits. Data analysed by one-way ANOVA with Tukey's post-hoc test; **p<0.01.

5.5.2 The neonatal mouse heart can regenerate following injury at P1

Additional hearts were collected at 21dpi and analysed by histology to assess scar resolution. H&E and Masson's Trichrome staining, of long axis sections, revealed little or no residual scar 21 days following myocardial infarction, comparable to uninjured controls, indicative of cardiac regeneration, as previously described (Figure 5.5.2) (Porrello et al., 2011, 2013).

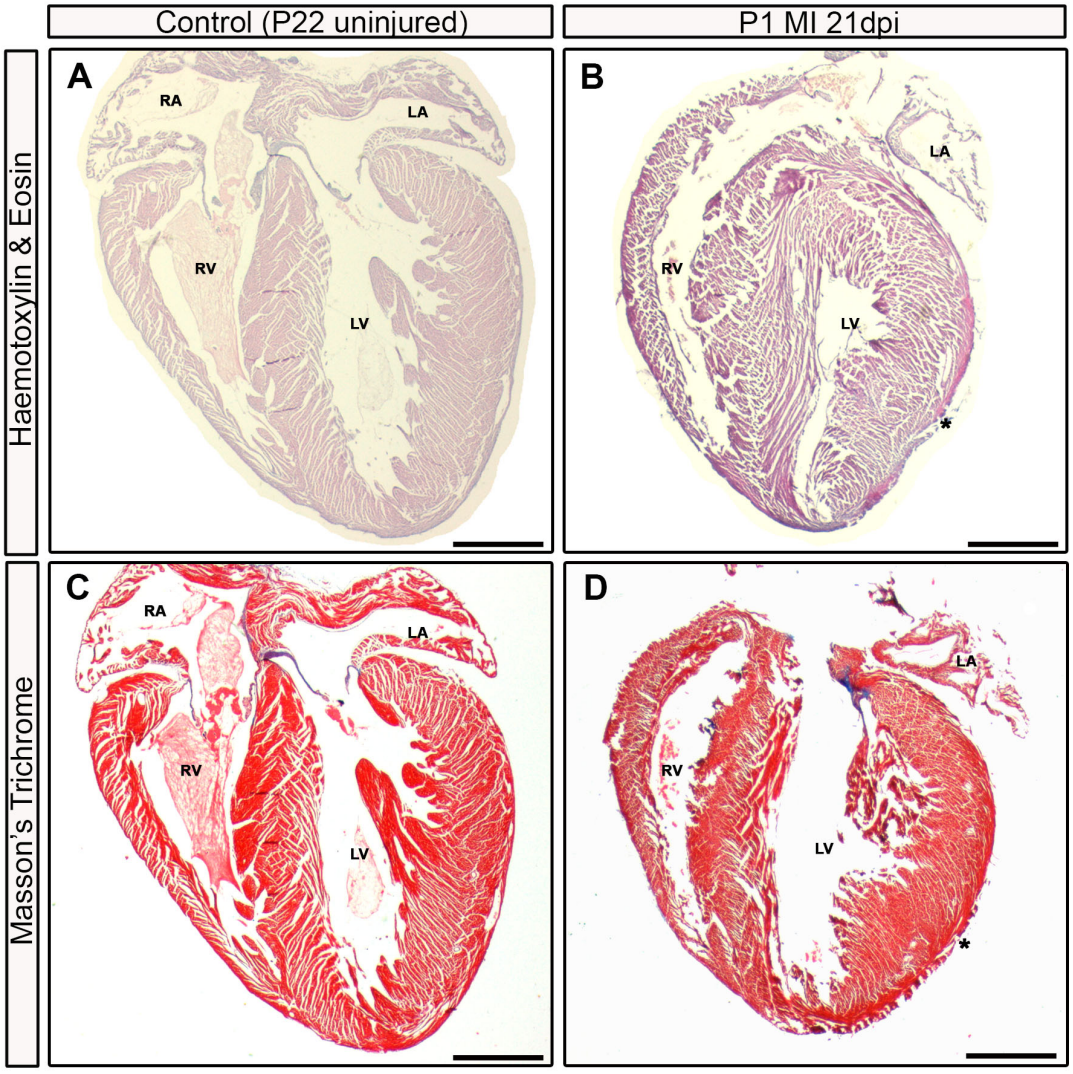


Figure 5.5.2 The neonatal mouse heart can regenerate in 21 days, following myocardial infarction at P1.

A-B. H&E histological staining of the mouse heart at **A**. P22 uninjured (control) and **B**. P22, following ligation of the LAD at P1 (21dpi). **C-D**. Masson's Trichrome stained serial sections to show cardiac muscle fibre (red) and collagen deposition (blue). RA= right atria, RV= right ventricle, LA= left atria, LV= left ventricle. * indicates suture placement. Scale bars= 1mm, high magnification scale bars =0.5mm. Images representative of n=4 for controls, n=5 for injury.

5.6 Reactivation of the epicardium in the P7 heart after injury

5.6.1 The epicardium is partially reactivated following injury at P7

As the non-regenerative P7 model is the primary focus for the remainder of this thesis, a more in-depth assessment of epicardial and HIF activity, following ligation of the LAD at P7, was conducted. Initially, hearts were collected for analysis at 4dpi, when epicardial activity is highest (Masters, 2015), and either processed for RT-qPCR or immunostaining. Uninjured age-matched samples were also collected as controls. Expression levels of epicardial genes: *Wt1, Tbx18, Tcf21* and *Raldh2*, along with *Phd2* and *Glut1*, were measured by RT-qPCR of ventricular lysates (Figure 5.6.1 A-F). Expression of *Phd2* was decreased after infarction, indicating activation of HIF signalling, however, expression of HIF target, *Glut1*, remained unchanged (Figure 5.6.1A-B). Expression of *Wt1* was significantly increased (Mean fold change ± SEM; control: 0.73 ± 0.15; injury: 1.52 ± 0.21; n=4, p=0.0240; Figure 5.6.1C), expression of *Tbx18* and *Tcf21* remained unchanged (Figure 5.6.1D-E), and expression of *Raldh2* significantly decreased, following injury (Mean fold change ± SEM; control: 1.26 ± 0.10; injury: 0.81 ± 0.06; n=4, p=0.0074; Figure 5.6.1F).

Immunofluorescence, of apical transverse sections, stained for WT1 revealed a significant increase in WT1 protein in the epicardium following injury, when compared to intact controls (Mean number of $WT1^+$ in the epicardium per area ± SEM; control: ± ; infarct zone: ± ; remote zone: ± ; n=, p= [control vs infarct zone]; Figure 5.6.2). Of significance, WT1 expression was seen throughout the epicardium, but more prominently, proximal to the infarct region (infarct zone).

A recent study reported expression of WT1 in endothelial cells in the mouse, during development and in the adult following injury (Duim et al., 2015) . No endothelial expression of WT1 was observed in uninjured controls, however, 2 of the 5 infarcted hearts, which incidentally had the largest infarct sizes, had some weak WT1 expression in the myocardial layer of the infarct zone.

Co-staining of endothelial marker, EMCN, with smooth muscle marker, smooth muscle myosin heavy chain (SM-MHC) did not reveal any striking differences in mature coronary vasculature between uninjured and injured hearts. However, there was a noticeable increase in EMCN positive endothelial cells throughout the heart, following injury, indicating the start of neovascularistion (Figure 5.6.3).

Collectively these data reveal the epicardium responds to injury at P7, albeit to a lesser extent than the regenerative P1 heart, therefore augmenting the epicardial response to injury in the P7 heart could improve regeneration.

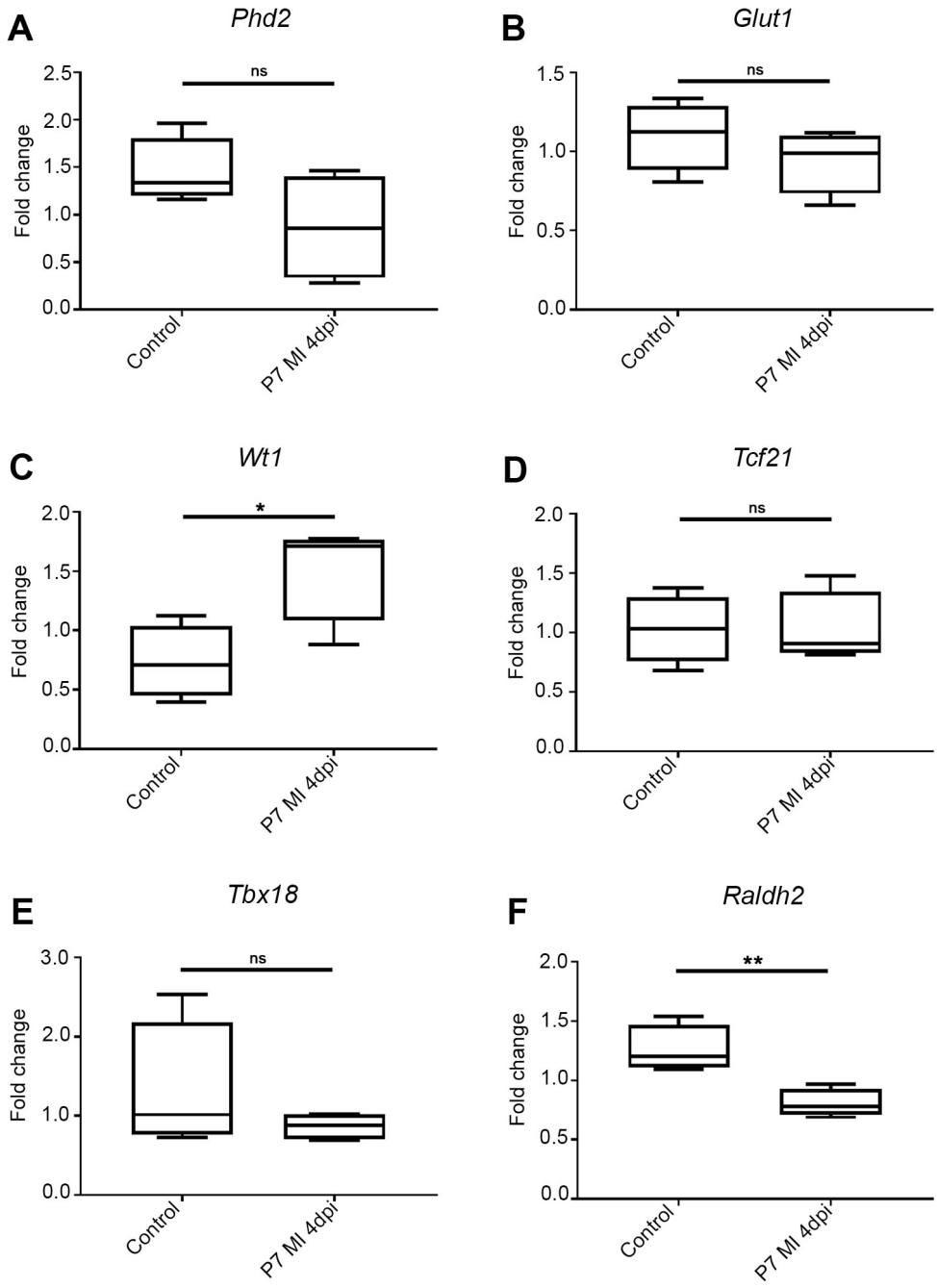


Figure 5.6.1 The epicardium is partially reactivated in response to injury at P7.

A-F. mRNA levels of **A**. *Phd2*, **B**. *Glut1* and epicardial genes **C**. *Wt1*, **D**. *Tcf21*, **E**. *Tbx18* and **F**. *Raldh2* taken from whole ventricles of P11 mice following myocardial infarction at P7, normalised to *Atp5b* and *Sdha* expression, compared to P11 uninjured controls and analysed by the $2^{-\Delta\Delta CT}$ method. n=4 mice per group. Data presented as median, IQR and upper and lower limits. Data analysed by Student t-test. *p<0.05; **p<0.01; ns=not significant.

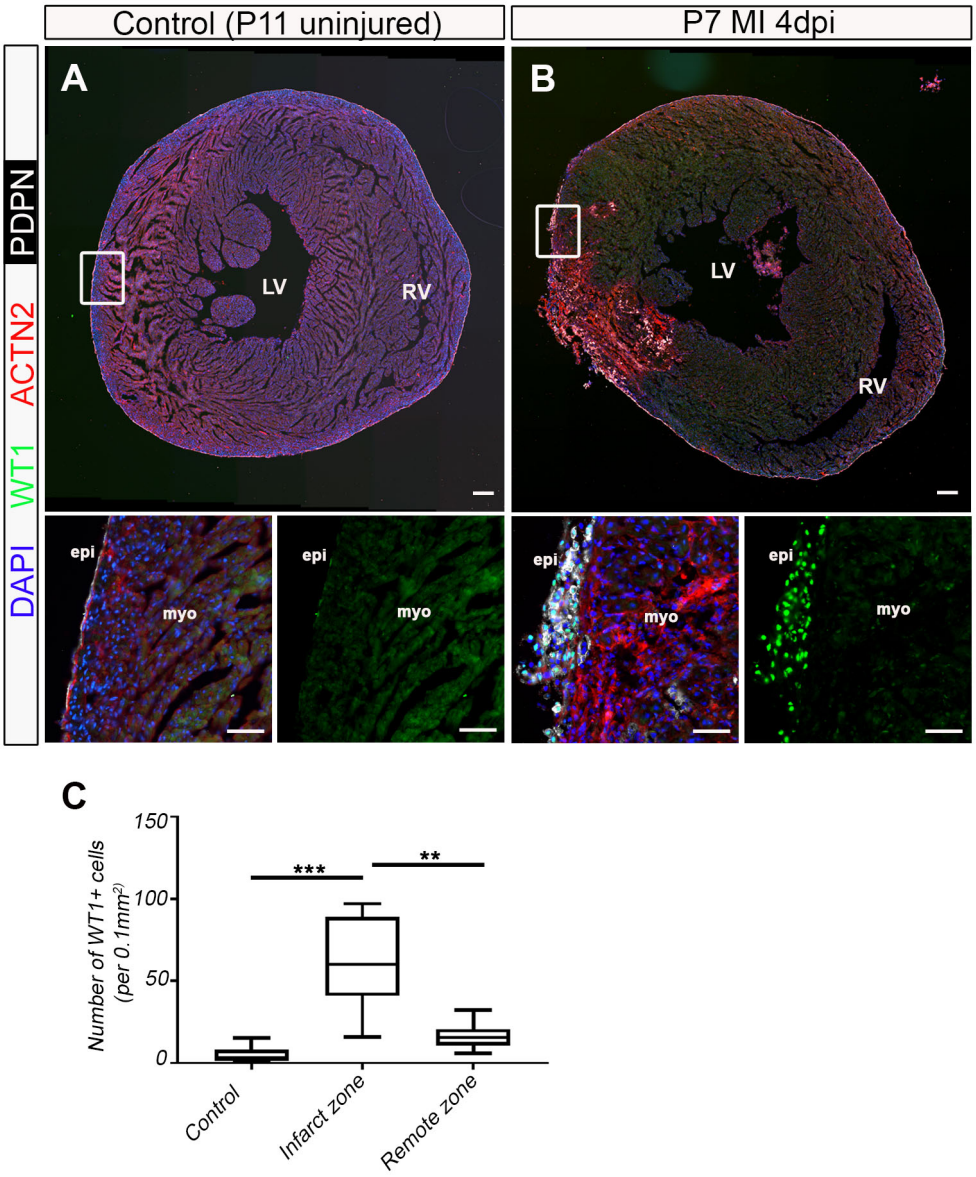


Figure 5.6.2 The epicardium is reactivated proximal to the infarct region.

A-B. Representative images of immunostaining for WT1 (green), ACTN22 (red), PDPN (white) and DAPI nuclear stain (blue) on transverse apical sections of hearts from C57BL/6 mice. **A**. P11, uninjured or **B**. P11 following myocardial infarction at P7 (4dpi). Images below represent high magnifications of boxed regions. Epi= epicardium, myo= myocardium. Scale bars are 200μm, high magnification scale bars = 100μm. **C**. Quantification number of WT1 positive cells in the epicardium, near the injury (infarct zone) and away from the injury (remote zone), compared to P11 uninjured hearts (control). n=4 hearts per group. Data presented as median, IQR and upper and lower limits. Data analysed by one-way ANOVA with Tukey's post-hoc test. **p<0.01; ***p<0.001.

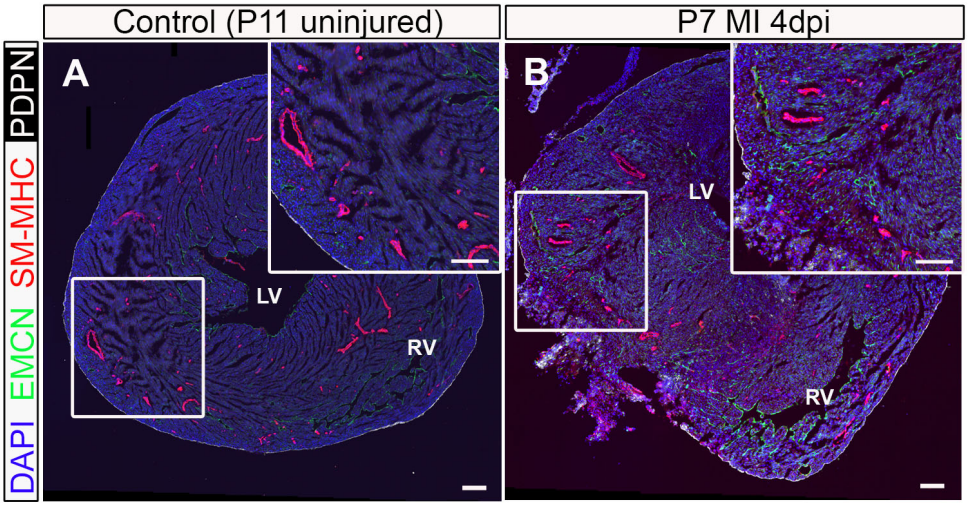


Figure 5.6.3 EMCN expression is increased following injury at P7.

A-B. Representative images of immunostaining for EMCN (green), SM-MHC (red) and DAPI (blue) on transverse apical sections of hearts from C57BL/6 mice. **A**. P11, uninjured (control) and **B**. P11 following MI at P7 (4dpi). Images in top right corner represent high magnifications of boxed region. n=4 hearts per group. Scale bars 200μm, high magnification scale bars= 100μm.

5.6.2 Myocardial infarction at P7 results in ventricular remodelling and persistent cardiac fibrosis

Additional hearts were collected for histological analysis, at 21dpi, to assess heart morphology and fibrosis (Figure 5.6.4). Uninjured age-matched controls were used for comparison. H&E staining revealed anterior wall thinning and dilation of the left ventricle, below the ligation (Figure 5.6.4A-D). Masson's trichrome staining of serial sections revealed presence of a persistent fibrotic scar (Figure 5.6.4E-H). These results support previous findings, that the regenerative capacity of the neonatal mouse heart is lost by P7. However, histological analysis also highlighted the variation in extent of injury. The injury represented in Figure 5.6.4D,H shows significant dilation of the left ventricle and substantial collagen deposition, in comparison to the heart represented in Figure 5.6.4C,G. This is likely due to variation in suture placement, and therefore, extent of LAD ligation, since the more severe injuries were achieved later in my surgery training.

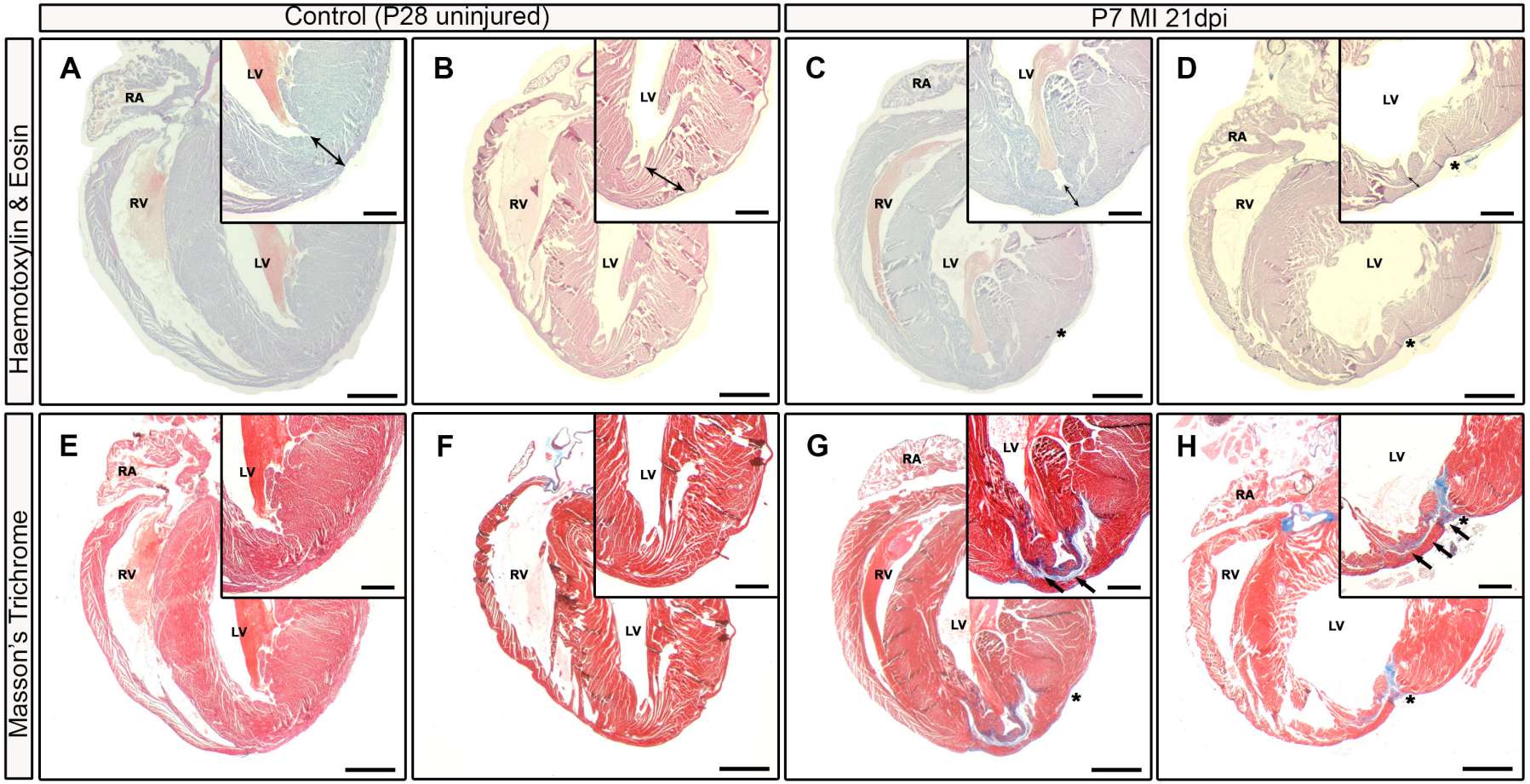

Control (P28 uninjured)
P7 MI 21dpi
Haemotoxylin & Eosin
Masson's Trichrome
A
B
C
D
E
F
G
H
RA
RV
LV
*

Figure 5.6.4 The neonatal mouse heart is unable to regenerate following myocardial infarction at P7.

A-D. H&E histological staining of the mouse heart at **A-B**. P28 uninjured (control) and **C-D**. P28, following ligation of the LAD at P7 (21dpi). **E-H**. Masson's Trichrome stained serial sections to show cardiac muscle fibre (red) and collagen deposition (blue). Images in top right represent high magnifications of boxed regions. RA= right atria, RV= right ventricle, LV= left ventricle. * indicates suture placement. Double arrow line highlights ventricle thickness. Arrows highlight collagen deposition and scarring. Scale bars= 1mm, high magnification scale bars =0.5mm. Images representative of n=4 for controls, n=8 for injury.

5.7 Discussion

5.7.1 Quiescence of the epicardium after birth

Previous work conducted in the lab indicated the epicardium becomes quiescent within the first week of life, occurring around P4, in CD1 mice (Masters, 2015). Data presented in this chapter, conducted on C57BL/6 mice, demonstrated a decrease in mRNA levels of hallmark epicardial genes after birth, but not until after P7. This disparity may reflect inherent differences between mice from different genetic backgrounds. In support of this, studies have reported differences, in cardiac function and response to myocardial infarction, between wildtype mice of different strains (Barnabei et al., 2010; van den Borne et al., 2009; Jelinek et al., 2018). Further, phenotype variability has been reported, following gene-targeting in different mouse strains (Baribault et al., 1994; Villar et al., 2004). This highlights the need to study baseline levels in the same background as the genetically modified strain.

Whilst transcript levels indicated expression of epicardial genes extended beyond P7, spatiotemporal analysis of WT1 protein revealed a significant decrease, in the master regulator of the epicardium, by P7, suggesting the epicardium does become quiescent within the first week of life. This discrepancy from the transcript levels may reflect differences between gene expression and protein translation. Further, since expression levels were measured in whole ventricular lysates, expression of *Wt1* elsewhere in the heart may have masked changes in epicardial gene expression at earlier stages (pre-P7).

5.7.2 HIF signalling in the heart after birth

Whilst the metabolism of foetal epicardial cells is unknown, it is generally thought that foetal cardiomyocytes generate energy from glycolysis and glucose oxidation (Lopaschuk et al., 1991). After birth, oxygen levels increase dramatically, resulting in a decrease in HIF-signalling in the heart. This was reported to act as a physiological switch, leading to mitochondrial maturation in postnatal cardiomyocytes, enabling them to generate energy via β-oxidation (Neary et al., 2014). In support of this, we observed a significant increase in expression of the HIFα inhibitor, *Phd2*, in the heart shortly after birth (P7), along with a dramatic decrease in cardiac expression of the glucose transporter, *Glut1*, immediately following birth (P1).

Transcript levels of *Hif1α* and *Hif2α* were not measured directly as HIF1α and HIF2α are regulated by post-translational modifications, thus, transcript levels does not reflect activity. Further, as HIF1/2α are rapidly degraded, immunostaining with antibodies against these proteins is particularly problematic. Whilst changes in *Phd2* and *Glut1* indicate HIF activity, they are only surrogate markers, and therefore an inability to measure HIF expression directly is a limiting factor in this study and more generally in the field.

5.7.3 Regeneration in the P1 mouse heart

Seminal work, by Porrello and colleagues in 2011, revealed the remarkable regenerative capacity of the P1 mouse (Porrello et al., 2011). Data presented in this chapter demonstrated that, following LAD ligation at P1, a robust regenerative response is seen, including prolonged activation and expansion

of the epicardium, resulting in complete regeneration of the cardiac tissue 21 days following injury.

5.7.4 The limited regenerative capacity of the P7 mouse heart

5.7.4.1 Partial re-activation of the epicardium

Porrello and colleagues also demonstrated that the regenerative capacity of the heart is lost one week after birth. Data in this chapter suggests that whilst the epicardium becomes quiescent within the first week of life, it is partially reactivated in response to injury at P7. A significant increase in WT1 expression, both at the transcript and protein level, was observed 4 days post injury, in comparison to baseline levels of uninjured age-matched controls.

Despite the increase in *Wt1*, expression of other hallmark epicardial genes *Tbx18* and *Tcf21* remained unchanged, and levels of *Raldh2* significantly decreased. Therefore, injury at P7 may result in a partial reactivation of the foetal epicardial gene programme, thus contributing to its limited regenerative capacity. Of significance, in the regenerating zebrafish, RA production, by the epicardium and endocardium was shown to be essential for regeneration (Kikuchi et al., 2011; Wang et al., 2015). Therefore, a significant reduction in the enzyme that catalyses the synthesis of RA, *Raldh2*, could be a factor contributing to the loss of regenerative capacity. However, changes in epicardial expression of *Tcf21*, *Tbx18* and *Raldh2*, may be masked by expression elsewhere in the heart, since their expression has been reported in mesenchymal cells, cardiomyocytes and the endocardium, respectively (Christoffels et al., 2009; Hidai et al., 1998; Kikuchi et al., 2011; Robb et al.,

1998). Therefore, immunostaining for TBX18, TCF21 and RALDH2 would need to be performed to assess this further, however, we were unable to find antibodies against these proteins that worked successfully on cryosections. Alternatively, the previously described epicardial reporter line *Wt1*^{GFPCre}, in which an EGFPCre fusion vector is knocked-in to the endogenous *Wt1* start codon (Zhou et al., 2008), could be used to selectively isolate WT1^{+}GFP^{+} epicardial cells by fluorescence activated cell sorting (FACS), mRNA could then be extracted from these cells, and transcript levels of *Tbx18, Tcf21* and *Raldh2* measured by RT-qPCR.

5.7.4.2 HIF signalling

Permanent ligation of the LAD restricts blood flow, reducing oxygen and nutrient supply to the cardiac muscle, and resulting in ischaemia. Fatty acid oxidation is the main source of energy for cardiac tissue, supplying 60-90% of the energy. Following myocardial infarction, a lack of available oxygen results in a metabolic switch, to anaerobic glycolysis (Stanley, 2001). Expression of the glucose transporter, and HIF target gene, *Glut1*, did not change following myocardial infarction at P7. GLUT1 is one of 14 known glucose transporters, and whilst its expression is upregulated in the adult mouse following MI, increased expression of GLUT4 has also been reported (Huang et al., 2009b), thus it is likely that a different glucose transporter may be important for glycolysis in the neonate heart following injury. Therefore, expression of other glucose transporters, including GLUT4, should be investigated further in this setting.

HIF signalling is activated in response to hypoxia, to promote cell survival. HIF activation should lead to the upregulation of HIF target genes which include *Phd2* and *Phd3* (Berra et al., 2003). However, upregulation of these HIF prolyl hydroxylases might then downregulate abundance of HIF via negative feedback, thereby limiting the size of the response seen. It is also important to note that PHD2 function is inhibited during hypoxia, due to the lack of oxygen as a substrate, therefore, variation in gene expression may not directly reflect changes in HIF activation. These factors make interpretation of the level of HIF activation based on variations in gene expression complicated. However, the lack of increase in *Glut1* and *Phd2* in the reported experiments suggests that any HIF response is not efficient to elicit a beneficial effect within this non-regenerative setting.

5.7.4.3 Neovascularisation

Following myocardial infarction in the non-regenerative P7 mouse, we found no observable difference in the number of mature EMCN and SM-MHC double-positive coronary vessels, near the infarct zone, 4 days after injury, compared to uninjured age-matched controls. However, a notable increase in EMCN staining was observed, indicating the presence of new endothelial cells and therefore the start of new coronary vessel formation. In the regenerating P1 heart, Porrello and colleagues reported the presence of new vessels 7dpi (Porrello et al., 2013), therefore, analysis of later time points would need to be conducted to probe this further. It is also important to note, the coronary vasculature continues to form and expand in the early postnatal period, therefore, at the stage analysed in these studies, neovascularisation may be

occurring in the uninjured controls, therefore large differences may not be observed (van Groningen et al., 1991; Tian et al., 2014; Tomanek et al., 1999).

5.7.4.4 Cardiac fibrosis

Histological analysis of P7 injured hearts at 21dpi, revealed anterior wall thinning, ventricular remodelling and the presence of a fibrotic scar, in agreement with previous findings, that the neonatal mouse heart is unable to regenerate beyond the first week of life. Whilst the extent of remodelling and fibrosis varied between pups, mainly due to variability in suture placement, ventricular wall thinning and residual fibrosis were evident in all experiments conducted on P7 mice, indicative of incomplete regeneration.

5.8 Conclusions

The findings documented in this chapter indicate the epicardium becomes quiescent within the first week of life of wild-type C57BL/6 mice, concurrent with a decrease in HIF-mediated signalling. Experiments on the P1 mouse demonstrate the epicardium remains activated following MI and confirm the remarkable regenerative capacity of the heart at this stage; whereas injury at P7 suggests the epicardium is only partially re-activated coincident with impaired regeneration, fibrosis and remodelling by 21dpi.

6 HIF signalling in neonatal cardiac regeneration

6.1 Background

The loss of function of HIF studies outlined in Chapter 3, suggest a role for HIF signalling in epicardial activation and EMT during development. Moreover, the *in vitro* studies outlined in Chapter 4, demonstrated enhanced epicardial EMT, following genetic knock-down or pharmacological inhibition of PHD2 and a corresponding gain-of-function of HIF.

Analysis of the regenerative window, in the previous Chapter, suggests the epicardium become quiescent within the first week of life, concurrent with a decrease in cardiac HIF signalling, and loss of regenerative capacity.

Taken together, we hypothesised that a reduction in HIF signalling after birth, resulted in quiescence of the epicardium, thus, contributing to the loss of regenerative capacity and consequently that stabilising HIF may act to increase and maintain epicardial activation to extend the window of neonatal cardiac regeneration.

6.2 Aims

Studies documented in this chapter sought to determine whether maintaining HIF signalling after birth could act to prolong epicardial activation, and thus promote cardiac regeneration following myocardial infarction at P7.

6.3 Maintaining HIF signalling after birth

Work in the previous chapter indicated expression of *Phd2* significantly increases in the heart, shortly after birth. Therefore, to prolong HIF signalling in the heart after birth, the genetic gain-of-function model, *Phd2$^{fl/fl}$;Rosa26$^{+/CreERT2}$* was used (as described in Chapter 4) to induce loss of *Phd2* and stabilisation of HIF, independent of tissue oxygen levels (Mazzone et al., 2009; Takeda et al., 2006). Work in Chapter 4 confirmed this model leads to efficient stabilisation of HIFα in epicardial cells, *in vitro*, and importantly, led to enhanced epicardial EMT.

6.3.1 HIF signalling can be activated postnatally.

Whereas tamoxifen administration, to achieve sufficient knockdown of *Phd2* in the adult mouse has been previously described (Arsenault et al., 2013; Hodson et al., 2016), there is no published protocol for neonatal administration. Initial studies were, therefore, used to optimise the route, dose and frequency of tamoxifen, in order to achieve efficient targeting of *Phd2* expression by postnatal day (P) 7, while causing least harm to the pup and, therefore, reducing the risk of maternal cannibalism.

To circumvent the difficulty of injecting neonatal pups shortly after birth, and because the lab had experience with prenatal tamoxifen administration, initially, a single dose of 100mg/kg of tamoxifen was administered to the pregnant dam, via either intraperitoneal (IP) or oral gavage, at embryonic stage E16.5 or E18.5. This injection regimen aimed to induce Cre-mediated recombination towards the end of gestation, i.e. loss of PHD2 within the first postnatal stages.

However, this method led to high incidence of abortion, stillbirths, or cannibalisation of the pups shortly after birth, most likely due to the oestrogen receptor antagonist function of tamoxifen being detrimental at the late stages of pregnancy (Shiau et al., 1998).

As an alternative, tamoxifen was administered to the lactating dam postnatally, via IP or oral gavage, at a dose of 100mg/kg per day, to deliver the tamoxifen to the pups via the milk (Cheval et al., 2012; Mayes et al., 2011). Earlier work (Chapter 5) demonstrated there was a significant increase in expression of *Phd2* in the heart during the first week of life. Therefore, we administered tamoxifen to the dam, 2 and 4 days after birth, to allow sufficient time for Cre activation and gene recombination in the pups by P7. To assess the efficacy of this strategy, ear biopsies were then taken from the pups at P7, and the resulting isolated DNA was used to investigate gene recombination, using previously described PCR primers (Adam et al., 2011). PCR amplification blots revealed no recombination of the “floxed” allele (data not shown), therefore, this method of tamoxifen delivery was considered insufficient.

As a consequence, an approach in which the tamoxifen was administered directly to the neonates could not be avoided and a report by Pitulescu et al. describing sufficient gene recombination arising from the administration of 50μl of 10mg/ml of tamoxifen on 3 consecutive days from P1-P3, was used as a reference (Pitulescu et al., 2010). Since this is a large volume in comparison to the size of the neonatal mouse, 2 doses of 10μl of 20mg/ml of tamoxifen were administered instead, at P2 and P4, for the same reasoning as outlined above. The litter was removed from the dam into a separate cage and all pups were

injected via IP; the entire litter was then returned to the dam, rather than one pup at a time, to cause minimal disturbance. Initially, high levels of maternal cannibalism were observed, so the protocol was modified to eliminate this as follows: Briefly, following injection, the pups were thoroughly cleaned with Hibiscrub antimicrobial skin cleanser diluted in sterile saline to remove any residues of peanut oil, in which the tamoxifen was dissolved, since mice readily consume peanut butter (Gonzales et al., 2014). Pups were then rolled in faeces from the breeding cage and warmed by an infra-red lamp, before being returned to the dam. Importantly, these additional steps significantly improved the neonate survival post-injection by reducing maternal cannibalism.

To assess the effect of administering tamoxifen directly to the pups on gene expression, mice were sacrificed at P7. DNA was isolated from ear biopsies to test for recombination by PCR and *Phd2* mRNA levels, derived from ventricular lysates, were measured via qPCR. These studies revealed that delivery of 10μl of 20mg/ml of tamoxifen at P2 and P4 was sufficient to induce gene recombination and reduce cardiac expression of *Phd2* by P7, to levels below baseline. To refine this protocol further and minimise the impact on the dam and litter, a single dose of 10μl of 20mg/ml of tamoxifen at P2 was tested. This dose was found to induce gene recombination and reduce levels of *Phd2* expression by over 90% in $Phd2^{fl/fl};Rosa26^{+/CreERT2}$ hearts compared to littermate controls (Mean fold change ± SEM; control: 2.99 ± 0.24, n=7; mutant: 0.25 ± 0.06 n=5; $p<0.0001$; Figure 6.3.1A). Therefore, this refined protocol was taken forward for future experiments.

In order to determine whether HIF signalling was activated, as a result of loss of *Phd2* expression, levels of the HIF target, *Glut1* were determined by RT-qPCR of P7 ventricular lysates. *Phd2$^{fl/fl}$;Rosa26$^{+/CreERT2}$* hearts showed a significant upregulation of *Glut1* expression at P7, compared to their littermate controls, suggesting HIF-mediated transcription is active in these pups (Mean fold change ± SEM; control: 0.78 ± 0.13, n=7; mutant: 1.61 ± 0.20 n=5; p=0.0050; Figure 6.3.1B). Baseline gene expression analysis in Chapter 5 revealed a dramatic decrease in *Glut1* expression, by almost 4-fold, from P0 to P1. Whilst loss of *Phd2* was not sufficient to increase *Glut1* levels to that seen at P0, expression was still comparatively high to that observed at P1-P7.

6.3.2 Loss of *Phd2* results in a significant increase in expression of WT1.

As discussed in Chapter 5, the expression of essential regulators such as *Wt1*, *Tbx18*, *Tcf21* and *Raldh2* is lost during the first postnatal weeks, leading to epicardial quiescence. To investigate the effect of loss of *Phd2* on epicardial gene expression, RT-qPCR was also used and whilst there were no notable changes in expression of *Tbx18, Tcf21* and *Raldh2* (Figure 6.3.1D-F), a significant upregulation in *Wt1* expression in *Phd2$^{fl/fl}$;Rosa26$^{+/CreERT2}$* hearts was found (Mean fold change ± SEM; control: 0.84 ± 0.10, n=7; mutant: 1.37 ± 0.09 n=5; p=0.0030; Figure 6.3.1C). To determine whether the increase in gene expression was reflected at a protein level, hearts were collected at P7 and prepared for immunostaining. Quantification of the number of WT1+ cells in the epicardium, revealed a significant increase in WT1 positive cells in *Phd2$^{fl/fl}$;Rosa26$^{+/CreERT2}$* pups compared to their littermate controls (Mean

number of WT1+ cells in the epicardium per area ± SEM; control: 9.75 ± 1.31, n=4; mutant: 16.70 ± 0.30 n=2; p=0.0243; Figure 6.3.2).

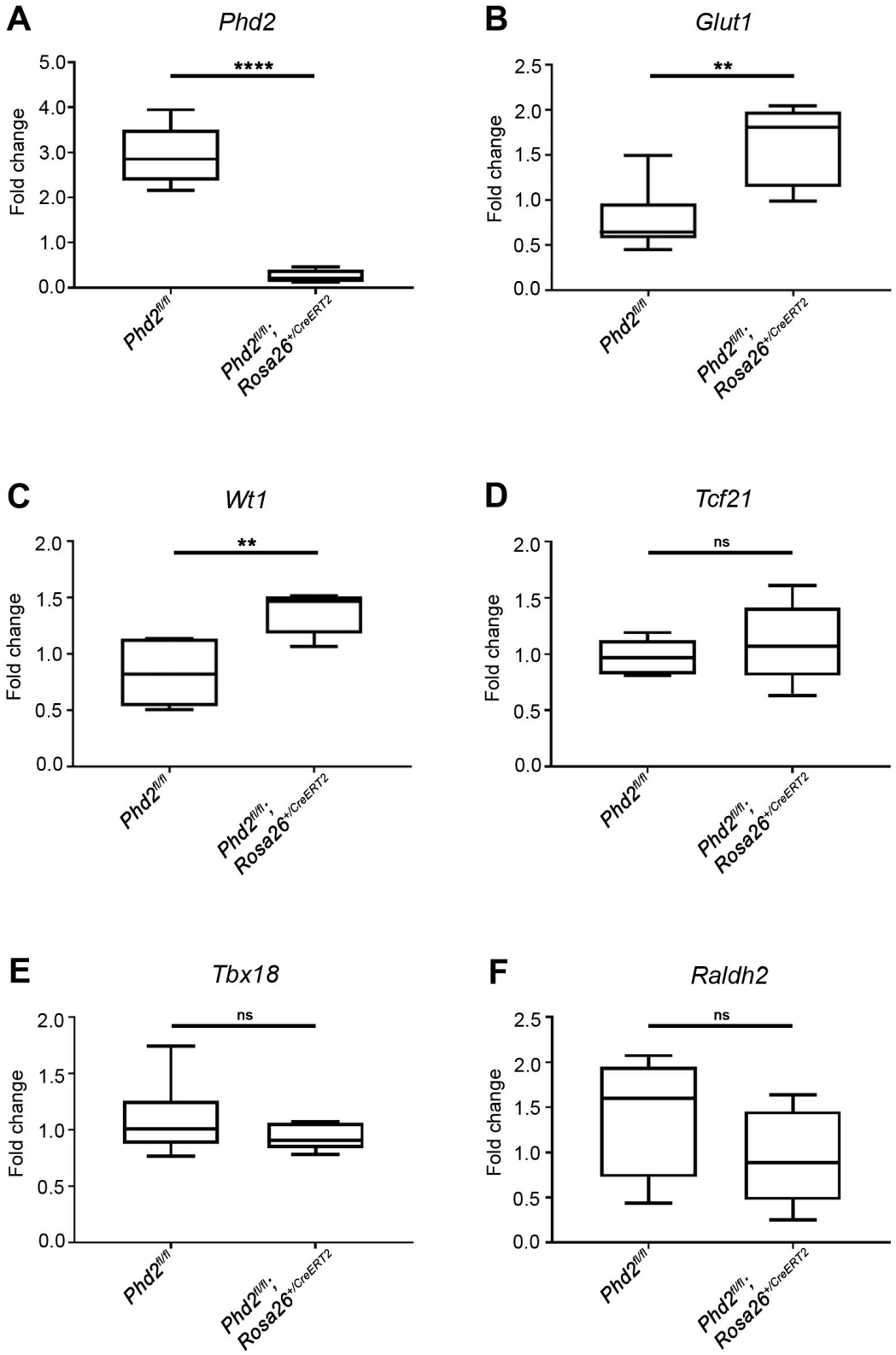

A
Phd2
****
Fold change
5.0
4.0
3.0
2.0
1.0
0.0
Phd2fl/fl
Phd2fl/fl; Rosa26+/CreERT2
B
Glut1
**
Fold change
2.5
2.0
1.5
1.0
0.5
0.0
Phd2fl/fl
Phd2fl/fl; Rosa26+/CreERT2
C
Wt1
**
Fold change
2.0
1.5
1.0
0.5
0.0
Phd2fl/fl
Phd2fl/fl; Rosa26+/CreERT2
D
Tcf21
ns
Fold change
2.0
1.5
1.0
0.5
0.0
Phd2fl/fl
Phd2fl/fl; Rosa26+/CreERT2
E
Tbx18
ns
Fold change
2.0
1.5
1.0
0.5
0.0
Phd2fl/fl
Phd2fl/fl; Rosa26+/CreERT2
F
Raldh2
ns
Fold change
2.5
2.0
1.5
1.0
0.5
0.0
Phd2fl/fl
Phd2fl/fl; Rosa26+/CreERT2

Figure 6.3.1 Tamoxifen administration to neonates at P2 successfully results in reduced *Phd2* and increased *Glut1* and *Wt1* expression by P7.

A-F. mRNA levels of **A**. *Phd2*, **B**. *Glut1*, **C**. *Wt1*, **D**. *Tcf21*, **E**. *Tbx18* and **F**. *Raldh2* taken from whole ventricles of *Phd2$^{fl/fl}$;Rosa26$^{+/CreERT2}$* P7 mice, normalised to *Atp5b* and *Sdha* expression, compared to *Phd2$^{fl/fl}$* controls, and analysed by the $\Delta\Delta$CT method. n=7 control mice and n=5 *Phd2$^{fl/fl}$;Rosa26$^{+/CreERT2}$* mice. Data presented as median, inter-quartile range (IQR) and upper and lower limits. Data analysed by Student t-test; **p<0.01; ****p<0.0001; ns= not significant.

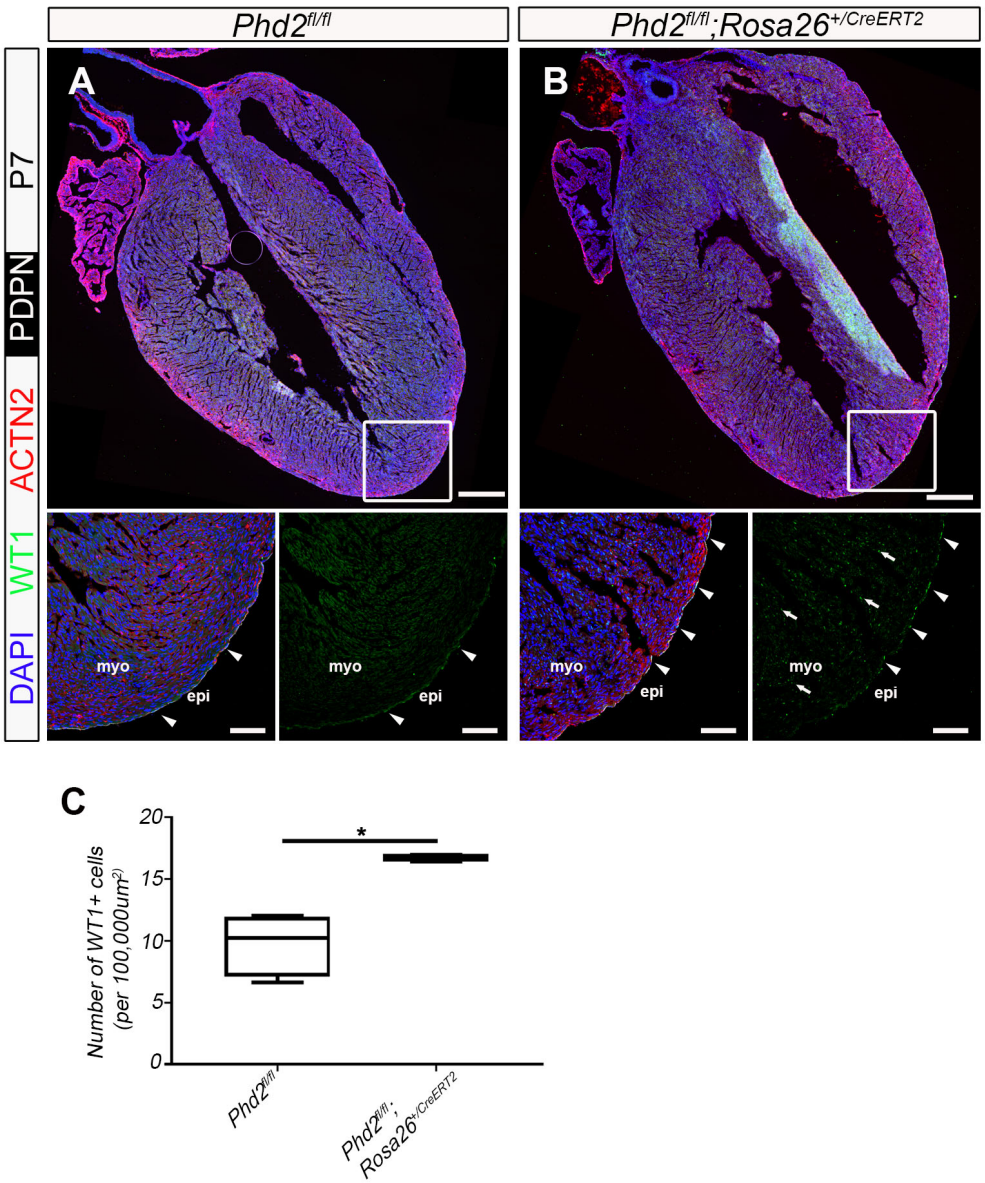


Figure 6.3.2 Loss of *Phd2* results in a significant increase in WT1

A-B. Representative images of immunostaining for WT1 (green), ACTN2 (red), PDPN (white) and DAPI nuclear stain (blue) on cryosections of P7 hearts, from **A**. *Phd2*$^{fl/fl}$ (control) and **B**. *Phd2*$^{fl/fl}$*;Rosa26*$^{+/CreERT2}$ mice. Images below represent high magnifications of boxed regions. Arrowheads highlight expression of WT1 in the epicardium. Epi= epicardium, myo= myocardium. Scale bars are 200μm, high magnification scale bars= 100μm. **C**. Quantification of number of Wt1+ cells in the epicardium per field of view, n=4 hearts for control and n=2 hearts for mutant. Data presented as median, IQR and upper and lower limits. Data analysed by Student t-test; *p<0.05.

6.4 Response to myocardial infarction in the HIF genetic gain-of-function model.

Since the epicardium is predominantly dormant by P7 (see section 5.3), we sought to determine whether prolonged expression of the "master regulator" of epicardial EMT (i.e. WT1), downstream of HIF signalling, would have a beneficial effect on the postnatal heart response to myocardial infarction. With that in mind, stabilisation of HIF signalling was tamoxifen-induced in *Phd2*$^{fl/fl}$;*Rosa26*$^{+/CreERT2}$ pups as outlined above, and LAD ligation surgery was performed at P7, a time point when the regenerative capacity of neonate mice has been lost (Porrello et al., 2011, 2013). Hearts were collected for analysis at 4dpi, to evaluate epicardial activation, and 21dpi to assess scar resolution. This experimental protocol is summarised in Figure 6.4.1 below.

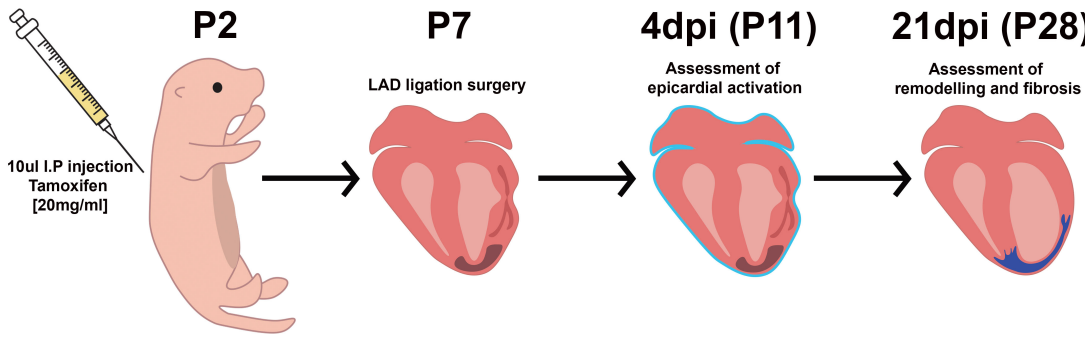


Figure 6.4.1 Myocardial infarction following activation of HIF signalling

Schematic of LAD ligation experiments, following postnatal activation of HIF signalling.

6.4.1 Loss of *Phd2* results in extensive WT1 expression, following myocardial infarction.

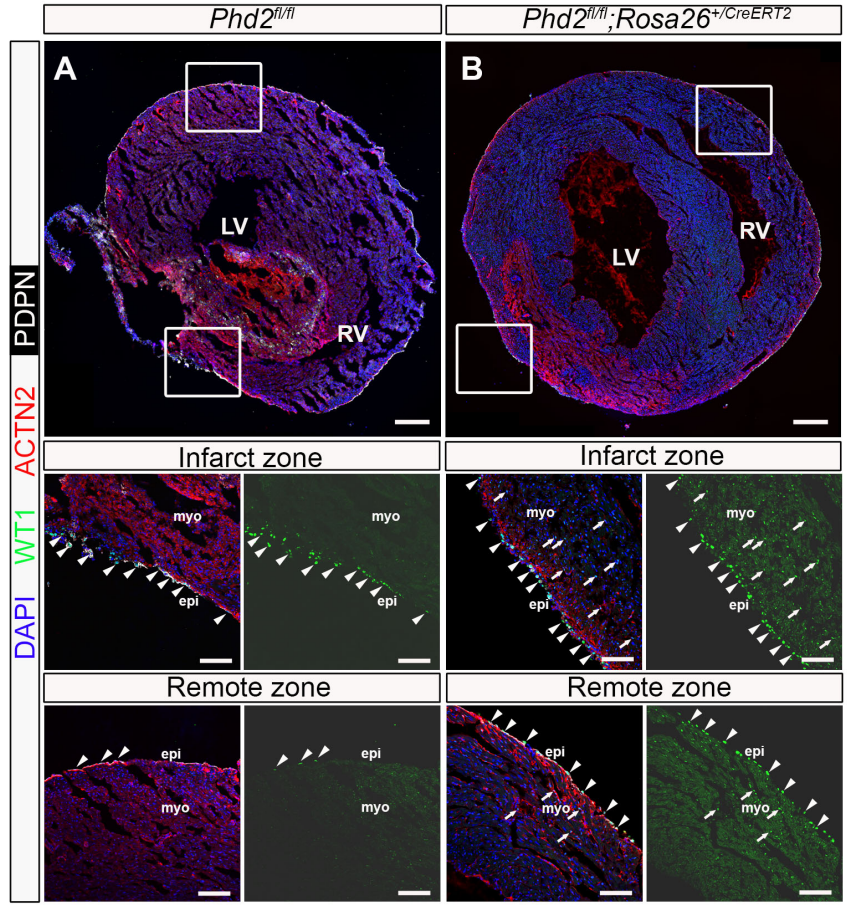
Despite high levels of maternal cannibalisation following surgery, a total of six *Phd2*$^{fl/fl}$ hearts and five *Phd2*$^{fl/fl}$*;Rosa26*$^{+/CreERT2}$ hearts were collected at 4dpi, when epicardial activation is highest (Masters, 2015). However, three hearts were excluded from further analysis, due to incorrect placement of the suture, likely due to twisting of the heart following manipulation out of the thoracic cavity. As such, the data described below refers to a total of four hearts per group.

Immunostaining for WT1, on transverse, apical sections of hearts collected at 4dpi, revealed an increase in WT1-positive cells within the epicardial layer, proximal to the infarct zone, in both the *Phd2*$^{fl/fl}$*;Rosa26*$^{+/CreERT2}$ and the *Cre* negative littermate controls. In addition, WT1 expression was found to be significantly enriched remotely, in relation to the injury area, in the epicardium of the non-infarcted right ventricle of *Phd2*$^{fl/fl}$*;Rosa26*$^{+/CreERT2}$, but not of littermate control hearts, suggesting organ-wide expansion of epicardial activation (Mean number of WT1+ epicardial cells ± SEM; [control infarct zone: 51.00 ± 16.43; mutant infarct zone: 34.14 ± 7.57, n=4, p= 0.3270]; [control remote zone: 2.60 ± 1.21; mutant remote zone: 15.29 ± 2.90, n=4, p= 0.0057]; Figure 6.4.A-D). Likewise, WT1 expression was observed in the myocardium, both in the infarct and remote zone, of *Phd2*-deficient hearts (Mean number of WT1+ cells in myocardial layer ± SEM; [control infarct zone: 2.22 ± 1.44; injury infarct zone: 52.09 ± 12.61, n=4, p= 0.0023]; [control remote zone: 2.63 ± 2.49; injury remote zone: 59.20 ± 16.51, n=4, p= 0.0080]; Figure 6.4.A-B, E-F). It is

likely that some of these WT1-expressing cells were EPDCs, though studies in chick embryos suggest the majority of transitioning epicardial cells downregulate *Wt1* expression following delamination and differentiation (Perez-Pomares et al., 2002), albeit this is in the absence of an injury-induced response. Another possibility for WT1 enrichment within the myocardial compartment could be due to ectopic expression in the other non-epicardial cell types of the heart. In support of the latter, *Rosa26*^{CreER} drives *Cre* expression in a ubiquitous manner, meaning that following tamoxifen delivery, HIF signalling is potentially stabilised in all cardiovascular cell types. Of significance, WT1 expression in murine endothelial cells, in development and in the adult following MI has previously been described (Duim et al., 2015), therefore, we hypothesised that the cells in the myocardial layer expressing WT1 were endothelial cells. To test this hypothesis WT1 was co-stained with the endothelial marker, endomucin (EMCN). Extensive co-expression of WT1 and EMCN throughout the myocardium was observed, supporting an endothelial identity for these WT1+ cells (Figure 6.4.2A).

Whilst the majority of WT1+ cells in the myocardium co-stained with EMCN, there was evidence of WT1^{+}EMCN^{-} cells. Lineage-tracing studies based on *Wt1* activity have reported some co-expression of a WT1-lineage reporter with cardiomyocyte markers, both in development and adult heart following myocardial infarction. It is possible that these cardiomyocytes originated from WT1^{+} precursors, and are not themselves expressing WT1 (Smart et al., 2011; Zhou et al., 2008). Indeed, endogenous expression of WT1 in cardiomyocytes has not been reported to-date. To determine whether loss of *Phd2* driven by *Rosa26*^{CreER} resulted in ectopic expression of WT1 in myocytes within the

injured neonatal heart, WT1 was co-stained against the marker α-sarcomeric actinin (ACTN2). Co-localisation of WT1 with ACTN2 was not observed (Figure 6.4.2B), suggesting ectopic expression of WT1 in cardiomyocytes, following loss of *Phd2*, does not occur.


Phd2fl/fl
Phd2fl/fl;Rosa26+/CreERT2
A
B
LV
RV
LV
RV
PDPN
ACTN2
WT1
DAPI
Infarct zone
Infarct zone
Remote zone
Remote zone
myo
epi

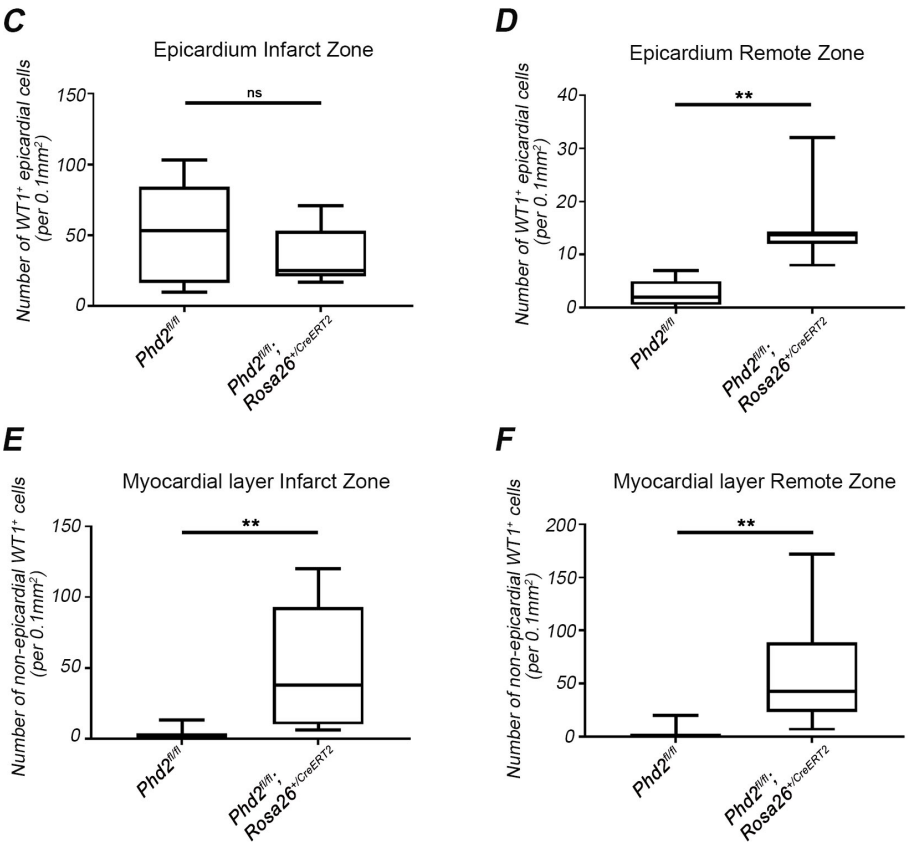

C
Epicardium Infarct Zone
Number of WT1+ epicardial cells (per 0.1mm²)
ns
150
100
50
0
Phd2fl/fl
Phd2fl/fl; Rosa26+/CreERT2
D
Epicardium Remote Zone
Number of WT1+ epicardial cells (per 0.1mm²)
**
40
30
20
10
0
Phd2fl/fl
Phd2fl/fl; Rosa26+/CreERT2
E
Myocardial layer Infarct Zone
Number of non-epicardial WT1+ cells (per 0.1mm²)
**
150
100
50
0
Phd2fl/fl
Phd2fl/fl; Rosa26+/CreERT2
F
Myocardial layer Remote Zone
Number of non-epicardial WT1+ cells (per 0.1mm²)
**
200
150
100
50
0
Phd2fl/fl
Phd2fl/fl; Rosa26+/CreERT2

Figure 6.4.1 Loss of *Phd2* results in a significant increase in WT1 expression post-MI

A-B. Representative images of immunostaining for WT1 (green), ACTN2 (red), PDPN (white) and DAPI nuclear stain (blue) on transverse apical sections of hearts from **A**. Control *Phd2*$^{fl/fl}$ and **B**. *Phd2*$^{fl/fl}$*;Rosa26*$^{+/CreERT2}$ mice. Images below represent high magnifications of boxed regions. Arrowheads highlight expression of WT1 in the epicardium (determined by co-expression with PDPN), arrows highlight WT1 expression in cells outside of epicardial layer. Epi= epicardium, myo= myocardium. Scale bars are 200μm, high magnification bars are 100μm. **C-F**. Quantification of number of WT1 positive cells, per Xμm area, in **C-D**. the epicardium or **E-F**. outside of the epicardial layer, in **C, E.** the infarct zone or **D, F.** the remote zone. n=4 hearts per group. Data presented as median, IQR and upper and lower limits. Data analysed by Student t-test; **p<0.01; ns= not significant.

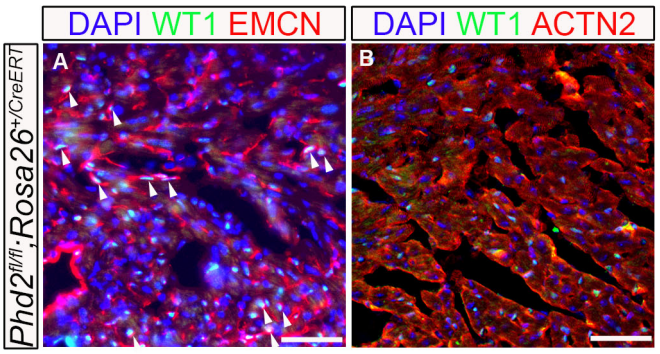


Figure 6.4.2 WT1 is expressed in endothelial cells following activation of HIF.

A-B. Representative images of co-staining of WT1 (green) with **A**. the endothelial cell marker, EMCN (Red) or **B.** the cardiomyocyte marker, ACTN2 (Red). Arrowheads highlight co-expression of WT1 with EMCN. Scale bars are 50μm.

6.4.2 Stabilisation of HIF does not increase neovascularisation at four days post injury.

In order to determine whether the widespread expression of WT1 resulting from ubiquitous loss of *Phd2* promoted neovascularisation, immunostaining against the endothelial marker EMCN and smooth muscle marker SM-22α was done on sections from mutant and control hearts collected at 4dpi. No gross differences in marker expression, nor in the number of mature EMCN+ SM-22α^{+} coronary vessels were observed (Figure 6.4.3), suggesting that the neovascularisation response, at 4dpi, is not substantially affected by stabilisation of HIF.

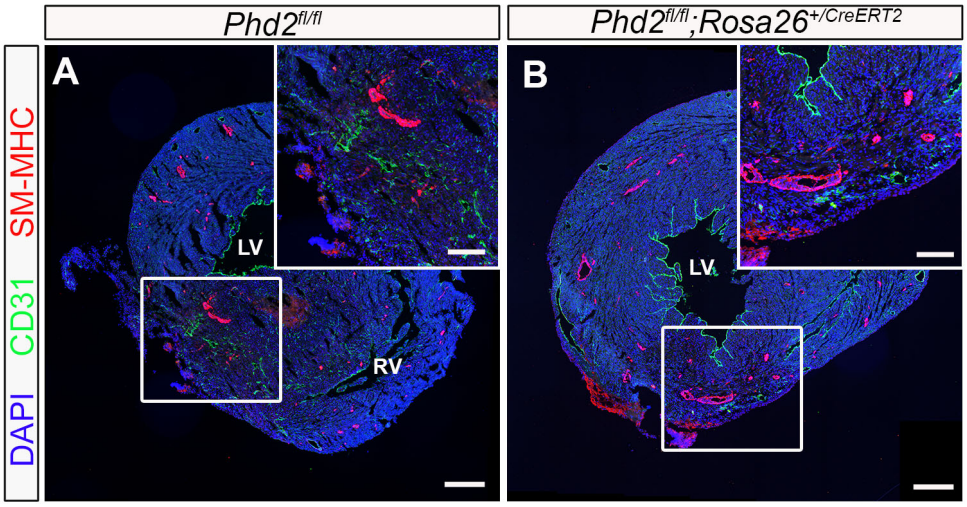


Figure 6.4.3 Loss of *Phd2* does not lead to changes in vessel formation, four days after myocardial infarction at P7.

A-B. Representative images of immunostaining for EMCN (green), SM-MHC (red) and DAPI (blue) on transverse apical sections of hearts from **A**. Control (*Phd2*$^{fl/fl}$) and **B**. *Phd2*$^{fl/fl}$;*Rosa26*$^{+/CreERT2}$ hearts 4dpi, following MI at P7. Images in top right corner represent high magnifications of boxed region. n=4 hearts per group. RV= right ventricle, LV= left ventricle. Scale bars 200μm, high magnification scale bars= 50μm.

6.4.3 Loss of *Phd2* does not lead to gross changes in cell proliferation nor monocyte/macrophage recruitment, four days post-infarction.

Complete regeneration requires the generation of new muscle and vessels combined with the complex modulation of the inflammatory response. Macrophages, key mediators of inflammation, are essential for mouse neonatal cardiac regeneration (Aurora et al., 2014). A study on hind-limb ischaemia, by Takeda and colleagues, demonstrated that *Phd2* haplo-deficiency induced arteriogenesis, due to expansion of tissue-resident reparative macrophages (Takeda et al., 2011). Immunostaining against proliferation marker PHH3, was used to look at global proliferation in the heart 4dpi, following loss of *Phd2*. Further, co-staining with the monocyte/macrophage marker, CD68, was used to determine if there was an effect on monocyte/macrophage recruitment and expansion specifically. Both control and $Phd2^{fl/fl};Rosa26^{+/CreERT2}$ hearts displayed global PHH3 expression, with no notable differences between the two groups. Concomitantly, significant expression of CD68 was observed in the infarct zone, in both $Phd2^{fl/fl};Rosa26^{+/CreERT2}$ and control hearts with no observable differences between them. Instead, expression of CD68 and PHH3 increased with infarct size, across both groups (Figure 6.4.4). This suggests loss of *Phd2* does not affect overall cell proliferation, and monocyte/macrophage recruitment and proliferation, following MI at P7. To determine if there were any differences in cardiomyocyte proliferation specifically, co-staining with the cardiomyocyte marker ACTN2 would need to be performed and quantified.

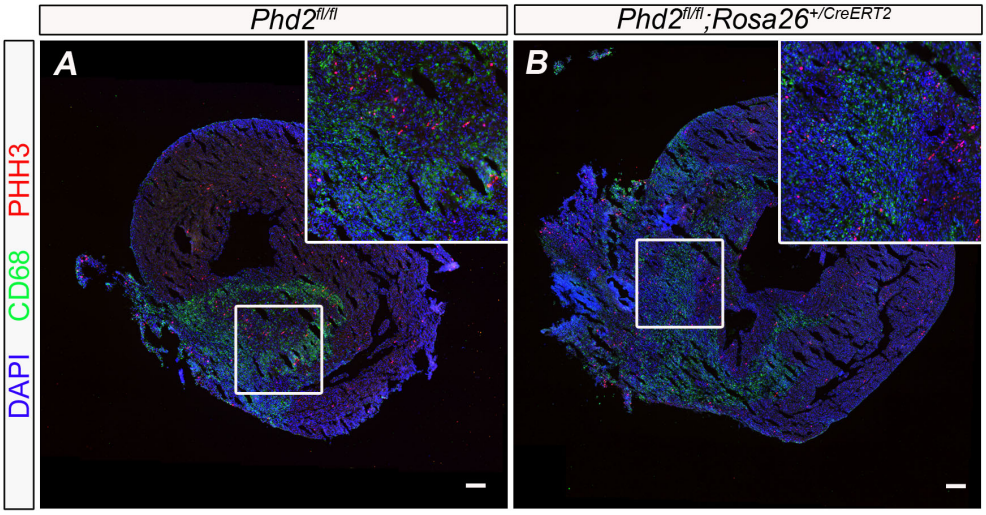


Figure 6.4.4 Activation of HIF does not lead to notable changes in global cell proliferation or monocyte/macrophage proliferation/recruitment, four days following MI.

A-B. Representative images of immunostaining for CD68 (green), PHH3 (red) and DAPI (blue) on transverse apical sections of hearts from **A**. Control (*Phd2*$^{fl/fl}$) and **B**. *Phd2*$^{fl/fl}$*;Rosa26*$^{+/CreERT2}$ hearts 4dpi, following MI at P7. Images in top right corner represent high magnifications of boxed region. RV= right ventricle, LV= left ventricle n=4 hearts per group. Scale bars 200μm, high magnification scale bars= 50μm.

6.4.4 Loss of *Phd2* in cardiac remodelling and fibrosis

As demonstrated in chapter 5, 21 days post infarction, the P1 heart is fully regenerated, with little or no residual scar, whilst the P7 heart presents with substantial ventricular remodelling and persistent scar deposition. Given the role of WT1+ epicardial cells in cardiomyocyte proliferation, and coronary vessel formation during development, we hypothesised, the observed increase in WT1 expression, at 4dpi, would have a downstream consequence on both of these processes at a later time-point, thus resulting in a decrease in pathological remodelling and reduced scar deposition.

To this end, samples were collected at 21dpi, for histological analysis, to assess ventricular remodelling and scar resolution (Figure 1.5.1). Of all the surgeries performed in P7 neonates only three *Phd2*$^{fl/fl}$ and one *Phd2*$^{fl/fl}$*;Rosa26*$^{+/CreERT2}$ pups survived to 21dpi, 4 out 30 animals. The remaining pups were either cannibalised in the immediate days after surgery or died shortly thereafter. Of significance, this animal loss was observed in both experimental groups so is likely to reflect tamoxifen toxicity. Despite the low n numbers, samples were analysed, to look for potential differences in the extent of regeneration. Histological analysis of control hearts revealed a decline in cardiac muscle around the site of the injury (Figure 6.4.5A), accompanied by a transmural scar, which extended to the epicardial surface (Figure 6.4.5C). Further, control hearts presented with dilation of the left ventricle and a thinned right ventricle, suggestive of pathological remodelling. Analysis of the *Phd2*$^{fl/fl}$*;Rosa26*$^{+/CreERT2}$ heart revealed a thicker, more intact myocardium, at the site of injury, in comparison to controls (Figure 6.4.5B), suggesting loss of *Phd2* may have improved cardiac muscle survival post-MI. However, the heart also presented with a transmural scar, which extended to the epicardial surface (Figure 6.4.5D), therefore, loss of *Phd2* may not be sufficient to stimulate scar-free regeneration in the normally non-regenerative P7 heart. Despite this large scar, minimal remodelling in the left ventricle was observed, and none in the right, suggestive of a decrease in pathological remodelling compared to control hearts. Care was taken not to over-interpret the results and more samples need to be analysed before making any conclusions. This is fully discussed in section 6.6.5.

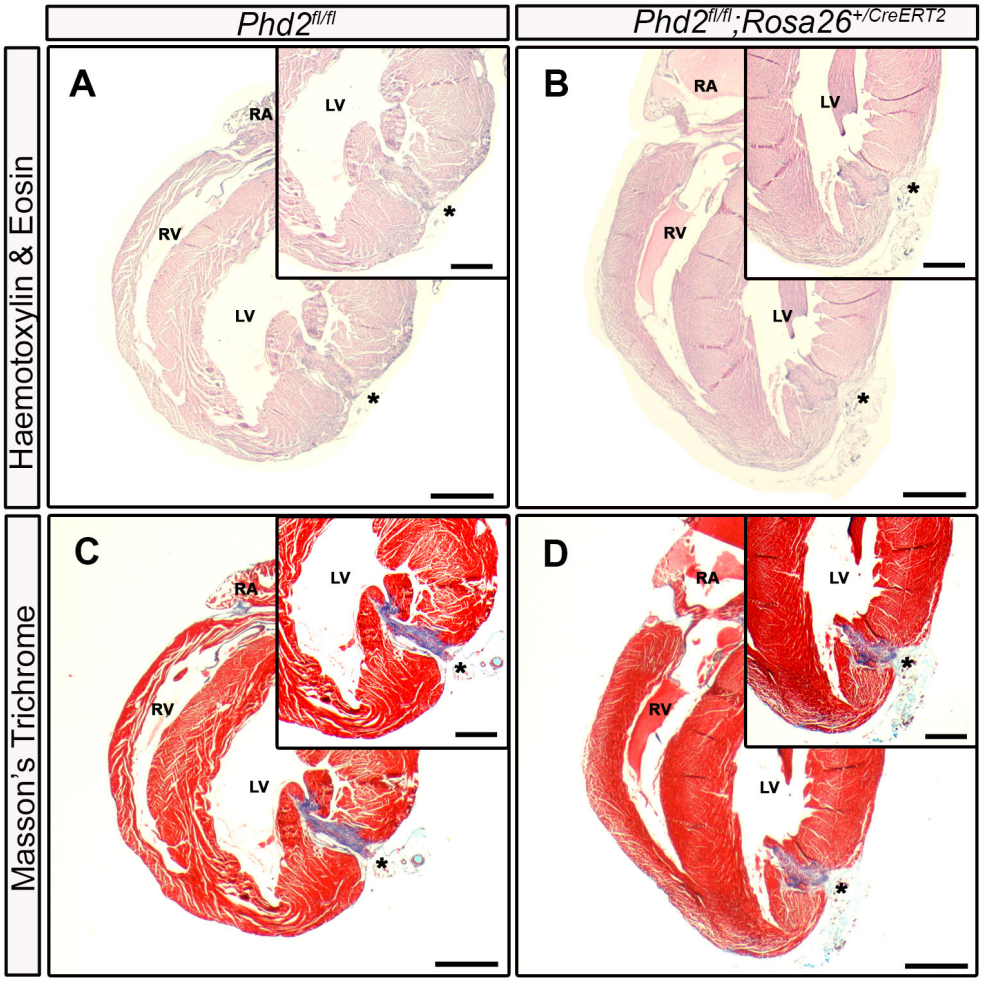


Figure 6.4.5 Potential improved myocardial survival and reduced ventricular remodelling following loss of *Phd2*.

A-B. Haematoxylin and Eosin staining of **A**. Control (*Phd2*$^{fl/fl}$) and **B**. *Phd2*$^{fl/fl}$;*Rosa26*$^{+/CreERT2}$ hearts 21 days following LAD ligation at P7. **C-D**. Masson's Trichrome stained serial sections to show cardiac fibrosis (blue). Images in top right represent high magnifications of boxed regions. RA= right atria, RV= right ventricle, LV= left ventricle. * indicates suture placement. Arrows highlight collagen deposition and scarring. Scale bars= 1mm, high magnification scale bars =0.5mm. Images representative of n=3 for controls, n=1 for *Phd2*$^{fl/fl}$;*Rosa26*$^{+/CreERT2}$.

6.5 Pharmacological activation of HIF signalling

Genetic knock-down of *Phd2,* acting as a gain-of-function of HIF signalling, resulted in a significant increase in WT1 expression in the postnatal heart, following LAD ligation at P7. However, due to the toxic effects of tamoxifen administration postnatally, the histological and functional impact of WT1 enrichment on the regenerative response could not be assessed in full. Further, whilst a genetic approach to activate HIF signalling ensures specificity at the level of the targeted PHD2 pathway, it is not applicable therapeutically. Pharmacological activation of HIF signalling, through PHD inhibition, circumvents the need for tamoxifen administration in terms of the neonatal mouse studies, and provides a potential therapeutic approach to regenerate the heart post-MI in human patients.

Experiments conducted in Chapter 4 demonstrated FG-4592 is capable of stabilising HIF1α in murine epicardial cells *in vitro*. This resulted in a significant increase in WT1 expression, akin to genetic loss of *Phd2* (see Chapter 4). Moreover, *in vitro* treatment with FG-4592 led to an increase in SNAI1/2 expression and proportion of mesenchymal cells, indicating augmentation of EMT.

We aimed to replicate the increased WT1 expression observed in our genetic *Phd2*$^{fl/fl}$*;Rosa26*$^{+/CreERT2}$ model post-MI following injury at P7, via pharmacological inhibition of PHDs, with FG-4592 and to assess the downstream consequences on the regenerative response of the heart.

6.5.1 FG-4592 dose administration.

Whilst HIF was activated prior to surgery in the previous experiments, regenerative therapies in the clinic would need to be implemented post-infarction, therefore, FG-4592 was administered following LAD ligation, to signify a more therapeutically relevant approach. FG-4592 has a reported half-life of approximately 12 hours (Provenzano et al., 2016b), and previous studies have administered the drug daily, in adult mice, at a dose of 10mg/kg body weight (Tang et al., 2018). As such, in a pilot study, wildtype C57BL/6 P7 pups were injected, via IP, with 10mg/kg of FG-4592, immediately after LAD surgery, and then once daily for 3 days thereafter. However, this dosing regimen resulted in significant maternal cannibalism, which may have been due to repeated disturbance of the litter, or due to drug toxicity, resulting in death followed by cannibalisation.

Hoppe and colleagues reported HIF stabilisation, for at least 24 hours, following a single IP injection of 10mg/kg FG-4592 in neonatal mice, and reported a half-life of 2-3 days (Hoppe et al., 2016). Therefore, for subsequent studies, a single dose of 10mg/kg was administered immediately following surgery and was found to be well tolerated (Figure 6.5.1). Hearts were then collected at 4dpi, to evaluate epicardial activation, and 21dpi to assess scar deposition and cardiac remodelling. Wildtype C57BL/6 untreated pups were collected as controls.

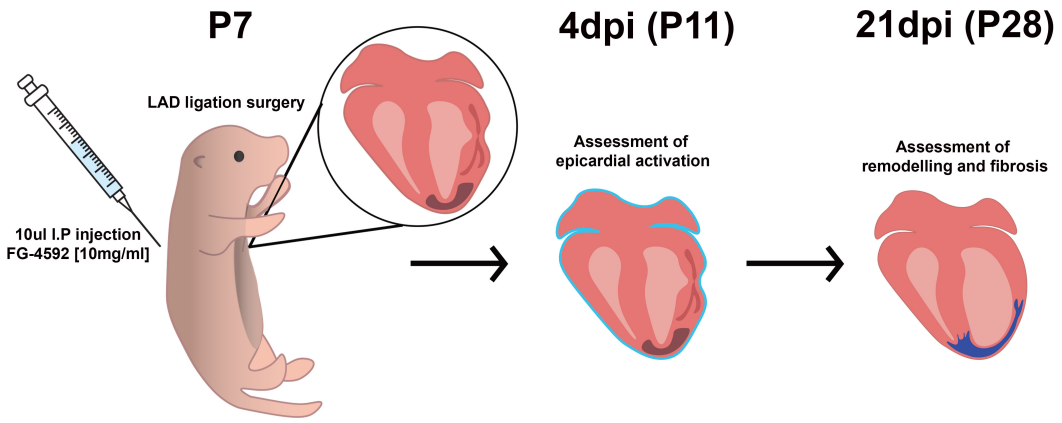
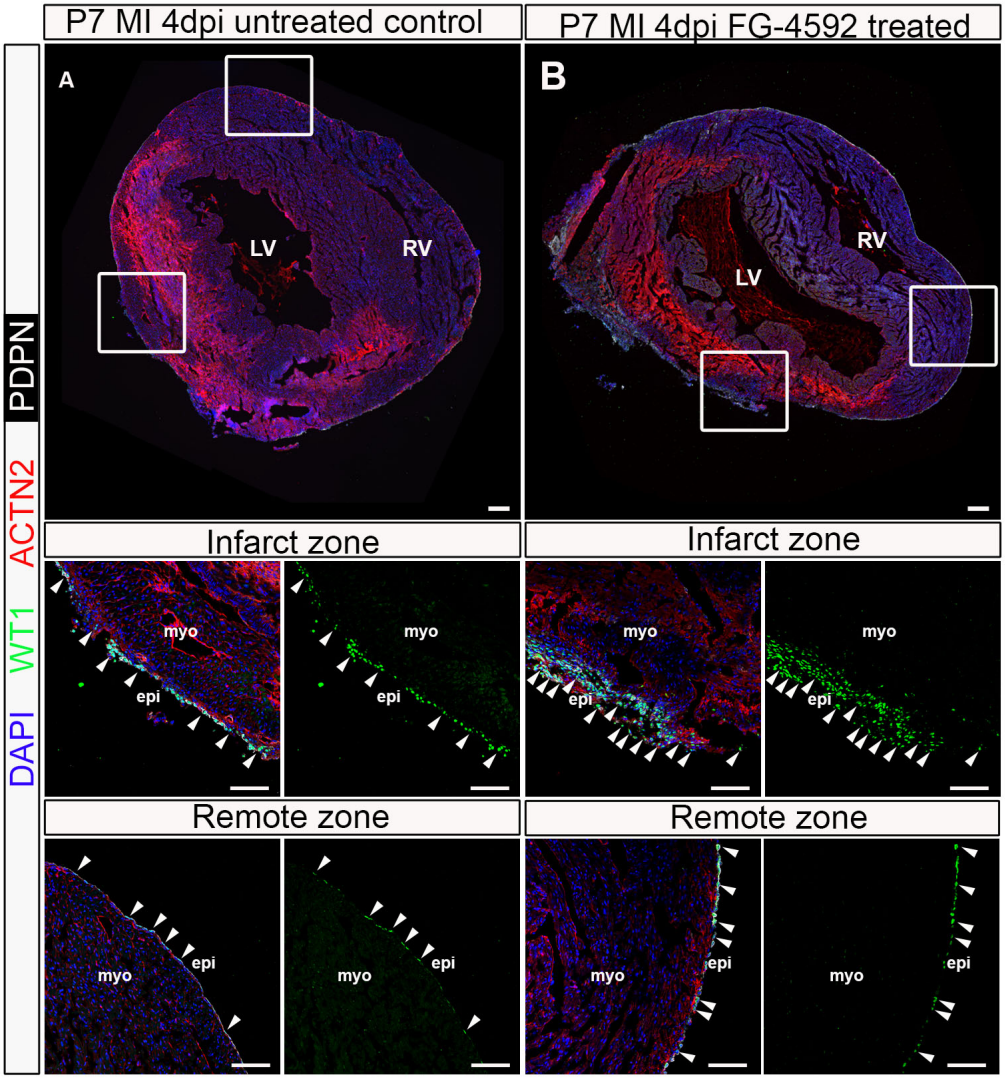


Figure 6.5.1 Pharmacological activation of HIF signalling following myocardial infarction.

Schematic of neonatal LAD ligation studies, with treatment with FG-4592.

6.5.2 Inhibition of PHDs, post-MI leads to a significant upregulation of epicardial WT1.

Immunostaining for WT1, on transverse, apical section of hearts, collected at 4dpi, revealed a significant increase in epicardial WT1 expression in the infarct zone, in FG-4592 treated hearts compared to controls (Mean number of WT1+ epicardial cells ± SEM; control infarct zone: 55.46 ± 7.89, n=4; treated infarct zone: 118.20 ± 19.65, n=6; p= 0.0210; Figure 6.5.2A-C). In contrast to genetic *Phd2* loss-of-function, no differences in epicardial WT1 expression in the remote zone were observed (Mean number of WT1+ epicardial cells ± SEM; control remote zone: 15.71 ± 3.05, n=4; treated remote zone: 12.08 ± 2.94, n=6; p= 0.4135; Figure 6.5.2D). Moreover, WT1 expression was observed predominately in the epicardial layer, with little or no expression in the myocardial compartment,


P7 MI 4dpi untreated control
P7 MI 4dpi FG-4592 treated
A
B
LV
RV
LV
RV
PDPN
ACTN2
WT1
DAPI
Infarct zone
Infarct zone
Remote zone
Remote zone
myo
epi
myo
epi
myo
epi
myo
epi
myo
epi
myo
epi
myo
epi
myo
epi

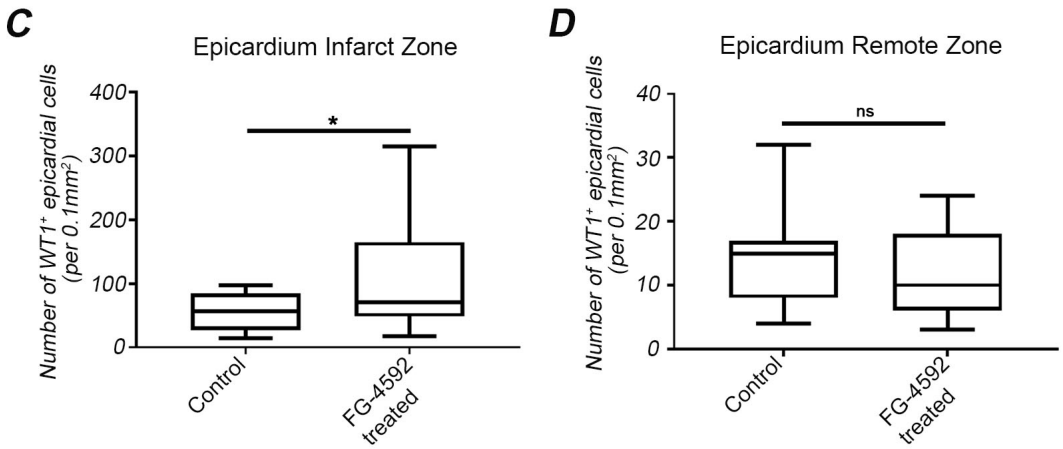

C
Epicardium Infarct Zone
Number of WT1+ epicardial cells (per 0.1mm²)
400
300
200
100
0
*
Control
FG-4592 treated
D
Epicardium Remote Zone
Number of WT1+ epicardial cells (per 0.1mm²)
40
30
20
10
0
ns
Control
FG-4592 treated

Figure 6.5.2 Pharmacological inhibition of PHDs increases epicardial WT1 expression following myocardial infarction

A-B. Representative images of immunostaining for WT1 (green), ACTN2 (red), PDPN (white) and DAPI nuclear stain (blue) on transverse apical sections of hearts from C57BL/6 pups, following LAD ligation surgery at P7, collected 4dpi. **A**. Control (non-treated) and **B.** FG-4592 treated. Images below represent high magnifications of boxed regions. Arrowheads highlight expression of WT1 in the epicardium. Epi= epicardium, myo= myocardium. Scale bars are 200μm, high magnification bars are 100μm. **C-D**. Quantification of number of WT1 positive cells, per 0.1mm^2 area, **C**. in the infarct zone or **D.** in the remote zone. n=4 control, n=6 treated mice. Data analysed by Student t-test; *<0.05; ns= not significant.

6.5.3 Activation of HIF does not lead to increased neovascularisation, four days post-MI.

In order to determine whether the observed increase in epicardial WT1, following treatment with FG4592, promoted neovascularisation, immunostaining against the endothelial marker EMCN and smooth muscle marker SM-22α was performed on sections from treated and control hearts collected at 4dpi. No notable differences between marker expression, or the number of mature EMCN+ SM-22α+ vessels were observed between the two groups (Figure 6.5.3), suggesting the neovascularisation response was not affected, following treatment with FG-4592, as early as 4dpi.

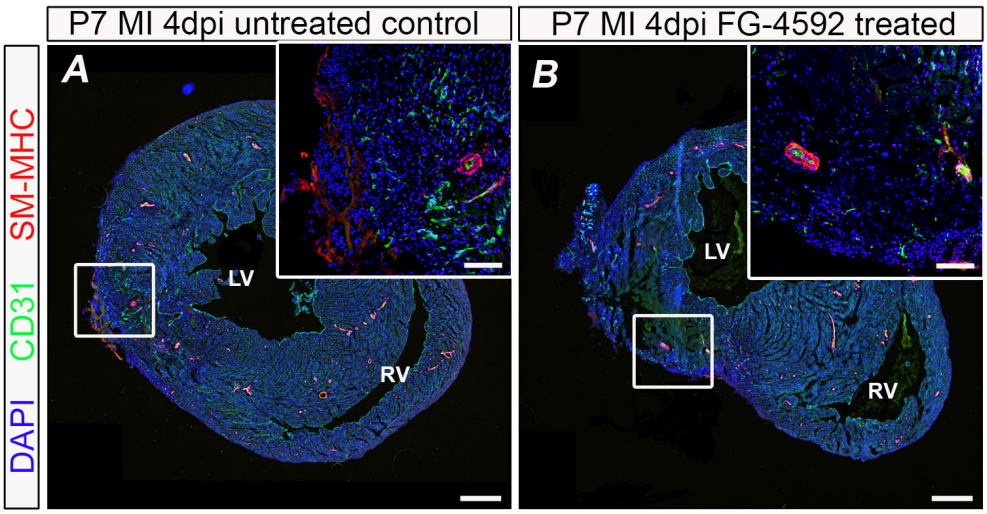


Figure 6.5.3 Pharmacological activation of HIF does not lead to notable differences in neovascularisation, four days post injury.

A-B. Representative images of immunostaining for EMCN (green), SM-MHC (red) and DAPI (blue) on transverse apical sections of hearts from C57BL/6 pups, following LAD ligation surgery at P7, collected 4dpi. **A**. Control (non-treated) and **B.** FG-4592 treated. Images in top right corner represent high magnifications of boxed region. RV= right ventricle, LV= left ventricle. n=4 control, n=6 treated mice. Scale bars 200μm, high magnification scale bars= 50μm.

6.5.4 Inhibition of PHDs post-MI does not alter global proliferation nor early macrophage proliferation/recruitment.

To determine whether treatment with FG-4592 stimulated cell proliferation, along with recruitment and proliferation of monocytes/macrophages, immunostaining against the proliferation marker, PHH3 and the monocyte/macrophage marker CD68 was performed. No gross differences in global proliferation were observed, nor differences in the recruitment and proliferation of monocytes/macrophages (Figure 6.5.4), suggesting absolute proliferation and monocyte/macrophage recruitment are not affected by treatment with FG-4592, 4 days after injury.

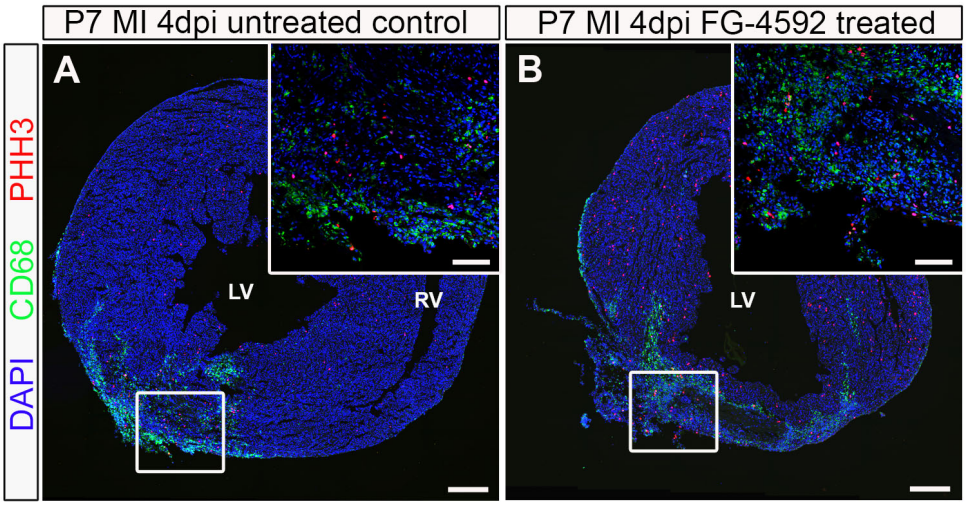


Figure 6.5.4 Global proliferation and early monocyte/macrophage proliferation/recruitment are not altered following inhibition of PHDs post-MI.

A-B. Representative images of immunostaining for CD68 (green), PHH3 (red) and DAPI (blue) on transverse apical sections of hearts from C57BL/6 pups, following LAD ligation surgery at P7, collected 4dpi. **A**. Control (non-treated) and **B.** FG-4592 treated. Images in top right corner represent high magnifications of boxed region. n=4 control, n=6 treated mice. Scale bars 200μm, high magnification scale bars= 100μm.

6.5.5 A single dose of FG-4592 results in a decrease in pathological remodelling post-MI.

Unlike tamoxifen treatment, injection with FG-4592 was well-tolerated, therefore, hearts were collected at 21dpi to assess the impact of treatment on the regenerative response. H&E staining of control hearts revealed significant damage to the myocardium at the suture site, thinning and dilation of the left ventricle, along with evidence of thinning and remodelling of the right ventricle. FG-4592-treated hearts presented with comparatively less dilation and thinning of the left ventricle, with a less severely damaged myocardium at the site of suture, and the right ventricle appeared normal (Figure 6.5.5A-D). However,

Masson's trichrome staining revealed the presence of a transmural scar, in all treated hearts, indicating treatment with FG-4592 was not sufficient to prevent fibrosis (Figure 6.5.5E-H). Nonetheless, the observed reduction in pathological remodelling, despite the presence of a fibrotic collagen scar, suggests the presence of a more viable myocardium and that pharmacological inhibition of PHDs to stabilise HIF signalling leads to an improved regenerative response following MI at P7. More samples will need to be collected to confirm this finding and to determine the mechanism of action of HIF signalling and the corresponding epicardial activation in this context.

Haemotoxylin & Eosin
Masson's Trichrome
Control
P7 MI 21dpi
FG-4592 treated
P7 MI 21dpi
A
B
C
D
E
F
G
H
RA
RV
LV

Figure 6.5.5 Assessment of cardiac remodelling and collagen deposition 21dpi.

A-D. Haematoxylin and Eosin staining of **A-B**. Control (untreated) and **C-D**. FG-4592 treated hearts 21 days following LAD ligation at P7. **E-H**. Masson's Trichrome stained serial sections to show cardiac fibrosis (blue). Images in top right represent high magnifications of boxed regions. RA= right atria, RV= right ventricle, LV= left ventricle. * indicates suture placement. Arrows highlight collagen deposition and scarring. Scale bars= 1mm, high magnification scale bars =0.5mm. Images representative of n=4 for each group.

6.6 Discussion

6.6.1 HIF signalling in the quiescence of the epicardium

Postnatal loss of *Phd2* expression led to a significant increase in cardiac expression of the HIF target gene, *Glut1*, suggesting HIF signalling was activated. Further a significant increase in *Wt1* expression was observed, and immunostaining revealed expression was predominantly in the epicardium, with some WT1+ cells in the myocardial layer. HIF1α has previously been shown to induce expression of *Wt1* (Wagner et al., 2003), and ChIP-seq analysis on ccRCC cells confirmed a direct interaction, therefore, stabilised HIF1α may be directly upregulating expression of *Wt1* in these hearts. Moreover, it suggests the observed increase in *Phd2* expression after birth (Chapter 5), may contribute to the reduction in *Wt1* expression, and therefore quiescence of the epicardium, in the first week of life. To confirm a direct interaction between HIF and *Wt1*, CHIP-seq on isolated epicardial cells would need to be performed.

Whilst expression of *Wt1* was significantly increased, expression of other epicardial genes, *Tcf21, Tbx18* and *Raldh2* remained unchanged. Previous work in the lab indicated the developing zebrafish epicardium is a heterogenous population, with three, spatially restricted, sub-populations, characterised by differential expression of *Wt1b, Tbx18* and *Tcf21* (Weinberger, 2017). Additional work demonstrated that, following injury, the reactivated adult mammalian epicardium is highly heterogenous, with different subpopulations exhibiting varied cardiovascular potential (Bollini et al., 2014), therefore, HIF signalling may only be important in the activation of a distinct

population of epicardial cells, notably a WT1^{+} sub-population. However, it could also be because gene expression was measured in whole ventricular lysates, thus changes in epicardial gene expression may be masked by expression elsewhere in the heart (Christoffels et al., 2009; Hidai et al., 1998; Kikuchi et al., 2011; Robb et al., 1998). To overcome this issue, immunostaining, to determine the extent and distribution of TCF21, TBX18 and RALDH2 protein should be performed, we were however unable to find antibodies against these proteins that worked successfully on cryosections.

6.6.2 Activation of WT1 by HIF.

Phd2$^{fl/fl}$*;Rosa26*$^{+/CreERT2}$ hearts showed a substantial increase in epicardial WT1 expression, proximal to the injury, although surprisingly, this did not significantly differ from the control hearts. However, whilst in control hearts minimal epicardial expression of WT1 was observed in the remote zone, a significant increase was observed following loss of *Phd2*. Thus, indicating activation of HIF, by inhibition of *Phd2,* enhanced the epicardial response to injury. Importantly, expression was higher than previously observed following loss of *Phd2* in the uninjured P7 hearts, suggesting this response was injury dependant.

Correspondingly, a striking increase in WT1 throughout the entire myocardial layer was observed in all *Phd2*$^{fl/fl}$*;Rosa26*$^{+/CreERT2}$ hearts. Work in Chapter 4 suggested HIF signalling promotes epicardial EMT via SNAI1/2, therefore, some of these cells are likely to be activated epicardial cells which have undergone EMT and migrated into the underlying myocardium. To confirm this, immunostaining of sections, with antibodies against WT1 and SNAI1/2, could

be used to look for co-expression, however, both available antibodies are raised in rabbit, therefore, an approach using serial sections would need to be used.

Nonetheless, given the extent of WT1 expression, it is unlikely all these cells are EPDCs, moreover, it has been reported in chick embryos that the majority of EPDCs downregulate expression of WT1, following migration into the myocardium and differentiation (Perez-Pomares et al., 2002), therefore, it is likely that WT1 was also activated in other cell types of the heart. In support of this possibility, the *Rosa26*$^{+/CreERT2}$ is a ubiquitous Cre, thus HIF signalling is stabilised in all cell types of the heart.

Substantial co-expression of WT1 with the endothelial marker EMCN, indicated the majority of the observed WT1+ cells were endothelial. Endothelial cell expression of WT1, in both rats and adult mice, following myocardial infarction, has previously been reported (Duim et al., 2015; Wagner et al., 2002), suggesting a role for WT1 in the endothelial cell response to injury. However, contrary to their findings, we did not observe substantial WT1 expression in endothelial cells in wildtype controls, but instead observed only minimal endothelial expression, similar to levels reported by Zhou and colleagues (Zhou et al., 2011). Interestingly, both groups demonstrated a role for hypoxia and HIF in this response. Taken together with our findings, this suggest loss of *Phd2* enhances expression of *Wt1* in endothelial cells, via HIF-mediated transcription. Whilst endothelial WT1 expression has previously been described, its function has not been fully elucidated. Duim and colleagues suggested a role in endothelial cell proliferation, since knockdown of *Wt1* in human umbilical endothelial cells (HUVECs), resulted in a decrease in

expression of CyclinD1, a regulator of cell cycle progression and a direct target of WT1 (Duim et al., 2015). Interestingly, WT1 is frequently over-expressed in endothelial cells in tumours, and was shown to be a key factor in hypoxia-mediated tumour angiogenesis via direct activation of VEGF transcription (McCarty et al., 2011). Therefore, the observed increase in endothelial WT1 expression, following loss of *Phd2*, may promote neovascularisation and angiogenesis, thus improving the regenerative response. To test this sections were immunostained with EMCN and SM-MHC to assess the coronary vessels, however, there were no observable differences between control and *Phd2*$^{fl/fl}$*;Rosa26*$^{+/CreERT2}$ hearts. That said, hearts were collected at 4dpi, when epicardial activation was highest, but formation of new vessels may not have occurred. Porrello and colleagues reported formation of new vessels from 7dpi in the regenerative P1 heart, but did not examine P7 hearts (Porrello et al., 2013), therefore, for future studies samples should be collected along a time-course, to include 7dpi, to assess neo-vessel formation.

6.6.3 Epicardial specific deletion of WT1

Whilst the observed increase in WT1+ epicardial cells, and migratory EPDCs, following loss of *Phd2*, suggests enhancement of the epicardial response to injury, the use of the ubiquitous Cre driver, Rosa26;$^{+/CreERT2}$, makes it difficult to determine whether any downstream effects on the regenerative response were as a direct result of epicardial activation, or were from the effect of activation of HIF signalling on the pathway itself. For example, in development WT1^{+} EPDCs secrete FGF9 and IGF2, to stimulate cardiomyocyte proliferation (Brade et al., 2011; Lavine et al., 2005). Correspondingly, HIFα represses cell

stress pathways in foetal cardiomyocytes, enabling them to proliferate (Guimarães-Camboa et al., 2015). Therefore, if an increase in cardiomyocyte proliferation was observed at later stages, there would be no way to distinguish if this was as a result of paracrine signalling from the activated epicardium, or from the direct role of HIF on cardiomyocyte cell cycle progression.

This major caveat to the approach could not be avoided, due to the lack of a postnatal/adult epicardial-specific Cre-driver. Previously reported genetic models all rely on the expression of genes only expressed in the epicardium during development, therefore, activation of the Cre at postnatal or adult stages, when the epicardium is quiescent, is not possible. Work in Chapter 5 demonstrated expression of WT1 decreases shortly after birth, with very few $WT1^{+}$ cells in the epicardium from P4 onwards. Therefore, use of the epicardial specific $WT1^{CreERT2/+}$ line, employed in Chapter 3 of this thesis, would have resulted in HIF activation in only a very small set of cells postnatally, and would therefore have been unlikely to have a significant impact. To that end it was decided to conduct preliminary studies using the ubiquitous $Rosa26^{+/CreERT2}$, but with a focus on the epicardial response specifically. Given the observed impact of HIF signalling on the epicardium, and WT1 specifically, future studies will utilise the $WT1^{CreERT2/+}$ line to determine whether loss of *Phd2* in only a subset of epicardial cells is enough to elicit a response. Further, given that activation of HIF signalling increased WT1 expression, an initial dose of tamoxifen could increase WT1 expression, leading to recombination in more cells upon a second administration. However, multiple doses of tamoxifen may not be practical, as discussed in section 6.6.5. Alternatively, tamoxifen could be administered shortly after LAD surgery, since injury alone results in an

upregulation of WT1, and would therefore target *Phd2* expression in a greater number of cells.

6.6.4 Loss of *Phd2* in the regenerative response

To determine whether loss of *Phd2* was sufficient to invoke a regenerative response similar to that seen in the P1 heart, samples were collected at 21dpi to investigate levels of scar deposition and cardiac remodelling. Only one *Phd2*$^{fl/fl}$*;Rosa26*$^{+/CreERT2}$ heart was collected at 21dpi due to impaired survival of tamoxifen treated animals, however, the presence of a collagen scar suggests loss of *Phd2* alone is insufficient to stimulate complete regeneration. Despite the presence of a fibrotic scar, the *Phd2*$^{fl/fl}$*;Rosa26*$^{+/CreERT2}$ heart had less cardiac remodelling and a thicker myocardium, suggesting an improvement in the regenerative response, however, insufficient n-numbers mean no real conclusions, on the consequence of *Phd2* loss on the regenerative response, can be drawn.

6.6.5 Tamoxifen toxicity in the neonate

Whilst the optimised tamoxifen protocol, described in section 6.4, sufficiently reduced *Phd2* expression, activated HIF signalling, and avoided maternal cannibalism following injection, it had a significant negative impact on the LAD ligation surgery. Initial survival rates, following myocardial infarction, were lower than wildtype C57BL/6 mice, and therefore the protocol had to be adapted accordingly.

Initially the tamoxifen protocol consisted of two injections, at P2 and P4, however, pups were unable to recover after myocardial infarction, following this

regimen. Importantly, the lack of recovery was irrespective of genotype, suggesting it was, in fact, as a result of the tamoxifen administration, as opposed to an effect of loss of *Phd2*. Moreover, sham operations, in which the heart was manipulated out of the chest but no suture through the heart was placed, resulted in full recovery. Therefore, the cardiac insult alone caused the lack of recovery, suggesting tamoxifen was affecting cardiac function, a phenomenon which has previously been described. Several patients treated with tamoxifen, for childhood gliomas, developed long-QT syndrome (LQTS) (Pollack et al., 1997). Tamoxifen is known to inhibit multiple ion channels in the sarcoplasmic reticulum and plasma membrane which may have resulted in the prolonged action potential, characteristic of LQTS (Beca et al., 2008; Ponce-Balbuena et al., 2010). Further, mice, with a tamoxifen inducible, cardiac specific transgene (Tg(αMHC-MerCreMer), developed severe transient dilated cardiomyopathy after tamoxifen treatment, independent of gene excision. This was attributed to nuclear accumulation of tamoxifen, which subsequently altered transcription of genes related to cardiac function and metabolism (Koitabashi et al., 2009). Additionally, isolated wildtype rat cardiomyocytes displayed decreased contractility and calcium handling, following tamoxifen treatment (Asp et al., 2013). As such the protocol was modified, to one dose of tamoxifen at P2, to reduce the amount of tamoxifen given, and to allow sufficient time for the heart to recover before surgery. This refinement still resulted in sufficient loss of *Phd2* expression and significantly improved recovery following MI.

Tamoxifen administration severely stunted the growth of all pups. At the time of surgery, pups were substantially smaller than an average P7 mouse, making

the surgical procedure technically challenging. Further, mice collected at 21pi were around half the size of age-matched, wildtype C57BL6 mice, who had also undergone ligation surgery. Since pre-weaned mice rely solely on milk from the lactating dam, this reduction in size could be attributed to maternal rejection, and therefore insufficient feeding. However, tamoxifen has been shown to diminish growth hormone secretion in boys (Metzger and Kerrigan, 1994), and growth hormone, along with one of its targets, insulin-like growth factor 1 (IGF1), are major signals of growth in the postnatal mouse (Stratikopoulos et al., 2008). Therefore, the tamoxifen itself may be the cause of the retarded growth, presenting a significant limitation of postnatal cre-mediated gene targeting.

Normally, general anaesthesia is induced, prior to surgery, via inhalation of 4% isoflurane, until the righting reflex is lost, usually taking 1-2 minutes. Following tamoxifen administration, pups showed an increased sensitivity to isoflurane induction, with the righting reflex lost within 30 seconds. To prevent over inhalation, pups were closely monitored during isoflurane induction, and removed immediately after the righting reflex was lost.

6.6.6 Maternal cannibalism

Maternal cannibalism, following surgery, was substantially higher than levels observed in wildtype C57BL/6 mice. Cannibalism is often caused by maternal stress (Weber and Olsson, 2008), therefore, the increased incidence of cannibalism, may have been as a result of the repeated removal of the litter from the cage, for tamoxifen administration and then later for surgery. As part of the standard protocol used in the lab, pups are rolled in faeces from the

breeding cage before returning to the dam. In addition, where possible, only females who had previously had a litter were used, as they are known to be more nurturing (Mahmoud et al., 2014), and another female was kept in the cage as communal nesting is known to decrease cannibalism (Jo Manning et al., 1995). *Phd2*$^{fl/fl}$ mice are on a pure C57BL/6 background, which are known to have higher rates of maternal cannibalism (Weber et al., 2013), therefore, in future experiments pups could be fostered using CD1 mothers, as they are known for their nurturing tendencies, as suggested by Mahmoud and colleagues (Mahmoud et al., 2014).

However, dams will also commonly cannibalise their pups that have died, therefore, the increased levels of maternal cannibalism may have been as a direct result of decreased pup survival. This theory would be difficult to prove or disprove however, as the mice consume the evidence. Nevertheless, it is important to note that, of the pups that did survive, preference towards one genotype was not observed, suggesting that any decrease in survival rates was down to tamoxifen and not loss of *Phd2*.

Due to the above-mentioned complications associated with tamoxifen and maternal cannibalism, and to present a more therapeutically relevant approach, treatment with the PHD inhibitor, FG-4592, was trialled.

6.6.7 Differences between the genetic and pharmacological approach.

In contrast to the genetic gain-of-function of HIF studies, hearts from pups treated with FG-4592, showed a significant increase in epicardial WT1 expression in the infarct zone but not the remote zone. Moreover, only 2 of the

6 treated hearts displayed myocardial WT1 expression, and this was minimal compared to the genetic studies. The reason for these differences between the genetic and pharmacological approach may reflect the differences in protocol. In the genetic studies, tamoxifen was administered several days prior to surgery, meaning *Phd2* expression was already significantly downregulated at the time of infarction. Conversely FG-4592 was administered immediately after the surgery, to represent a more therapeutically relevant approach, therefore, HIF signalling was only activated after the infarction. Moreover, in the genetic studies, tamoxifen administration results in stable loss of *Phd2* and therefore prolonged HIF activation, whilst the pharmacological approach results in transient inhibition of PHDs1-3 and therefore a transient activation of HIF. Taken together, the differences in expression in WT1 may be attributed to length of HIF activation. HIF-mediated activation of WT1 in the epicardium, may be an early response, i.e. to acute hypoxia, whilst endothelial expression of WT1 may be a late response i.e. to chronic hypoxia. Moreover, it is possible many of the WT1 positive cells observed in the myocardium, following genetic loss of *Phd2*, were activated epicardial cells which underwent EMT and migrated into the myocardium. Whereas, in the pharmacological approach, which activated HIF signalling later, the $WT1^+$ cells would not have undergone EMT and as such remained in the epicardium, thus accounting for the increased epicardial expression, and decreased myocardial expression.

Another reason for the difference, already discussed in Chapter 4, could be because the genetic approach only targets *Phd2*, whilst the pharmacological approach targets all PHDs. All PHD enzymes are capable of inhibiting both HIF1α and HIF2α, however, PHD2 appears to preferentially regulate HIF1α,

whilst PHD1 and PHD3 appear to be more important for controlling HIF2α (Appelhoff et al., 2004; Berra et al., 2003). Therefore, HIF1α may be more important for activating transcription of WT1 in endothelial cells, whilst HIF2α may upregulate epicardial expression. The *Phd2*$^{fl/fl}$ line could be crossed onto both *Hif1α*$^{fl/fl}$ and *Hif2α*$^{fl/fl}$ lines, to determine whether the observed increase in *Wt1* is HIF1α or HIF2α dependant.

The genetic approach resulted in a significant increase in epicardial WT1 in the remote zone, whilst the pharmacological approach did not. Interestingly, organ-wide activation of the epicardium was observed in the FG-4592 treated hearts, similar to *Phd2*$^{fl/fl}$*;Rosa26*$^{+/CreERT2}$ hearts. However, whilst *Phd2*$^{fl/fl}$ control hearts exhibited little or no remote epicardial activation, wildtype C57BL/6 control hearts exhibited comparable activation to FG-4592 treated hearts. This difference between the two control groups may reflect differences between wildtype and genetically modified mice (wildtype C57BL/6 vs. *Phd2*$^{fl/fl}$) or may reflect the extent of injury. In general, the infarcts in the pharmacological study were more extensive than in the genetic. This is likely due to the toxic effects associated with tamoxifen administration, meaning those with substantial infarcts did not survive to collection.

6.6.8 FG-4592 in the regenerative response

Unlike tamoxifen administration, treatment with FG-4592 was well tolerated and hearts were successful collected at 21dpi. All FG-4592-treated hearts displayed left ventricular dilation and scar deposition, suggesting one dose of FG-4592 is insufficient to prevent fibrosis, warranting further studies testing

multiple doses and different concentrations of FG-4592. The presence of a fibrotic scar is unsurprising, since $WT1^+$ epicardial cells are known to contribute to cardiac fibroblast activation (Zhou et al., 2011). However, treated hearts also appeared to display less cardiac remodelling, despite the significant scar. $WT1^+$ epicardial cells are known to stimulate proliferation of cardiomyocytes and coronary vessel formation during development. Moreover, Zhou and colleagues demonstrated reactivated EPDCs, following MI in the adult, promoted angiogenesis, reduced infarct size and improved cardiac function (Zhou et al., 2011). Therefore, the observed extensive epicardial activation following treatment, may have led to an increase in secretion of paracrine signals, promoting angiogenesis, cardiomyocyte survival and/or proliferation, thus, resulting in a less severely damaged myocardium, as observed by histological staining. To further investigate this, more samples would need to be collected at 21dpi, along with samples at 1dpi to assess cardiomyocyte apoptosis and survival and at 7 and 14dpi, to assess cardiomyocyte proliferation and neovascularisation.

6.7 Conclusions

The data presented in this chapter demonstrates that loss of *Phd2* is sufficient to maintain epicardial WT1 expression in the first postnatal week. Further genetic and pharmacological activation of HIF post-MI results in a significant increase in WT1 expression and preliminary data suggests this may improve the regenerative response via reduced chamber dilation and improved cardiomyocyte survival.

7 General discussion

7.1 Discussion of aims

This chapter discusses the overall findings of this thesis, with reference to the experimental aims outlined in Chapter 1, which were as follows:

1. To characterise levels of hypoxia and HIF in the epicardium during development.

2. To investigate a functional requirement for HIF in epicardial development.

3. To explore a role for HIF signalling in epicardial EMT.

4. To characterise the epicardial response to neonatal cardiac regeneration.

5. To determine the effect of activation of HIF signalling on the epicardial response to injury in the neonate.

The extent to which these aims were achieved, the limitations of the findings, and the implications the findings have on the wider field are discussed below.

7.1.1 Levels of hypoxia and HIF in the epicardium during development

The experimental data presented in Chapter 3 provides a characterisation of levels of hypoxia in the heart during mid to late gestation, when the epicardium has fully formed. At E12.5 hypoxia was restricted to areas of compact myocardium, most significantly in the compact myocardium of the AV groove, situated close to where the coronary plexus first forms (Chen et al., 2014). By E14.5, hypoxia was restricted to the IVS, which incidentally, is perfused later than the muscle of the free wall (Tian et al., 2013). Taken together, these findings suggest a role for hypoxia in stimulating vascularisation of the

embryonic heart. Of significance, by E16.5, when the heart is sufficiently perfused by the coronaries, hypoxia was restricted to the epicardium, with substantial overlap with the key epicardial marker WT1. It has been reported that the adult epicardium is less perfused than the rest of the heart (Ball et al., 1975; Kocabas et al., 2012), which may also be the case for the embryonic epicardium. Given that the embryonic heart resides in a comparatively lower oxygen environment to the adult (Fisher et al., 1980), this may result in hypoxia in the epicardium during development.

Perhaps the more important question is whether the hypoxic environment has a functional role. Hypoxia in the epicardium coincides with the presence of WT1+ EPDCs which have undergone EMT and migrated into the underlying myocardium. Hypoxia induced HIF signalling is a known promoter of EMT (Scully et al., 2016; Xu et al., 2015), therefore, we hypothesised that the hypoxic epicardium stimulates epicardial cells to undergo EMT, via HIF-mediated signalling. To test this, genetic loss-of-function of HIF studies, coupled with *in vitro* gain-of-function studies, were used.

It is important to note that having determined that the epicardium is hypoxic at later stages of development, experiments conducted in this thesis, focused on the HIF-dependant response to hypoxia, given the known role of HIF in EMT, and its capacity to regulate WT1 (Scully et al., 2016; Wagner et al., 2003; Xu et al., 2015). Whilst hypoxia and HIF are intrinsically linked (Elvidge et al., 2006), HIF-independent responses to hypoxia have been described. For example, exposure of human embryonic kidney (HEK-293) to hypoxia resulted in inhibition of mRNA translation, through hypo-phosphorylation of mechanistic target of rapamycin (mTOR) and its effectors, in a HIF-independent manner

(Arsham et al., 2003). Therefore, HIF-independent responses to the hypoxic environment may have been overlooked and may therefore require separate investigation.

7.1.2 A functional requirement for HIF in the developing epicardium

To address a functional requirement for HIF signalling in the epicardium during development, genetic lines were generated, which enabled epicardial specific knock-out of *Hif1α* or *Hif2α* during development. Loss of *Hif1α* and *Hif2α,* resulted in a strikingly similar phenotype, characterised by a significant reduction of WT1+ cells in the epicardium and underlying myocardial layer, along with a decrease in the number of coronary vessels. Furthermore, loss of *Hif2α* also specifically resulted in reduced cardiomyocyte proliferation in the compact layer and hyper-trabeculation. These observed phenotypes are indicative of a defect in epicardial EMT and migration (von Gise et al., 2011; Moore et al., 1999), thus implicating these transcription factors in an as yet unappreciated requirement for heart development.

Whilst HIF1α and HIF2α, bind the same consensus site, they are reported to have predominantly distinct expression patterns and target genes (Jain et al., 1998; Schodel et al., 2011). The remarkably similar phenotype observed, following loss of *Hif1α* or *Hif2α* herein, suggests they are both expressed in the embryonic epicardium, in contrast to the prevailing dogma. However, the presence of a phenotype, following loss of only one HIFα isoform, suggests an inability to compensate and therefore, a lack of functional redundancy between

them. Thus, suggesting they have unique yet complimentary roles in epicardial development.

7.1.2.1 Limitations of the Cre-lox system

There are limitations to the experimental approach used, pertaining to the use of an inducible Cre-system. Firstly, whilst inducible CreERT lines enable activation of the Cre in the target cell type, at specific developmental stages, they require injection of tamoxifen, an oestrogen receptor agonist, during pregnancy, which can have detrimental effects on the developing embryos. The Riley lab has extensive experience with prenatal tamoxifen administration, and a protocol for targeting epicardial development has been optimised, however, early abortions still occasionally occurred, meaning some samples had to be collected at earlier time points than planned. To account for the toxic effects associated with prenatal tamoxifen administration, mutant embryos were only compared to littermate controls, negative for the Cre driver.

Prenatal tamoxifen administration also results in variable dosing between embryos of the same litter which may account for the variation in phenotype observed. However, it may also be the result of Cre mosaicism, due to the Cre not being expressed in all anticipated cells or varied expression within cells, resulting in inconsistency in Cre recombination between littermates (Heffner et al., 2012). This highlights the need for large sample numbers in order to determine a consistent and genuine phenotype, due to loss of the gene of interest.

Finally, a limitation of the loss-of-function studies presented in Chapter 3, is the use of the *Wt1*$^{CreERT2/+}$ driver. This line, first described by Zhou and colleagues in 2008, is frequently used as an epicardial specific Cre driver, due to the extensive and widespread expression of WT1 in the epicardium during development (Zhou et al., 2008). However, whilst WT1 expression was thought to be restricted to the epicardium during cardiac development, recent studies have reported expression in endothelial cells (Duim et al., 2015; Rudat and Kispert, 2012), prompting Zhou and colleagues to assess the specificity and effectiveness of the *Wt1*$^{CreERT2/+}$ driver (Zhou and Pu, 2012). Following activation of the Cre at E14.5 and P4, they reported expression of WT1 in endothelial cells at E18.5 and P7 respectively. Since the Cre was activated at late stages of development, when the majority of EPDCs would have undergone EMT, differentiated and thus downregulated WT1, it is unlikely the observed WT1+ endothelial cells were derived from EPDCs, therefore indicating WT1 is expressed in endothelial cells in development. However, of significance, they reported only rare labelling of endothelial cells, following activation of the Cre at E10.5, suggesting WT1 is expressed in endothelial cells primarily at later stages of development (Zhou and Pu, 2012).

Experiments conducted in Chapter 3, activated the Cre at E9.5 and E11.5, therefore, likely targeting predominantly epicardial cells. However, minimal targeting of *Hif1*α or *Hif2*α in WT1+ endothelial cells cannot be discounted. Therefore, the observed reduction in coronary vessel formation, following loss of *Hif1*α or *Hif2*α*,* may be the result of aberrant HIF signalling in WT1+ endothelial cells, as opposed to loss of pro-angiogenic factors from the defective epicardium. Despite this possibility, the observed significant reduction

in epicardial WT1 expression suggests a role for *Hif1α* and *Hif2α* in the development of the epicardium, irrespective of their role in endothelial cells.

The observed reduction in expression of WT1, following loss of *Hif1α* or *Hif2α,* brings an additional caveat to the use of the *Wt1*$^{CreERT2/+}$ driver, as the reduction in expression will therefore effect Cre. This means the system could not be used to target *Wt1* from the onset of expression, as *Wt1* must first be expressed in order to target *Hif1α* or *Hif2α.* Other epicardial Cre drivers have previously been described, such as *Tbx18*$^{CreERT2/+}$ and *Tcf21*$^{CreERT2/+}$, however, *Tbx18* and *Tcf21* are expressed in cardiomyocytes and fibroblasts during development, respectively, therefore, the *Wt1*$^{CreERT2/+}$ driver is currently the best tool for epicardial genetic loss-of-function studies.

Notwithstanding the limitations with the approach, the developmental loss-of-function studies, outlined in Chapter 3, demonstrate an important role for HIF signalling in epicardial development. Future studies, outlined in section 7.3.1, will aim to determine the relative importance of both HIF1α and HIF2α and investigate the mechanism by which HIF signalling may act as the upstream regulator for epicardial EMT.

7.1.3 A role for HIF signalling in epicardial EMT

Loss of *Hif1α* and *Hif2α* in the epicardium during development suggested a role for HIF signalling in epicardial EMT. To further investigate this, an *in vitro* epicardial explant approach was used (Chapter 4). Pharmacological inhibition of all PHD enzymes, and thus stabilisation of HIF independent of oxygen levels, resulted in a significant increase in the EMT inducing transcription factors WT1

and SNAI1/2. During epicardial EMT, WT1 is known to directly bind to and regulate *Snai1* (Martínez-Estrada et al., 2010), therefore, HIF may be acting as the upstream regulator of this process. However, genetic loss of *Phd2*, resulted in upregulation of SNAI1/2, whilst levels of WT1 remained unaffected, suggestive of a second WT1-independent pathway regulating EMT, whereby HIFα may directly induce expression of *Snai1/2*, thus stimulating EMT.

The observed dissimilarities between genetic and pharmacological approach are likely due to differences in experimental protocol, along with the fact that the latter approach resulted in the inhibition of all PHD enzymes. Despite these differences, in both instances, activation of HIF signalling in cultured primary epicardial cells led to enhanced epicardial EMT. Taken together, with the *in vivo* loss-of-function studies, this suggests a role for HIF in stimulating epicardial cells to undergo EMT during development and presents a novel approach for augmenting epicardial EMT.

7.1.4 The epicardial response in neonatal cardiac regeneration

Findings presented in Chapter 5 demonstrated the epicardium became quiescent within the first week of life, characterised by decreased expression of WT1, and concurrent with a decrease in HIF-mediated signalling in the heart. Experiments on the P1 mouse demonstrated the epicardium remains activated following MI and confirmed the remarkable regenerative capacity of the heart at this stage. Experiments on the P7 mouse revealed the epicardium is partially re-activated following injury, and confirmed the heart is unable to regenerate by 21dpi.

Complete regeneration, following myocardial infarction, requires both the replacement of lost cardiomyocytes and the formation of new blood vessels. Given the paracrine role of the epicardium during development, in promoting cardiomyocyte proliferation and coronary vessel formation, the observed quiescence of the epicardium within the first week of life may contribute to the loss of regeneration. Therefore, augmenting epicardial re-activation post-MI, in the non-regenerative P7 heart, may represent a novel approach for extending the regenerative response.

Foetal circulation is shunt-dependant, resulting in significant mixing of arterial and venous blood (Dawes et al., 1954). After birth, an increase in oxygen (O_2) tension induces shunt closure, dramatically increasing O_2 saturation in the heart (Smith, 1998), meaning the postnatal heart is comparatively less hypoxic than the foetal heart. In keeping with this we observed a significant reduction in *Glut1*, from P0 to P1, suggesting a rapid switch from anaerobic glycolysis to oxygen-dependant metabolism. Further, a significant increase in *Phd2* was observed over the first postnatal week, suggesting a decline in HIF-mediated transcription. Significantly, this coincides with quiescence of the epicardium. Earlier work presented in this thesis demonstrated the epicardium is hypoxic during the later stages of development and suggested that HIF-mediated transcription is important for epicardial activation and EMT. Therefore, the switch to a postnatal circulation, and hence an increase in oxygenation of the heart, including the epicardium, may result in decreased HIF signalling, which feeds back to induce quiescence of the epicardium.

7.1.5 The effect of HIF signalling in the epicardial response to injury in the neonate

Chapter 6 addressed the question as to whether a decline in HIF signalling in the heart after birth contributed to quiescence of the epicardium. Following loss of *Phd2*, persistent WT1 expression was observed in the epicardium at P7, similar to levels observed in a wildtype P1 heart. This suggested that maintaining HIF signalling after birth is sufficient to maintain activation of the epicardium beyond the first week, and that the switch to a postnatal circulation, and therefore an increase in O_2 saturation, contributes towards quiescence of the epicardium. We therefore hypothesised that maintenance of HIF signalling, and thus epicardial activation, would improve the response to injury at P7.

Indeed, loss of *Phd2* augmented epicardial re-activation post-MI, characterised by organ-wide upregulation of WT1 in the epicardium, and the presence of WT1+ EPDCs in the underlying myocardium. Additionally, substantial expression of WT1 in endothelial cells was observed, suggesting a role for HIF signalling in endothelial cell activation and angiogenesis, via WT1-mediated transcription (McCarty et al., 2011).

The experimental design in Chapter 6 outlined a robust protocol for inducing genetic recombination in neonatal mice, via tamoxifen administration. This will enable members of the lab, and collaborators, to decipher the impact of specific genes and pathways on early postnatal development. However, caveats associated with the technique, coupled with the severity of the LAD surgery, are significantly limiting.

To circumvent the caveats of neonatal tamoxifen administration, and to test a more therapeutically relevant approach, treatment with the potent and selective PHD inhibitor, FG-4592, was implemented. Initial *in vitro* studies demonstrated that stimulation with FG-4592 led to an upregulation of WT1 expression coupled with enhanced SNAI1/2 mediated EMT. Following MI, FG-4592 administration induced a significant upregulation of epicardial WT1. Whilst an effect specifically on epicardial EMT has yet to be determined, the findings from the *in vitro* studies and enhanced expression of key EMT mediator, WT1, suggest this is likely.

During development, $WT1^+$ epicardial cells secrete mitogens, such as RA, EPO and FGFs, which stimulate cardiomyocyte proliferation and angiogenesis (Chen et al., 2002; Lavine et al., 2006; Stuckmann et al., 2003), therefore, an improvement was anticipated for both parameters following augmentation of the epicardium post-MI. Whilst no notable differences were observed in vasculature or global proliferation, at the 4dpi time-point analysed, following activation of HIF, assessment of later time-points, such as 7dpi may be more appropriate for assessing the downstream effects of increased epicardial activity. Furthermore, whilst global proliferation was apparently not affected, further studies are required to exclude an effect on cardiomyocyte proliferation specifically.

Histological analysis of hearts collected 21 days after myocardial infarction, following either genetic loss of *Phd2* or chemical inhibition of PHDs, revealed the presence of a persistent fibrotic scar, suggesting activation of HIF signalling is insufficient to prevent a fibrotic response. This is unsurprising, since $WT1^+$ epicardial cells are known to contribute to cardiac fibroblast activation post-MI

(Zhou et al., 2011). Despite the presence of a fibrotic scar, PHD loss-of-function hearts displayed less cardiac remodelling in comparison to controls suggesting a cardioprotective effect, and/or stimulation of new cardiac muscle, and indicating that activation of HIF signalling post-MI may improve the regenerative response at P7. Given the paracrine role of WT1+ epicardial cells in stimulating cardiomyocyte proliferation and angiogenesis, it raises the possibility that the observed expansion of the epicardium post-MI promoted cardiomyocyte proliferation and angiogenesis and reinforces the need to investigate these processes at later stages post-MI as highlighted above. Additionally, different dosing regimens of FG-4592 should be tested, in an attempt to further improve the response. This may, in turn, lead to a decrease in cardiac fibrosis, since in the regenerating P1 heart, an initial scar forms which is subsequently replaced by newly formed myocardium (Porrello et al., 2013).

Whilst the observed increase in epicardial WT1 is likely to have a downstream impact on the regenerative response, the use of the ubiquitous *Rosa26*$^{+/CreERT2}$, for the genetic gain-of-function studies, due to the difficulties associated with epicardial specific Cre drivers after birth, makes it difficult to confirm the exact role of the epicardium. Further, FG-4592 was injected via IP, likely resulting in systemic activation of HIF signalling, again making the contribution of the activated epicardium difficult to determine. To that end, future studies (discussed in section 7.3.3) will use the epicardial specific *Wt1*$^{CreERT2/+}$ driver, using the activated epicardium post-injury to drive loss of *Phd2*.

7.1.5.1 Systemic hypoxia on the regenerative response

It is important to note that invoking a hypoxic response to stimulate regeneration in the adult mouse has previously been described. Nakeda and colleagues subjected adult mice to severe hypoxia, prior to, and following myocardial infarction (Nakada et al., 2017). This led to substantial proliferation in both myocardial and non-myocardial cells, 14 days after injury, and was accompanied by an improvement in cardiac function. They attributed the observed increase in cardiomyocyte proliferation to a decrease in reactive oxygen species (ROS) and DNA damage, bought about by a metabolic shift, thus stimulating cardiomyocyte cell-cycle re-entry. A direct role of HIF signalling was not investigated, nor the impact of non-myocyte populations, including the epicardium, on the regenerative response. Given the findings in this thesis, it raises the question whether chronic hypoxia led to epicardial activation in these hearts, contributing to the observed improvement in regeneration. Of note, whilst improved cardiac function in the Nakada study was observed 14dpi, increased mortality was observed after 3 weeks exposure to hypoxia, suggesting long term exposure to hypoxia is detrimental to heart function. Similarly, persistent activation of HIF signalling, via deletion of PHD2, or VHL (which ubiquitinates HIFα, tagging it for proteasomal degradation), in uninjured, adult mice, led to dilated cardiopathies (Lei et al., 2008; Moslehi et al., 2010).

Whilst these studies highlight the need to assess the effect of FG-4592 treatment on long term cardiac function, and determine the optimal dose, it is likely that the detrimental effects observed in the above described studies (Lei et al., 2008; Moslehi et al., 2010; Nakada et al., 2017) were as a result of sustained activation of HIF signalling. Therefore, treatment with FG-4592,

leading to the transient activation of HIF may augment the acute response to injury without adverse side-effects.

7.1.5.2 Limitations of the LAD ligation model

Despite being widely used in the study of cardiac regeneration, the neonatal LAD ligation model has its limitations. Ligation of the LAD more closely recapitulates human MI, than apical resection or cryo-injury (Jesty et al., 2012; Porrello et al., 2011), however, it is still far from what happens in the clinical setting. Firstly, the surgery is performed on young healthy mice, in contrast to the older diseased patients who present with an MI in the clinic. Furthermore, human MI is primarily caused by thrombolytic occlusion, following plaque rupture (Fuster et al., 1990), as oppose to ligation. Moreover, in the clinical setting, the occluded artery is reopened, resulting in ischemia reperfusion injury (IRI) (Carden and Granger, 2000). HIF1α is known to protect against IRI, therefore, the response following treatment with a PHD inhibitor, such as FG-4592, could be different following reperfusion. However, whilst an ischaemia reperfusion model in the adult mouse has previously been described (Michael et al., 1995), generally in the neonatal model the ligation is permanent. For the mouse neonatal surgery protocol, the duration of the procedure is critical, as protracted hypothermia reduces the ability to recover, and prolonged separation from the dam increases the risk of maternal cannibalism (Mahmoud et al., 2014). Therefore, ligation of the LAD, followed by reperfusion 30-60 minutes later as performed in the adult mouse, would not be practical for the neonatal model.

Significant variability in size of infarct is also observed following LAD ligation, making differences in regenerative responses, between experimental and control groups, difficult to interpret. This highlights the need for large cohorts in myocardial infarction studies, however, this is limited by the number of genetically-modified mice available per litter (on average 6-8 pups per litter), surgery hours (~15-20 minutes is needed per pup for surgery and recovery), cannibalisation post-surgery and abidingness to the home office regulations. To minimise experimental variability where possible, all surgeries presented in this thesis were performed by myself as the surgeon. Further, upon harvesting, samples in which the suture was incorrectly placed were not taken forward for analysis.

An effective way to exclude variability, would be to determine the extent of infarct immediately after surgery. Studies in adult mice have assessed infarct size via serum levels of cardiac troponin I (cTnI) (Xu et al., 2014b), or via *in vivo* magnetic resonance imaging (MRI) (Ross et al., 2002). Whilst blood testing in neonates is not possible, due to their low total blood volume, our lab recently established a protocol to enable longitudinal MRI, in the neonate following myocardial infarction (Gunadasa-Rohling et al., 2018). Routine implementation of this would not only enable assessment of extent of injury, but also quantitative analysis of changes in cardiac function over time.

7.2 Conclusions

The data presented in this thesis demonstrated that the epicardium is hypoxic at later stages of development and have implicated a role for HIF1α and HIF2α in epicardial activation and EMT. Maintaining HIF signalling after birth was sufficient to retain activation of the epicardium, suggesting the oxygen rich postnatal environment contributes to quiescence of the epicardium after birth. Moreover, genetic and pharmacological activation of HIF augmented the epicardial response to injury, and preliminary results suggested an improvement in the regenerative response, presenting a potential novel therapeutic approach to improve cardiac regeneration following MI.

7.3 Future work

Following on from the findings of this thesis, the aims of future work are:

1. To further investigate the role of HIF1α and HIF2α in the epicardium during development

2. To determine if there is an effect of stabilisation of HIF on epicardial development.

3. To further investigate how activation of HIF improves myocardial function after MI.

4. To determine whether loss of HIF signalling is sufficient to cause early quiescence of the epicardium and inhibit the neonatal regenerative response.

5. To determine a role for HIF signalling in adult mouse regeneration.

How these experimental aims will be addressed, and how they could further our understanding of the work undertaken in this thesis, is now discussed.

7.3.1 To Further investigate the role of HIF1α and HIF2α in the epicardium during development

The findings in this thesis indicate a role for both HIF1α and HIF2α in epicardial development, however, a full analysis was not conducted due to limited numbers of transgenic mice, therefore, further characterisation, on their relative contributions is required. Firstly, *Hif1α*$^{fl/fl}$*; Wt1*$^{CreERT2/+}$ litters will be collected at E16.5 and analysed using precisely the same approaches as the *Hif2α*$^{fl/fl}$*; Wt1*$^{CreERT2/+}$ hearts described in this thesis. This will determine if the relatively

more severe phenotype, following loss of *Hif2α* is genuine, or simply because *Hif1α$^{fl/fl}$; Wt1$^{CreERT2/+}$* samples were collected at an earlier time-point (due to issues with tamoxifen toxicity). Additional *Hif2α$^{fl/fl}$; Wt1$^{CreERT2/+}$* hearts will also be collected, to prevent any severity of phenotype being masked by variability in tamoxifen dosing and mosaicism. The effect of loss of epicardial *Hif1α* or *Hif2α* on coronary vessels formation and patterning will then be assessed, via whole mount immunostaining against endothelial marker EMCN and smooth muscle marker SM22α. Formation of the lymphatic vasculature will also be assessed, using markers PROX1 and LYVE-1, since the epicardium has been reported as a source of VEGF-C (Chen et al., 2014), which is known to stimulate cardiac lymphangiogenesis during development and following injury (Karkkainen et al., 2004; Klotz et al., 2015).

To determine whether epicardial HIF signalling is essential for cardiac development, both *Hif1α$^{fl/fl}$; Wt1$^{CreERT2/+}$* and *Hif2α$^{fl/fl}$; Wt1$^{CreERT2/+}$* hearts will be collected at a later timepoint in gestation (E18.5), and in the postnatal period, to determine whether these mice are viable. Further hearts will be collected at an earlier time-point, E11.5, following tamoxifen administration at E7.5 and E9.5, to determine whether HIF signalling is important for migration of the PEO and formation of the epicardium.

Surprisingly, loss of either *Hif1α* or *Hif2α* in the epicardium resulted in remarkably similar phenotypes, suggesting complimentary or partially redundant roles. Therefore, we hypothesise that complete loss of HIF signalling in the epicardium will result in an increased severity of phenotype, thus, we will cross *Hif1α$^{fl/fl}$; Wt1$^{CreERT2/+}$* with *Hif2α$^{fl/fl}$* mice for two generations to generate a

Hif1α$^{fl/fl}$; Hif2α$^{fl/fl}$; Wt1$^{CreERT2/+}$ double knock-out line. This will eliminate any potential redundancy between the two genes, and also disrupt the entire pathway if they are acting co-operatively.

To determine a direct interaction of HIF with *Wt1*, and other epicardial genes, WT1+ epicardial cells will be isolated from *Wt1^{CreEGFP}* embryos via FACs sorting. ChIP-seq analysis will then be performed, using antibodies against HIF1α and HIF2α, to determine whether either or both transcription factors bind.

The *in vitro* studies presented in this thesis focused on a gain-of-function of HIF due to the limited number of *Hif1$\alpha^{fl/fl}$/Hif2$\alpha^{fl/fl}$* mice available. However, future studies will further investigate the effect of loss of *Hif1α* and/or *Hif2α* on epicardial explant cultures, using the same approaches used for the gain-of-function studies, to determine the relative importance of both HIF1α and HIF2α in epicardial EMT.

7.3.2 Determine if there is an effect of stabilisation of HIF on epicardial development.

In vitro studies presented in this thesis suggested that loss of *Phd2* in epicardial cells promotes EMT. To confirm this *in vivo*, we will cross the *Phd2$^{fl/fl}$* mouse line with the epicardial specific Cre driver *Wt1$^{CreERT2/+}$* to induce a gain of function of HIF signalling in the epicardium in development. We will then collect and analyse hearts using the same approaches used for the loss-of-function studies described in Chapter 3. Whilst we expect to see an increase in EMT in these hearts this may not be beneficial for cardiac development. Various

studies have highlighted the importance of the tight regulation of HIF signalling during cardiac development, since both loss-of-function (through deletion of *Hif1*α and/or *Hif2*α), or gain-of-function (through loss of *Phd1,2/3*) resulted in developmental defects such as myocardial hypoplasia and poorly formed trabeculae (Ryan et al., 1998; Tian et al., 1998). Further, a study in the chick reported that persistent HIF signalling *in ovo* impaired epicardial EMT, through inhibition of VEGF (Tao et al., 2013). That said, since the epicardium is hypoxic in development, HIFα may already be stabilised, thus, loss of *Phd2* may not have an effect. As a proof-of-principle, pilot studies have been conducted using the Rosa26$^{+/CreERT2}$ promoter. Following Cre activation at E9.5 and E11.5, and collection at E16.5, mice were grossly abnormal, therefore, setting a precedent for crossing these mice onto an epicardial specific Cre.

7.3.3 To investigate if activation of HIF improves myocardial function

Data presented in this thesis suggested that postnatal gain-of-function of HIF, through genetic or pharmacological inhibition of PHDs, resulted in an improvement in the regenerative response at P7. However, low n numbers and variability in infarct size made it challenging to draw any concrete conclusions. Given the caveats of neonatal tamoxifen administration, and the therapeutic benefit of a pharmacological approach, future experiments will focus on the regenerative response, following treatment with FG-4592.

Firstly, we will confirm activation of HIF signalling, following treatment with FG-4592, by injecting C57BL6 pups with FG-4592 and then collect hearts at 6, 12 and 24 hours post injection. We will then assess levels of HIF targets genes,

such as *Glut1* to confirm activation of HIF signalling. We will try several different administration regimens to determine the optimal dose and frequency of FG-4592.

We will then perform a longitudinal MRI study, using in-house imaging protocols (Gunadasa-Rohling et al., 2018), in which a large cohort of C57BL/6 mice will undergo LAD ligation surgery at P7, followed by treatment with FG-4592 or DMSO diluted in PBS (vehicle control). Pups will then be scanned by MRI, immediately following surgery, and then again at 4, 7, and 21dpi. Mice will then be sacrificied at 21dpi, following the final scan, to increase n numbers for looking at scar resolution and cardiac remodelling. The MRI data will then be used to allow comparison of experimental and control samples of equivalent infarct size, and importantly, to determine if there are any improvements in cardiac function following treatment. In parallel, more hearts will be collected at 4dpi to strengthen the samples already collected at this time point. Additionally, mice will be sacrificed at 7dpi, to determine the downstream consequences on cardiomyocyte proliferation and neovascularisation.

Whilst studies will focus on the pharmacological approach, LAD surgery will also be performed on *Phd2*$^{fl/fl}$; *Wt1*$^{CreERT2/+}$ pups, followed by tamoxifen administration. This will result in re-activation of Wt1 in the epicardium in response to injury, which in turn will lead to loss of *Phd2* in WT1+ epicardial cells. This will enable us to decipher the specific role of the epicardium in the HIF-mediated response to injury.

7.3.4 To determine whether loss of HIF signalling is sufficient to cause early quiescence of the epicardium and inhibit the neonatal regenerative response.

Experiments outlined in this thesis demonstrated the epicardium becomes quiescent shortly after birth, characterised by loss of expression of embryonic epicardial transcription factor WT1. However, maintaining HIF signalling after birth, via loss of P*hd2*, was sufficient to maintain expression of WT1, suggesting a role for HIF signalling in quiescence of the epicardium. Future studies will therefore target *Hif1α* and *Hif2α*, at early postnatal stages, to determine if loss of HIF signalling is sufficient to cause early quiescence of the epicardium. Initial studies will be trialled using the ubiquitous *Rosa26*$^{+/CreERT2}$ Cre driver, given the previously discussed issue of effective gene targeting with epicardial specific Cre drivers after birth. Further, these mice will be subjected to LAD ligation surgery at P1, to determine if loss of HIF signalling is sufficient to prevent regeneration. Preliminary studies have been conducted on *Hif1α; Rosa26*$^{+/CreERT2}$ pups to optimise tamoxifen administration. Pups were injected with 10mg/kg of tamoxifen at P0 using the protocol outlined in this thesis. Hearts were then collected at P1, P2 and P3, and RT-qPCR of ventricular lysates was used to determine levels of *Hif1α.* However, at each time-point analysed, expression of *Hif1α* was not decreased in *Hif1α; Rosa26*$^{+/CreERT2}$ hearts compared to controls. This could be due to the length of time needed for Cre recombination to occur or could be due to the difficulties with injecting into very small pups, therefore, further protocol optimisation is required before undertaking these studies.

7.3.5 To determine a role for HIF signalling in adult mouse regeneration

Comparative analysis between the regenerative P1 heart and the non-regenerative P7 heart is a novel approach to determine the signalling pathways which are essential for mammalian heart regeneration. The P1 neonatal mouse enables the determination of signalling pathways essential for mammalian heart regeneration. Direct comparison with the non-regenerative as a model to study heart regeneration

To that end, we will activate HIF signalling in the adult mouse and determine whether there is an effect on the regenerative response. Initially, we will take a genetic approach, using *Phd2; Rosa26*$^{+/CreERT2}$ mice, whereby we will induce loss of *Phd2* expression in the adult mouse, prior to ligation of the LAD. In a proof-of-principle experiment we will collect hearts at 4dpi and assess epicardial activation. Later, in a larger cohort, samples will be collected at 4, 7, 14 and 21dpi, and coupled with MRI scanning to determine if activation of HIF signalling in the adult can invoke a regenerative response.

A similar approach will then be used to study the effect of treatment with FG-4592, on the adult response to injury, in wildtype C57BL/6 mice. Initial studies will be used to determine the optimal dose and frequency of treatment, followed by a longitudinal MRI study, as outlined above. If the outcome of these studies are positive, this could provide the basis for a therapy to stimulate regeneration in the human adult following MI.

8 Appendices

8.1 Funding

This DPhil was funded by the British Heart Foundation (BHF) Oxbridge Centre of Regenerative Medicine (CRM) 4-year DPhil studentship (1-year rotation & 3-year DPhil).

8.2 Timing and venue of research

The research presented in this thesis was performed from October 2015 to September 2018 in the Department of Physiology, Anatomy and Genetics (DPAG), University of Oxford. The supervisors were Professor Paul Riley (DPAG) and Dr Joaquim Vieira (DPAG). I also had a co-supervisor, Dr Sanjay Sinha, at the University of Cambridge, as part of BHF Oxbridge CRM.

8.3 Publications

8.3.1 Manuscript in preparation

Price E L, Vieira J M, Rohling M, Bishop T, Ratcliffe P J, Riley P R. The role of Hypoxia and HIF-mediated signalling in epicardial development and neonatal cardiac regeneration.

8.3.2 Review in preparation

Price E L, Vieira J M, Riley P R. Animal models of cardiac regeneration. Disease Models and Mechanisms.

8.4 Presentations at scientific meetings

8.4.1 Oral presentations

DPAG final year DPhil student symposium, 2018 (awarded runner-up prize for presentation).

The BHF Oxbridge CRM annual meeting, Royal Society London, 2017.

Development and Cell Biology meeting, Oxford, 2017

8.4.2 Poster Presentations

Weinstein Cardiovascular Development and Regeneration conference, Kyoto, Japan, 2018.

Therapeutic targeting of Hypoxia-sensitive pathways, Keystone conference, Oxford, 2018.

Joint Nordic/BSDB developmental biology and regeneration conference, Stockholm, Sweden, 2017.

The BHF CRM joint Centres meeting, Cambridge, (2016), Nottingham (2017), Edinburgh (2018).

The annual BHF Centre of Research Excellence (CRE) symposium, Oxford, 2015, 2016, 2017.

9 Bibliography

Acharya, A., Baek, S.T., Banfi, S., Eskiocak, B., and Tallquist, M.D. (2011). Efficient inducible Cre-mediated recombination in Tcf21 cell lineages in the heart and kidney. Genesis *49*, 870–877.

Adam, J., Hatipoglu, E., O'Flaherty, L., Ternette, N., Sahgal, N., Lockstone, H., Baban, D., Nye, E., Stamp, G.W., Wolhuter, K., et al. (2011). Renal Cyst Formation in Fh1-Deficient Mice Is Independent of the Hif/Phd Pathway: Roles for Fumarate in KEAP1 Succination and Nrf2 Signaling. Cancer Cell *20*, 524–537.

Ali, S.R., Ranjbarvaziri, S., Talkhabi, M., Zhao, P., Subat, A., Hojjat, A., Kamran, P., Muller, A.M.S., Volz, K.S., Tang, Z., et al. (2014). Developmental heterogeneity of cardiac fibroblasts does not predict pathological proliferation and activation. Circ. Res. *115*, 625–635.

Appelhoff, R.J., Tian, Y.-M., Raval, R.R., Turley, H., Harris, A.L., Pugh, C.W., Ratcliffe, P.J., and Gleadle, J.M. (2004). Differential function of the prolyl hydroxylases PHD1, PHD2, and PHD3 in the regulation of hypoxia-inducible factor. J. Biol. Chem. *279*, 38458–38465.

Aros, F., Loma-Osorio, A., Vila, J., Lopez-Bescos, L., Cunat, J., Rodriguez, E., San Jose, J.M., Heras, M., and Marrugat, J. (2006). [Effect of combined beta-blocker and angiotensin-converting enzyme inhibitor treatment on 1-year survival after acute myocardial infarction: findings of the PRIAMHO-II registry]. Rev. Esp. Cardiol. *59*, 313–320.

Arsenault, P.R., Pei, F., Lee, R., Kerestes, H., Percy, M.J., Keith, B., Simon, M.C., Lappin, T.R.J., Khurana, T.S., and Lee, F.S. (2013). A knock-in mouse model of human PHD2 gene-associated erythrocytosis establishes a haploinsufficiency mechanism. J. Biol. Chem. *288*, 33571–33584.

Arsham, A.M., Howell, J.J., and Simon, M.C. (2003). A novel hypoxia-inducible factor-independent hypoxic response regulating mammalian target of rapamycin and its targets. J. Biol. Chem. *278*, 29655–29660.

Arteel, G.E., Thurman, R.G., Yates, J.M., and Raleigh, J.A. (1995). Evidence that hypoxia markers detect oxygen gradients in liver: pimonidazole and retrograde perfusion of rat liver. Br. J. Cancer *72*, 889–895.

Asp, M.L., Martindale, J.J., and Metzger, J.M. (2013). Direct, differential effects of tamoxifen, 4-hydroxytamoxifen, and raloxifene on cardiac myocyte contractility and calcium handling. PLoS One *8*, e78768.

Aurora, A.B., Porrello, E.R., Tan, W., Mahmoud, A.I., Hill, J.A., Bassel-Duby, R., Sadek, H.A., and Olson, E.N. (2014). Macrophages are required for neonatal heart regeneration. J. Clin. Invest. *124*, 1382–1392.

Ball, R.M., Bache, R.J., Cobb, F.R., and Greenfield, J.C.J. (1975). Regional myocardial blood flow during graded treadmill exercise in the dog. J. Clin. Invest. *55*, 43–49.

Baribault, H., Penner, J., Iozzo, R. V, and Wilson-Heiner, M. (1994). Colorectal hyperplasia and inflammation in keratin 8-deficient FVB/N mice. Genes Dev. *8*, 2964–2973.

Barnabei, M.S., Palpant, N.J., and Metzger, J.M. (2010). Influence of genetic background on ex vivo and in vivo cardiac function in several commonly used inbred mouse strains. Physiol. Genomics *42A*, 103–113.

Bax, N.A.M., van Oorschot, A.A.M., Maas, S., Braun, J., van Tuyn, J., de Vries, A.A.F., Groot, A.C.G., and Goumans, M.-J. (2011). In vitro epithelial-to-mesenchymal transformation in human adult epicardial cells is regulated by TGFbeta-signaling and WT1. Basic Res. Cardiol. *106*, 829–847.

Beca, S., Pavlov, E., Kargacin, M.E., Aschar-Sobbi, R., French, R.J., and Kargacin, G.J. (2008). Inhibition of a cardiac sarcoplasmic reticulum chloride channel by tamoxifen. Pflugers Arch. *457*, 121–135.

Beck, H., Jeske, M., Thede, K., Stoll, F., Flamme, I., Akbaba, M., Erguden, J.-K., Karig, G., Keldenich, J., Oehme, F., et al. (2018). Discovery of Molidustat (BAY 85-3934): A Small-Molecule Oral HIF-Prolyl Hydroxylase (HIF-PH) Inhibitor for the Treatment of Renal Anemia. ChemMedChem *13*, 988–1003.

Bergmann, O., Bhardwaj, R.D., Bernard, S., Zdunek, S., Barnabe-Heider, F., Walsh, S., Zupicich, J., Alkass, K., Buchholz, B.A., Druid, H., et al. (2009). Evidence for cardiomyocyte renewal in humans. Science *324*, 98–102.

Berra, E., Benizri, E., Ginouves, A., Volmat, V., Roux, D., and Pouyssegur, J. (2003). HIF prolyl-hydroxylase 2 is the key oxygen sensor setting low steady-state levels of HIF-1alpha in normoxia. EMBO J. *22*, 4082–4090.

Besarab, A., Provenzano, R., Hertel, J., Zabaneh, R., Klaus, S.J., Lee, T., Leong, R., Hemmerich, S., Yu, K.-H.P., and Neff, T.B. (2015). Randomized placebo-controlled dose-ranging and pharmacodynamics study of roxadustat (FG-4592) to treat anemia in nondialysis-dependent chronic kidney disease (NDD-CKD) patients.

Nephrol. Dial. Transplant *30*, 1665–1673.

Bollini, S., Vieira, J.M.N., Howard, S., Dube, K.N., Balmer, G.M., Smart, N., and Riley, P.R. (2014). Re-activated adult epicardial progenitor cells are a heterogeneous population molecularly distinct from their embryonic counterparts. Stem Cells Dev. *23*, 1719–1730.

van den Borne, S.W.M., van de Schans, V.A.M., Strzelecka, A.E., Vervoort-Peters, H.T.M., Lijnen, P.M., Cleutjens, J.P.M., Smits, J.F.M., Daemen, M.J.A.P., Janssen, B.J.A., and Blankesteijn, W.M. (2009). Mouse strain determines the outcome of wound healing after myocardial infarction. Cardiovasc. Res. *84*, 273–282.

Brade, T., Kumar, S., Cunningham, T.J., Chatzi, C., Zhao, X., Cavallero, S., Li, P., Sucov, H.M., Ruiz-Lozano, P., and Duester, G. (2011). Retinoic acid stimulates myocardial expansion by induction of hepatic erythropoietin which activates epicardial Igf2. Development *138*, 139–148.

Braitsch, C.M., Combs, M.D., Quaggin, S.E., and Yutzey, K.E. (2012). Pod1/Tcf21 is regulated by retinoic acid signaling and inhibits differentiation of epicardium-derived cells into smooth muscle in the developing heart. Dev. Biol. *368*, 345–357.

Bruick, R.K., and McKnight, S.L. (2001). A conserved family of prolyl-4-hydroxylases that modify HIF. Science *294*, 1337–1340.

Brutsaert, D.L., and Andries, L.J. (1992). The endocardial endothelium. Am. J. Physiol. *263*, H985-1002.

Cai, C.-L., Martin, J.C., Sun, Y., Cui, L., Wang, L., Ouyang, K., Yang, L., Bu, L., Liang, X., Zhang, X., et al. (2008). A myocardial lineage derives from Tbx18 epicardial cells. Nature *454*, 104–108.

Candia Carnevali, M.D., Bonasoro, F., Patruno, M., and Thorndyke, M.C. (1998). Cellular and molecular mechanisms of arm regeneration in crinoid echinoderms: the potential of arm explants. Dev. Genes Evol. *208*, 421–430.

Cano-Martinez, A., Vargas-Gonzalez, A., Guarner-Lans, V., Prado-Zayago, E., Leon-Oleda, M., and Nieto-Lima, B. (2010). Functional and structural regeneration in the axolotl heart (Ambystoma mexicanum) after partial ventricular amputation. Arch. Cardiol. Mex. *80*, 79–86.

Cano, E., Carmona, R., Ruiz-Villalba, A., Rojas, A., Chau, Y.-Y., Wagner, K.D., Wagner, N., Hastie, N.D., Muñoz-Chápuli, R., and Pérez-Pomares, J.M. (2016). Extracardiac septum transversum/proepicardial endothelial cells pattern embryonic coronary arterio–venous

connections. Proc. Natl. Acad. Sci. *113*, 656 LP-661.

Captur, G., Lopes, L.R., Patel, V., Li, C., Bassett, P., Syrris, P., Sado, D.M., Maestrini, V., Mohun, T.J., McKenna, W.J., et al. (2014). Abnormal cardiac formation in hypertrophic cardiomyopathy: fractal analysis of trabeculae and preclinical gene expression. Circ. Cardiovasc. Genet. *7*, 241–248.

Captur, G., Zemrak, F., Muthurangu, V., Petersen, S.E., Li, C., Bassett, P., Kawel-Boehm, N., McKenna, W.J., Elliott, P.M., Lima, J.A.C., et al. (2015). Fractal Analysis of Myocardial Trabeculations in 2547 Study Participants: Multi-Ethnic Study of Atherosclerosis. Radiology *277*, 707–715.

Captur, G., Wilson, R., Bennett, M.F., Luxán, G., Nasis, A., de la Pompa, J.L., Moon, J.C., and Mohun, T.J. (2016). Morphogenesis of myocardial trabeculae in the mouse embryo. J. Anat. *229*, 314–325.

Carden, D.L., and Granger, D.N. (2000). Pathophysiology of ischaemia–reperfusion injury. J. Pathol. *190*, 255–266.

Chan, M.C., Atasoylu, O., Hodson, E., Tumber, A., Leung, I.K.H., Chowdhury, R., Gómez-Pérez, V., Demetriades, M., Rydzik, A.M., Holt-Martyn, J., et al. (2015). Potent and selective triazole-based inhibitors of the hypoxia-inducible factor prolyl-hydroxylases with activity in the murine brain. PLoS One *10*, 1–17.

Chazotte, B. (2010). Labeling cytoskeletal F-actin with rhodamine phalloidin or fluorescein phalloidin for imaging. Cold Spring Harb. Protoc. *2010*, pdb.prot4947.

Chen, H.I., Sharma, B., Akerberg, B.N., Numi, H.J., Kivela, R., Saharinen, P., Aghajanian, H., McKay, A.S., Bogard, P.E., Chang, A.H., et al. (2014). The sinus venosus contributes to coronary vasculature through VEGFC-stimulated angiogenesis. Development *141*, 4500–4512.

Chen, Q.K., Lee, K., Radisky, D.C., and Nelson, C.M. (2013). Extracellular matrix proteins regulate epithelial-mesenchymal transition in mammary epithelial cells. Differentiation. *86*, 126–132.

Chen, T.H.P., Chang, T.C., Kang, J.O., Choudhary, B., Makita, T., Tran, C.M., Burch, J.B.E., Eid, H., and Sucov, H.M. (2002). Epicardial induction of fetal cardiomyocyte proliferation via a retinoic acid-inducible trophic factor. Dev. Biol. *250*, 198–207.

Cheval, H., Guy, J., Merusi, C., De Sousa, D., Selfridge, J., and Bird, A. (2012). Postnatal inactivation reveals enhanced requirement for MeCP2 at distinct age windows. Hum. Mol. Genet. *21*, 3806–3814.

Cho, K.H., Yu, S.L., Cho, D.Y., Park, C.G., and Lee, H.Y. (2015). Breast cancer metastasis suppressor 1 (BRMS1) attenuates TGF-β1-induced breast cancer cell aggressiveness through downregulating HIF-1aα expression. BMC Cancer *15*, 1–9.

Christoffels, V.M., Grieskamp, T., Norden, J., Mommersteeg, M.T.M., Rudat, C., and Kispert, A. (2009). Tbx18 and the fate of epicardial progenitors. Nature *458*, E8-9; discussion E9-10.

Compernolle, V., Brusselmans, K., Franco, D., Moorman, A., Dewerchin, M., Collen, D., and Carmeliet, P. (2003). Cardia bifida, defective heart development and abnormal neural crest migration in embryos lacking hypoxia-inducible factor-1alpha. Cardiovasc. Res. *60*, 569–579.

Covello, K.L., Kehler, J., Yu, H., Gordan, J.D., Arsham, A.M., Hu, C.-J., Labosky, P.A., Simon, M.C., and Keith, B. (2006). HIF-2alpha regulates Oct-4: effects of hypoxia on stem cell function, embryonic development, and tumor growth. Genes Dev. *20*, 557–570.

Dawes, G.S. (1955). Physiological effects of anoxia in the foetal and newborn lamb. Lect. Sci. Basis Med. *5*, 53–66.

Dawes, G.S., Mott, J.C., and Widdicombe, J.G. (1954). The foetal circulation in the lamb. J. Physiol. *126*, 563–587.

Dawydoff, C. (1954). [Studies on regeneration in primitive Annelida, Saccocirrus and Polygordius]. C. R. Hebd. Seances Acad. Sci. *238*, 2378–2380.

DeRuiter, M.C., Poelmann, R.E., VanderPlas-de Vries, I., Mentink, M.M., and Gittenberger-de Groot, A.C. (1992). The development of the myocardium and endocardium in mouse embryos. Fusion of two heart tubes? Anat. Embryol. (Berl). *185*, 461–473.

Dettman, R.W., Denetclaw, W.J., Ordahl, C.P., and Bristow, J. (1998). Common epicardial origin of coronary vascular smooth muscle, perivascular fibroblasts, and intermyocardial fibroblasts in the avian heart. Dev. Biol. *193*, 169–181.

Downes, N.L., Laham-Karam, N., Kaikkonen, M.U., and Ylä-Herttuala, S. (2018). Differential but Complementary HIF1α and HIF2α Transcriptional Regulation. Mol. Ther. *26*, 1735–1745.

Duim, S.N., Kurakula, K., Goumans, M.-J., and Kruithof, B.P.T. (2015). Cardiac endothelial cells express Wilms' tumor-1: Wt1 expression in the developing, adult and infarcted heart. J. Mol. Cell. Cardiol. *81*, 127–135.

Dunwoodie, S.L. (2009). The Role of Hypoxia in Development of the

Mammalian Embryo. Dev. Cell *17*, 755–773.

Dyer, L., Pi, X., and Patterson, C. (2014). Connecting the coronaries: How the coronary plexus develops and is functionalized. Dev. Biol. *395*, 111–119.

Elvert, G., Kappel, A., Heidenreich, R., Englmeier, U., Lanz, S., Acker, T., Rauter, M., Plate, K., Sieweke, M., Breier, G., et al. (2003). Cooperative interaction of hypoxia-inducible factor-2alpha (HIF-2alpha) and Ets-1 in the transcriptional activation of vascular endothelial growth factor receptor-2 (Flk-1). J. Biol. Chem. *278*, 7520–7530.

Elvidge, G.P., Glenny, L., Appelhoff, R.J., Ratcliffe, P.J., Ragoussis, J., and Gleadle, J.M. (2006). Concordant regulation of gene expression by hypoxia and 2-oxoglutarate-dependent dioxygenase inhibition: The role of HIF-1α, HIF-2α, and other pathways. J. Biol. Chem. *281*, 15215–15226.

Ema, M., Taya, S., Yokotani, N., Sogawa, K., Matsuda, Y., and Fujii-Kuriyama, Y. (1997). A novel bHLH-PAS factor with close sequence similarity to hypoxia-inducible factor 1alpha regulates the VEGF expression and is potentially involved in lung and vascular development. Proc. Natl. Acad. Sci. U. S. A. *94*, 4273–4278.

Epstein, A.C., Gleadle, J.M., McNeill, L.A., Hewitson, K.S., O'Rourke, J., Mole, D.R., Mukherji, M., Metzen, E., Wilson, M.I., Dhanda, A., et al. (2001). C. elegans EGL-9 and mammalian homologs define a family of dioxygenases that regulate HIF by prolyl hydroxylation. Cell *107*, 43–54.

Feil, R., Wagner, J., Metzger, D., and Chambon, P. (1997). Regulation of Cre recombinase activity by mutated estrogen receptor ligand-binding domains. Biochem. Biophys. Res. Commun. *237*, 752–757.

Fisher, D.J., Heymann, M.A., and Rudolph, A.M. (1980). Myocardial oxygen and carbohydrate consumption in fetal lambs in utero and in adult sheep. Am. J. Physiol. Circ. Physiol. *238*, H399–H405.

Flamme, I., Frohlich, T., von Reutern, M., Kappel, A., Damert, A., and Risau, W. (1997). HRF, a putative basic helix-loop-helix-PAS-domain transcription factor is closely related to hypoxia-inducible factor-1 alpha and developmentally expressed in blood vessels. Mech. Dev. *63*, 51–60.

Forsythe, J.A., Jiang, B.H., Iyer, N. V, Agani, F., Leung, S.W., Koos, R.D., and Semenza, G.L. (1996). Activation of vascular endothelial growth factor gene transcription by hypoxia-inducible factor 1. Mol. Cell. Biol. *16*,

4604–4613.

Fratz, S., Hager, A., Schreiber, C., Schwaiger, M., Hess, J., and Stern, H.C. (2011). Long-Term Myocardial Scarring After Operation for Anomalous Left Coronary Artery From the Pulmonary Artery. Ann. Thorac. Surg. *92*, 1761–1765.

Fuhrmann-Benzakein, E., García-Gabay, I., Pepper, M.S., Vassalli, J.-D., and Herrera, P.L. (2000). Inducible and irreversible control of gene expression using a single transgene. Nucleic Acids Res. *28*, e99–e99.

Fuster, V., Stein, B., Ambrose, J.A., Badimon, L., Badimon, J.J., and Chesebro, J.H. (1990). Atherosclerotic plaque rupture and thrombosis. Evolving concepts. Circulation *82*, II47-59.

Gates, G.E. (1950). Regeneration in an earthworm, Eisenia foetida (Savigny) 1826. III. Regeneration from simultaneous anterior and posterior transections. Biol. Bull. *99*, 425–438.

Gerdes, J., Schwab, U., Lemke, H., and Stein, H. (1983). Production of a mouse monoclonal antibody reactive with a human nuclear antigen associated with cell proliferation. Int. J. Cancer *31*, 13–20.

Gheorghiade, M., Zannad, F., Sopko, G., Klein, L., Pina, I.L., Konstam, M.A., Massie, B.M., Roland, E., Targum, S., Collins, S.P., et al. (2005). Acute heart failure syndromes: current state and framework for future research. Circulation *112*, 3958–3968.

von Gise, A., and Pu, W.T. (2012). Endocardial and epicardial epithelial to mesenchymal transitions in heart development and disease. Circ. Res. *110*, 1628–1645.

von Gise, A., Zhou, B., Honor, L.B., Ma, Q., Petryk, A., and Pu, W.T. (2011). WT1 regulates epicardial epithelial to mesenchymal transition through beta-catenin and retinoic acid signaling pathways. Dev. Biol. *356*, 421–431.

Gittenberger-de Groot, A.C., Vrancken Peeters, M.P., Mentink, M.M., Gourdie, R.G., and Poelmann, R.E. (1998). Epicardium-derived cells contribute a novel population to the myocardial wall and the atrioventricular cushions. Circ. Res. *82*, 1043–1052.

Gonzales, C., Zaleska, M.M., Riddell, D.R., Atchison, K.P., Robshaw, A., Zhou, H., and Sukoff Rizzo, S.J. (2014). Alternative method of oral administration by peanut butter pellet formulation results in target engagement of BACE1 and attenuation of gavage-induced stress responses in mice. Pharmacol. Biochem. Behav. *126*, 28–35.

Gonzalez-Rosa, J.M., and Mercader, N. (2012). Cryoinjury as a myocardial

infarction model for the study of cardiac regeneration in the zebrafish. Nat. Protoc. *7*, 782–788.

Gonzalez-Rosa, J.M., Peralta, M., and Mercader, N. (2012). Pan-epicardial lineage tracing reveals that epicardium derived cells give rise to myofibroblasts and perivascular cells during zebrafish heart regeneration. Dev. Biol. *370*, 173–186.

Gooskens, S.L., Klasson, T.D., Gremmels, H., Logister, I., Pieters, R., Perlman, E.J., Giles, R.H., and van den Heuvel-Eibrink, M.M. (2018). TCF21 hypermethylation regulates renal tumor cell clonogenic proliferation and migration. Mol. Oncol. *12*, 166–179.

Grego-Bessa, J., Luna-Zurita, L., del Monte, G., Bolos, V., Melgar, P., Arandilla, A., Garratt, A.N., Zang, H., Mukouyama, Y.-S., Chen, H., et al. (2007). Notch signaling is essential for ventricular chamber development. Dev. Cell *12*, 415–429.

van Groningen, J.P., Wenink, A.C., and Testers, L.H. (1991). Myocardial capillaries: increase in number by splitting of existing vessels. Anat. Embryol. (Berl). *184*, 65–70.

Gruber, M., Hu, C.-J., Johnson, R.S., Brown, E.J., Keith, B., and Simon, M.C. (2007). Acute postnatal ablation of Hif-2alpha results in anemia. Proc. Natl. Acad. Sci. U. S. A. *104*, 2301–2306.

Guadix, J.A., Ruiz-Villalba, A., Lettice, L., Velecela, V., Munoz-Chapuli, R., Hastie, N.D., Perez-Pomares, J.M., and Martinez-Estrada, O.M. (2011). Wt1 controls retinoic acid signalling in embryonic epicardium through transcriptional activation of Raldh2. Development *138*, 1093–1097.

Guimarães-Camboa, N., Stowe, J., Aneas, I., Sakabe, N., Cattaneo, P., Henderson, L., Kilberg, M.S., Johnson, R.S., Chen, J., McCulloch, A.D., et al. (2015). HIF1α Represses Cell Stress Pathways to Allow Proliferation of Hypoxic Fetal Cardiomyocytes. Dev. Cell *33*, 507–521.

Gunadasa-Rohling, M., Masters, M., Maguire, M., Smart, S., Schneider, J., and Riley, P. (2018). Magnetic resonance imaging of the regenerating neonatal mouse heart. BioRxiv.

Ham, R.G., and Eakin, R.E. (1958). Time sequence of certain physiological events during regeneration in hydra. J. Exp. Zool. *139*, 33–53.

Hansson, A., Thevis, M., Cox, H., Miller, G., Eichner, D., Bondesson, U., and Hedeland, M. (2017). Investigation of the metabolites of the HIF stabilizer FG-4592 (roxadustat) in five different in vitro models and in a human doping control sample using high resolution mass

spectrometry. J. Pharm. Biomed. Anal. *134*, 228–236.

Hara, S., Hamada, J., Kobayashi, C., Kondo, Y., and Imura, N. (2001). Expression and characterization of hypoxia-inducible factor (HIF)-3alpha in human kidney: suppression of HIF-mediated gene expression by HIF-3alpha. Biochem. Biophys. Res. Commun. *287*, 808–813.

Hasegawa, Y., Daitoku, Y., Sekiguchi, K., Tanimoto, Y., Mizuno-Iijima, S., Mizuno, S., Kajiwara, N., Ema, M., Miwa, Y., Mekada, K., et al. (2013). Novel ROSA26 Cre-reporter knock-in C57BL/6N mice exhibiting green emission before and red emission after Cre-mediated recombination. Exp. Anim. *62*, 295–304.

Haubner, B.J., Schneider, J., Schweigmann, U., Schuetz, T., Dichtl, W., Velik-Salchner, C., Stein, J.-I., and Penninger, J.M. (2016). Functional Recovery of a Human Neonatal Heart After Severe Myocardial Infarction. Circ. Res. *118*, 216–221.

Heffner, C.S., Herbert Pratt, C., Babiuk, R.P., Sharma, Y., Rockwood, S.F., Donahue, L.R., Eppig, J.T., and Murray, S.A. (2012). Supporting conditional mouse mutagenesis with a comprehensive cre characterization resource. Nat. Commun. *3*, 1218.

Hellemans, J., Mortier, G., De Paepe, A., Speleman, F., and Vandesompele, J. (2007). qBase relative quantification framework and software for management and automated analysis of real-time quantitative PCR data. Genome Biol. *8*, R19.

Hidai, H., Bardales, R., Goodwin, R., Quertermous, T., and Quertermous, E.E. (1998). Cloning of capsulin, a basic helix-loop-helix factor expressed in progenitor cells of the pericardium and the coronary arteries. Mech. Dev. *73*, 33–43.

Higgins, D.F., Biju, M.P., Akai, Y., Wutz, A., Johnson, R.S., and Haase, V.H. (2004). Hypoxic induction of Ctgf is directly mediated by Hif-1. Am. J. Physiol. Renal Physiol. *287*, F1223-32.

Hirakow, R. (1992). Epicardial formation in staged human embryos. Kaibogaku Zasshi. *67*, 616–622.

Hodson, E.J., Nicholls, L.G., Turner, P.J., Llyr, R., Fielding, J.W., Douglas, G., Ratnayaka, I., Robbins, P.A., Pugh, C.W., Buckler, K.J., et al. (2016). Regulation of ventilatory sensitivity and carotid body proliferation in hypoxia by the PHD2/HIF-2 pathway. J. Physiol. *594*, 1179–1195.

Hoppe, G., Yoon, S., Gopalan, B., Savage, A.R., Brown, R., Case, K., Vasanji, A., Chan, E.R., Silver, R.B., and Sears, J.E. (2016). Comparative

systems pharmacology of HIF stabilization in the prevention of retinopathy of prematurity. Proc. Natl. Acad. Sci. U. S. A. *113*, E2516-25.

Hu, C.-J., Wang, L.-Y., Chodosh, L.A., Keith, B., and Simon, M.C. (2003a). Differential roles of hypoxia-inducible factor 1alpha (HIF-1alpha) and HIF-2alpha in hypoxic gene regulation. Mol. Cell. Biol. *23*, 9361–9374.

Hu, C., Wang, L., Chodosh, L. a, Keith, B., and Simon, M.C. (2003b). Differential Roles of Hypoxia-Inducible Factor 1 alpha (HIF-1 alpha) and HIF-2 alpha in Hypoxic Gene Regulation. Mol. Cell. Biol. *23*, 9361–9374.

Huang, C.-H., Yang, W.-H., Chang, S.-Y., Tai, S.-K., Tzeng, C.-H., Kao, J.-Y., Wu, K.-J., and Yang, M.-H. (2009a). Regulation of membrane-type 4 matrix metalloproteinase by SLUG contributes to hypoxia-mediated metastasis. Neoplasia *11*, 1371–1382.

Huang, J.-P., Huang, S.-S., Deng, J.-Y., and Hung, L.-M. (2009b). Impairment of insulin-stimulated Akt/GLUT4 signaling is associated with cardiac contractile dysfunction and aggravates I/R injury in STZ-diabetic rats. J. Biomed. Sci. *16*, 77.

Iyer, N. V, Kotch, L.E., Agani, F., Leung, S.W., Laughner, E., Wenger, R.H., Gassmann, M., Gearhart, J.D., Lawler, A.M., Yu, A.Y., et al. (1998). Cellular and developmental control of O2 homeostasis by hypoxia-inducible factor 1 alpha. Genes Dev. *12*, 149–162.

Jaakkola, P., Mole, D.R., Tian, Y.-M., Wilson, M.I., Gielbert, J., Gaskell, S.J., Kriegsheim, A. von, Hebestreit, H.F., Mukherji, M., Schofield, C.J., et al. (2001). Targeting of HIF-α to the von Hippel-Lindau Ubiquitylation Complex by O₂-Regulated Prolyl Hydroxylation. Science (80-.). *292*, 468 LP-472.

Jain, S., Maltepe, E., Lu, M.M., Simon, C., and Bradfield, C.A. (1998). Expression of ARNT, ARNT2, HIF1 alpha, HIF2 alpha and Ah receptor mRNAs in the developing mouse. Mech. Dev. *73*, 117–123.

Jelinek, M., Wallach, C., Ehmke, H., and Schwoerer, A.P. (2018). Genetic background dominates the susceptibility to ventricular arrhythmias in a murine model of β-adrenergic stimulation. Sci. Rep. *8*, 2312.

Jesty, S.A., Steffey, M.A., Lee, F.K., Breitbach, M., Hesse, M., Reining, S., Lee, J.C., Doran, R.M., Nikitin, A.Y., Fleischmann, B.K., et al. (2012). c-kit+ precursors support postinfarction myogenesis in the neonatal, but not adult, heart. Proc. Natl. Acad. Sci. U. S. A. *109*, 13380–13385.

Jiang, X., Rowitch, D.H., Soriano, P., McMahon, A.P., and Sucov, H.M. (2000).

Fate of the mammalian cardiac neural crest. Development *127*, 1607–1616.

Jo Manning, C., Dewsbury, D.A., Wakeland, E.K., and Potts, W.K. (1995). Communal nesting and communal nursing in house mice, Mus musculus domesticus. Anim. Behav. *50*, 741–751.

Johnson, D.S., Mortazavi, A., Myers, R.M., and Wold, B. (2007). Genome-wide mapping of in vivo protein-DNA interactions. Science *316*, 1497–1502.

Jopling, C., Sleep, E., Raya, M., Marti, M., Raya, A., and Izpisua Belmonte, J.C. (2010). Zebrafish heart regeneration occurs by cardiomyocyte dedifferentiation and proliferation. Nature *464*, 606–609.

Jopling, C., Suñé, G., Faucherre, A., Fabregat, C., and Izpisua Belmonte, J.C. (2012). Hypoxia induces myocardial regeneration in zebrafish. Circulation *126*, 3017–3027.

Joseph, J. V., Conroy, S., Pavlov, K., Sontakke, P., Tomar, T., Eggens-Meijer, E., Balasubramaniyan, V., Wagemakers, M., den Dunnen, W.F.A., and Kruyt, F.A.E. (2015). Hypoxia enhances migration and invasion in glioblastoma by promoting a mesenchymal shift mediated by the HIF1α-ZEB1 axis. Cancer Lett. *359*, 107–116.

Kang, J.-O., and Sucov, H.M. (2005). Convergent proliferative response and divergent morphogenic pathways induced by epicardial and endocardial signaling in fetal heart development. Mech. Dev. *122*, 57–65.

Karkkainen, M.J., Haiko, P., Sainio, K., Partanen, J., Taipale, J., Petrova, T. V, Jeltsch, M., Jackson, D.G., Talikka, M., Rauvala, H., et al. (2004). Vascular endothelial growth factor C is required for sprouting of the first lymphatic vessels from embryonic veins. Nat. Immunol. *5*, 74–80.

Katz, T.C., Singh, M.K., Degenhardt, K., Rivera-Feliciano, J., Johnson, R.L., Epstein, J.A., and Tabin, C.J. (2012). Distinct Compartments of the Proepicardial Organ Give Rise to Coronary Vascular Endothelial Cells. Dev. Cell *22*, 639–650.

Kelly, B.D. (2003). Cell Type-Specific Regulation of Angiogenic Growth Factor Gene Expression and Induction of Angiogenesis in Nonischemic Tissue by a Constitutively Active Form of Hypoxia-Inducible Factor 1. Circ. Res. *93*, 1074–1081.

Kelly, R.G., and Buckingham, M.E. (2002). The anterior heart-forming field: voyage to the arterial pole of the heart. Trends Genet. *18*, 210–216.

Kikuchi, K., Holdway, J.E., Werdich, A.A., Anderson, R.M., Fang, Y., Egnaczyk, G.F., Evans, T., Macrae, C.A., Stainier, D.Y.R., and Poss, K.D. (2010).

Primary contribution to zebrafish heart regeneration by gata4(+) cardiomyocytes. Nature *464*, 601–605.

Kikuchi, K., Holdway, J.E., Major, R.J., Blum, N., Dahn, R.D., Begemann, G., and Poss, K.D. (2011). Retinoic acid production by endocardium and epicardium is an injury response essential for zebrafish heart regeneration. Dev. Cell *20*, 397–404.

Klotz, L., Norman, S., Vieira, J.M., Masters, M., Rohling, M., Dube, K.N., Bollini, S., Matsuzaki, F., Carr, C.A., and Riley, P.R. (2015). Cardiac lymphatics are heterogeneous in origin and respond to injury. Nature *522*, 62–67.

Kocabas, F., Mahmoud, A.I., Sosic, D., Porrello, E.R., Chen, R., Garcia, J.A., Deberardinis, R.J., and Sadek, H.A. (2012). The hypoxic epicardial and subepicardial microenvironment. J. Cardiovasc. Transl. Res. *5*, 654–665.

Koitabashi, N., Bedja, D., Zaiman, A.L., Pinto, Y.M., Zhang, M., Gabrielson, K.L., Takimoto, E., and Kass, D.A. (2009). Avoidance of transient cardiomyopathy in cardiomyocyte-targeted tamoxifen-induced MerCreMer gene deletion models. Circ. Res. *105*, 12–15.

Krishnan, J., Ahuja, P., Bodenmann, S., Knapik, D., Perriard, E., Krek, W., and Perriard, J.-C. (2008). Essential role of developmentally activated hypoxia-inducible factor 1alpha for cardiac morphogenesis and function. Circ. Res. *103*, 1139–1146.

Kumar, S., Das, A., and Sen, S. (2014). Extracellular matrix density promotes EMT by weakening cell-cell adhesions. Mol. Biosyst. *10*, 838–850.

Kwee, L., Baldwin, H.S., Shen, H.M., Stewart, C.L., Buck, C., Buck, C.A., and Labow, M.A. (1995). Defective development of the embryonic and extraembryonic circulatory systems in vascular cell adhesion molecule (VCAM-1) deficient mice. Development *121*, 489–503.

de Lange, F.J., Moorman, A.F.M., Anderson, R.H., Manner, J., Soufan, A.T., de Gier-de Vries, C., Schneider, M.D., Webb, S., van den Hoff, M.J.B., and Christoffels, V.M. (2004). Lineage and morphogenetic analysis of the cardiac valves. Circ. Res. *95*, 645–654.

Lavine, K.J., Yu, K., White, A.C., Zhang, X., Smith, C., Partanen, J., and Ornitz, D.M. (2005). Endocardial and epicardial derived FGF signals regulate myocardial proliferation and differentiation in vivo. Dev. Cell *8*, 85–95.

Lavine, K.J., White, A.C., Park, C., Smith, C.S., Choi, K., Long, F., Hui, C., and Ornitz, D.M. (2006). Fibroblast growth factor signals regulate a wave of Hedgehog activation that is essential for coronary vascular

development. Genes Dev. *20*, 1651–1666.

Lee, Y.M., Jeong, C.H., Koo, S.Y., Son, M.J., Song, H.S., Bae, S.K., Raleigh, J.A., Chung, H.Y., Yoo, M.A., and Kim, K.W. (2001). Determination of hypoxic region by hypoxia marker in developing mouse embryos in vivo: a possible signal for vessel development. Dev. Dyn. *220*, 175–186.

Lei, L., Mason, S., Liu, D., Huang, Y., Marks, C., Hickey, R., Jovin, I.S., Pypaert, M., Johnson, R.S., and Giordano, F.J. (2008). Hypoxia-inducible factor-dependent degeneration, failure, and malignant transformation of the heart in the absence of the von Hippel-Lindau protein. Mol. Cell. Biol. *28*, 3790–3803.

Lepilina, A., Coon, A.N., Kikuchi, K., Holdway, J.E., Roberts, R.W., Burns, C.G., and Poss, K.D. (2006). A Dynamic Epicardial Injury Response Supports Progenitor Cell Activity during Zebrafish Heart Regeneration. Cell *127*, 607–619.

Li, X., Cui, X.-X., Chen, Y.-J., Wu, T.-T., Xu, H., Yin, H., and Wu, Y.-C. (2018). Therapeutic Potential of a Prolyl Hydroxylase Inhibitor FG-4592 for Parkinson's Diseases in Vitro and in Vivo: Regulation of Redox Biology and Mitochondrial Function. Front. Aging Neurosci. *10*, 121.

Livak, K.J., and Schmittgen, T.D. (2001). Analysis of relative gene expression data using real-time quantitative PCR and the 2-ΔΔCT method. Methods *25*, 402–408.

Lopaschuk, G.D., Spafford, M.A., and Marsh, D.R. (1991). Glycolysis is predominant source of myocardial ATP production immediately after birth. Am. J. Physiol. *261*, H1698-705.

Maezawa, Y., Onay, T., Scott, R.P., Keir, L.S., Dimke, H., Li, C., Eremina, V., Maezawa, Y., Jeansson, M., Shan, J., et al. (2014). Loss of the podocyte-expressed transcription factor Tcf21/Pod1 results in podocyte differentiation defects and FSGS. J. Am. Soc. Nephrol. *25*, 2459–2470.

Mahmoud, A.I., Porrello, E.R., Kimura, W., Olson, E.N., and Sadek, H.A. (2014). Surgical models for cardiac regeneration in neonatal mice. Nat. Protoc. *9*, 305–311.

Mahon, P.C., Hirota, K., and Semenza, G.L. (2001). FIH-1: a novel protein that interacts with HIF-1α and VHL to mediate repression of HIF-1 transcriptional activity. Genes Dev. *15*, 2675–2686.

Mahtab, E.A.F., Wijffels, M.C.E.F., Van Den Akker, N.M.S., Hahurij, N.D., Lie-Venema, H., Wisse, L.J., Deruiter, M.C., Uhrin, P., Zaujec, J., Binder,

B.R., et al. (2008). Cardiac malformations and myocardial abnormalities in podoplanin knockout mouse embryos: Correlation with abnormal epicardial development. Dev. Dyn. *237*, 847–857.

Manner, J. (1992). The development of pericardial villi in the chick embryo. Anat. Embryol. (Berl). *186*, 379–385.

Marinas, I.D., Marinas, R., Pirici, I., and Mogoanta, L. (2012). Vascular and mesenchymal factors during heart development: a chronological study. Rom. J. Morphol. Embryol. = Rev. Roum. Morphol. Embryol. *53*, 135–142.

Martínez-Estrada, O.M., Lettice, L.A., Essafi, A., Guadix, J.A., Slight, J., Velecela, V., Hall, E., Reichmann, J., Devenney, P.S., Hohenstein, P., et al. (2010). Wt1 is required for cardiovascular progenitor cell formation through transcriptional control of Snail and E-cadherin. Nat. Genet. *42*, 89–93.

Masters, M. (2015). Epicardial signalling in mammalian heart regeneration. University of Oxford.

Maxwell, P.H., Pugh, C.W., and Ratcliffe, P.J. (1993). Inducible operation of the erythropoietin 3' enhancer in multiple cell lines: evidence for a widespread oxygen-sensing mechanism. Proc. Natl. Acad. Sci. U. S. A. *90*, 2423–2427.

Mayes, D.A., Rizvi, T.A., Cancelas, J.A., Kolasinski, N.T., Ciraolo, G.M., Stemmer-Rachamimov, A.O., and Ratner, N. (2011). Perinatal or adult Nf1 inactivation using tamoxifen-inducible PlpCre each cause neurofibroma formation. Cancer Res. *71*, 4675–4685.

Mazzone, M., Dettori, D., de Oliveira, R.L., Loges, S., Schmidt, T., Jonckx, B., Tian, Y.-M., Lanahan, A.A., Pollard, P., de Almodovar, C.R., et al. (2009). Heterozygous deficiency of PHD2 restores tumor oxygenation and inhibits metastasis via endothelial normalization. Cell *136*, 839–851.

McCarty, G., Awad, O., and Loeb, D.M. (2011). WT1 protein directly regulates expression of vascular endothelial growth factor and is a mediator of tumor response to hypoxia. J. Biol. Chem. *286*, 43634–43643.

Mercer, S.E., Odelberg, S.J., and Simon, H.-G. (2013). A dynamic spatiotemporal extracellular matrix facilitates epicardial-mediated vertebrate heart regeneration. Dev. Biol. *382*, 457–469.

Metzger, D.L., and Kerrigan, J.R. (1994). Estrogen receptor blockade with tamoxifen diminishes growth hormone secretion in boys: evidence for a stimulatory role of endogenous estrogens during male adolescence.

J. Clin. Endocrinol. Metab. *79*, 513–518.

Michael, L.H., Entman, M.L., Hartley, C.J., Youker, K.A., Zhu, J., Hall, S.R., Hawkins, H.K., Berens, K., and Ballantyne, C.M. (1995). Myocardial ischemia and reperfusion: a murine model. Am. J. Physiol. *269*, H2147-54.

Mikawa, T., and Fischman, D.A. (1992). Retroviral analysis of cardiac morphogenesis: discontinuous formation of coronary vessels. Proc. Natl. Acad. Sci. U. S. A. *89*, 9504–9508.

Mikawa, T., and Gourdie, R.G. (1996). Pericardial mesoderm generates a population of coronary smooth muscle cells migrating into the heart along with ingrowth of the epicardial organ. Dev. Biol. *174*, 221–232.

Del Monte-Nieto, G., Ramialison, M., Adam, A.A.S., Wu, B., Aharonov, A., D'Uva, G., Bourke, L.M., Pitulescu, M.E., Chen, H., de la Pompa, J.L., et al. (2018). Control of cardiac jelly dynamics by NOTCH1 and NRG1 defines the building plan for trabeculation. Nature *557*, 439–445.

Moore, A.W., McInnes, L., Kreidberg, J., Hastie, N.D., and Schedl, A. (1999). YAC complementation shows a requirement for Wt1 in the development of epicardium, adrenal gland and throughout nephrogenesis. Development *126*, 1845–1857.

Morgan, T.H. (1898). Experimental studies of the regeneration of Planaria maculata (Leipzig: W. Engelmann).

Moslehi, J., Minamishima, Y.A., Shi, J., Neuberg, D., Charytan, D.M., Padera, R.F., Signoretti, S., Liao, R., and Kaelin, W.G.J. (2010). Loss of hypoxia-inducible factor prolyl hydroxylase activity in cardiomyocytes phenocopies ischemic cardiomyopathy. Circulation *122*, 1004–1016.

Nahirney, P.C., Mikawa, T., and Fischman, D.A. (2003). Evidence for an extracellular matrix bridge guiding proepicardial cell migration to the myocardium of chick embryos. Dev. Dyn. *227*, 511–523.

Nakada, Y., Canseco, D.C., Thet, S., Abdisalaam, S., Asaithamby, A., Santos, C.X., Shah, A.M., Zhang, H., Faber, J.E., Kinter, M.T., et al. (2017). Hypoxia induces heart regeneration in adult mice. Nature *541*, 222–227.

Nanka, O., Valasek, P., Dvorakova, M., and Grim, M. (2006). Experimental hypoxia and embryonic angiogenesis. Dev. Dyn. *235*, 723–733.

Neary, M.T., Ng, K.E., Ludtmann, M.H.R., Hall, A.R., Piotrowska, I., Ong, S.B., Hausenloy, D.J., Mohun, T.J., Abramov, A.Y., and Breckenridge, R.A. (2014). Hypoxia signaling controls postnatal changes in cardiac mitochondrial morphology and function. J. Mol. Cell. Cardiol. *74*, 340–

352.

Niederreither, K., Fraulob, V., Garnier, J.-M., Chambon, P., and Dolle, P. (2002). Differential expression of retinoic acid-synthesizing (RALDH) enzymes during fetal development and organ differentiation in the mouse. Mech. Dev. *110*, 165–171.

O'Reilly, V.C., Lopes Floro, K., Shi, H., Chapman, B.E., Preis, J.I., James, A.C., Chapman, G., Harvey, R.P., Johnson, R.S., Grieve, S.M., et al. (2014). Gene-environment interaction demonstrates the vulnerability of the embryonic heart. Dev. Biol. *391*, 99–110.

Osterreicher, C.H., Penz-Osterreicher, M., Grivennikov, S.I., Guma, M., Koltsova, E.K., Datz, C., Sasik, R., Hardiman, G., Karin, M., and Brenner, D.A. (2011). Fibroblast-specific protein 1 identifies an inflammatory subpopulation of macrophages in the liver. Proc. Natl. Acad. Sci. U. S. A. *108*, 308–313.

Ouiddir, A., Planes, C., Fernandes, I., VanHesse, A., and Clerici, C. (1999). Hypoxia upregulates activity and expression of the glucose transporter GLUT1 in alveolar epithelial cells. Am. J. Respir. Cell Mol. Biol. *21*, 710–718.

Peng, J., Zhang, L., Drysdale, L., and Fong, G.H. (2000). The transcription factor EPAS-1/hypoxia-inducible factor 2alpha plays an important role in vascular remodeling. Proc. Natl. Acad. Sci. U. S. A. *97*, 8386–8391.

Peralta, M., Steed, E., Harlepp, S., Gonzalez-Rosa, J.M., Monduc, F., Ariza-Cosano, A., Cortes, A., Rayon, T., Gomez-Skarmeta, J.-L., Zapata, A., et al. (2013). Heartbeat-driven pericardiac fluid forces contribute to epicardium morphogenesis. Curr. Biol. *23*, 1726–1735.

Perez-Pomares, J.M., Macias, D., Garcia-Garrido, L., and Munoz-Chapuli, R. (1998). The origin of the subepicardial mesenchyme in the avian embryo: an immunohistochemical and quail-chick chimera study. Dev. Biol. *200*, 57–68.

Perez-Pomares, J.M., Phelps, A., Sedmerova, M., Carmona, R., Gonzalez-Iriarte, M., Munoz-Chapuli, R., and Wessels, A. (2002). Experimental studies on the spatiotemporal expression of WT1 and RALDH2 in the embryonic avian heart: a model for the regulation of myocardial and valvuloseptal development by epicardially derived cells (EPDCs). Dev. Biol. *247*, 307–326.

Pfeffer, M.A., and Braunwald, E. (1990). Ventricular remodeling after myocardial infarction. Experimental observations and clinical implications. Circulation *81*, 1161 LP-1172.

Pitulescu, M.E., Schmidt, I., Benedito, R., and Adams, R.H. (2010). Inducible gene targeting in the neonatal vasculature and analysis of retinal angiogenesis in mice. Nat. Protoc. *5*, 1518–1534.

Pollack, I.F., DaRosso, R.C., Robertson, P.L., Jakacki, R.L., Mirro, J.R.J., Blatt, J., Nicholson, S., Packer, R.J., Allen, J.C., Cisneros, A., et al. (1997). A phase I study of high-dose tamoxifen for the treatment of refractory malignant gliomas of childhood. Clin. Cancer Res. *3*, 1109–1115.

Ponce-Balbuena, D., Moreno-Galindo, E.G., Lopez-Izquierdo, A., Ferrer, T., and Sanchez-Chapula, J.A. (2010). Tamoxifen inhibits cardiac ATP-sensitive and acetylcholine-activated K+ currents in part by interfering with phosphatidylinositol 4,5-bisphosphate-channel interaction. J. Pharmacol. Sci. *113*, 66–75.

Porrello, E.R., Mahmoud, A.I., Simpson, E., Hill, J.A., Richardson, J.A., Olson, E.N., and Sadek, H.A. (2011). Transient regenerative potential of the neonatal mouse heart. Science (80-.). *331*, 1078–1080.

Porrello, E.R., Mahmoud, A.I., Simpson, E., Johnson, B.A., Grinsfelder, D., Canseco, D., Mammen, P.P., Rothermel, B.A., Olson, E.N., and Sadek, H.A. (2013). Regulation of neonatal and adult mammalian heart regeneration by the miR-15 family. Proc. Natl. Acad. Sci. *110*, 187–192.

Poss, K.D., Wilson, L.G., and Keating, M.T. (2002). Heart regeneration in zebrafish. Science *298*, 2188–2190.

Provenzano, R., Besarab, A., Sun, C.H., Diamond, S.A., Durham, J.H., Cangiano, J.L., Aiello, J.R., Novak, J.E., Lee, T., Leong, R., et al. (2016a). Oral Hypoxia-Inducible Factor Prolyl Hydroxylase Inhibitor Roxadustat (FG-4592) for the Treatment of Anemia in Patients with CKD. Clin. J. Am. Soc. Nephrol. *11*, 982–991.

Provenzano, R., Besarab, A., Wright, S., Dua, S., Zeig, S., Nguyen, P., Poole, L., Saikali, K.G., Saha, G., Hemmerich, S., et al. (2016b). Roxadustat (FG-4592) Versus Epoetin Alfa for Anemia in Patients Receiving Maintenance Hemodialysis: A Phase 2, Randomized, 6- to 19-Week, Open-Label, Active-Comparator, Dose-Ranging, Safety and Exploratory Efficacy Study. Am. J. Kidney Dis. *67*, 912–924.

Puente, B.N., Kimura, W., Muralidhar, S.A., Moon, J., James, F., Phelps, K.L., Grinsfelder, D., Rothermel, B.A., Chen, R., Garcia, J.A., et al. (2014). The Oxygen Rich Postnatal Environment Induces Cardiomyocyte Cell Cycle Arrest Through DNA Damage Response. Cell *157*, 565–579.

Puymirat, E., Simon, T., Steg, P.G., Schiele, F., Gueret, P., Blanchard, D., Khalife, K., Goldstein, P., Cattan, S., Vaur, L., et al. (2012).

Association of changes in clinical characteristics and management with improvement in survival among patients with ST-elevation myocardial infarction. JAMA *308*, 998–1006.

Raleigh, J.A., Chou, S.C., Arteel, G.E., and Horsman, M.R. (1999). Comparisons among pimonidazole binding, oxygen electrode measurements, and radiation response in C3H mouse tumors. Radiat. Res. *151*, 580–589.

Red-Horse, K., Ueno, H., Weissman, I.L., and Krasnow, M.A. (2010). Coronary arteries form by developmental reprogramming of venous cells. Nature *464*, 549.

Ren, B., Robert, F., Wyrick, J.J., Aparicio, O., Jennings, E.G., Simon, I., Zeitlinger, J., Schreiber, J., Hannett, N., Kanin, E., et al. (2000). Genome-wide location and function of DNA binding proteins. Science *290*, 2306–2309.

Risebro, C.A., Vieira, J.M., Klotz, L., and Riley, P.R. (2015). Characterisation of the human embryonic and foetal epicardium during heart development. Development *142*, 3630 LP-3636.

Robb, L., Mifsud, L., Hartley, L., Biben, C., Copeland, N.G., Gilbert, D.J., Jenkins, N.A., and Harvey, R.P. (1998). epicardin: A novel basic helix-loop-helix transcription factor gene expressed in epicardium, branchial arch myoblasts, and mesenchyme of developing lung, gut, kidney, and gonads. Dev. Dyn. *213*, 105–113.

Rosenberger, C., Mandriota, S., Jurgensen, J.S., Wiesener, M.S., Horstrup, J.H., Frei, U., Ratcliffe, P.J., Maxwell, P.H., Bachmann, S., and Eckardt, K.-U. (2002). Expression of hypoxia-inducible factor-1alpha and -2alpha in hypoxic and ischemic rat kidneys. J. Am. Soc. Nephrol. *13*, 1721–1732.

Ross, A.J., Yang, Z., Berr, S.S., Gilson, W.D., Petersen, W.C., Oshinski, J.N., and French, B.A. (2002). Serial MRI evaluation of cardiac structure and function in mice after reperfused myocardial infarction. Magn. Reson. Med. *47*, 1158–1168.

Rudat, C., and Kispert, A. (2012). Wt1 and epicardial fate mapping. Circ. Res. *111*, 165–169.

Ryan, H.E., Lo, J., and Johnson, R.S. (1998). HIF1-alpha is required for solid tumor formation and embryonic vascularization. EMBO J. *17*, 3005–3015.

Saker, D.M., Walsh-Sukys, M., Spector, M., and Zahka, K.G. (1997). Cardiac recovery and survival after neonatal myocardial infarction. Pediatr.

Cardiol. *18*, 139–142.

Schodel, J., Oikonomopoulos, S., Ragoussis, J., Pugh, C.W., Ratcliffe, P.J., and Mole, D.R. (2011). High-resolution genome-wide mapping of HIF-binding sites by ChIP-seq. Blood *117*, e207-17.

Scully, D., Keane, E., Batt, E., Karunakaran, P., Higgins, D.F., and Itasaki, N. (2016). Hypoxia promotes production of neural crest cells in the embryonic head. Development *143*, 1742–1752.

Sedmera, D., and Thomas, P.S. (1996). Trabeculation in the embryonic heart. Bioessays *18*, 607.

Sedmera, D., Reckova, M., DeAlmeida, A., Coppen, S.R., Kubalak, S.W., Gourdie, R.G., and Thompson, R.P. (2003). Spatiotemporal pattern of commitment to slowed proliferation in the embryonic mouse heart indicates progressive differentiation of the cardiac conduction system. Anat. Rec. A. Discov. Mol. Cell. Evol. Biol. *274*, 773–777.

Semenza, G.L., and Wang, G.L. (1992). A nuclear factor induced by hypoxia via de novo protein synthesis binds to the human erythropoietin gene enhancer at a site required for transcriptional activation. Mol. Cell. Biol. *12*, 5447–5454.

Serluca, F.C. (2008). Development of the proepicardial organ in the zebrafish. Dev. Biol. *315*, 18–27.

Shiau, A.K., Barstad, D., Loria, P.M., Cheng, L., Kushner, P.J., Agard, D.A., and Greene, G.L. (1998). The structural basis of estrogen receptor/coactivator recognition and the antagonism of this interaction by tamoxifen. Cell *95*, 927–937.

Simoes, F.C., and Riley, P.R. (2018). The ontogeny, activation and function of the epicardium during heart development and regeneration. Development *145*.

Simon, A., and Tanaka, E.M. (2013). Limb regeneration. Wiley Interdiscip. Rev. Dev. Biol. *2*, 291–300.

Smart, N., Risebro, C.A., Melville, A.A.D., Moses, K., Schwartz, R.J., Chien, K.R., and Riley, P.R. (2007). Thymosin beta4 induces adult epicardial progenitor mobilization and neovascularization. Nature *445*, 177–182.

Smart, N., Bollini, S., Dubé, K.N., Vieira, J.M., Zhou, B., Davidson, S., Yellon, D., Riegler, J., Price, A.N., Lythgoe, M.F., et al. (2011). De novo cardiomyocytes from within the activated adult heart after injury. Nature *474*, 640.

Smith, G.C.S. (1998). The Pharmacology of the Ductus Arteriosus. Pharmacol.

Rev. *50*, 35 LP-58.

Smith, C.L., Baek, S.T., Sung, C.Y., and Tallquist, M.D. (2011). Epicardial-derived cell epithelial-to-mesenchymal transition and fate specification require PDGF receptor signaling. Circ. Res. *108*, e15-26.

Stanley, W.C. (2001). Changes in cardiac metabolism: a critical step from stable angina to ischaemic cardiomyopathy. Eur. Hear. J. Suppl. *3*, O2–O7.

Stratikopoulos, E., Szabolcs, M., Dragatsis, I., Klinakis, A., and Efstratiadis, A. (2008). The hormonal action of IGF1 in postnatal mouse growth. Proc. Natl. Acad. Sci. *105*, 19378 LP-19383.

Stuckmann, I., Evans, S., and Lassar, A.B. (2003). Erythropoietin and retinoic acid, secreted from the epicardium, are required for cardiac myocyte proliferation. Dev. Biol. *255*, 334–349.

Takeda, K., Ho, V.C., Takeda, H., Duan, L.-J., Nagy, A., and Fong, G.-H. (2006). Placental but not heart defects are associated with elevated hypoxia-inducible factor alpha levels in mice lacking prolyl hydroxylase domain protein 2. Mol. Cell. Biol. *26*, 8336–8346.

Takeda, Y., Costa, S., Delamarre, E., Roncal, C., Leite de Oliveira, R., Squadrito, M.L., Finisguerra, V., Deschoemaeker, S., Bruyere, F., Wenes, M., et al. (2011). Macrophage skewing by Phd2 haplodeficiency prevents ischaemia by inducing arteriogenesis. Nature *479*, 122–126.

Tallquist, M.D., and Molkentin, J.D. (2017). Redefining the identity of cardiac fibroblasts. Nat. Rev. Cardiol. *14*, 484.

Tang, D., Zhang, J., Yan, T., Wei, J., Jiang, X., Zhang, D., Zhang, Q., Jia, J., and Huang, Y. (2018). FG-4592 Accelerates Cutaneous Wound Healing by Epidermal Stem Cell Activation via HIF-1alpha Stabilization. Cell. Physiol. Biochem. *46*, 2460–2470.

Tao, J., Doughman, Y., Yang, K., Ramirez-Bergeron, D., and Watanabe, M. (2013). Epicardial HIF signaling regulates vascular precursor cell invasion into the myocardium. Dev. Biol. *376*, 136–149.

Tao, J., Barnett, J. V, Watanabe, M., and Ramirez-Bergeron, D. (2018). Hypoxia Supports Epicardial Cell Differentiation in Vascular Smooth Muscle Cells through the Activation of the TGFbeta Pathway. J. Cardiovasc. Dev. Dis. *5*.

Tetzlaff, M.T., Curry, J.L., Ivan, D., Wang, W.-L., Torres-Cabala, C.A., Bassett, R.L., Valencia, K.M., McLemore, M.S., Ross, M.I., and Prieto, V.G. (2013). Immunodetection of phosphohistone H3 as a surrogate of

mitotic figure count and clinical outcome in cutaneous melanoma. Mod. Pathol. an Off. J. United States Can. Acad. Pathol. Inc *26*, 1153–1160.

Theriault, J.R., Perez, J., Gilbert, S., Palmer, M., Schreiber, S.L., Lindsley, C.W., Dawson, E.S., Engers, J.L., Felts, A.S., Bates, B.S., et al. (2010). Discovery of a Small Molecule Activator of the Hypoxia Inducible Factor Pathway. (Bethesda (MD)), p.

Tian, H., McKnight, S.L., and Russell, D.W. (1997). Endothelial PAS domain protein 1 (EPAS1), a transcription factor selectively expressed in endothelial cells. Genes Dev. *11*, 72–82.

Tian, H., Hammer, R.E., Matsumoto, A.M., Russell, D.W., and McKnight, S.L. (1998). The hypoxia-responsive transcription factor EPAS1 is essential for catecholamine homeostasis and protection against heart failure during embryonic development. Genes Dev. *12*, 3320–3324.

Tian, X., Hu, T., Zhang, H., He, L., Huang, X., Liu, Q., Yu, W., He, L., Yang, Z., Zhang, Z., et al. (2013). Subepicardial endothelial cells invade the embryonic ventricle wall to form coronary arteries. Cell Res. *23*, 1075.

Tian, X., Hu, T., Zhang, H., He, L., Huang, X., Liu, Q., Yu, W., He, L., Yang, Z., Yan, Y., et al. (2014). De novo formation of a distinct coronary vascular population in neonatal heart. Science (80-.). *345*, 90–94.

Tomanek, R.J., Ratajska, A., Kitten, G.T., Yue, X., and Sandra, A. (1999). Vascular endothelial growth factor expression coincides with coronary vasculogenesis and angiogenesis. Dev. Dyn. *215*, 54–61.

Towbin, J.A., Lorts, A., and Jefferies, J.L. (2015). Left ventricular non-compaction cardiomyopathy. Lancet (London, England) *386*, 813–825.

Vega-Hernandez, M., Kovacs, A., De Langhe, S., and Ornitz, D.M. (2011). FGF10/FGFR2b signaling is essential for cardiac fibroblast development and growth of the myocardium. Development *138*, 3331–3340.

Velagaleti, R.S., Pencina, M.J., Murabito, J.M., Wang, T.J., Parikh, N.I., D'Agostino, R.B., Levy, D., Kannel, W.B., and Vasan, R.S. (2008). Long-term trends in the incidence of heart failure after myocardial infarction. Circulation *118*, 2057–2062.

Vicente-Steijn, R., Scherptong, R.W.C., Kruithof, B.P.T., Duim, S.N., Goumans, M.J.T.H., Wisse, L.J., Zhou, B., Pu, W.T., Poelmann, R.E., Schalij, M.J., et al. (2015). Regional differences in WT-1 and Tcf21 expression during ventricular development: implications for

myocardial compaction. PLoS One *10*, e0136025.

Villar, A.J., Kim, J., De Blank, P., Gillespie, A.M., Kozy, H.M., Ursell, P.C., and Epstein, C.J. (2004). Effects of genetic background on cardiovascular anomalies in the Ts16 mouse. Dev. Dyn. *232*, 131–139.

Vinas-Castells, R., Beltran, M., Valls, G., Gomez, I., Garcia, J.M., Montserrat-Sentis, B., Baulida, J., Bonilla, F., de Herreros, A.G., and Diaz, V.M. (2010). The hypoxia-controlled FBXL14 ubiquitin ligase targets SNAIL1 for proteasome degradation. J. Biol. Chem. *285*, 3794–3805.

Viragh, S., and Challice, C.E. (1981). The origin of the epicardium and the embryonic myocardial circulation in the mouse. Anat. Rec. *201*, 157–168.

Vooijs, M., Jonkers, J., and Berns, A. (2001). A highly efficient ligand-regulated Cre recombinase mouse line shows that LoxP recombination is position dependent. EMBO Rep. *2*, 292–297.

Wagner, K.-D., Wagner, N., Bondke, A., Nafz, B., Flemming, B., Theres, H., and Scholz, H. (2002). The Wilms' tumor suppressor Wt1 is expressed in the coronary vasculature after myocardial infarction. FASEB J. Off. Publ. Fed. Am. Soc. Exp. Biol. *16*, 1117–1119.

Wagner, K.-D., Wagner, N., Wellmann, S., Schley, G., Bondke, A., Theres, H., and Scholz, H. (2003). Oxygen-regulated expression of the Wilms' tumor suppressor Wt1 involves hypoxia-inducible factor-1 (HIF-1). FASEB J. Off. Publ. Fed. Am. Soc. Exp. Biol. *17*, 1364–1366.

Wang, G.L., Jiang, B.H., Rue, E.A., and Semenza, G.L. (1995). Hypoxia-inducible factor 1 is a basic-helix-loop-helix-PAS heterodimer regulated by cellular O2 tension. Proc. Natl. Acad. Sci. U. S. A. *92*, 5510–5514.

Wang, J., Panáková, D., Kikuchi, K., Holdway, J.E., Gemberling, M., Burris, J.S., Singh, S.P., Dickson, A.L., Lin, Y.-F., Sabeh, M.K., et al. (2011). The regenerative capacity of zebrafish reverses cardiac failure caused by genetic cardiomyocyte depletion. Development *138*, 3421 LP-3430.

Wang, J., Cao, J., Dickson, A.L., and Poss, K.D. (2015). Epicardial regeneration is guided by cardiac outflow tract and Hedgehog signalling. Nature *522*, 226–230.

Watt, A.J., Battle, M.A., Li, J., and Duncan, S.A. (2004). GATA4 is essential for formation of the proepicardium and regulates cardiogenesis. Proc. Natl. Acad. Sci. U. S. A. *101*, 12573–12578.

Weber, E.M., and Olsson, I.A.S. (2008). Maternal behaviour in Mus musculus sp.: An ethological review. Appl. Anim. Behav. Sci. *114*, 1–22.

Weber, E.M., Algers, B., Wurbel, H., Hultgren, J., and Olsson, I.A.S. (2013). Influence of strain and parity on the risk of litter loss in laboratory mice. Reprod. Domest. Anim. *48*, 292–296.

Weinberger, M. (2017). Epicardial heterogeneity during zebrafish heart development. University of Oxford.

White, J.A., Boffa, M.B., Jones, B., and Petkovich, M. (1994). A zebrafish retinoic acid receptor expressed in the regenerating caudal fin. Development *120*, 1861–1872.

Wiesener, M.S., Turley, H., Allen, W.E., Willam, C., Eckardt, K.U., Talks, K.L., Wood, S.M., Gatter, K.C., Harris, A.L., Pugh, C.W., et al. (1998). Induction of endothelial PAS domain protein-1 by hypoxia: characterization and comparison with hypoxia-inducible factor-1alpha. Blood *92*, 2260–2268.

van Wijk, B., Gunst, Q.D., Moorman, A.F.M., and van den Hoff, M.J.B. (2012). Cardiac Regeneration from Activated Epicardium. PLoS One *7*, e44692.

Wills, A.A., Holdway, J.E., Major, R.J., and Poss, K.D. (2008). Regulated addition of new myocardial and epicardial cells fosters homeostatic cardiac growth and maintenance in adult zebrafish. Development *135*, 183–192.

Wisneski, J.A., Gertz, E.W., Neese, R.A., Gruenke, L.D., Morris, D.L., and Craig, J.C. (1985). Metabolic fate of extracted glucose in normal human myocardium. J. Clin. Invest. *76*, 1819–1827.

Witman, N., Murtuza, B., Davis, B., Arner, A., and Morrison, J.I. (2011). Recapitulation of developmental cardiogenesis governs the morphological and functional regeneration of adult newt hearts following injury. Dev. Biol. *354*, 67–76.

Wouters, B.G., and Koritzinsky, M. (2008). Hypoxia signalling through mTOR and the unfolded protein response in cancer. Nat. Rev. Cancer *8*, 851–864.

Wu, B., Zhang, Z., Lui, W., Chen, X., Wang, Y., Chamberlain, A.A., Moreno-Rodriguez, R.A., Markwald, R.R., O'Rourke, B.P., Sharp, D.J., et al. (2012). Endocardial Cells Form the Coronary Arteries by Angiogenesis through Myocardial-Endocardial VEGF Signaling. Cell *151*, 1083–1096.

Xu, J., Nie, X., Cai, X., Cai, C.-L., and Xu, P.-X. (2014a). Tbx18 is essential for normal development of vasculature network and glomerular mesangium in the mammalian kidney. Dev. Biol. *391*, 17–31.

Xu, X., Tan, X., Tampe, B., Sanchez, E., Zeisberg, M., and Zeisberg, E.M. (2015). Snail Is a direct target of hypoxia-inducible factor 1α (HIF1α) in hypoxia-induced endothelial to mesenchymal transition of human coronary endothelial cells. J. Biol. Chem. *290*, 16553–16664.

Xu, Z., Alloush, J., Beck, E., and Weisleder, N. (2014b). A Murine Model of Myocardial Ischemia-reperfusion Injury through Ligation of the Left Anterior Descending Artery. J. Vis. Exp. 51329.

Yamashita, T., Ohneda, O., Nagano, M., Iemitsu, M., Makino, Y., Tanaka, H., Miyauchi, T., Goto, K., Ohneda, K., Fujii-Kuriyama, Y., et al. (2008). Abnormal heart development and lung remodeling in mice lacking the hypoxia-inducible factor-related basic helix-loop-helix PAS protein NEPAS. Mol. Cell. Biol. *28*, 1285–1297.

Yang, J.T., Rayburn, H., and Hynes, R.O. (1995). Cell adhesion events mediated by alpha 4 integrins are essential in placental and cardiac development. Development *121*, 549–560.

Yuan, X., Qi, H., Li, X., Wu, F., Fang, J., Bober, E., Dobreva, G., Zhou, Y., and Braun, T. (2017). Disruption of spatiotemporal hypoxic signaling causes congenital heart disease in mice. J. Clin. Invest. *127*, 2235–2248.

Zhang, C., Li, Y., Cornelia, R., Swisher, S., and Kim, H. (2012). Regulation of VEGF expression by HIF-1α in the femoral head cartilage following ischemia osteonecrosis. Sci. Rep. *2*, 650.

Zhang, W., Chen, H., Qu, X., Chang, C.-P., and Shou, W. (2013). Molecular mechanism of ventricular trabeculation/compaction and the pathogenesis of the left ventricular noncompaction cardiomyopathy (LVNC). Am. J. Med. Genet. C. Semin. Med. Genet. *163*, 144–156.

Zhang, W., Shi, X., Peng, Y., Wu, M., Zhang, P., Xie, R., Wu, Y., Yan, Q., Liu, S., and Wang, J. (2015). HIF-1alpha Promotes Epithelial-Mesenchymal Transition and Metastasis through Direct Regulation of ZEB1 in Colorectal Cancer. PLoS One *10*, e0129603.

Zhou, B., and Pu, W.T. (2012). Genetic Cre-loxP assessment of epicardial cell fate using Wt1-driven Cre alleles. Circ. Res. *111*, e276-80.

Zhou, B., Ma, Q., Rajagopal, S., Wu, S.M., Domian, I., Rivera-Feliciano, J., Jiang, D., von Gise, A., Ikeda, S., Chien, K.R., et al. (2008). Epicardial progenitors contribute to the cardiomyocyte lineage in the developing heart. Nature *454*, 109–113.

Zhou, B., Honor, L.B., He, H., Ma, Q., Oh, J.-H., Butterfield, C., Lin, R.-Z., Melero-Martin, J.M., Dolmatova, E., Duffy, H.S., et al. (2011). Adult

mouse epicardium modulates myocardial injury by secreting paracrine factors. J. Clin. Invest. *121*, 1894–1904.

Zhou, B., Honor, L.B., Ma, Q., Oh, J.-H., Lin, R.-Z., Melero-Martin, J.M., von Gise, A., Zhou, P., Hu, T., He, L., et al. (2012). Thymosin beta 4 treatment after myocardial infarction does not reprogram epicardial cells into cardiomyocytes. J. Mol. Cell. Cardiol. *52*, 43–47.

Zou, J., Ma, W., Li, J., Littlejohn, R., Zhou, H., Kim, I., Fulton, D.J.R., Chen, W., Weintraub, N.L., Zhou, J., et al. (2018). Neddylation mediates ventricular chamber maturation through repression of Hippo signaling. Proc. Natl. Acad. Sci. *115*, E4101 LP-E4110.